Periodic structures and metamaterials for absorption purposes

Costanza HERRERA

Supervisor:
Prof. dr. ir. Guy A. E. Vandenbosch

Members of the Examination Committee:
Prof. dr. Gustaaf Borghs
Prof. dr.ir. Georges Gielen
Prof. dr. Robert Mertens
Prof. dr. Anton G. Tijhuis
Prof. dr.ir. Emmanuel Van Lil

Dissertation presented in partial fulfilment of the requirements for the degree of Doctor in Engineering

December 2015

I thank everyone who in different ways, directly or indirectly, has contributed and helped me with the realization of this PhD.

For his invaluable and generous help, to Prof.em.dr.ing. Antoine Van de Capelle.

To Prof. dr.ir.Dominique Schreurs and to Prof. dr.ir Emmanuel van Lil for his help and support prior to his appointment as jury-member, specially to Prof.dr. A.G.Tijhuis and Prof.em. dr.ir.Yves Willems within the Examinatory Committee, to Prof.dr.ir Bart Nauwelaers.

To Monesia program and to KU Leuven.

Among my colleagues at Telemic, to Ilja, Sen, Song, Gustavo, Jan-willem, Pawel, Tomislav, Vladimir, Marco, Xuezhi, Zhanna, Jack, Maciej, Dongpin and Ma.
To Xueru, Qinju and Yuanyuan.
To Enas and Mohamed, Huda, Mai, Rafael, Valeria, to Urmimala and Swaraj.
To Ann Deforce, Anne Ons, Natalie Buyckx, Lut Vanderbracht, Carine Decock, Ethel Claes, Paul Konijn, Anke Van Noten, Chantal Deboes. Thanks to Rudi Casteels at CMW.
I am surely forgetting someone.

To Gemengd Parochiaal Koor Heverlee for their continuous interest, to Elisabeth and Francois for their concern and support. I would not have survived this last year and a half without Katrien! To Fabienne. To the Jesuit Community Jezuïetenshuis Heverlee, to Fathers Juan Carlos Tinjacá and Paul Aerts in Sint-Michielskerk, to the community of Sint-Jan-de-Doperkerk (UP), to Zuster Christiane and Zuster Ana.
To my unforgettable colleagues at BROU, specially to Luis, Manuel, Marcelo, Guille and Santiago. To Prof. Ing. Alejandro Rodríguez, gone in February 2010, for his advice and recommendation. To wise Dr. Alfredo Corvalán.
To many people at GIFT community; I specially remember Mercedes with her supporting words, Fernanda and Chris.

For the very last leg of this journey, very special thanks to Koen Maesmans and Joske Maesmans -Van Den Plas. Also infinite thanks to Pater Jan Françoois, to Vero, Blanca and Jaime, Nati and Claudia, Silvia, María Antonia, Lilián, Marina and Rainer, Gisela and Markus, Ana Lucía and Camilo, Carolina and Pablo, to Rosita, Cristina M., Cristina F., Aurelina and Pedro, my uncles José Luis, Humberto, Marcelo and Carlitos, my aunts Amparo and Alicia, to my cousin Carolina, to my great-aunt Amancia, and to my mother, to whom I cannot be thankful enough.

To my grandmother, my grandfather and my father who have never stopped supporting me, even after they were gone, my aunt Graciela, my great-aunt Tota, my dear neighbour Milagros, and all of those who join them in that wonderful Community.

Abstract

Nowadays the demand for more broadband and multi-band operability is increasing in different electronic and electric applications, and absorbing capabilities of materials will be required to go hand in hand with this demand. The use of wearable technologies and devices can additionally give a more relevant role to absorbing materials and devices.
Apart from this, artificial complex media, and metamaterials among them, have not only promised to exhibit extraordinary properties, but have proven in many cases to be more tuneable to applications' operational frequency ranges, to be potentially more adaptable to applications' requirements and to possess a number of structural or functional advantages with respect to conventional materials.
In this context our research has focused in a specific application of artificial complex media and periodic structures: microwave absorbers, more specifically in attempting to widen periodic structure's absorption bandwidth and in seeking for designs with wider absorption bandwidths. These designs should additionally have as less extra resonators, layers and complementary elements as possible, in view of the increasing demand for further miniaturization of electrical and electronic components and devices, tuneable and flexible materials and devices, and the continuous expectations for new materials exhibiting multiple features and properties in a single structure. Metamaterials and periodic structures, due to their typical resonant character, have intrinsically narrowband responses, which is typically the opposite of what is required from an electromagnetic absorber. Therefore the effort for achieving wideband absorptive responses has classically been important and at the same time the narrowband nature of most metamaterial and periodic structures makes obtaining a genuine broadband behaviour difficult. On the other hand, as a general advantage, many metamaterial and periodic absorbing structures have turned out to be thinner and more tuneable than conventional absorbers. They are typically more suitable for small-sized devices and potentially for applications and environments requiring strong structural constraints.

In this framework, first, a systematic analysis is performed in order to gain further insight in the relationship between a structure's parameters and its absorptive capabilities, and eventually find contributions to absorption bandwidth widening mechanisms. A multiple-layer narrowband metamaterial absorber is fully validated through a vast amount of numerical results and through measurements. Then, wideband absorbing structures made with single-resonators are proposed, accompanied by measurement results of equivalent designs.
Regarding initial investigation performed on pure metamaterials -viewed as mere materials whose design is not directed towards any specific kind of application-, additional results on a specific type of metamaterial, NRI metamaterials, are included. This is realized prior to the research on absorbing structures.

Samenvatting

Tegenwoordig wordt de vraag naar breedband en multiband mogelijkheden steeds groter voor verschillende elektronische en elektrische toepassingen, en materialen met absorberende eigenschappen zullen nodig zijn om aan deze vraag te voldoen.
Het gebruik van draagbare technologieën en apparaten kan bovendien een meer relevante rol betekenen voor absorberende materialen en apparaten.
Daarnaast vertonen kunstmatige complexe media, waaronder ook metamaterialen, niet alleen uitzonderlijke eigenschappen, maar zijn in veel gevallen beter af te stemmen voor operationele bandbreedtes van toepassingen, makkelijker aan te passen aan de vereisten van bepaalde toepassingen, en hebben een aantal structurele en functionele voordelen ten opzichte van conventionele materialen.
In die context heeft ons onderzoek zich gericht op een specifieke toepassing van kunstmatige complexe media en periodieke structuren: microwave absorbers, meer bepaald in een poging om de structuur van absorptie bandbreedte te verbreden en in het zoeken naar ontwerpen met grotere absorptie bandbreedtes. Die ontwerpen zouden bovendien zo weinig mogelijk extra resonatoren, lagen en aanvullende elementen mogen hebben, gezien de toenemende vraag naar verdere miniaturisering van elektrische en elektronische componenten en apparaten, afstelbare en flexibele materialen en apparaten, en de blijvende verwachting naar nieuwe materialen met meerdere kenmerken en eigenschappen in één enkele structuur. Metamaterialen en periodieke structuren hebben vanwege hun typische resonante aard intrinsieke korteband reacties, wat net het tegenovergestelde is van wat een elektromagnetische absorber nodig heeft. Daarom is het altijd belangrijk geweest om te proberen absorptieve gedragingen in breedband te zoeken. Tegelijkertijd maakt het smalband gedrag van de meeste metamaterialen en structuren het moeilijk om een echt breedband gedrag te verkrijgen. Anderzijds is het een voordeel gebleken dat vele metamaterialen en periodieke absorberende structuren dunner en beter afstelbaar zijn dan conventionele absorbers. Ze zijn meer geschikt voor kleine apparaten en mogelijk voor toepassingen die sterke structurele beperkingen vereisen.

In dit kader hebben we ten eerste een systematische analyse uitgevoerd om meer inzicht te krijgen in de relatie tussen de parameters van een structuur en haar absorberende capaciteiten, en tenslotte mechanismen te zoeken die bijdragen tot de verbreding van absorberende bandbreedte. Een meerlagen smalband absorber uit metamateriaal is volledig onderbouwd door een enorme hoeveelheid numerieke resultaten en door metingen. Vervolgens stellen we breedband absorberende constructies met enkelvoudige resonatoren voor , samen met de meetresultaten van gelijkaardige ontwerpen.
De resultaten van eerder onderzoek naar zuivere metamaterialen – louter beschouwd als materialen waarvan het ontwerp niet gericht is op een specifieke toepassing- zoals NRI metamaterialen, zijn eveneens toegevoegd, en dit vóór het onderzoek naar absorberende eigenschappen.

Contents

1 Introduction

1.1 Artificial complex materials: Metamaterials

From a general point of view we can say metamaterials are artificially crafted materials exhibiting physical properties that are not meant to be found in nature, which rely on their structure rather than on their chemical composition. In 1999 Rodger Walser (University of Austin, Texas) said "Metamaterials are macroscopic composites having man-made, three-dimensional, periodic cellular architecture designed to produce an optimized combination, not available in nature, of two or more responses to specific excitation". The physical structure of metamaterials is therefore always engineered at macroscopic level, not at the atomic level, no matter how reduced this macroscopic scale is. The interaction with small inclusions in the structure affects the macroscopic properties of the composite medium, resulting in a specific behaviour of the new material. These small inclusions are usually arranged in a periodic fashion within the "base material" (bulk material) that is used to accomplish the metamaterial. They can exhibit extraordinary physical properties –many of them still to be adequately proved-, or offer advantageous characteristics, frequently structural, with respect to conventional materials when exhibiting more ordinary properties or used for more conventional purposes like absorption, reduction of different types of interference, unwanted radiation in antennas -and radars-, among others. Some of the most common extraordinary properties claimed are invisibility, sub-wavelength image resolution, left handedness and negative refraction.

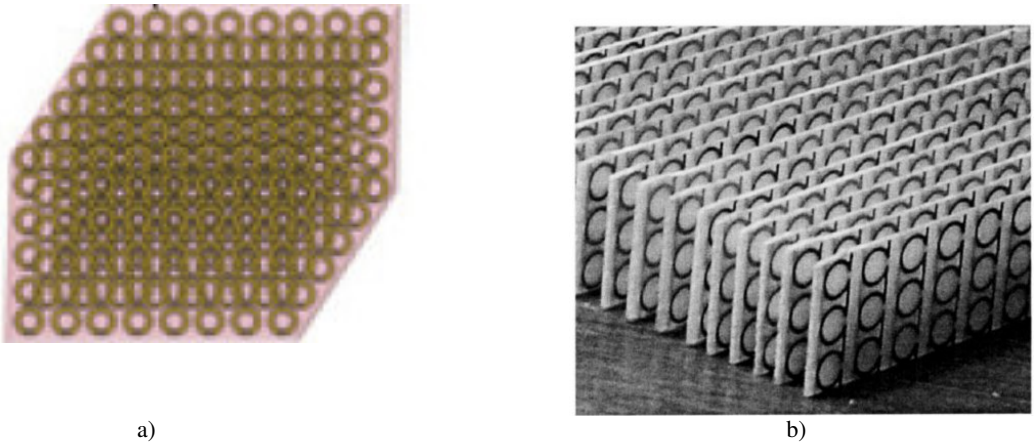

a) b)

Fig. 1. a) Schematic view of a piece of metamaterial with plasmonic resonators as inclusions.[1] b) A simple metamaterial fabricated on PCB boards. [2]

Different kinds of materials that could be classified as metamaterials, artificial complex materials or electromagnetic composite media have been studied and developed over the past nearly ten years, after a group of researchers at the University of California (2001) managed to build the first metamaterial made up of resonant structures (metal split-ring resonators and wires) [1]. Before this, theoretical research in artificially tuned electromagnetic materials was led mainly by Victor Veselago in 1968 [2] and John Pendry already in 1999 [3]. In the early 90s other groups have theoretically studied and built photonic crystals or Electromagnetic

[1] Source: Nikolay I. Zheludev, "A roadmap for metamaterials", OPN Optics & Photonics News, Vol.22, Issue 3, p.31, 2011

[2] Source: N. Engheta, Richard W. Ziolkowski, "Metamaterials: Physics and Engineering Explorations", IEEE Press, John Willey and Sons, Inc, 2006, chapter 4, section 4.3.2 "Measurements of various rings"

Bandgap (EBG) materials [4], [5], which have also been considered an important kind of metamaterial. Double-Negative metamaterials (DNG), more often called negative index materials, and Electromagnetic Bandgap materials were the first kind of metamaterials introduced, but more have been proposed since then like transmission-line metamaterials [6], actively and dynamically reconfigurable metamaterials [7], [8], high-impedance surfaces have also been considered metamaterials [9], gradient index metamaterials [10], [11], metasurfaces [12], [13], [14], among others, many of which can be found in several review papers (for instance [15]). Metamaterials have also been used in combination with graphene [16]. We will briefly report on the first two and on metamaterial absorbers which together with periodic absorbing materials have been our main line of research.

These artificial materials have found applications not only in the electrical and optical fields, comprising electrical engineering, semiconductors, nanotechnology and photonics, but also in mechanical waves (acoustics and seismic applications) [17] and even in thermal radiation, where applications even to energy saving are possible [18]. In electrical engineering, applications to alternative and many times improved solutions to conventional issues, in the field of radiation and antennas for instance, have been proposed and carried out in [19] and [43]. Some common applications are shown in figure 2.

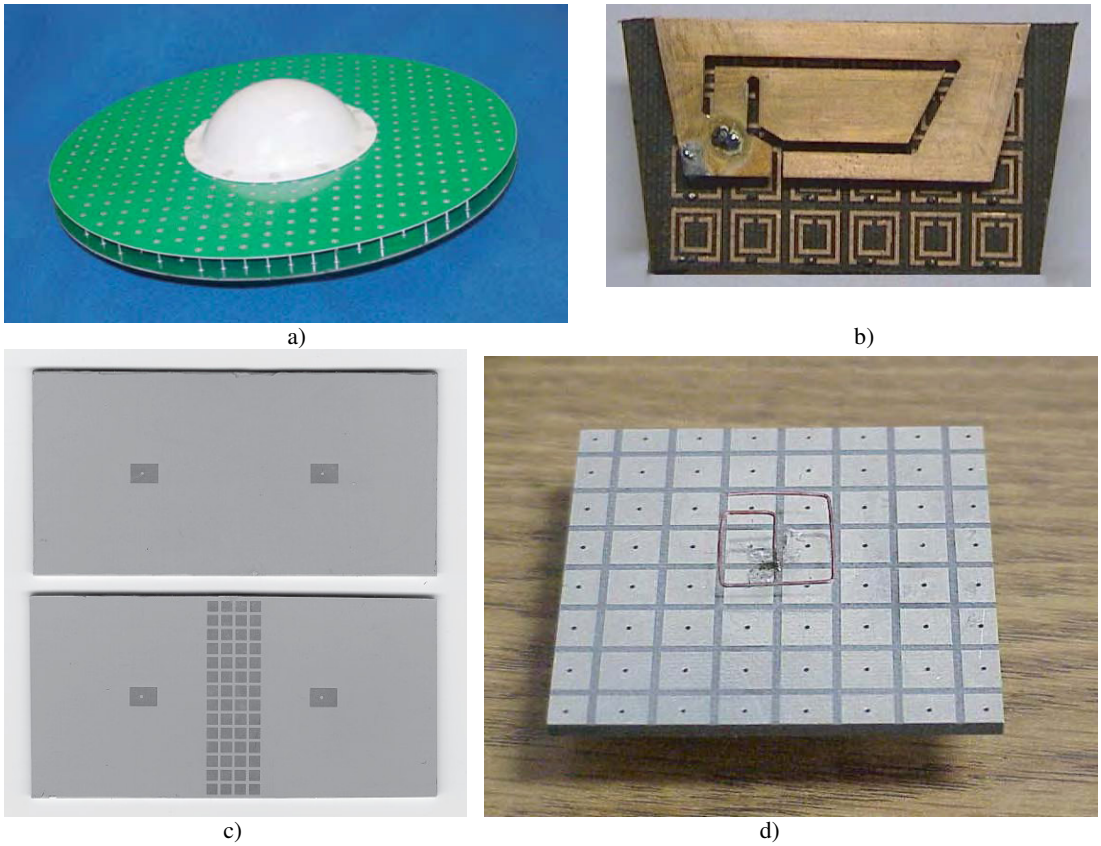

Fig. 2. a) GPS antenna presumably made with EBG technology. b) Top view of a mobile phone antenna fabricated with EBG technology, the pattern of split-ring-resonators printed can be observed.[3] c) Photograph of a typical microstrip antenna, two elements (top) and the same array with EBG material embedded in

[3] Source: N. Engheta, Richard W. Ziolkowski, "Metamaterials: Physics and Engineering Explorations", IEEE Press, John Willey and Sons, Inc, 2006, chapter 9, section 9.4 "Current and future applications of EBG systems"

between both elements to suppress interference. d) Photograph of a circularly polarized curl antenna over an EBG ground plane.[4]

Metamaterial absorbers or filters used as sensors and thermal detectors specially in the infrared regime and terahertz range of the spectrum have been proposed as well [41].
In the next years the use of quantum interference devices to create quantum artificial electromagnetic media [15], the combination of metamaterials with other materials such as the recently awarded graphene [16] and the use of metamaterials as active and non-linear source of devices [15] promises even more productive applications. Interesting review publications enumerating further exciting applications have been published (among others [15], [41], [42]).

Main working principle in metamaterials: resonance

The most common functional mechanism found to be the origin of metamaterials' behaviour is resonance. The inspiration to design and build metamaterials with this working principle came from natural materials: the dispersive Lorentz, Drude, Debye models are used to characterize a material's electrical or magnetic susceptibility, and describe in a simplified way the mechanical motion of subatomic particles (electrons) in conventional material, making reference to its resonant behaviour. Regarding this, (1) is the equation of the motion of an electron following Lorentz's model

$$m_e \frac{d^2\mathbf{x}(t)}{dt^2} + m_e\gamma \frac{d\mathbf{x}(t)}{dt} + \kappa\mathbf{x}(t) = -e\mathbf{E}(t) \qquad (1)$$

(with x being position, t time, m_e the electron's mass, γ damping factor, $\kappa = m_e\omega_0^2$ and E electric field). Ultimately they can therefore be used to describe the permittivity and permeability of a certain natural material more accurately, as these parameters have actually a dispersive nature as it is known. In metamaterials its microscopic inclusions are the ones that yield resonant characteristics.

For metamaterials it has been necessary to introduce generalizations and combinations of these classical material models, as explained in [43] to some extent.
To the best of our knowledge Pendry made the first proposal [20] of this kind, which can give more insight on the principle. His aim was to obtain a negative effective electromagnetic parameter, namely effective permittivity, based on plasma´s electromagnetic response, which shows a negative permittivity below its plasma frequency ω_p -it would be the "cuttoff" frequency in an analogy with waveguides-. Again we could make reference to natural materials, specifically metals, which essentially could be seen as an ionized "gas" of free electrons, but with their natural plasma frequencies normally occuring in the ultraviolet region of the electromagnetic spectrum, in which wavelengths are extremely short. Pendry proposed an array of thin metallic wires aiming to "shift" the plasma frequency to a more convenient region in the EM spectrum, and derived (2) for infinitely long wires

$$\varepsilon_{\text{eff}} = 1 - \frac{\omega_p^2}{\omega\left(\omega + i\varepsilon_0 a^2\omega_p^2/\pi r^2\sigma\right)} \qquad (2)$$

[4] Source: N. Engheta, Richard W. Ziolkowski, "Metamaterials: Physics and Engineering Explorations", IEEE Press, John Willey and Sons, Inc, 2006, chapter 12, section 12.4.1 "Enhanced performance of microstrip antennas and arrays" for figure 2c) and section 12.4.4 "Low-Profile circularly polarized antennas: Curl and dipole designs" for figure 2d).

with *a* being the lattice constant –separation between wires-, r the radii of the wires, ω_p its plasma frequency and σ the conductivity of the metal chosen to fabricate the wires. According to his analysis the small radii of the wires is to account for the reduction in the structure's plasma frequency. The formula could be rewritten in a Drude-Lorentz form in (3)

$$\varepsilon_{\text{eff}}(\omega) = 1 - \frac{\omega_{\text{ep}}^2 - \omega_{e0}^2}{\omega^2 - \omega_{e0}^2 + i\gamma\omega} \qquad (3)$$

with ω_{ep} being the electric plasma frequency, ω_{e0} a resonant frequency which would stand for the low-frequency edge of the electrical forbidden band and γ the damping factor. In the case of infinitely large wires ω_{e0} =0. This form was later used in the experiments that put these ideas into practice.

Following the same way[5] in 1999 he derived the dispersive behaviour of permeability for a periodic array of split-ring resonators (SRR) with the structure shown in figure 3,

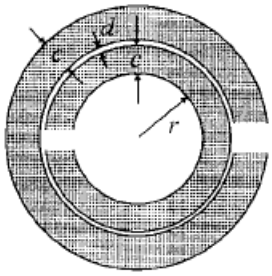

Fig. 3. A classic circular SRR shape being c the width in both rings, r the inner ring radius and d the separation between inner and outer ring.[6]

being (4) one of the possible forms to describe these resonators' permeability

$$\mu_{\text{eff}} = 1 - \frac{F\omega^2}{\omega^2 - \omega_0^2 + i\omega\Gamma} \qquad (4)$$

with *F* being the fractional area of the unit cell occupied by the interior of the split ring, Γ is a damping factor and ω_0 again a resonant frequency associated with the SRR's capacitance , internal radius, among other parameters. In the end the single structure shows both inductive and capacitive responses yielding analogy with LC-circuits and its consequent resonant behaviour. Basically the design of the SRRs and their combination into a periodic medium that achieves a strong magnetic coupling between them seems to be able to achieve unique properties in the macroscopic structure. μ_{eff} (ω) is negative near the high frequency side of the resonance.

Perhaps the major achievement of Pendry et.al was to be able to create designs that could be quite easily tuned to have its resonant frequencies at more convenient frequency regions (no longer in the ultraviolet region), that is, where the wavelength of electromagnetic waves would allow a feasible fabrication of inclusions due to its size.

Different shapes of resonant structures have been developed following from Pendry's original idea. Among other reasons, they have been implemented to address different issues –even

[5] except that a "gas" of isolated magnetic charges is more difficult to model as there are no physical existing magnetic "charges" or magnetic monopoles

[6] Source: J. B. Pendry, A. J. Holden, D. J. Robbins, W. J. Stewart, "Magnetism from Conductors and Enhanced Nonlinear Phenomena", IEEE Transactions on Microwave Theory and Techniques, Vol. 47, no. 11, p.2075, 1999.

issues related to experiments- and optimize the metamaterial's electromagnetic response. The same structures have been used and miniaturized in order to obtain responses at higher frequencies, above all in the infrared and optical regions, although simply scaling down the inclusions has proven not to be sufficient to achieve the desired effects. Among others, size effects start to appear when we scale down structures as free electrons start to collide with the boundary of the structure. This phenomenon is of course relevant in nanoparticles which can also be seen as resonators and have also found application in metamaterials.

Also, most metamaterials are designed and fabricated in a way that enables the effective medium theory to be applied to them and therefore they can be regarded as an effective medium with effective parameters. This imposes the condition on their inclusions and the spacing between them to be sub-wavelength, meaning that the unit cells that compose the typically periodic structure have to be much smaller than the operational wavelength. This is, the wavelength that corresponds to the frequency at which the resonance occurs; this is generally one order smaller than the free-space wavelength of the resonance frequency.
EBG materials or photonic crystals typically involve distances of half a wavelength or more and thus would not comply with the effective medium theory, they rather rely on other mechanisms to characterize their behaviour. Artificial magnetic conductors, also considered by many as metamaterials [43], do not rely on their constituting parts to be sub-wavelength either. Some even do not consider periodic structures that do not qualify as effective medium as metamaterials, while others have an even broader conception of what can be considered a metamaterial. Thus when the periodicity in a structure with characteristics of metamaterial is too large to be considered effective medium, the structure –or rather material- can be just defined as periodic structure, frequency selective surface, or even composite media or artificial complex material, instead of metamaterial. In this Introduction we will take the broader approach to the term and include most examples and publications under the umbrella of metamaterials, as long as they are periodic structures artificially composed, indistinctively of whether the size of their unit cells is an order smaller than the wavelength or not. In fact, in literature many periodic structures are referred simply as metamaterials despite not being sub-wavelength –there are cases where they are even not periodic and rather "metamaterial-like"-. It is not the aim of this introduction to give a full view of the extremely vast universe of artificially complex materials but to explain the main idea behind them and report on the ones that can be more useful for the rest of this work.

Some extraordinary metamaterials' properties: Negative refraction index and left-handed media

Veselago was, to the best of our knowledge, the first scientist that theoretically proposed what could happen if a material with simultaneous negative permittivity and permeability was found in nature or artificially fabricated. One of the most known properties he predicted was a resultant negative refractive index: he took the dispersion equation for a monochromatic wave

$$\left| \frac{\omega^2}{c^2} \varepsilon_{il} \mu_{lj} - k^2 \delta_{ij} + k_i k_j \right| = 0 \qquad (5)$$

(with ω being the angular frequency, k the wave number or wave vector, ε the electric permittivity, μ magnetic permeability, c the speed of light in vacuum and δ the skin depth, as usual) and to simplify the analysis assumed –as is also broadly done in the literature for

metamaterials – that it was propagating in an isotropic medium, so that the equation took the form

$$k^2 = \frac{\omega^2}{c^2} n^2 \qquad (6)$$

with $n^2 = \varepsilon\mu$. He further supposed that losses were negligible which makes $\varepsilon=\varepsilon_r$ and $\mu= \mu_r$ with ε_r and μ_r being real values. Finally we can write $n=\pm\sqrt{\mu_r\varepsilon_r}$ and because ε_r and μ_r were supposed to be negative, the negative sign has to be chosen for the square root, giving a negative refractive index n (NRI).

Analogously we could have said that if ε and μ can be considered effective parameters in the material then the media can be considered homogeneous. If we also assume the propagation of a plane wave in an isotropic medium with negligible losses the following is valid for its phase velocity

$$v_{phase} = \frac{1}{\sqrt{\mu\varepsilon}} \qquad (7)$$

with ε and μ being scalar and real values.
By definition

$$n \equiv \frac{c}{v_{phase}} \rightarrow n^2 = \frac{c}{v_{phase}}^2 = \frac{\mu\varepsilon}{\mu_0\varepsilon_0} = \mu_r\varepsilon_r \qquad (8)$$

with ε_r and μ_r being again scalar values (isotropic, homogeneous) and real (no losses) in this case, which takes us again to $n=-\sqrt{\mu_r\varepsilon_r}$ and a negative refractive index.

One of the immediate consequences of having simultaneously negative permittivity and permeability is the creation of a left-handed triplet: in the case of a TEM (Transverse ElectroMagnetic) wave propagating in a medium were n>0, the electrical field vector E, magnetic field vector H and the wave vector k would form a "right-handed triplet". This term is used as they follow the "right-handed rule" which indicates the direction of the resultant vector of the cross product, in this case the vector k has a direction resultant from the cross product of vectors E and H. In a medium with n<0 we would have a "left-handed triplet", as k would point in the opposite direction.
Veselago proved theoretically the "left-handedness" of negative-refractive- index media using mainly Maxwell's equations and the constitutive relations:

$$\nabla \times E = -j\omega B \qquad \nabla \times H = j\omega D \text{ (for a lossless media)} \quad (9)$$
$$B = \mu H \qquad D = \varepsilon E$$

The simplest solutions for Maxwell's equations in the case of a TEM wave are $E(z, t)= E_0e^{j\omega t-jkz}$ and $H(z, t)= H_0e^{j\omega t-jkz}$, being E_0 and H_0 magnitudes that can be complex -the amplitudes of the electric and magnetic fields with its respective initial phases-. We must bear in mind that $\nabla(e^{-jkz}) = -jk(e^{-jkz})$, so that after cancelling the common factors $e^{j\omega t-jkz}$ the two Maxwell's equations can be rewritten as follows:

$$\begin{aligned} -jk \times E_0 &= -j\omega\mu H_0 \\ -jk \times H_0 &= j\omega\epsilon E_0 \end{aligned} \quad \Rightarrow \quad \begin{aligned} k \times E_0 &= \omega\mu H_0 \\ k \times H_0 &= -\omega\epsilon E_0 \end{aligned} \qquad (10)$$

were we can easily see that if we have a medium with ε and μ simultaneously negative the signs of the cross products will indicate that not a right-handed but a left-handed triplet is present.

In addition to this, for any kind of electromagnetic wave the Poynting vector will always form a right-handed triplet with the electric and magnetic field vectors as follows from

$$\overline{S} = \overline{E} \times \overline{H} \qquad (11)$$

whereas in left-handed media the propagation vector k forms a left-handed triplet with the field vectors, as we have seen before. That means that in negative-refractive-index media the Poynting vector will always point in the direction opposite to that of the propagation vector k. The fact that the propagation and the Poynting vectors point in opposite directions also indicates that the electromagnetic energy flux and the wave propagate in opposite directions, which should lead in theory to a reverse Doppler and Cerenkov effects.These will not be analyzed in the scope of this text. More interestingly though is the fact that a backward-travelling wave is established, as the direction of the flow of power of the wave propagating in a left-handed medium will be opposite to that of the positive phase advance of the same wave.

Another consequence of the left-handedness of NRI materials is that Snell's law should be written in a different form: the electromagnetic boundary conditions at the interface of two media are

$$\begin{aligned} E_{t1} &= E_{t2} \\ H_{t1} &= H_{t2} \end{aligned} \quad \text{and} \quad \begin{aligned} \varepsilon_1 E_{n1} &= \varepsilon_2 E_{n2} \\ \mu_1 H_{n1} &= \mu_2 H_{n2} \end{aligned} \qquad (12)$$

again for isotropic, homogeneous media. So if one of the two media has negative permittivity and permeability, the normal or perpendicular components of the electric and magnetic fields will have opposite signs when transversing the boundary, while the tangential components remain the same. As a consequence Snell's law should be rewritten

$$\frac{\sin\theta_1}{\sin\theta 2} = \frac{n_2}{n_1} = \pm\left|\sqrt{\frac{\varepsilon_2\mu_2}{\varepsilon_1\mu_1}}\right| \qquad (13)$$

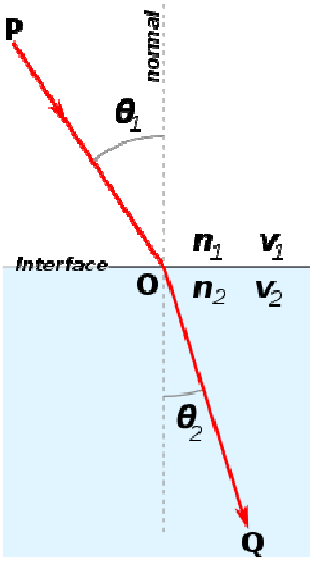

Fig. 4. Schematic draw of how a beam with normal incidence would refract in conventional media. Parameters used in Snell's law equation (13) are indicated.[7]

[7] Source:Snell's law at www.wikipedia.com

The negative sign should be taken if the two media have different handedness (one of them is right-handed while the other is left-handed).

However some authors have argued that the effects of some of these properties cannot physically take place and therefore negative-refractive index media would not really be physically realizable; violations to thermodynamics' laws and even the necessity of negative time have been mentioned. At the same time until now, although some have proved to be difficult to built, mainly in the optical region, numerous LHM metamaterials have been fabricated confirming these properties.

1.2 DNG materials

Double-negative (DNG) materials have an effective simultaneously negative permittivity and permeability for a certain frequency region, thus DNG metamaterials have evidently this particular feature. To the best of our knowledge the first designs proposed were previously mentioned Pendry's designs in 1996 and 1999, where the array of wires also had an effective permeability but at a frequency region that did not overlap the region of negative effective permittivity, thus being the structure by its own not able to yield the simultaneous $\varepsilon,\mu<0$ needed.
The first implementation of a material based on these kinds of structures, that additionally directly showed a negative refraction angle, was realized in 2001 at microwave frequencies (8-12GHz), which allowed the construction of a sample of left-handed material in the order of millimetres (figure 5b). A beam of electromagnetic waves impinged on the sample and the negative angle of the refracted beam could be directly measured (figure 5c). The metallic wires and slightly modified SRRs (see figure 5a) were implemented to achieve a frequency region where the negative ε_{eff} and μ_{eff} overlapped.

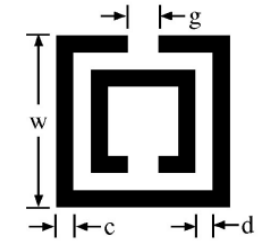

a)

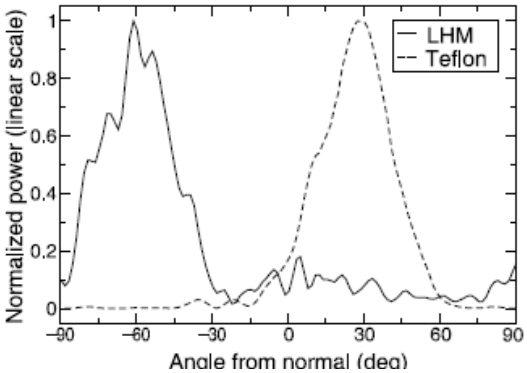

Fig. 5. a) Shape of the SRR resonator used in [1].[8] b) Photograph of the finished metamaterial slab used in [1] c) Normalized resulting power transmitted through the metamaterial and a teflon slab in [1]. [9]

[8] Source: R. A. Shelby, D. R. Smith, S. Schultz, "Experimental verification of a negative index of refraction", Science, Vol. 292, p. 77, 2001 ([1]).
[9] Source of figures b) and c) : R. A. Shelby, D. R. Smith, S. C. Nemat-Nasser, S. Schultz, "Microwave transmission through a two-dimensional, isotropic, left-handed metamaterial", Appl. Phys. Lett., Vol. 78, no. 4, p.489, 2001.

b) c)

Copper was used for the metallizations and the bulk material was a dielectric, circuit board material. The left-handed behaviour region of the composite material proved to be extended approximately around the frequency band of 10-10.8 GHz.

Many others followed since then, often fabricated using standard PCB material [44]-[64].

1.3 Electromagnetic Bandgap Materials or Photonic Crystals

Although this type of metamaterial is not part of our core research, it is an important line of research worth presenting in this Introduction and that bears some analogy with metamaterial absorbers or filters, as both do not allow transmission of waves in a certain frequency band.
As previously mentioned, unlike most double-negative metamaterials, EBG metamaterials typically do not qualify as effective medium regarding their structure. EBG materials yield a forbidden frequency band or gap in which all propagating states are prohibited for the electromagnetic waves within it. They are also referred as Photonic Bandgap Materials or Photonic Crystals, although this term should be more strictly used to define EBG materials that show bandgaps in the optical range. EBGs bear analogy with semiconductors as semiconductors have forbidden electronic energy bands that affect electrons' motion, while EBG materials have forbidden frequency bands that affect electromagnetic waves' motion. EBGs accomplish this by yielding periodic electromagnetic parameters (i.e. refractive index, dielectric constant or permittivity) as they are built from different materials with also different electromagnetic parameters, generally periodically built nanostructures. It must though be born in mind that in the case of EBGs periodicity alone does not guarantee the existence of a complete bandgap (we will define later what a complete or full bandgap means). Also, unlike NRI materials, EBG materials final structures do not necessarily conform an effective medium and therefore the sub-wavelength condition presented before is not a pre-requisite in these materials. EBG materials rather rely on Brillouin's ideas: media with periodically changing dielectric properties impose periodic boundary conditions on the electromagnetic modes that propagate through them, imposing restrictions on them.

Again a very wide variety of structures has been built using different methods, but
EBGs have commonly been classified as one, two or three-dimensional according to how properties vary on them, that is, if there is periodicity only along one direction it is classified as a one-dimensional EBG, and so on.

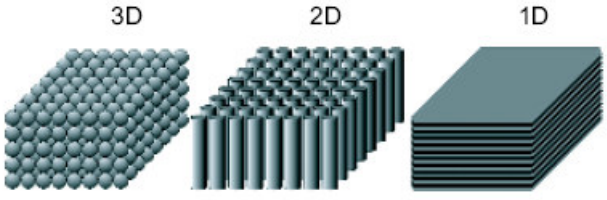

Fig. 6. Simplified schematic drawing to illustrate what should differentiate 1-, 2- and 3-D structures, for 2-D structure periodicity exists in 2 direcions, for 3-D structures in 3 directions and therefore we would have spheres.[10]

[10] Source: Paras N.Prasad, "Nanophotonics", John Wiley & Sons Inc, 2004, chapter 9 "Photonic Crystals"

The way that one-dimensional EBGs allow the propagation of only certain wavelengths is the same principle that two and three –dimensional structures use, just extended to more directions.

1D-EBGs

Is the simplest kind of photonic crystal, being the most widely studied structure the multilayer film, Bragg mirror or Bragg reflector. Such a multiple layer construction can be considered the basic idea used to build photonic crystals from which more complicated structures have been developed. A Bragg reflector is conformed by multiple layers of dielectric material with alternating refractive indexes as shown in figure 7,

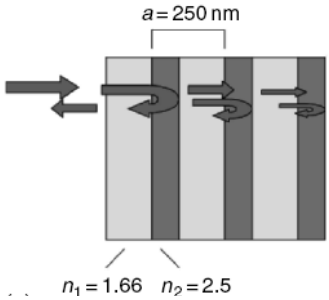

Fig. 7. Schematic draw of a simple Bragg reflector constituted by multiple layers of materials with different refractive indexes n, 1.66 and 2.5 in this case, differently refracting incident waves. [11]

complying with Bragg's condition for a certain wavelength range according to (14)

$$2n_{average}\,d\cos(\theta) = m\lambda \qquad (14)$$

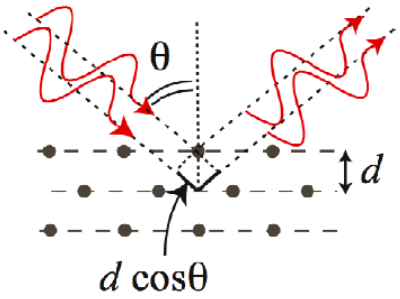

Fig. 8. Bragg's condition reflected in (14) and illustrated in the figure.[12]

being d the thickness of each layer and m an integer number, so that we have a material with a periodicity of d. In each layer boundary, waves are reflected and with m being an odd integer for those wavelengths that fulfil Bragg's condition there is destructive interference , as illustrated in figure 8. The structure acts then as a reflector and a forbidden bandgap is built for those wavelengths, as they are totally reflected and cannot propagate through the structure. If we consider that the incident angle of the wave is normal instead of oblique –which is the most common approach used to explain multilayer film structures-, and we use a instead to define the periodicity of the material we can write

[11] Source: L.Pavesi, G.Guillot, "Optical Interconnects. The Silicon Approach ", Springer, Springer Series in Optical Sciences, Vol.119, 2006, chapter 9 "Photonic Crystal Microcircuits"

[12] Source:Notes of the course "Optical properties of solids" 2010-2011 (K.U.Leuven), 4.Optics in dielectrics, Prof.G.Borghs

$2n_{av}a = m\lambda$ that can be rewritten as $k = m\frac{\pi}{a}$, being k the wave vector. We can plot the dispersion relation ω(k) but it has to be considered that the refractive index n is not a constant number, and thus when the total reflection condition is met a bandgap is opened, as shown in figure 9

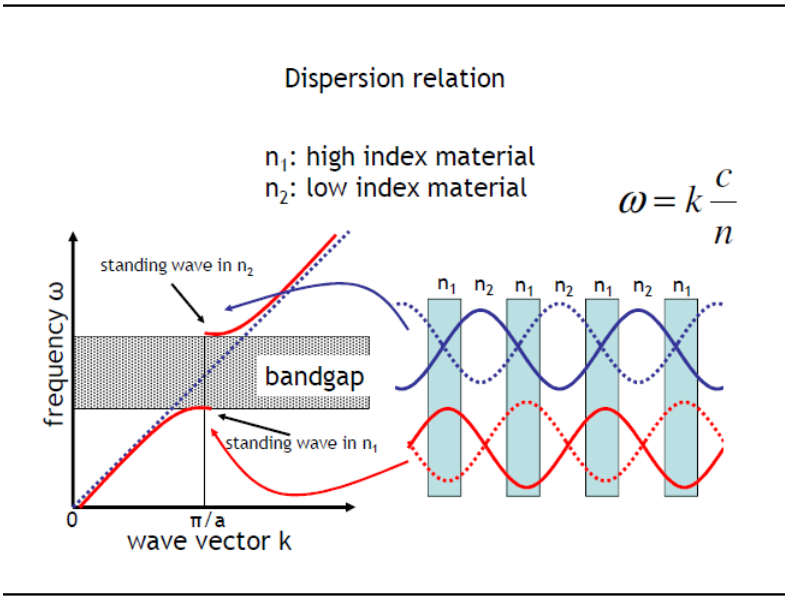

Fig. 9. Schematic explanation using the dispersion relation of how a bandgap is created with a high and low index material.[13]

When the wavelength approaches the condition, most of the wave starts to get reflected and a standing-wave appears. This is repeated every odd multiple of $\frac{\pi}{a}$.

This concept is extended and used in periodic 2-dimensional and 3-dimensional structures, but Brillouin zones are preferably used to describe the band structure of crystals.

It might be interesting to mention that a crystal is said to have a complete bandgap when it reflects waves of any polarization incident at any angle for a particular frequency range, so that no wave modes can propagate within that band.

Besides this the "width" of the bandgap (how broad the forbidden frequency band is) depends on how different the indexes of refraction are, what is called the contrast: the more contrast between the high and low indexes, the broader the bandgap, as illustrated in figure 10 for GaAs and air. This gives the first idea on how EBGs can be designed to be more or less frequency selective, according to their final application.

[13] Source:Notes of the course "Optical properties of solids" 2010-2011 (K.U.Leuven), 4.Optics in dielectrics, Prof.G.Borghs

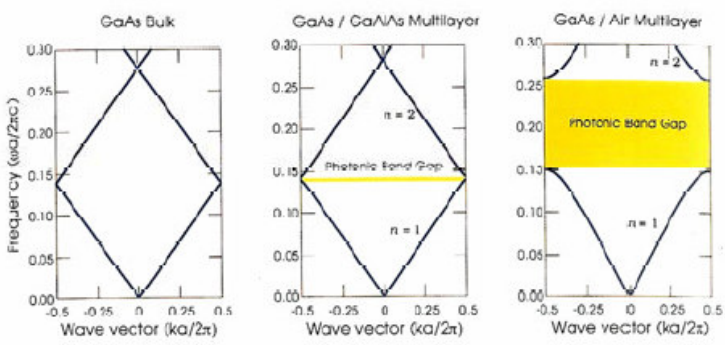

Fig. 10. Photonic bandgap in three different multilayer combinations, having each layer in all cases width 0.5a: at the left, with only GaAs there is as expected no bandgap, in the center using GaAs and Al there is a smal bandgap (refractive indexes 12 and 12) and at the right side with GaAs and air, where contrast is bigger (refr.indexes 13 and 1), the bandgap is also much larger. The images correspond to simulations' results. [14]

Besides the fact that fabricated photonic crystals are very unlikely to exhibit a sharp and perfect bandgap , different kinds of "defects" can be introduced just as doping is developed in semiconductors, as exemplified in figure 11

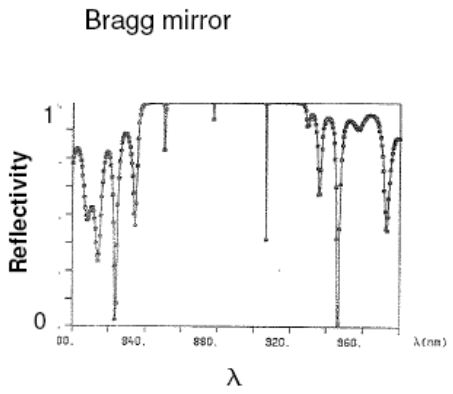

Fig. 11. Measured reflectivity of a Bragg mirror structure as a function of wavelength, where the distorting effect of "doping" in the bandgap can be seen.[15]

2D-EBGs

The most known case of a 2–dimensional EBG structure is a photonic waveguide, which can be simply produced by cutting out a channel in what could be called the bulk material. This bulk material could consist of small silicon pillars, as shown in figure 12, or other kind of material.

[14] Source: J.D.Joannopoulos, R.D.Meade, J.N.Winn, "Photonic Crystals: Molding the flow of light", Princeton University Press, 2nd edition, 2008, chapter 4, "The multilayer film"
[15] Source:Notes of the course "Optical properties of solids" 2010-2011 (K.U.Leuven), 4.Optics in dielectrics, Prof.G.Borghs

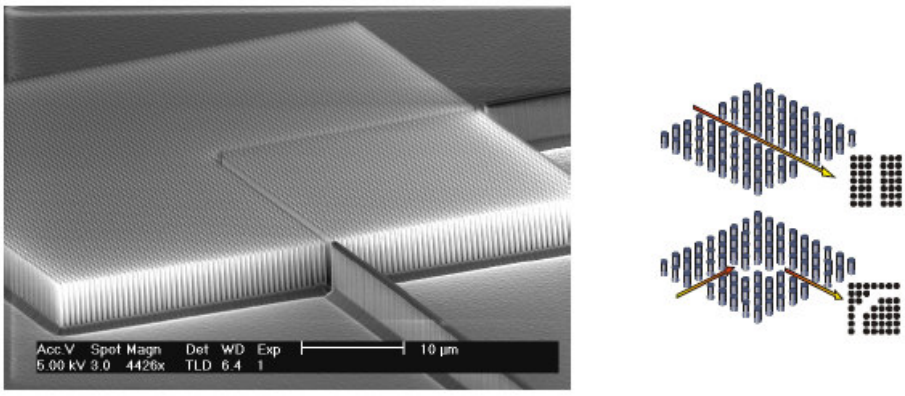

Fig. 12. Left: Microscope photograph of a photonic waveguide built by removing a row of rods in the two-dimensional array of rods. Right: schematic draw of of how rods can be removed to build waveguides.[16]

In figure 13 we can see an inversed example: a W1 waveguide which consists of a line of missing holes (a channel of one unit cell width).

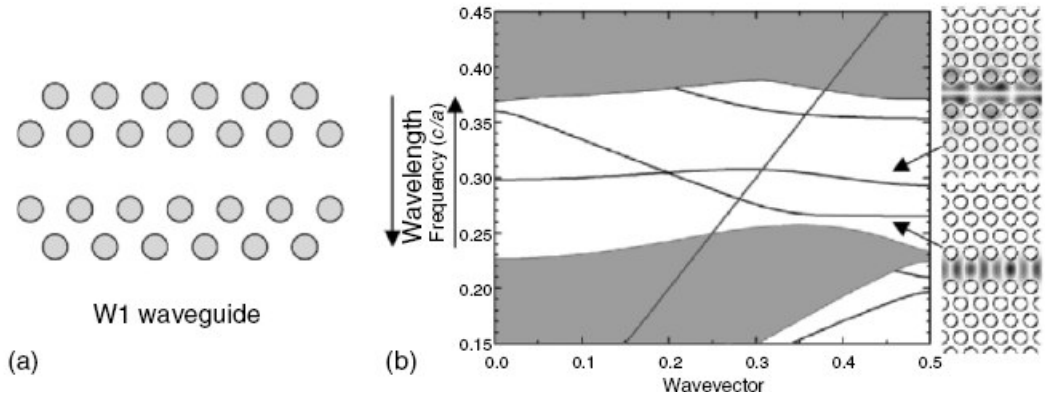

Fig. 13.a) Schematic draw of waveguide made of a row of missing holes. b) Resulting bandgap structure of a such a waveguide. [17]

Photonic waveguides can then be combined to conform more complex circuits.

3D-EBGs

The first three-dimensional EBG structure consisted in cylindrical holes drilled through a dielectric block, in a diamond- like lattice, the Yablonovite named after its discoverer Yablonovitch [5]. It has a full bandgap. A microscope photograph of a fabricated Yablonovite can be seen in figure 14.

[16] Source:Notes of the course "Optical properties of solids" 2010-2011 (K.U.Leuven), 4.Optics in dielectrics, Prof.G.Borghs

[17] Source: L.Pavesi, G.Guillot, "Optical Interconnects. The Silicon Approach ", Springer, Springer Series in Optical Sciences, Vol.119, 2006, chapter 9 "Photonic Crystal Microcircuits"

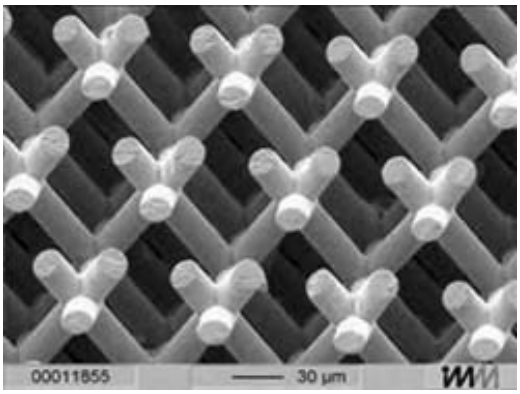

Fig. 14. Microscope view of an inverse Yablonovitch three-cylinder structure fabricated.[18]

The first woodpile structure designed in 1994 by Ho,. Chan, Soukoulis et. al., a layer-by-layer structure with a full three-dimensional bandgap at 12 to 14 GHz [21]. A photograph of a fabricated prototype to illustrate the structure can be seen in figure 15.

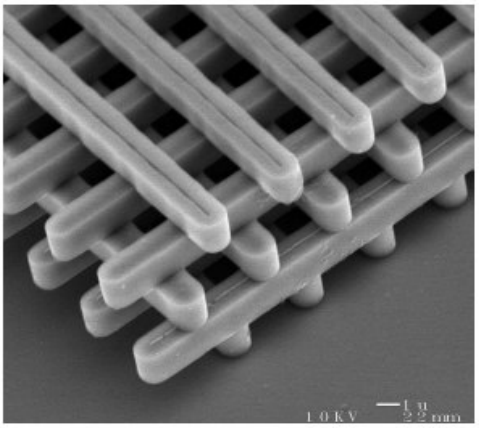

Fig. 15. Microscope view of a wood-pile structure fabricated [19]

Many other structures have been published after these, being those operating in the optical and infrared regime still the most difficult to realize.

In the antennas field EBG materials have already proved to find application in reducing the mutual coupling between arrays of patch antennas, attenuation of surface waves, enhancement of gain, creation of high-precision GPS antennas, are even promising in the use of wearable antennas, among many other applications.

1.4 Metamaterial and periodic absorbers

"Metamaterial absorbers try to take advantage of the lossy character that most metamaterials present due to their resonant behaviour. This behaviour also causes their spectral response to be often narrowband, which represents a drawback for electromagnetic absorbers, generally required to cover wider spectra. Since the first metamaterial absorber has been conceived

[18] Source: N. Engheta, Richard W. Ziolkowski, "Metamaterials: Physics and Engineering Explorations", IEEE Press, John Willey and Sons, Inc, 2006, chapter 8, section 8.1 "Introduction"
[19] Source: J.D.Joannopoulos, R.D.Meade, J.N.Winn, "Photonic Crystals: Molding the flow of light", Princeton University Press, 2nd edition, 2008, chapter 6, "The woodpile crystal"

[22]", also claimed to be a perfect absorber, "several others have been analyzed and built with different kinds of topologies and absorptions, that have gone up to 99.9%. Their level of complexity has also gone through a wide range, specially regarding the geometrical parameters of resonators, ranging from fairly simple to very complex [23]-[35]. The operational frequency spectrum has reached the optical range [36]-[40]. Also many efforts have been directed towards trying to make the absorption bandwidth of these materials broader, being one of the techniques applied the addition of multiple absorption peaks, adjacent in frequency."[20]

By using this technique also multiple-band narrowband absorbers or even filters could be produced, instead of aiming at a wideband absorber.

Regarding absorption bandwidth, it is typically more difficult to find topologies that can achieve a wide bandwidth by using a single resonator and not only multiple resonators or multiple layers are used to try to broaden the bandwidth, also embedded resistors, capacitors and even diodes, more frequently referred to as lumped elements. Using multiple layers can make the final structure much more bulky [26], using multiple resonators can also be disadvantageous for specific applications and the use of lumped elements can also make the structure more bulky, and thus less attractive for many applications and less advantageous with respect to most conventional absorbers [28]. For the first perfect metamaterial absorber reported [22] the measured bandwidth at FWHM (approximately 50% of absorption) was 8.7%, but the simulated result not more than 2.7% at -10 dB. In [36] three designs are presented using single-resonators each, being the highest bandwidth in the terahertz region 14.6% at FWHM, approximately 9.7% at -10 dB. [38] also in the terahertz region exhibits 13%, also at FWHM. In [39] a single gold rectangular patch is used for operation in the near-optical region, with a maximum 23.7% bandwidth measured at FWHM, 5% at -10 dB, whereas in [40] a single ELC resonator in gold in the terahertz region reports a maximum of 18.7% at FWHM again. Back in the microwave region, [27] uses a single-resonator with multiple resonances separated from each other in frequency, not more than 5 % is reached at FWHM and 2.5% at -10 dB. In [35] which also uses a single-resonator with double-resonance, bandwidth at FWHM is 11% as a result of the addition of both peaks, at -10 it is of around 1.5 % for each peak. [32] with several design in the microwave range, reaches nearly 10 % at -10 dB.

Going to structures that use multiple resonators, [30] uses multiple nested CRR resonators, but not more than 4.3% is reached at FWHM. In [25], where multiple combinations of several ELC resonators are used in a single-layer, not more than 5.4% is reached at FWHM as well. In [37] gold cross wires are used in the infrared region and three resonances added, with maximum 14 % of bandwidth at 80% of absorption, using a double-layer structure. In [65] which uses three layers of cross resonators in the terahertz range again, 38% bandwidth is reached at FWHM.

Designs using lumped elements can reach wider bandwidths, approximately 30% in [28], but again at FWHM and around 50% in [29] at FWHM.

[20] Source: Herrera C., Vandenbosch G.A.E., "Systematic study of double-layered ultra-thin stacked patch absorbers", Proc.EMC Europe 2013, (p.998), Brugge, Belgium, Sep.2013

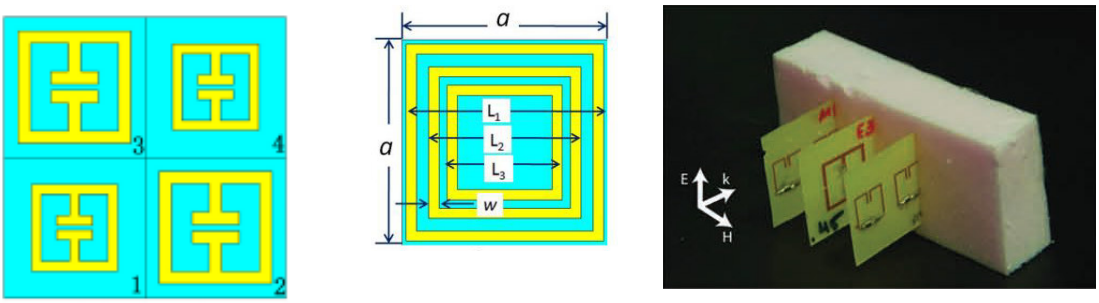

a) b) c)

Fig. 16. a) One of the co-planar designs with two different sizes of ELC resonators presented in [25] b) Nested CRR resonators in [30]. c) A unit of one ELC resonator sandwiched between two units of two SRR resonators, with embedded lumped resistors and capacitors, mechanically suppoted by a piece of foam in [28].

A simple example of a metamaterial absorber fabricated with copper in PCB is shown in figure 17. These designs actually produce two (figure 17a) and a single absorbing peak (17b) with a very narrow bandwidth, for which they should be actually denominated metamaterial filters. However the term absorber is more widely applied in metamaterials [27]. Figure 18 shows the schematic design of an absorber that uses crosses as metallic resonators, with three resonant modes [65]. Figure 19 shows a special absorber, with pyramidal shape made of 20 layers of copper and dielectric material that although not electrically small (5mm-thick, which is the height of the pyramids), it can yield a very broadband absorption of around 50% [26].

(a) (b)

Fig. 17. a) Metamaterial absorber design with double-resonant absorption.b) Metamaterial absorber design with single-resonant absorption.[21]

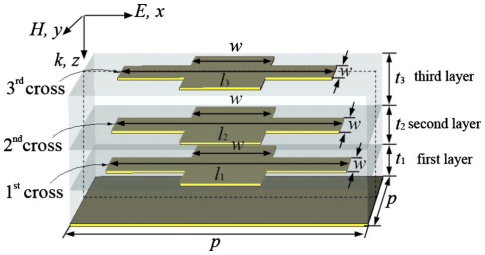

Fig. 18. Structure of 3-layer metamaterial absorber. [22]

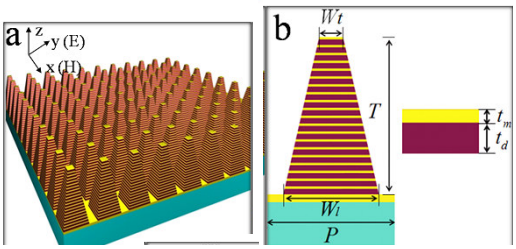

Fig. 19. a) Pyramidal metamaterial absorber built in [26]. b) a unit cell of the metamaterial absorber.[23]

This last kind of metamaterials has inspired our core research and has finally been part of our main research line, in addition to initial investigations in negative-refractive-index metamaterials. Nevertheless not only metamaterial absorbers but also materials with resonators periodically arranged as non-effective medium – sharing this characteristic with EBG materials and typically no longer defined as metamaterials- have constituted our

[21] Source: [27]
[22] Source: [65]
[23] Source: [26]

research, having both them in common the capacity to absorb electromagnetic radiation. Thus the focus was made on this particular application of the engineered materials, rather than distinguishing whether they could be considered effective medium or not. The same approach was taken for publications and references of the state of the art regarding absorbing materials: they are all periodically arranged structures, frequency selective surfaces or complex material, independently of whether they are effective medium or not.
More details on the working principle of periodically structured absorbers will be given in chapter 3.

1.5 Objectives

Our first main objective is to make a general research on an application of metamaterials, specifically metamaterial absorbers and periodically arranged structures as absorbing materials, though focusing on investigating the structures as materials and its properties. Secondly we particularly aim at the obtainment of designs that can provide a broad absorption bandwidth, with additionally as less extra resonators, layers and complementary elements as possible, in view of the increasing demand for more broadband and multi-band applications, for further miniaturization of electrical and electronic components and devices, tunable and flexible materials and devices, and the continuous expectations for new materials exhibiting multiple features and properties in a single structure –as has been the case of graphene-. Metamaterials and periodic structures, because of their typical resonant character, have intrinsically narrowband responses which is classically the opposite of what is required from an electromagnetic absorber. Therefore the effort for achieving wideband responses has classically been important and at the same time the narrowband nature of most metamaterial and periodic structures makes obtaining a genuine broadband behaviour difficult. Part of the difficulty is that an increase in bandwidth will also typically come at the expense of absorption level.
To acquire a better and deeper knowledge of metamaterials and periodic structures, together with further experience in its manufacturing and experimentation is at the end also an important goal.

1.6 Structure of this work

The thesis is structured as follows: in chapter 2 we present part of our initial research and first experimental experience with a metamaterial. Fundamental practical know-how and experience about the planning, design, manufacture and implementation of a metamaterial structure was acquired.
A very good example of a fully validated metamaterial-like structure is perhaps the most attractive fact presented in chapter 3. First a meticulous progressive analysis of a simple sub-wavelength absorbing structure and its corresponding results are displayed. Mainly links between variations in structural properties of the design and its absorbing performance are sought. Then a very thin filter-like metamaterial absorbing structure is manufactured, with accessible standard fabrication technologies, producing excellent experimental results that validate the two corresponding numerical analyses.
Chapter 4 proposes a very wideband design of a periodically arranged absorber, made of unit cells with a size in the order of its wavelength –that could therefore eventually be defined as electromagnetic bandgap material-and inspired in a structure previously used in antennas. Results are very interesting for the state of the art, specially considering that a single resonating shape is required to produce its broadband response.

The structure presented here shows the first real wideband absorbing response obtained in the doctoral research.
The widest absorption performance obtained with numerical calculations is presented in chapter 5. The original aim of the research that produced most of the results presented in this chapter was to further explore wideband topologies, specially pursuing advantages and enhancement with respect to previous designs' performances obtained. The ultimate aim of trying to improve the manufacturability of the design presented in chapter 4 was also kept in mind and finally achieved. Polarization and non-polarization insensitive designs are presented in this chapter.
Finally chapter 6 contains the core conclusions of the doctoral research, possible applications and future outlook for the field.
It is worth mentioning that from chapter 3 on, the analyses of the structures are performed focusing on a unit cell approach, specially for electromagnetic simulations. This is explained in more detail in the introductory section of chapter 3, 3.1.

1.7 References

[1] R. A. Shelby, D. R. Smith, S. Schultz, "Experimental verification of a negative index of refraction", Science, Vol. 292, p. 77, 2001

[2] V. G. Veselago, "The electrodynamics of substances with simultaneously negative values of ε and μ", Sov. Phys. Uspekhi. Vol.10, no.4, p.509, 1968

[3] J. B. Pendry, A. J. Holden, D. J. Robbins, W. J. Stewart, "Magnetism from Conductors and Enhanced Nonlinear Phenomena", IEEE Transactions on Microwave Theory and Techniques, Vol. 47, no. 11, p.2075, 1999.

[4] J.D.Joannopoulos, R.D.Meade, J.N.Winn, "Photonic Crystals: Molding the flow of light", Princeton University Press, 1995

[5] E. Yablonovitch, T. J. Gmitter, K. M. Leung, "Photonic band structure: The face-centered-cubic case employing nonspherical atoms," Phys. Rev. Lett., Vol. 67, no.17, p. 2295, 1991.

[6] N. I. Zheludev, E. Plum, V. A. Fedotov, "Metamaterial polarization spectral filter: Isolated transmission line at any prescribed wavelength" , Appl. Phys. Lett, Vol. 99, No. 171915, 2011

[7] D. R. Chowdhury,R.Singh,J. F. O'Hara,H. Chen, A. J. Taylor,A.K.Azad, "Dynamically reconfigurable terahertz metamaterial through photo-doped semiconductor",Appl.Phys.Lett, Vol. 99, No. 231101, 2011.

[8] W.M.Zhu,A.Q.Liu,X.M.Zhang,D.P.Tsai,T.Bourouina,J.H.Teng,et.al,,"Switchable magnetic metamaterials using micromachining processes", Advanced Materials, Vol.23, No.15, pp.1792-1796, 2011

[9] L.Yousefi,O.M.Ramahi, "Artificial Magnetic Materials Using Fractal Hilbert Curves", IEEE Transactions on Antennas and Propagation, Vol. 58, No. 8, 2010

[10] Z.L.Mei,J.Bai,T.M.Niu,T.J.Cui, "A Half Maxwell Fish-Eye lens antenna based on gradient-index metamaterials", IEEE Transactions on Antennas and Propagation, Vol.60, No.1, 2012

[11] D.Bao,W.Qin,J.Tong,X.M.Yang,Q.Cheng,T.J.Cui ,"Gradient index metamaterials based on dielectric disks", Proc. International workshop on Metamaterials 2008, (pp.394-396), Nanjing, China, Nov. 2008

[12] C.L.Holloway,P.Kabos,M.A.Mohamed,E.F.Kuester,J.A.Gordon,M.D.Janezic,J.Baker-Jarvis, "Realisation of a controllable metafile/metasurface composed of resonant magnetodielectric particles: measurements and theory", IET Microwaves, Antennas &Propagation, Vol.4, No.8, pp.1111-1112, 2010

[13] L.B.Wang,K.Y.See,J.W.Zhang,B.Salam,"Ultrathin and Flexible Screen-Printed Metasurfaces for EMI Shielding Applications", IEEE Transactions on Electromagnetic Compatibility, Vol.53, No.3, 2011

[14] S.Bashir,A.Chauraya,R.M.Edwards,J.Vardaxoglou, "A flexible fabric metasurface for on body communication applications", Proc. Loughborough Antennas & Propagation Conference 2009, (pp.725-728), Loughborough , UK, Nov.2009.

[15] Nikolay I. Zheludev, "A roadmap for metamaterials", OPN Optics & Photonics News, Vol.22, Issue 3, p.31, 2011

[16] D.L.Sounas, C.Caloz, "Graphene-Based Non-Reciprocal Metasurface", Proc. 5th European Conference on Antennas and Propagation EuCAP, (pp. 2419-2422), Rome, Italy, Apr.2011

[17] A. Vora, J. Gwamuri, N. Pala, A. Kulkarni, J.M. Pearce, D. Ö. Güney, "Exchanging ohmic losses in metamaterial absorbers with useful optical absorption for photovoltaics," Sci. Rep. Vol. 4, No. 4901, 2014.

[18] M. Brun, S. Guenneau, A. B. Movchan,"Achieving control of in-plane elastic waves", Appl. Phys. Lett. , Vol.94, No.6, p.061903, 2009.

[19] Y.Dong, T.Itoh, "Miniaturized patch antennas loaded with Complementary Split-Ring Resonators and Reactive Impedance Surface", Proc. 5th European Conference on Antennas and Propagation EuCAP, (pp. 2415-2418), Rome, Italy, Apr.2011

[20] J. B. Pendry, A. J. Holden and W. J. Stewart, I. Youngs, "Extremely Low Frequency Plasmons in Metallic Mesostructures", Phys. Rev. Lett., Vol.76, no.25 , p.4773 , 1996

[21] E. Ozbay, A. Abeyta, G. Tuttle, M. C. Tringides, R. Biswas, M. Sigalas, C. M. Soukoulis, C. T. Chan, and K. M. Ho, “Measurement of a three-dimensional photonic band gap in a crystal structure made of dielectric rods,” Phys. Rev. B, Vol. 50,pp. 1945–1948, July 1994.

[22] N.I.Landy, S.Sajuyigbe, J.JMock, D.R.Smith, W.J.Padilla, "Perfect metamaterial absorber", Physical Review Letters, Vol.100, No.207402

[23] Sun, Liu, Dong, Zhou, “An extremely broad band metamaterial absorber based on destructive interference”, Optics Express,Vol.19 , No.22, 21155,2011

[24] Mias, Yap, "A varactor-tunable high impedance surface with a resistive-lumped-element biasing grid", IEEE Transaction on Antennas and Propagation, Vol.55, No.7,2007

[25] Li, Yuan, Zhou et.al, "Ultrathin multiband gigahertz metamaterial absorbers",Journal of Applied Physics Vol.110, No.014909,2011

[26] Ding, Cui, Ge, Jin, He, "Ultra-broadband microwave metamaterial absorber", Applied Physics Letters, Vol.100, No.103506,2012

[27] Li, Yang, Liang, "A wide -angle polarization-insensitive ultra-thin metamaterial absorber with three resonant modes ", Journal of Applied Physics,Vol.110, No.063702,2011

[28] Gu, Barrett, Hand, Popa, Cummer, "A broadband low-reflection metamaterial absorber", Journal of Applied Physics700MHzol.108, 064913,2010

[29] Cheng, Wang, Nie, Gong, Xioing, Wang, "Design fabrication and measurement of a broadband polarization-insensitive metamaterial absorber based on lumped elements", Journal of Applied Physics, Vol.111 , No.044902,2012

[30] Shen, Cui, Zhao, Ma, Jiang, Li, "Polarization-independent wide-angle triple-band metamaterial absorber", Optics Express, Vol.19, No.10,2011

[31] Xu, Zhou, Zhang, Chen, Deng, "A wide-angle planar metamaterial absorber based on split ring resonator coupling", Journal of Applied Physics, Vol.110, No.044102,2011

[32] Alici, Bilotti, Vegni, Ozbay, “Experimental verification of metamaterial based subwavelength microwave absorbers”, Journal of Applied Physics, Vol.108, No.083113,2010

[33] Costa, Monorchio, Manara , “Analysis and Design of Ultra Thin Electromagnetic Absorbers Comprising Resistively Loaded High Impedance Surfaces”, IEEE Transactions on Antennas and Propagation, Vol.58, No.5,2010

[34] Pang, Zhou, Wang, “Equivalent circuit method analysis of the influence of frequency selective surface resistance on the frequency response of metamaterial absorbers” , Journal of Applied Physics, Vol.110, No.023704,2011

[35] Lee,Lim,"Bandwidth-enhanced and polarization-insensitive metamaterial absorber using double resonance", Electronic Letters, Vol.47, No. 1,2011

[36] Alves, Kearney, Grbovic, Lavrik, Karunasiri; “Strong terahertz absorption using SiO2/Al based metamaterial structures”; Applied Physics Letters,Vol.110, No.111104,2012

[37] Chen, Cheng, Yang, Li, Duan, Gu,Tian; "Polarization insensitive and omnidirectional broadband near perfect planar metamaterial absorber in the near infrared regime"; Applied Physics Letters; Vol.99; No.253104,2011

[38] Landy, Bingham, Tyler, Jokerst, Smith, Padilla; “Design, theory and measurement of a polarization-insensitive absorber for terahertz imaging”;Physical Review B ,Vol.79, No.125104,2009

[39] Hao, Wang, Liu, Padilla, Zhou, Qiu; “High performance optical absorber based on a plasmonic metamaterial”; Applied Physics Letters, vol.96, No.251104,2010

[40] Tao, Bingham, Strikwerda et.al; “Highly flexible wide angle of incidence terahertz metamaterial absorber: Design, fabrication, and characterization”;Physical Review B, Vol.78, No.241103,2008

[41] C.M.Watts, X.Liu, W.J.Padilla, “Metamaterial Electromagnetic Wave Absorbers”, Advanced Materials, Vol.24, No.23, pp.98-120, 2012.

[42] D. R. Smith,J. B. Pendry, M. C. K. Wiltshire, “Metamaterials and Negative Refractive Index”, Science, Vol.305, p.788, 2004

[43] N. Engheta, Richard W. Ziolkowski, “Metamaterials: Physics and Engineering Explorations”, IEEE Press, John Willey and Sons, Inc, 2006

[44] R. A. Shelby, D. R. Smith, S. C. Nemat-Nasser, S. Schultz, “Microwave transmission through a two-dimensional, isotropic, left-handed metamaterial”, Appl. Phys. Lett., Vol. 78, no. 4, p.489, 2001.

[45] D. R. Smith, Willie J. Padilla, D. C. Vier, S. C. Nemat-Nasser, S. Schultz, “Composite Medium with Simultaneously Negative Permeability and Permittivity”, Phys. Rev. Lett., Vol.84, no.18 , p.4184, 2000.

[46] D.R.Smith, P.Rye, D.C.Vier, A.F.Starr, J.J.Mock, T.Perram, “Design and measurement of anisotropic metamaterials that exhibit negative refraction”, IEICE Trans. Electron., vol.E87-C, no.3, 2004.

[47] Andrew A. Houck, Jeffrey B. Brock, Isaac L. Chuang, “Experimental Observations of a Left-Handed Material That Obeys Snell’s Law”, Phys.Rev. Letters, vol.90, no.13, 137401, 2003.

[48] L. Ran, X. Zhang, K.Chen, T. M. Grzegorczyk, J. Au Kong, “Left-handed metamaterial and its experimental verifications”, Chinese Science Bulletin, vol. 48, no.13, p. 1325, 2003.

[49] C.G. Parazzoli, R. B. Greegor, K. Li, B. E.C. Koltenbah, M. Tanielian , “Experimental Verification and Simulation of Negative Index of Refraction Using Snell’s Law”, Phys.Rev. Letters, vol.90, no.10, 107401, 2003.

[50] Kin Li, S. J. McLean, R. B. Greegor, C. G. Parazzoli, M. H. Tanielian, “Free-space focused-beam characterization of left-handed materials”, Appl. Phys. Lett., vol.82, no.15, p.2535, 2003.

[51] R. W. Ziolkowski, “Design, fabrication, and testing of double negative metamaterials”, IEEE Trans. Antennas Propag., vol. 51, no.7, p.1516, 2003.

[52] J. Huangfu, L. Ran, H. Chen, X. Zhang, K. Chen, T. M. Grzegorczyk, J. A. Kong, "Experimental confirmation of negative refractive index of a metamaterial composed of omega-like metallic patterns", Appl. Phys. Lett., vol.84, no.9, p.1537, 2004.

[53] A. F. Starr, P. M. Rye, D. R. Smith, S. Nemat-Nasser, "Fabrication and characterization of a negative-refractive-index composite metamaterial", Phys. Rev. B, vol. 70, 113102, 2004.

[54] H. Chen, L. Ran, J. Huangfu, X. Zhang, K. Chen, T. M. Grzegorczyk, J. A.Kong, "Metamaterial exhibiting left-handed properties over multiple frequency bands", J. Appl. Phys., vol. 96, no. 9, p. 5338, 2004.

[55] H. Chen, L. Ran, J. Huangfu, X. Zhang, K. Chen, T. M. Grzegorczyk, J. A. Kong, "Left-handed materials composed of only S-shaped resonators", Phys. Rev. E, vol. 70, 057605, 2004.

[56] K.Aydin, K. Guven, C. M. Soukoulis, E. Ozbay, "Observation of negative refraction and negative phase velocity in left-handed metamaterials", Appl. Phys. Lett., vol. 86, 124102, 2005.

[57] S. Zhang, W. Fan, N. C. Panoiu, K. J. Malloy, R. M. Osgood, S. R. J. Brueck, "Experimental demonstration of near-infrared negative-index metamaterials", Phys. Rev. Lett. , vol.95, 137404, 2005.

[58] J. Zhou, T. Koschny, L. Zhang, G. Tuttle, C. M. Soukoulis, "Experimental demonstration of negative index of refraction", Appl. Phys. Lett., vol. 88, 221103, 2006.

[59] K.Guven, M. D. Caliskan, E.Ozbay, "Experimental observation of left-handed transmission in a bilayer metamaterial under normal-to-plane propagation", Optics Express, vol.14, no. 19, p. 8685, 2006.

[60] K.Aydin, I.Bulu, E.Ozbay, "Subwavelength resolution with a negative-index metamaterial superlens", Appl. Phys. Lett., vol. 90, 254102, 2007.

[61] R. Liu, A. Degiron, J. J. Mock, D. R. Smith, "Negative index material composed of electric and magnetic resonators", Appl. Phys. Lett.,vol. 90, 263504 , 2007.

[62] J. Zhang, H. Chen, L. Ran, Y. Luo, B-I. Wu, J. A. Kong, "Experimental characterization and cell interactions of a two-dimensional isotropic left-handed metamaterial", vol. 92, 084108, 2008.

[63] F. Zhang, D. P. Gaillot, C. Croënne, E. Lheurette, X. Mélique, D. Lippens, "Low-loss left-handed metamaterials at millimeter waves", Appl. Phys. Lett., vol. 93, 083104, 2008.

[64] W. Zhu , X. Zhaoa, "Adjusting the resonant frequency and loss of dendritic left-handed metamaterials with fractal dimension", Journal of Appl. Phys., vol.106, 093511, 2009

[65] Yu Qian Ye, Jin, and He, "Omnidirectional, polarization-insensitive and broadband thin absorber in the terahertz regime",Journal of the Optical Society of America B, Vol. 27, Issue 3, 498-504, 2010.

[66] G.V. Eleftheriades, K.G. Balmain, "Negative-Refraction Metamaterials, Fundamental Principles and Applications ", IEEE Press, John Wiley & Sons, Inc, 2005

[67] Ben A.Munk, "Metamaterials: Critique and Alternatives", John Wiley & Sons, Inc 2009

[68] I. V. Lindell, S. A. Tretyakov, K. I. Nikoskinen, S. Ilvonen, "BW Media-Media with negative parameters, capable of supporting backward waves", Microwave and Optical Technology Letters, Vol. 31, No. 2, p.129, 2001.

2 Building a first piece of metamaterial and analyzing NRI materials

2.1 Introduction

Different kinds of materials that could be classified as metamaterials have been studied and developed over the past nearly ten years, after a group of researchers at the University of California (2001) managed to build the first metamaterial made up of resonant structures (metal split-ring resonators and wires) [1]. To the best of our knowledge this should also be the first Negative-Refractive-Index (NRI) metamaterial ever built.
Left-handed metamaterials (LHM), Negative-Refractive-Index metamaterials (NRI) or Double-Negative materials (DNG) were the first and technologically most simple kind of metamaterials to be proposed and built. Over the years they have usually been designed and fabricated in a way that enabled the effective medium theory to be applied to them and therefore they could be regarded as an effective medium with effective parameters. This common characteristic allows the properties of left-handed media to be expressed more conveniently, further easing analysis and calculations, but imposing the condition on their inclusions and the spacing between them to be sub-wavelength. This means that the unit cells that compose the typically periodic structure have to be considerably smaller than the operational wavelength, which should correspond to the resonant frequency of the structure.
DNG materials are, in brief, all those that have simultaneously a negative permittivity and a negative permeability. Materials with these electric characteristics have so far not been found in nature, to the best of our knowledge, and can therefore only be artificial. As mentioned in the Introduction, chapter 1, Veselago [26] is widely assumed to have been the first scientist to propose the negative refractive index of a DNG material, if found. To briefly expose his postulate: he took the dispersion equation for a monochromatic wave

$$\left| \frac{\omega^2}{c^2} \varepsilon_{il} \mu_{lj} - k^2 \delta_{ij} + k_i k_j \right| = 0 \qquad (1)$$

(with ω being the angular frequency, k the wave number or wave vector, ε the electric permittivity, μ magnetic permeability, c the speed of light in vacuum and δ the skin depth, as usual) . He assumed that the wave was propagating in an isotropic medium obtaining (2)

$$k^2 = \frac{\omega^2}{c^2} n^2 \qquad (2)$$

with $n^2 = \varepsilon\mu$. Then he supposed negligible losses so that permittivity and permeability were real, thus $\varepsilon=\varepsilon_r$ and $\mu=\mu_r$ being ε_r and μ_r real values, and then the refractive index n can be written $n=\pm\sqrt{\mu_r\varepsilon_r}$. As ε_r and μ_r were supposed to be negative, the negative sign has to be chosen for the square root, giving a negative refractive index n.
Physically a negative refractive index would fundamentally imply that normal incident waves would be refracted with a “negative” angle, that is, they would be refracted on the same side as the incident ray with respect to the normal of the interface, as depicted in figure 1. Here the dotted line is the normal of the interface between two media, medium 2 where the refracted waves propagate is characterized in grey and the black line indicates the trajectory of the incident wave in medium 1. The green line then corresponds to the refracted beam in a medium with a positive index of refraction, the red line corresponds to the refracted beam in a medium with a negative index of refraction.

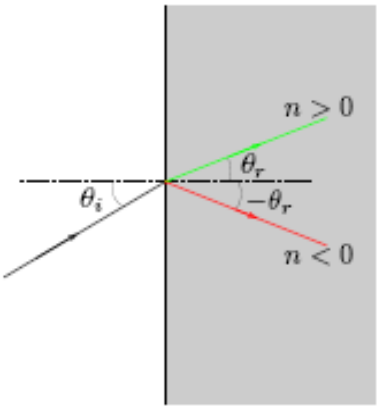

Fig. 1. Schematich draw of how waves with normal incidence would refract in normal (green) and NRI media (red). The angle of incidence is indicate with the suffix "i", angle of refraction is indicated with suffix "r".

Among other consequences, the negative refraction could lead in theory to invisibility [29], if realized in the optical range.

Since [1] further NRI topologies have been published, generally more complex [4]-[25] and typically relying in the resonant characteristics of metallic patterns, fabricated on top of standard PCB material when the operational frequency range is the microwave range. Not all of them have been fabricated and for fewer of them experiments in order to really directly demonstrate negative refractive behaviour have been carried out. Above all in the early years, getting closer to the creation of an invisibility cloak was a strong motivation, and some have claimed to have achieved a good approximation in the microwave frequency, as [27] claimed in 2010.

In this chapter we expose the processes of partial design, full numerical analysis, set-up and sample fabrication and measurement of a NRI metamaterial in order to try to replicate an experiment already carried out and observe which results are obtained. Our ultimate aim as later exposed in this chapter, is to study the behaviour of a negative-refractive index metamaterial. These kind of metamaterials do not require extremely complex technologies to be built -as previously mentioned-, as opposite to others where nanotechnology is required, and also comparably few of them have really been realized and tested, which together with criticism about the feasibility of this kind of materials makes experimentation with them more challenging and interesting. The simpler and less costly manufacturing process was what mainly motivated the election of negative-refractive index materials above others for a first experiment.
Besides this the topology to be tested had to meet certain criteria in order to ensure that the experiment was developed within the scope and reach of the PhD: among the relative simplicity of negative-refractive index metamaterials, a topology with a relatively simple building process was the target, with dimensions that did not approach nano-scale sizes neither were too large to handle, covering an operational frequency range within the scope of the available measurement equipment (not less than 5GHz, not more than 100GHz), if possible requiring relatively standard equipment, and being a known, not scarcely studied structure so as to avoid technical complexities beyond the scope of a first experiment as much as possible. In order to look for a known topology with the mentioned characteristics a selection process was carried out among the ones that had already been built in the literature ([4]-[25], [28]), giving as result the first negative-refractive-index metamaterial been built: [1]. The paper showed that a sample of material with the characteristics of a so-called

negative-refractive-index (NRI) or left-handed metamaterial (LHM) "negatively refracted" a beam of microwaves under the conditions set for the experiment. Although the topology had been built before, an intense design process had to be carried out and the preparation of the experiment involved not only a brief planning but also the acquisition of the elements to build the metamaterial and to perform the experimental measurements. This was done not only as part of a learning process but also because the information given in the publication regarding sample's building process and experimental setup was not complete.

According to this also a brief, initial budget calculation had to be made, based mainly on the necessary elements to manufacture the metamaterial and the setup for the commissioning of the experiment. Even after deciding to manufacture the metamaterial sample locally at CDE (ESAT's prototyping workshop) the investigation of prices and material availability was still necessary, as most decisions were finally not to be made exclusively by CDE. Part of this process -which took several weeks- is described in section 2:

Item	**Cost (Max)**
4 aluminum plates (2 circular + 2 rectangular) for the experiment's setup	(Max) 7euro
0.4mm-thick FR4 material	21 euro
0.2mm-thick FR4 material	150 euro
milling process (12hsx2)	72 euro
used mills (1 or 2pcs)	44 euro
Total max. cost for 0.4mm-thick FR4	**144 euro**
Total max. cost for 0.2mm-thick FR4	**273 euro**

Table 1-Initial calculation of costs

Similarly, in section 3 the necessary design and fabrication process of the experimental set-up are described. Together with the process of building and testing the real metamaterial sample, a simulation was carried out with one of the electromagnetic solvers available in our research group. In section 4 the experiment's simulation, numerical analysis and necessary adjustments are exposed. Between the two available solvers, MAGMAS and CST, this last one was chosen mainly because the sample has a certain volume (its height is not negligible) and at the time the decision had to be made MAGMAS was not yet able to solve problems implying calculations over volumes. Carrying out the simulation also implied a learning process on the use and limitations of the solver, particularly in handling with materials showing negative electromagnetic parameters, limitations that finally proved to be quite high. It has to be taken into account that it was the first time in our group that a model of a material with these characteristics was used in CST.
The whole wedge-shaped piece of metamaterial was simulated as a bulk material with permittivity and permeability each defined by a separated function. This is different from the typical unit cell approach taken in publications. The aim was to simulate the behaviour of the material as a piece and observe whether it could refract incoming waves with a negative angle.
In section 5 the measurements results are presented, together with the necessary previous considerations. Section 6 contains this experiment's conclusions.

2.2 Design process for the sample's fabrication

A wedge-shaped sample of material, approaching a right-angled triangle form had to be built by assembling strips of circuit board material printed with specific copper patterns, designed to make the structure resonate in a determined frequency. The orthogonal assembly of the strips would conform a final piece of material periodically arranged in anisotropic unit cells that aims to have all the characteristics of the negative-refractive index material envisioned in the first metamaterial publications:

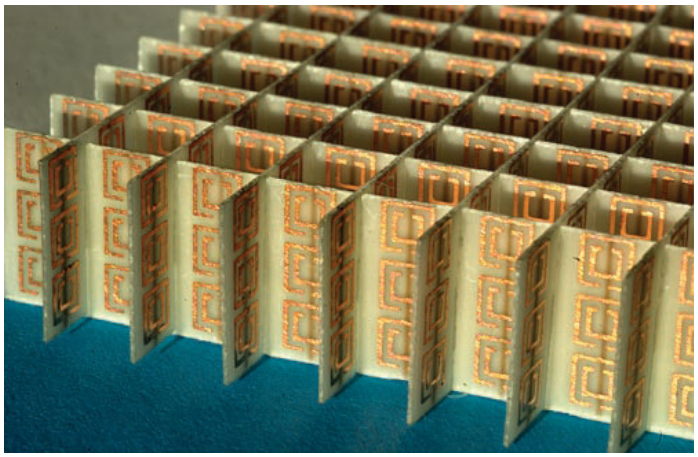

Fig. 2. View of the first NRI-metamaterial with its patterns lithographically printed[24]

The patterns were split-ring-resonators (SRR) on one side of the strip and wires on the other, this last ones centered in the gap of the SRRs. On the side of the SRRs three of them had to be printed equally spaced by 0.535 mm along the unit cell height.

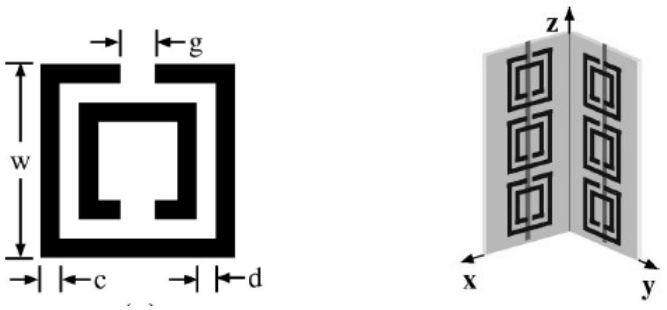

a) b)

Fig. 3. a) Diagram of an SRR b) Diagram of a unit cell, with 90° between x and y axes[25]

[24] Source:D. R. Smith, J. B. Pendry, M. C. K. Wiltshire; "Metamaterials and Negative Refractive Index"; Science, Vol. 305, p.788, Aug. 2004.

[25] [4] is the source of both figures: R. A. Shelby, D. R. Smith, S. C. Nemat-Nasser, S. Schultz, "Microwave transmission through a two-dimensional, isotropic, left-handed metamaterial", Appl. Phys. Lett., Vol. 78, no. 4, p.489, 2001.

Parameter	Value
g (SRR's gap)	0.46 mm
w (outer SRR height)	2.62 mm
d (ring spacing)	0.30 mm
wire length (unit cell height)	10 mm
c (track width, also for wires)	0.25 mm
copper thickness (preferably)	0.03 mm
unit cell width (lattice constant)	5 mm

Table 2-Copper patterns' dimensions

The form and sizes of these patterns are a result of the research and calculations performed by J.Pendry in the first theoretical studies made about negative-refractive-index materials ([2] and [3]) and the ones performed in the papers immediately preceding the one published by Shelby, Smith and Schultz ([4] and [5]). The dimensions of the patterns presented above were mentioned in these last publications and are meant to conform a material topology with its resonant frequency at 10.5GHz. Also according to these dimensions the sample is predicted to follow a behaviour approximately described by the dispersion equations (3) and (4)[26]:

$$\frac{\mu(\omega)}{\mu_0} = 1 - \frac{\omega_{mp}^2 - \omega_{mo}^2}{\omega^2 - \omega_{mo}^2 + i\gamma\omega} \quad (3) \qquad \frac{\varepsilon(\omega)}{\varepsilon_0} = 1 - \frac{\omega_{ep}^2 - \omega_{eo}^2}{\omega^2 - \omega_{eo}^2 + i\gamma\omega} \quad (4)$$

and to behave as an effective medium, since the unit cells' size was chosen to be relatively small compared to the wavelength size of the X-band (operational frequency region) center frequency. A reference to the X-band will be made later in this text.

The exact dimensions of the sample were not mentioned in the reference paper, but could be approximately deduced from subsequent publications and especially a paper published later by Smith [6]. Also with this information and the patterns' values given above, an arrangement of strips' and unit cell's quantities that was very close to the one used in the reference paper could be formulated: The wedge should be 5cm long in the propagation direction, 12.5cm long in the perpendicular direction and 1 cm high. Consequently and according to the unit cells' parameters, the structure should then have a periodicity of 10 unit cells in the direction of propagation and of 25 unit cells in the perpendicular direction.

9 strips of different lengths transversally assembled shaped the structure along the propagation direction and another 24 of different lengths did it in the other direction. All strips of circuit board were 1 cm wide in order to achieve the 1cm-high structure:

- 3 strips of 50 mm, 3 of 45 mm, 3 of 40, 3 of 35, 3 of 30, 3 of 25, 3 of 20 and 3 of 15
- 2 strips of 125 mm, 1 strip of 105 mm, 1 of 90, 1 of 75, 1 of 60, 1 of 45, 1 of 30, 1 of 15

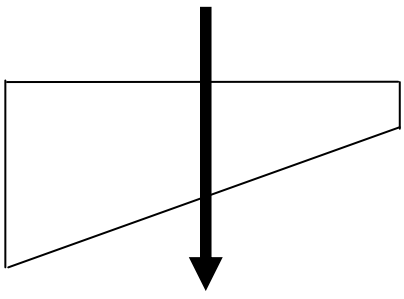

Fig. 4. Sample's sketch indicating the propagation direction of microwaves

[26] For Engineering notation, "i" (imaginary number) should be replaced by "j".

It was important to find out practically already in the design phase how to assemble the strips in order to achieve the sample's form showed in the publications, as it could have an influence in the design of the strips. In [6] was mentioned and showed that slots were half-cut into the strips in order to later interlock them orthogonally, and that was the approach finally chosen as it was apparently the most straightforward way to build the topology.

As it was mentioned before, the fabrication technique chosen in the reference paper to manufacture the topology was simple circuit board printing (shadow mask/etching technique), so the most efficient way to fabricate the sample for the purposes of the course seemed to be ordering the design of the PCBs at ESAT's central service for electronics, CDE. This implied making the designs with one of the software tools CDE uses and using the service to manufacture an unfamiliar kind of material for which these services have never been used before. This fact was presumably the main cause for designs and material having to be redone a number of times; at some point of the fabrication process the idea of outsourcing part or all the process was considered. Given that there was a certain familiarity with CST and this software was also going to be used as an electromagnetic solver, it was decided to use this tool to design the boards. Anyway the first Gerber designs issued with this tool posed several problems for CDE, among others being them different from what CDE was used to see at PCB design, and the designs had to be redone. The basic design with 10 unit cells is depicted in figure 5:

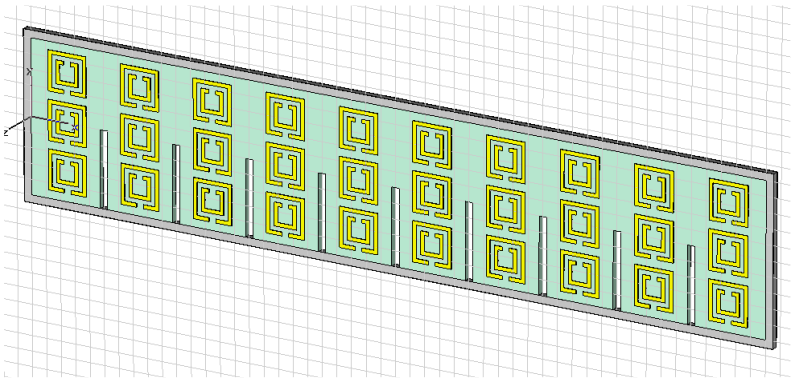

Fig. 5. SRR's side view of 10-unit-cell strip design

The circuit board material used in the reference paper was 0.25mm-thick G10 fiber-glass, the most affordable available option was standard FR4, also used in [8]. 0.4mm- and 0.8mm-thick FR4 were the most easily acquirable materials for CDE (a few days of delivery time), 0.25-mm thick FR4 had never been purchased before and only 0.2mm-thick FR4 could be acquired within a delivery time at first estimated of weeks. Finally this thickness turned out to be available at only one provider with a very variable delivery time -from weeks to months- dependable on the material's demand from other clients. In addition to this they required the purchase of at least one plate of 1.22m x 2m to make the delivery, which was for our experiment an excessive amount of material, being its cost 150 euros. Although this cost was already high compared to the estimated 21 euros for 0.4mm-thick FR4 material, the main issue was the delivery's uncertainty. Also taking into account that the metamaterial's periodicity was meant to be 5 mm, relatively large compared to the 0.4mm-thickness, and that even 0.5mm-thick FR4 had been used in a past experiment with a metamaterial's periodicity of 6 mm [7], it was finally decided to use 0.4mm-thick FR4.

There was also a choice to be made regarding the printing technique of the boards, the decision was mainly left to CDE taking into consideration its experience in board printing. The method chosen, although faster, less expensive and less risky -as it should minimize the probabilities of damaging the circuit board material- had as a major drawback a low repeatability: at some point of the PCB manufacturing process a spraying technique done through an automatic procedure was performed, which caused patterns to be not uniformly printed. Thus it was necessary to repeat the process several times and try different workarounds, and in the end the best shaped boards were chosen to be made strips. Anyhow the definition of the patterns (SRRs and wires) was not perfect in every one of them.
The order in which the different steps were performed during the whole circuit board printing and cutting process could not be arbitrary, especially concerning the cutting process of slots, so it was a real challenge for CDE to see how and at which points of the process the slots had to be made. Also the decision of which tools and method to use had to be taken. Although more expensive and risky, the milling technique was chosen as it was the most accurate option and a quite high level of precision and uniformity was required in order to achieve an assembly that made the sample be shaped as periodical as possible. The mill's process of purchase was similar to the circuit board material purchase process: not all mill's sizes are easy to acquire and also the most suitable size had to be chosen. Sizes in mills determine the width of the slot cut into the PCB strips, so they have to be at least as wide as the PCBs' thickness to make the orthogonal interlocking possible.1mm-mills were more "standard" and easy to acquire, but were certainly going to make the strip's assembly too poor and loose. 0.5mm- and more specifically 0.4mm-mills were more difficult to obtain but would achieve a finer adjustment, anyway 0.4mm-mills could be too tight or the 0.5mm-mill too loose. At the end samples of both mills were acquired and a few strips were tested with both mill-sizes. It was decided to use 0.4mm-mills, which could be too tight and make the building process of the sample too difficult at those points of the process when many strips were involved, but would make the sample mechanically more stable. A specification of the slot's width was not found in the papers read.

Finally, the assembly process of the finished strips was not trivial: the mechanism was quite simple but it was mechanically very difficult to interlock all the strips together orthogonally and at the same time, mainly due to the adjusted dimensions of the slots. Again it was important to try to keep the sample as uniform as possible to achieve a relatively high level of periodicity and the desired characteristics of an effective medium.

The finished sample used in the experiments is shown in figure 6:

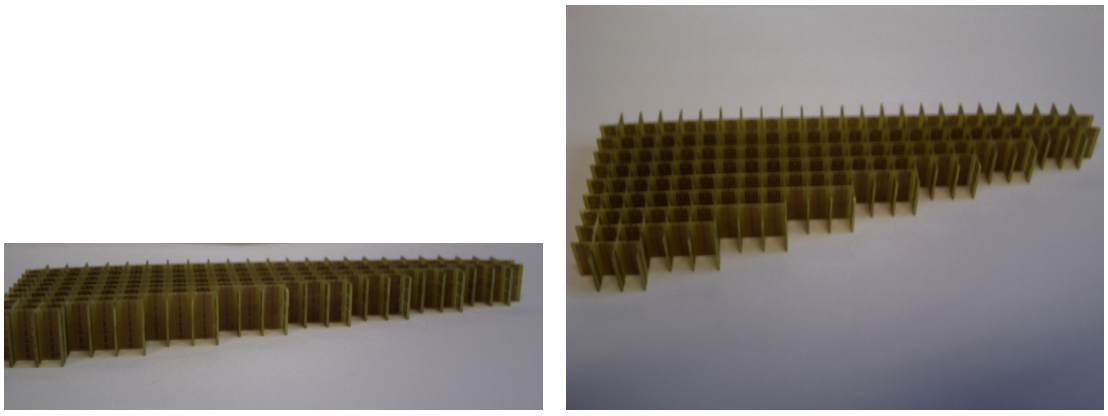

Fig. 6. Photographs of the finished sample, first one is an almost front view of the refraction surface.

2.3 Experimental setup

The primary objective of the experiment carried out by Shelby Smith and Schultz in 2001 was to find out whether a piece of negative-refractive index metamaterial could indeed refract normal incident waves with a negative angle. In order to do so they implemented a setup consisting of two circular aluminum plates that were placed on top and bottom of the metamaterial sample, followed by two rectangular ones, with microwave absorber placed on the sides and in between the aluminum plates, as shown in figure 7.

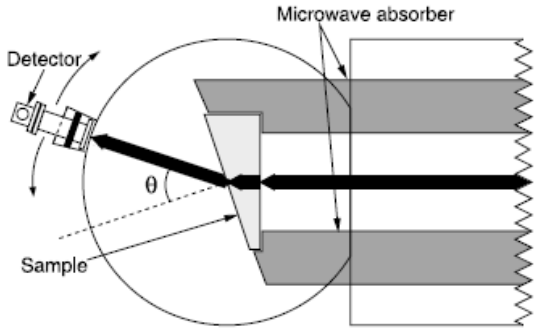

Fig. 7. [27]Schematic representation of the reference paper's experimental setup

This was presumably meant to accomplish a closed, waveguide environment, with the aim to shield the sample from possible external perturbations and, as indicated by other researchers within the same field, also the boundary conditions of such a setup would allow the sample to remain small and yet seem to have an infinite extension relative to the microwaves beam.
According to the reference paper, the microwaves's source would be placed 1m distant from the sample, so the rectangular plates should be approximately 1m-long. This is meant to allow the wave-front to flatten out in order to have waves as close as possible to plane waves. However the distance did not have to be necessarily 1m or more, subsequent repetitions of the experiment found out that a distance of 40cm was enough, but it was advisable that the waves' source was not be very close to the sample for the reason just mentioned before. From the information given on the reference paper it could be deduced that the rectangular plates used were 30 cm wide, as well as the circular plates' diameter, and the absorbers on the sides were placed 9.3 cm apart. Around the circumference of the circular plates a detector was rotated in order to measure the power transmitted through the sample in 1.5° steps. It is mentioned that the top circular plate has a pivot in the center around which the detector can be rotated, but the mechanism by which it is attached to the rest of the setup and can be accurately rotated is not described.
Diverse variations of this setup were implemented in subsequent related papers, but the main purpose of the configuration was always to conform an environment where waves were as close as possible to a clear beam and could be impinged in the sample without adding much noise from the outside environment.
In addition to the detector attached to a standard X-band waveguide the equipment used and mentioned in the reference paper was an HP8756A scalar network analyzer and a coaxial cable to waveguide adapter, this last one to introduce the microwaves in the aluminum plates-absorbers channel. In publications reproducing similar experiments the HP X281A adapter was mentioned and as detector HP11664A was mentioned.

[27] Source: R. A. Shelby, D. R. Smith, S. Schultz; "Experimental verification of a negative index of refraction"; Science, Vol. 292, p. 77, 2001

Complying with the dimensions of the sample and sample's unit cells the frequency range of the waves impinged in the sample would be the X-band (8-12GHz as defined by IEEE) in the microwave region, thus the source (sweep oscillator) and detection equipment should be used accordingly.

First the four aluminum plates were fabricated locally at CMW, they had to be modified later because no proper way was found to connect the circular and rectangular plates in a way that did not distort the traveling waves inside the channel. The final length of the effective linear channel was about 85cm.

Fig. 8. Photograph of the setup completely assembled, without the sample inside

The fabrication of a metal piece was also necessary to avoid unwanted radiation at the entrance of the channel, this is mainly, to avoid electromagnetic waves' "leakage" from the source waveguide adapter to the plates-absorbers channel. Thus, as the piece was going to constitute a connection between the adapter and the two aluminum plates it also had to ensure electrical contact between these elements. In figures 9 and 10 the piece's design finally used in the setup is presented:

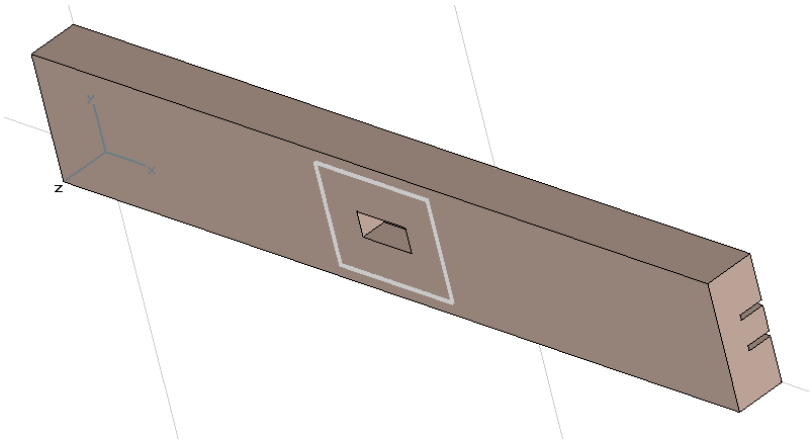

Fig. 9. Design of the metal piece connected between adapter and plates, view from the adapter's side

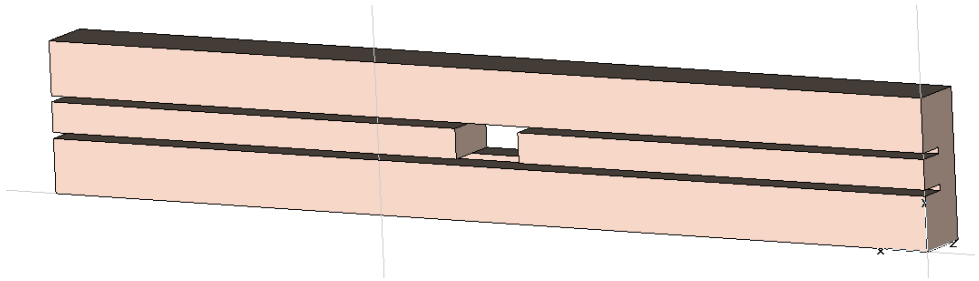

Fig. 10.Design of the metal piece, view from the plates' side

In figure 11 the plates can be seen couloured in grey and included in the design, so that the place to be introduced can be seen:

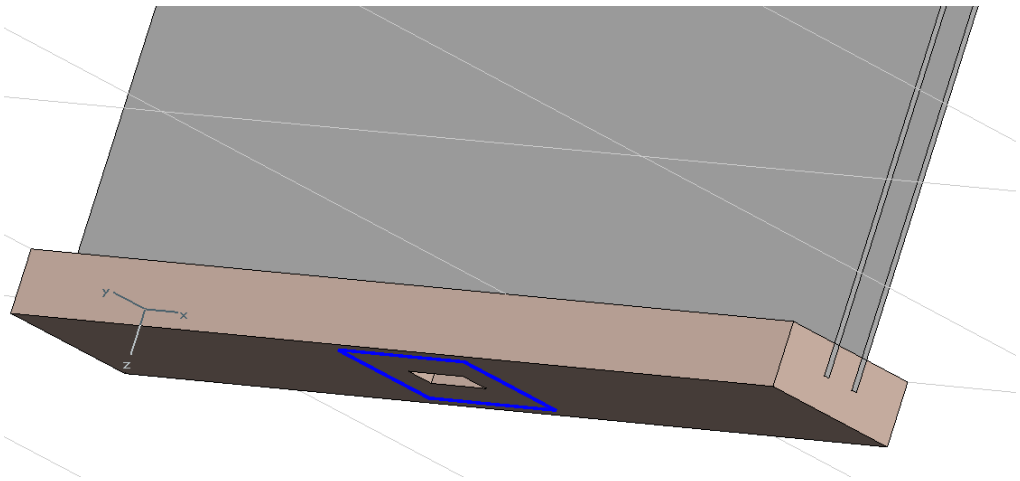

Fig. 11.Design of the metal piece with the aluminum plates already inserted

Obviously the piece had to be designed to suit the dimensions of the waveguide, the thickness of the aluminum plates and the necessary separation between them to contain the sample and taking into account the presence of the microwave absorbers.

In the meantime a proper absorber had to be obtained. At first when the initial costs calculation was done there seemed to be enough absorber available at ESAT, so that no purchases were necessary. However, the way they had to be cut and fit between the aluminum plates was not trivial and even the company Eccosorb was taken into consideration to acquire this material. First free samples of an absorber for the X-band were requested and particularly a product called Eccosorb SF-U seemed to be a good option. An absorber called Eccosorb SF-U-10.5 with resonant frequency at 10.5GHz was suggested by Eccosorb but only two free samples of 10 by 10cm could be sent, as the cost of one standard sheet size of 305 by 305mm was 100,17euro.

Also some absorbers got easily disintegrated when cut, so that obtaining a consistent and usable absorber sheet was not possible with these materials. It was not possible to cut the absorbers in any desired direction (transversally as well as longitudinally for instance) either. Finally a consistent absorber that could be cut longitudinally and still have a relatively appropriate length for the aluminum plates and sample's dimensions was found. Its absorption

capacity was tested with two horn antennas and a piece of absorber placed in between, and an attenuation of approximately -20 dB was found around the theoretical resonant frequency (10.5GHz). It fluctuated from around -15dB to around -20dB along the whole frequency range (8-12GHz) as illustrated in figure 12; the graph in blue shows the power transmitted without absorber, in red the transmission through the piece of absorber is represented:

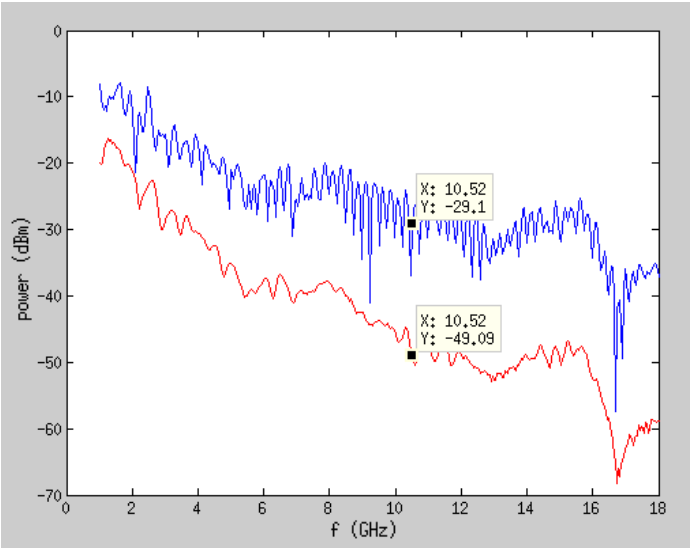

Fig. 12.Measured absorption capacity of the absorbers used in the setup

Thus it was considered a material good enough to be used in our experiment. The material could be finally cut in two strips with an automatic saw available at CMW.

In order to move the detector around the circumference of the circular part of the plates with a certain regularity and smoothness, a rotating mechanism had to be finally ordered also at CMW. A PVC bar –mechanically serving as arm- was fixed to the center of the semi-circumference that was the end of the upper aluminum plate. The detector was tightly screwed to the arm in such a way that it faced the aperture of the plates perpendicularly. The arm attached to the rest of the setup can be seen in figure 13:

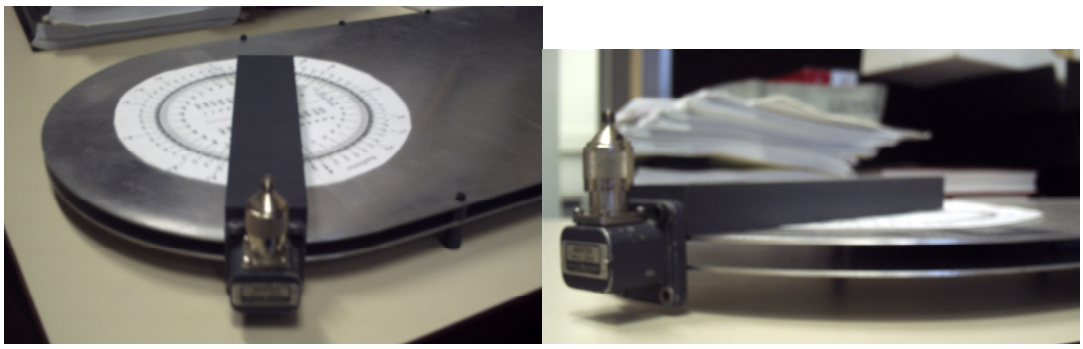

Fig. 13. PVC rotating arm screwed to the upper aluminum plate on one end, with the detector on the other, also screwed. The scale used to move the arm in approximately 2°-steps is attached to the upper plate too.

Also spacers were screwed to the aluminum plates every 10 cm along their linear section (channel), this aimed to ensure a constant separation between the plates that fitted the sample's height. It also allowed the absorbers' sheets to be uniformly compressed between the plates. The closed setup had to be opened to place the sample perpendicularly to the direction of the beam that was going to travel through the channel. The absorbers' strips were positioned touching the sample to avoid unwanted reflections and any kind of radiations as much as possible. This also kept the channel as "thin" as possible towards obtaining the "infinite-extension" effect of the sample mentioned at the beginning of this section.

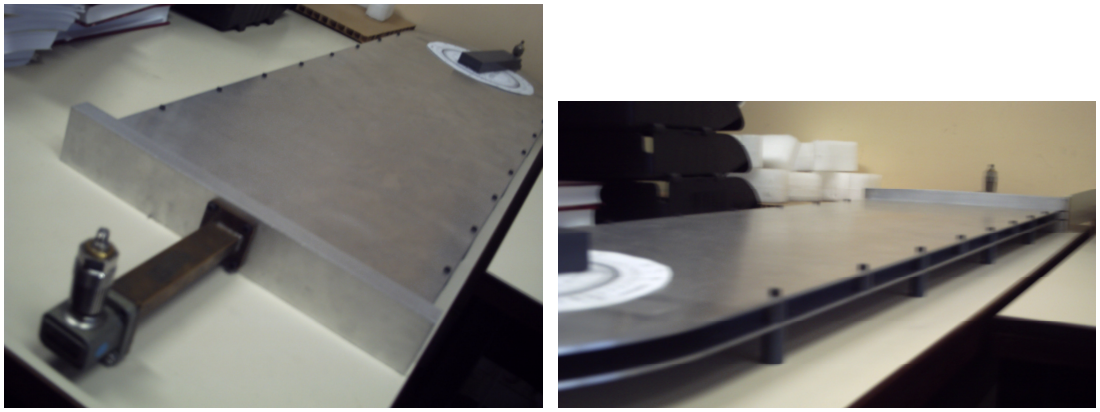

Fig. 14.Photographs of the setup where the spacers in between and under both plates can be seen.

Spacers were screwed below the bottom plate too in order to compensate the exceeding part of the metal piece attached at the beginning of the channel, thus giving more stability and portability to the whole experimental setup.

2.4 Numerical simulations

The main challenge in this phase was to be able to reproduce with simulations the NRI phenomenon linked to the experimental set-up defined before, under the conditions defined by the setup, particularly regarding the model of the sample. In order to see a negative refraction in the material it was important to try to model the metamaterial in such a way that it's behaviour in CST was as close as possible to the one a double-negative material (DNG, electric permittivity and magnetic permeability are negative) would have in real life -which has been described in previous sections and in the Introduction-. Consequently regarding accuracy the focus had to be made on the sample.

2.4.1 Considerations of computational simulation

CST Microwave Studio 2010 and 2011 were used alternatively first in a computer with an Intel Xeon (not 64-bit) processor of 2.8GHz, a RAM memory of 3.5GB and hard disc capacity of 38.8GB, and subsequently in a computer with 3.37GB of RAM memory, AMD Athlon processor of 2.41 GHz and a hard disc capacity of 46.5GB. Despite its apparently good computational characteristics the first computer was very slow when used with metamaterial simulations. The Frequency Domain solver was finally used for the definitive simulations. However the main improvement was noticed in calculation speed when the second computer started to be used.

CST capabilities were limited for our model and finally restricted our analysis. Additionally a software bug contributed to this restriction.This is explained in section the Annex and the consequences for the analysis are indicated along the subsequent subsections.

2.4.2 Sample and setup's modelling

First a simple setup was designed in CST in order to acquire a radiation that resembled plane waves (from now on referred as "plane wave´s setup") as much as possible, having a scatterer with the form of the sample. This was first tested with bulk materials to see if the desired effect was reached. Then the same had to be tested with a metamaterial.
To represent the metamaterial used in the wedge-like sample two options were considered at the beginning: modelling the whole sample in a realistic way or as bulk material. The first option demanded excessive amounts of computational resources just in order to design the material, so it was not going to be feasible to run a simulation with the metamaterial modelled in this way. On the other hand the representation of a periodic material through the design of only one unit cell, simulating its periodical repetition up to infinity –which was a new feature in CST 2011- was not suitable as it simulated an infinitely large piece of material and we wanted to observe the effect of the metamaterial used in a particular, finite, shape of sample. More importantly this new feature posed certain limitations on the way the unit cells were extended or repeated, making the resulting periodical arrange to stay very far from the model we needed for our metamaterial.

The representation of the material as a bulk-material implied that as it could be considered an effective medium, it could be represented as homogeneous media in CST: the materials used to model elements –scatterers in this case- in CST can be chosen from a library and eventually combined. Also new, user designed materials can be created with a certain freedom by defining some of its electromagnetic, mechanical and even thermal properties. Among the electromagnetic properties the electric permittivity and magnetic permeability can be described with certain restrictions, mainly:

1) by constant and uniform values, through one of the dispersive models available (in CST 2011 Lorentz, Drude, Debye first and second order, etc)
2) through a function with general parameters or
3) by entering a list of values assigning a certain permittivity and permeability for each frequency point in a frequency range (permittivity and permeability are frequency dependant parameters)

In the publications studied and in particular in references [2]-[6] a number of dispersion equations were proposed to describe the relative electric permittivity and permeability of a theoretical future negative-refractive index material. In our reference paper, [1], the authors used two of these to describe the new metamaterial -(3) and (4) in this chapter- so taking CST's available modelling tools previously mentioned into account, these equations were a promising information source for the model.
Anyhow these equations could not be accurately described by any of the common dispersion models available in CST, nor by a dispersion model equation with general parameters. This is because there was no way to set the parameters in any of the models accordingly to the equations, in particular the sign of one of the parameters was always opposite to what we needed with any possible combination tried.
So the most accurate option was to use the equations to produce a list of values and then use these with option 3 previously mentioned. CST requires the real and imaginary part of each

electromagnetic parameter to be shown in different columns and the imaginary part to be always positive, so MATLAB seemed to be a useful option to make the calculation.

2.4.2.1 Results with frequency dependant electric parameters

The first simulation attempts were made taking the experiment's complete range of frequencies into account, so the function was evaluated from 8 to 12GHz. 200 entries in the table had been an appropriate number in the past for simulations tried in CST within our group, so first 200 frequency points were used for the equations. CST's solver ran out of memory without even being able to reach a result –even when computers with RAM memory above 4 GB were additionally used- also when using 100 frequency points and with a number of different plane wave's setups. Also other parameters in CST were changed, general characteristics, type of material defined, type of problem as defined for CST, reduction of frequency range, even changing the source of the plane waves, without success.
Addressing a problem of excessive amount of unknowns to be calculated by the solver, the same actions were carried out using only three out of the 100 older frequency points, the ones that were closest to the resonant frequency of 10.5 GHz, without success.

The same setups were tested with a non-metamaterial sample and reached an end -did not run out of memory-, confirming that the problem appeared when the metamaterial was used in the sample. Anyhow this could either be caused by the use of non-traditional material in CST (for example by any of the negative parameters or its combination) or by the way in which the material was modelled.

2.4.2.2 Results with non-frequency dependant electric parameters

Pointing now at the use of the value´s list with a dispersion model of a double-negative (DNG) material as possible cause of the problem , the next step was to test a material with global, constant, uniform but very small permittivity and permeability values. More importantly, permittivity and permeability had to be forced to be no longer frequency dependant. Now the values used were an effective permittivity and permeability very close to zero, namely 0.002 and 0.001 respectively. The result was a slightly negative refraction in the far field, as can be seen in figure 15.

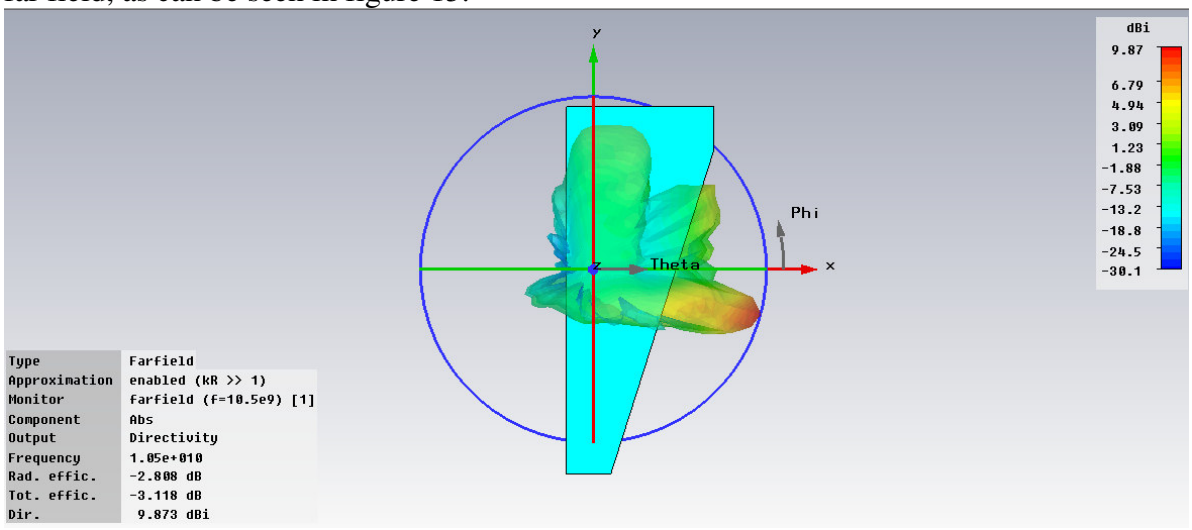

Fig. 15.Simulated farfield of the slab where the refracted angle of an hypothetic beam can be seen from above in the sample.

This was the closest we could get to negative effective electromagnetic parameters, as CST does not allow negative global values.

From then on the material model´s complexity was progressively increased: again a dispersion list with only three frequency points centered around the resonant frequency was used but with positive values. Permittivity values close to the absolute values of the reference dispersion function and smaller positive values were used: permittivity's real part is 14 at 10.45 GHz, 11 at 10.5 GHz and 9 at 10.55 GHz. Permittivity's imaginary part is 0.00001 in all cases (see table 3). The simulation corresponding to the list with permittivity values greater than or around 10 also matched CST's software bug described in the Annex–as learnt later on- and ran out of memory before a result was reached.

freq(GHz)	**Re{ε(ω)/ ε_0}**	**Im{ε(ω)/ ε_0}**
1.0450e01	14	0.00001
1.0500e01	11	0.00001
1.0550e01	9	0.00001

Table 3- Large positive permittivity values

However when permittivity values smaller than 10 were used the simulation reached an end, having a slightly positive refractive angle as result shown in figure 16. Corresponding permittivity values are shown in table 4.

freq(GHz)	**Re{ε(ω)/ ε_0}**	**Im{ε(ω)/ ε_0}**
1.0450e01	4	0.00001
1.0500e01	1	0.00001
1.0550e01	3	0.00001

Table 4- Small positive permittivity values

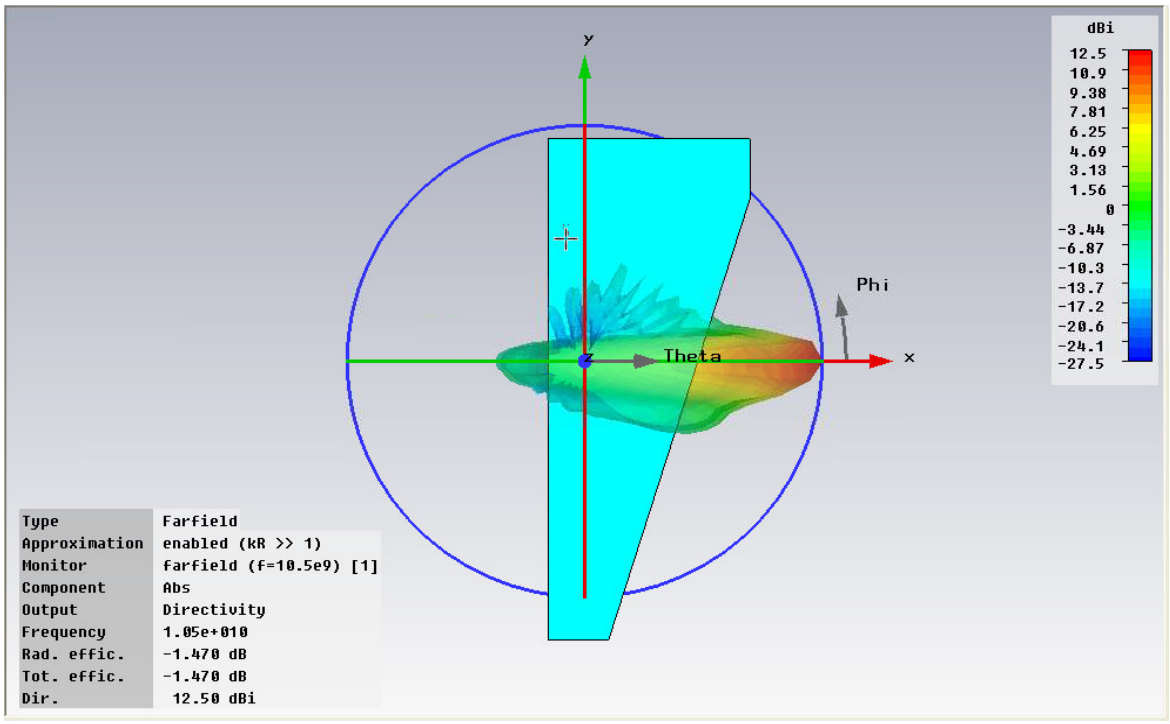

Fig. 16.Simulated farfield of the slab where the refracted angle of an hypothetic beam can be seen from above in the sample. Small positive permittivity values resulted in a slightly positive angle in this case.

Permeability values were always kept below or very close to 1.
Then the positive values were substituted by negative values below 10 in the permittivity and around 1 in the permeability, and negative angles were obtained in the refracted beams, as shown in the simulation result of figure 17. Corresponding permittivity values are shown in table 5.

freq(GHz)	Re{ε(ω)/ ε_0}	Im{ε(ω)/ ε_0}
1.0450e01	-4	0.00001
1.0500e01	-1	0.00001
1.0550e01	-3	0.00001

Table 5a)- Small negative permittivity values

freq(GHz)	Re{μ(ω)/ μ_0}	Im{μ(ω)/μ_0}
1.0450e01	-0.55	0.00001
1.0500e01	-1.01	0.00001
1.0550e01	-0.72	0.00001

Table 5b)- Small negative permeability values

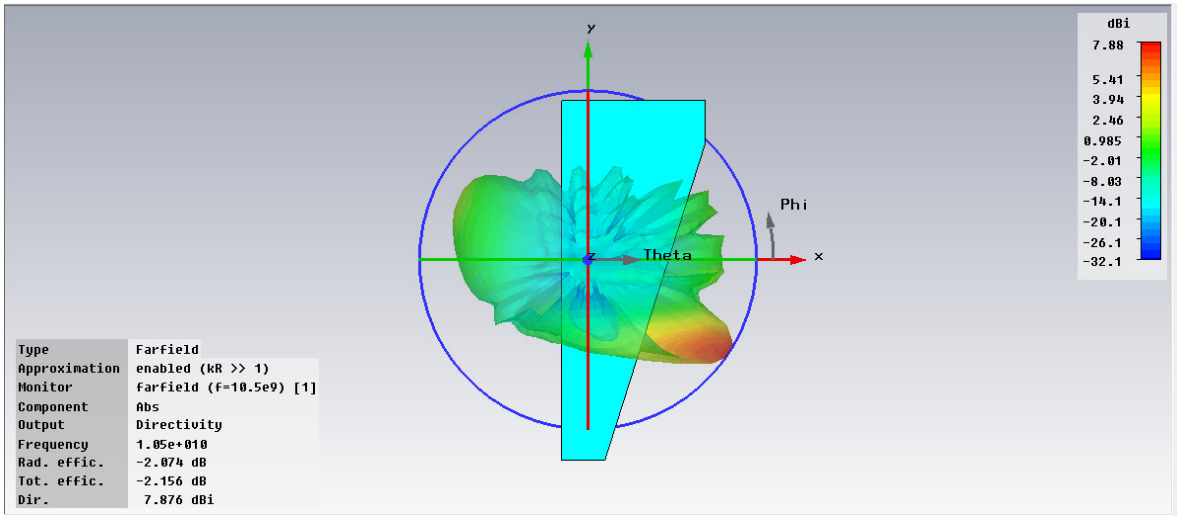

Fig. 17.Simulated farfield of the slab where the refracted angle of an hypothetic beam can be seen from above in the sample. Small negative permittivity values resulted in a negative angle in this case.

Then the same setups were run with smaller negative values -above 10 in absolute terms-, an example is shown in table 6. Permeability values are slightly changed as well and frequency points were permittivity and permeability values are defined are also changed. The imaginary part of the permittivity and permeability is however not the same as in the 3 frequency points of previous subsection. This new set of values also matched CST capability's problems and therefore no results could be obtained with them.

freq(GHz)	Re{ε(ω)/ ε_0}	Im{ε(ω)/ ε_0}
1.0480e01	-14.4392	0.00001
1.0500e01	-12.8820	0.00001
1.0520e01	-11.6079	0.00001

Table 6a) – New larger negative permittivity values

freq(GHz)	Re{μ(ω)/ μ_0}	Im{μ(ω)/μ_0}
1.0480e01	-1.1409	0.00001
1.0500e01	-1.0438	0.00001
1.0520e01	-0.9549	0.00001

Table 6b) – New larger negative permeability values

So finally, in order to see a finished simulation with the computational resources available, the best approximation obtained was a material model with small negative electromagnetic

parameters, relatively far from those obtained with the reference dispersion function but still negative around the theoretical resonant frequency. The specific values are the ones shown in table 5.
Consequently and as expected, the refraction angle obtained in the simulations using these smaller negative values could not coincide with the angle documented in [1] (the peak seen was around -30° instead of -60°, as shown in figures 17 and 18). In fact it would not be advisable to compare both results directly. Still the results of the simulations obtained with the smaller negative values showed a negative refraction angle, so we were able to simulate a negatively refracted beam of microwaves out of a material that behaved as a DNG in the frequencies of interest. In figure 18 a cartesian graph of figure 17 is shown, 327° would correspond to about -30° in the scale of [1].
In [1] results of the experiment's simulation are not shown. The only graph showing power transmitted is shown in figure 19, but power is actually normalized (linear scale) and most importantly, it is the power measured in [1].

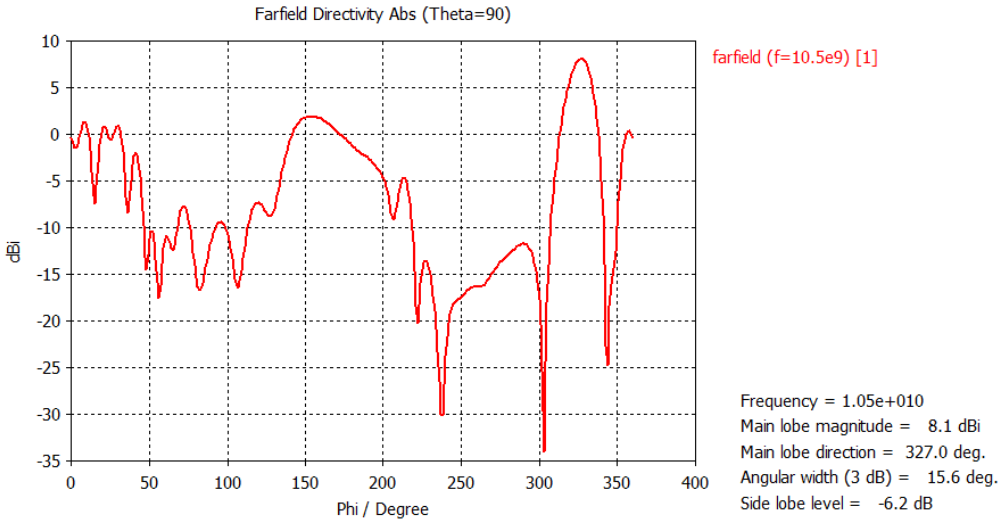

Fig. 18.Farfield directivity of the resulting refraction beam as a function of the angle.

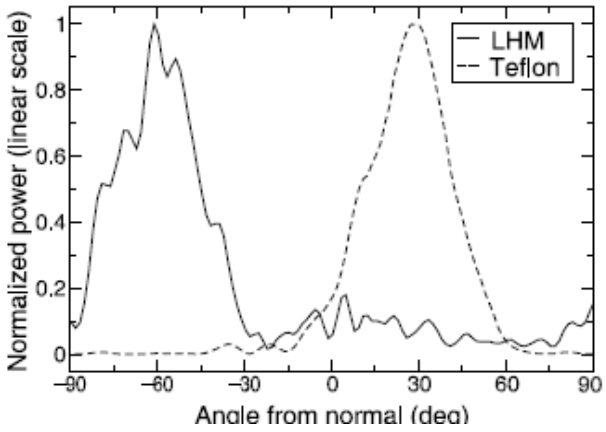

Fig. 19.Transmitted power measured in [1] as a function of refraction angle, for the LHM sample and a teflon sample.[28]

[28] Source: R. A. Shelby, D. R. Smith, S. Schultz, "Experimental verification of a negative index of refraction", Science, Vol. 292, p. 77, 2001

2.5 Measurement

The ultimate objective of the measurements was to see whether there was a significant increase in the power radiated at any point or region in the refractive face of the sample that could indicate that negative refraction was taking place. A higher level of power should indeed approximately indicate in which direction the incident microwaves' beam was being refracted by the sample. With this purpose the power level transmitted through the sample should be measured in the whole range of possible refracted angles - in a circumference around the refraction face- and for each angle the measurement should be made in the whole frequency band issued by the source. A network analyzer can perform a single measurement of the transmitted power within a wide range of frequencies in seconds, being an ideal tool to do the measurements. Although the specific angle and frequency in which the negative refraction took place were given in [1], the measurement should be made for a wider range of angles and frequencies taking into account that both refraction angle and frequency could not be the same in a similar experiment.

According to the information given in [1] the refractive surface of the sample was taken as the ground line to start the angular measurements (line P). They considered positive values the measurements taken in a clockwise direction from the normal to the surface to the ground line (90°) and the negative direction in the anticlockwise direction from the normal up to the ground line (-90°).Either they performed the measurements like this or they did not take the rest of the circumference into account. A schematic draw of the setup already shown in figure 7, now with our adjustments included, is depicted in figure 20.

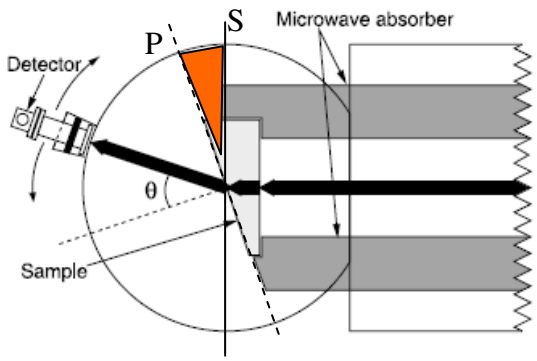

Fig. 20.Diagram of the setup showing mentioned angular ranges.

Instead we took a parallel line to the incident surface as the ground line (line S), so that our ground line coincided with our semi-circumference in the aluminum plates. This meant that we also had to dismiss the first angular range -marked in orange- which size should correspond to the smaller angle of the sample, we measured approximately[29] 30° in our case. We measured from the S line in the anticlockwise direction. This meant that -60° in the reference paper's scale should correspond to 180° (=150°+30°) in our scale. As we did not use a complete circumference as shown in the reference paper but rather a semi-circumference –because we did not find an appropriate way to connect the circular and rectangular plates as mentioned before- to rotate the detector, being the semi-circumference coincident with our 180° scale, the theoretical negative refraction angle would be positioned in a risky point. All

[29] It was "approximately" because the refractive surface is not a straight line, it is heavily corrugated as will be explained later

these meant that we were also “loosing” –not taking into account- the last 30° between lines S and P, the refraction angle should not be found there but this left very little margin if it turned out to be shifted to this region.
However, at the moment of starting the measurements the line of the refractive surface seemed –at first sight- to be at 45° with respect to the scale placed in the aluminum plates and this was also consistent with the results found, as will be later explained.
Without taking into account the first angular range, the measurements were made in 2°-steps.

S_{21} (and S_{12}) parameters were measured in the way described above in two different network analyzers in 400 frequency points. So from the network analyzer, for each angle a set of data at each frequency point was obtained and stored as a file. At first, Matlab scripts were written to show the levels as a function of frequency for each measured angle, later further scripts were written to plot transmission levels as a function of angle for several frequencies, among other scripts. It was indeed observed that the resonant frequency of our sample was shifted to a range centered at 11GHz instead of the reference paper’s 10.5GHz.
To seek for the approximate “location” of this sample’s resonant frequency within the X-band frequency range, first the highest transmission level for some angles –those closer to the theoretical negative refraction angle - as a function of frequency was searched, as shown in figure 21.

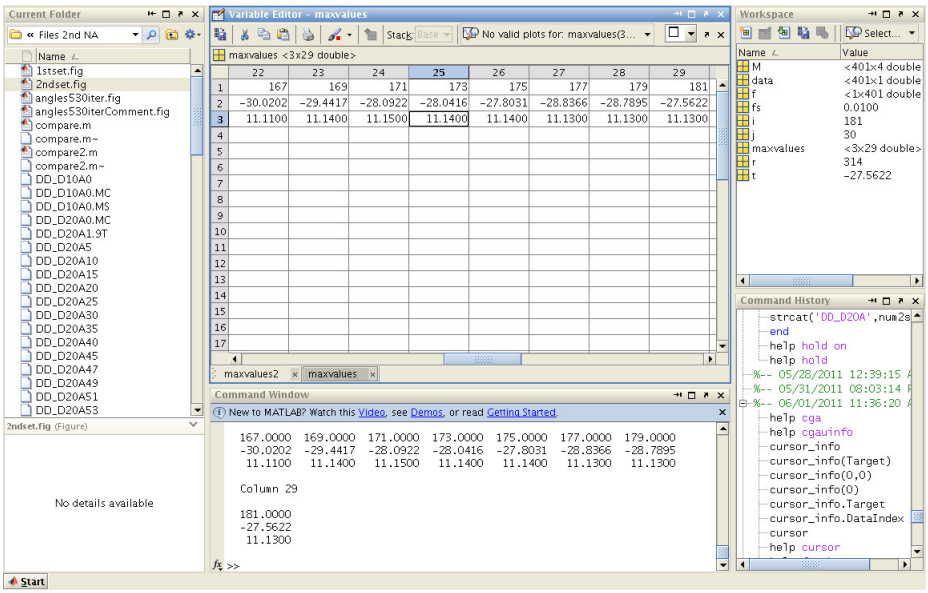

Fig. 21.Search for and extraction of maximum transmission values. Here we can see that specifically for angles between 167° and 181°, the maximum transmission levels were found always at around 11.13 or 11.14 GHz.

Matlab’s max function was used and the frequencies where most of the maximums were found were located close to 11 GHz, as observed in figure 21.
This could also be observed in graphs of the transmission level plotted as a function of frequency, for instance in figure 22, where different colours represent different angles, a peak can be seen around 11GHz. It was particularly plotted for all angles measured from 91° to 181° but a similar effect could be seen for most of the angles.

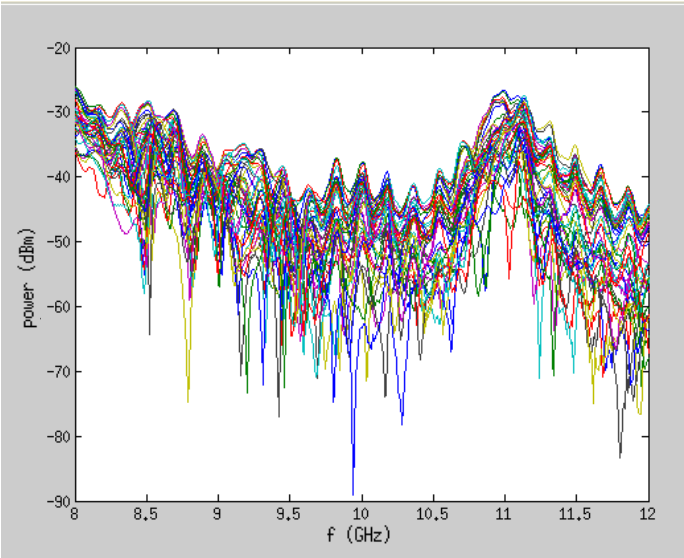

Fig. 22. Power transmitted through our metamamterial sample for each position of the detector between 91° and 181°, plotted as a function of frequency.

As mentioned before, further Matlab scripts were written in order to be able to handle the original data with dependency on the angle instead of as a function of frequency and graphs were made as a function of angle in several frequencies around 11GHz.
It must first be said that the transmission values from 0° to 45° were always inconsistently higher with respect to the rest of the scale, which we deemed could be linked to what was mentioned at the beginning of this section about the first range of angles or "orange region" that did not have to be taken into account.
For example in figure 23 we plotted several consecutive frequencies -each with a different colour- around 11 GHz as a function of the angle.

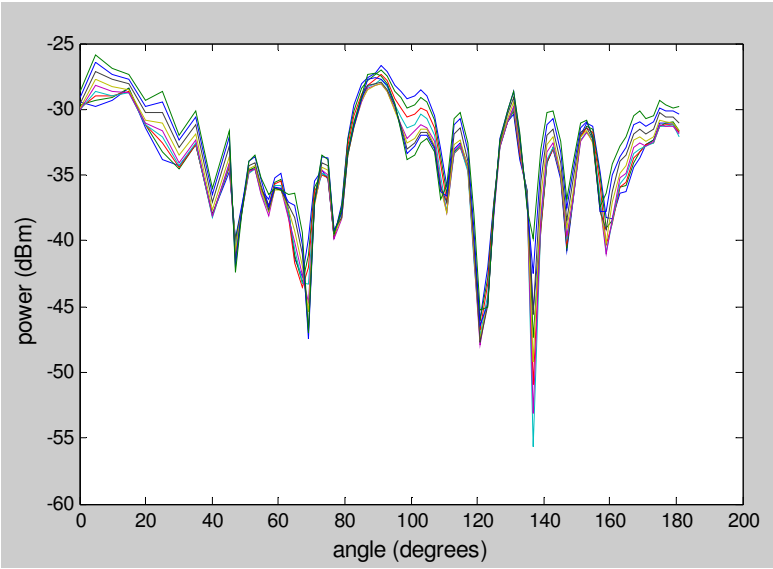

Fig. 23. Transmitted power measured at several consecutive frequency points close to 11 GHz, each frequency distinguished with a different colour, with the power plotted as a function of angle.

So we assumed the “orange region” had a size of 45° instead of 30° and did not take into account this range at the beginning of the scale for the rest of the analysis.

Among the frequencies close to 11GHz the one that showed the steepest growing tendency towards the theoretical negative refraction angle 180° was 11.3GHz, as depicted in figure 24:

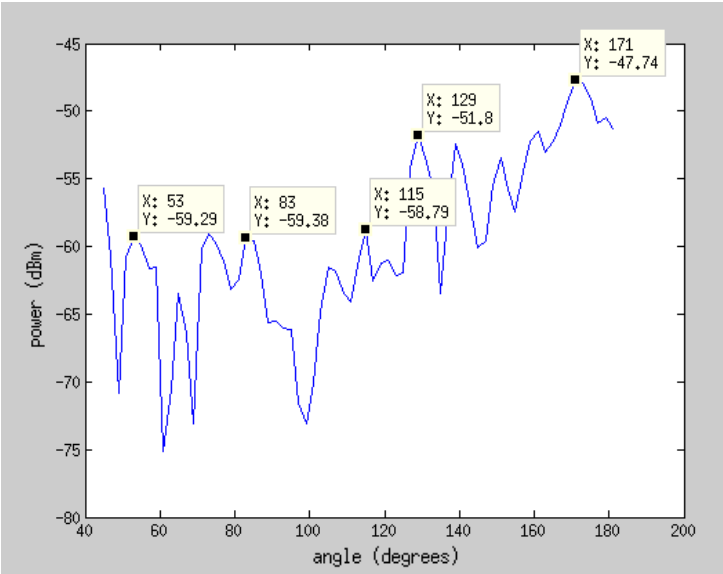

Fig. 24. Transmitted power measured at 11.3 GHz plotted as a function of angle

Despite the large variations or fluctuations in dB, a considerable increase in the transmission level towards 180° can be seen. The peak in dB is situated at around 171° and it reaches a difference of around 10 dB with the lowest values level at 115°. So we considered 171° as our negative refraction angle.
If we want to make a comparison with the measured result in [1], depicted in figure 17, it has to be taken into account again that power in [1] is normalized, although it can be easily appreciated that results in [1] are more clean. In [28], where measurements are also exhibited in dB, fluctuations similar to the ones observed in our measurements can be seen.

2.5.1 Fluctuations and further measurements

In order to find out if these fluctuations had been caused mostly by the experimental setup, S_{21} was measured in it without the sample. When plotting several frequencies together for all angles a much sharper peak could be appreciated (see figure 25), suggesting that the fluctuations were rather coming from the interaction between the sample and the setup and mostly by reflections in the sample.

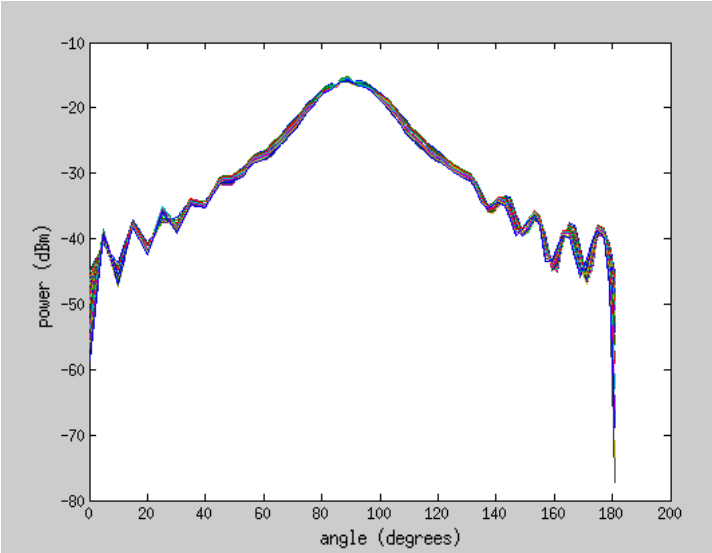

Fig. 25. Transmitted power for several different frequencies as a function of angle measured in the setup with no sample in it.

This could be observed at any single frequency too (for instance 11.14 GHz as plotted in figure 26):

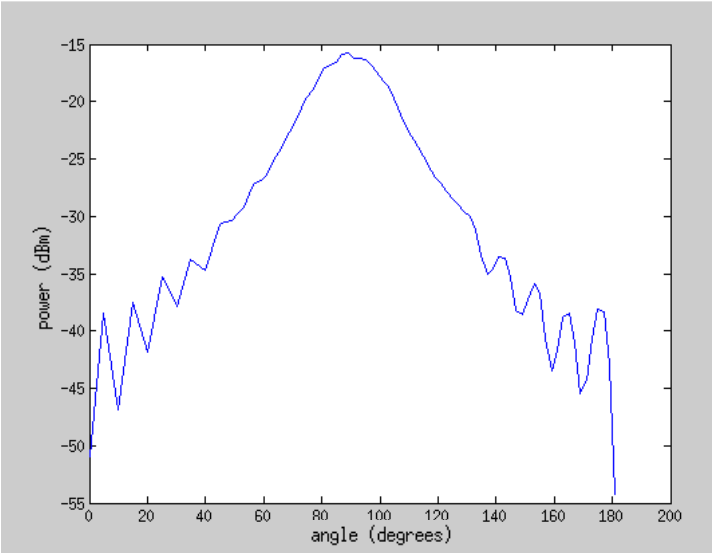

Fig. 26.Transmitted power at 11.14 GHz as a function of angle measured in the setup with no sample in it..

Anyway fluctuations of between approximately 5 and 10 dB could be seen when the measurement angle reaches approximately 140° and for angles below 50°, in this type of measurement.

It might be worth mentioning that a high number of this type of fluctuations could be observed too when graphs of different angles as a function of frequency were plotted, as in the first graphs showed with the sample. The fluctuations were not of the same size in dB but had a similar regularity and had comparable extensions in frequency, as illustrated in figure 27:

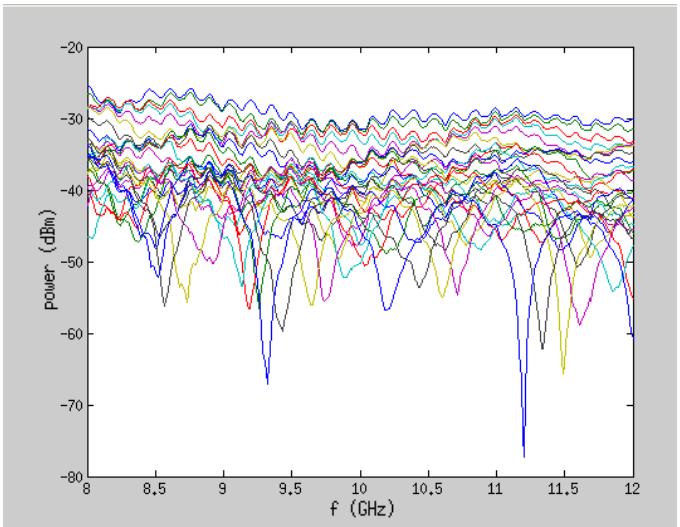

Fig. 27. Measured transmission at several different angles, each identified with a different colour, plotted as a function of frequency. Here also fluctuations can be observed as in previous cases.

Finally we realized that those fluctuations were probably linked to the "corrugation of the refraction surface" of the sample as mentioned in [1]. Indeed the refraction face of the sample has a staircase-like form, shaped by its unit cells, and this is unavoidable. The authors mention in the [1] that "this corrugation, in conjunction with reflection at the interface, introduces modulations into the observed angular transmission patterns" and that they made several measurements with the sample in eight different positions and averaged the results afterwards. These modulations they are talking about are probably the variations we observed. We did not make eight different measurements but we averaged the three measurements we had for a single frequency point, although the sample was not intentionally moved from its position. The result of this is shown in figure 28:

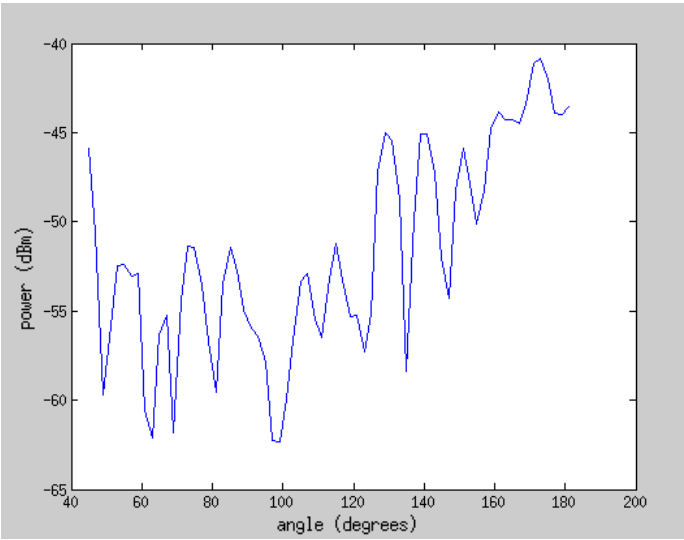

Fig. 28. Average of three full measurements of transmitted power, selecting only the sample at 11.3 GHz and plotted as a function of angle.

This resulting graph at 11.3GHz (figure 28) does not show a significant improvement with respect to the non-averaged graph (figure 24), as expected when several measurements are made on a sample that has remained with an unchanged position. Additionally this should also give an idea on the stability of the measurement. Anyhow, the growing tendency towards the 180 degrees or the difference in power level from the highest values (close to 180°) with respect to the lowest values is more noticeable in this graph. Again the highest peak is at 171-173° and has an approximate 10dB difference with the transmission level reached already at 115°-117°.

The contact issue between sample and aluminum plates was surely another source of perturbations: In the material model of most NRI metamaterials the wires' pattern should actually mimic a medium of infinite wires, to resemble a plasma-like effect. This shapes part of the NRI material behaviour and is best accomplished if the metal wires contact the metal parts of the waveguide channel in the setup. This was mentioned as an important issue in many publications related to experiments with NRI materials, as well sensitivity on the positioning of the sample with respect to the beam aperture, width of the aperture, waveguide channel's length and similar issues ([6],[7]), and for sure we can say that the wires in our sample were not always in contact with the plates.

2.6 Conclusions

We can say that although we did not obtain such a sharp peak as the one showed in [1], and the resonant frequency and up to a lesser extent the negative refraction angle did not coincide with the ones presented in the paper, we still found a clear anomaly in the power transmitted within the range of high frequencies in the X-band and in the region of negative refraction. This anomaly is a higher level of power transmitted through the sample around our negative refraction angle with respect to the angles that would correspond to a regular positive refraction.

Also, although we could not model the permittivity and permeability functions of the sample with accuracy in the electromagnetic solver, we could see that according to the simulations a material with negative electromagnetic parameters would refract an incoming beam of waves negatively, at least in a region of the microwave range.

As a first experience of fabricating a complete piece of metamaterial in our group, we can confirm that, as many authors in the field claim, in some cases it is indeed not trivial to properly fabricate a piece of metamaterial and perform a complete measurement , specially if negative refraction needs to be proved.

2.7 References

[1] R. A. Shelby, D. R. Smith, S. Schultz, "Experimental verification of a negative index of refraction", Science, Vol. 292, p. 77, 2001

[2] J. B. Pendry, A. J. Holden and W. J. Stewart, I. Youngs, "Extremely Low Frequency Plasmons in Metallic Mesostructures", Phys. Rev. Lett., Vol.76, no.25 , p.4773 , 1996

[3] J. B. Pendry, A. J. Holden, D. J. Robbins, W. J. Stewart, "Magnetism from Conductors and Enhanced Nonlinear Phenomena", IEEE Transactions on Microwave Theory and Techniques, Vol. 47, no. 11, p.2075, 1999.

[4] R. A. Shelby, D. R. Smith, S. C. Nemat-Nasser, S. Schultz, "Microwave transmission through a two-dimensional, isotropic, left-handed metamaterial", Appl. Phys. Lett., Vol. 78, no. 4, p.489, 2001.

[5] D. R. Smith, Willie J. Padilla, D. C. Vier, S. C. Nemat-Nasser, S. Schultz, "Composite Medium with Simultaneously Negative Permeability and Permittivity", Phys. Rev. Lett., Vol.84, no.18 , p.4184, 2000.

[6] D.R.Smith, P.Rye, D.C.Vier, A.F.Starr, J.J.Mock, T.Perram, "Design and measurement of anisotropic metamaterials that exhibit negative refraction", IEICE Trans. Electron., vol.E87-C, no.3, 2004.

[7] Andrew A. Houck, Jeffrey B. Brock, Isaac L. Chuang, "Experimental Observations of a Left-Handed Material That Obeys Snell's Law", Phys.Rev. Letters, vol.90, no.13, 137401, 2003.

[8] L. Ran, X. Zhang, K.Chen, T. M. Grzegorczyk, J. Au Kong, "Left-handed metamaterial and its experimental verifications", Chinese Science Bulletin, vol. 48, no.13, p. 1325, 2003.

[9] C.G. Parazzoli, R. B. Greegor, K. Li, B. E.C. Koltenbah, M. Tanielian , "Experimental Verification and Simulation of Negative Index of Refraction Using Snell's Law", Phys.Rev. Letters, vol.90, no.10, 107401, 2003.

[10] Kin Li, S. J. McLean, R. B. Greegor, C. G. Parazzoli, M. H. Tanielian, "Free-space focused-beam characterization of left-handed materials", Appl. Phys. Lett., vol.82, no.15, p.2535, 2003.

[11] R. W. Ziolkowski, "Design, fabrication, and testing of double negative metamaterials", IEEE Trans. Antennas Propag., vol. 51, no.7, p.1516, 2003.

[12] J. Huangfu, L. Ran, H. Chen, X. Zhang, K. Chen, T. M. Grzegorczyk, J. A. Kong, "Experimental confirmation of negative refractive index of a metamaterial composed of omega-like metallic patterns", Appl. Phys. Lett., vol.84, no.9, p.1537, 2004.

[13] A. F. Starr, P. M. Rye, D. R. Smith, S. Nemat-Nasser, "Fabrication and characterization of a negative-refractive-index composite metamaterial", Phys. Rev. B, vol. 70, 113102, 2004.

[14] H. Chen, L. Ran, J. Huangfu, X. Zhang, K. Chen, T. M. Grzegorczyk, J. A.Kong, "Metamaterial exhibiting left-handed properties over multiple frequency bands", J. Appl. Phys., vol. 96, no. 9, p. 5338, 2004.

[15] H. Chen, L. Ran, J. Huangfu, X. Zhang, K. Chen, T. M. Grzegorczyk, J. A. Kong, "Left-handed materials composed of only S-shaped resonators", Phys. Rev. E, vol. 70, 057605, 2004.

[16] K.Aydin, K. Guven, C. M. Soukoulis, E. Ozbay, "Observation of negative refraction and negative phase velocity in left-handed metamaterials", Appl. Phys. Lett., vol. 86, 124102, 2005.

[17] S. Zhang, W. Fan, N. C. Panoiu, K. J. Malloy, R. M. Osgood, S. R. J. Brueck, "Experimental demonstration of near-infrared negative-index metamaterials", Phys. Rev. Lett. , vol.95, 137404, 2005.

[18] J. Zhou, T. Koschny, L. Zhang, G. Tuttle, C. M. Soukoulis, "Experimental demonstration of negative index of refraction", Appl. Phys. Lett., vol. 88, 221103, 2006.

[19] K.Guven, M. D. Caliskan, E.Ozbay, "Experimental observation of left-handed transmission in a bilayer metamaterial under normal-to-plane propagation", Optics Express, vol.14, no. 19, p. 8685, 2006.

[20] K.Aydin, I.Bulu, E.Ozbay, "Subwavelength resolution with a negative-index metamaterial superlens", Appl. Phys. Lett., vol. 90, 254102, 2007.

[21] R. Liu, A. Degiron, J. J. Mock, D. R. Smith, "Negative index material composed of electric and magnetic resonators", Appl. Phys. Lett.,vol. 90, 263504 , 2007.

[22] J. Zhang, H. Chen, L. Ran, Y. Luo, B-I. Wu, J. A. Kong, "Experimental characterization and cell interactions of a two-dimensional isotropic left-handed metamaterial", vol. 92, 084108, 2008.

[23] F. Zhang, D. P. Gaillot, C. Croënne, E. Lheurette, X. Mélique, D. Lippens, "Low-loss left-handed metamaterials at millimeter waves", Appl. Phys. Lett., vol. 93, 083104, 2008.

[24] W. Zhu , X. Zhaoa, "Adjusting the resonant frequency and loss of dendritic left-handed metamaterials with fractal dimension", Journal of Appl. Phys., vol.106, 093511, 2009.

[25] Nikolay I. Zheludev, "A roadmap for metamaterials", OPN Optics & Photonics News, Vol.22, Issue 3, p.31, 2011

[26] V. G. Veselago, "The electrodynamics of substances with simultaneously negative values of ε and μ", Sov. Phys. Uspekhi. Vol.10, no.4, p.509, 1968

[27] Q. Cheng, T. J. Cui, W. X. Jiang, B. G. Cai, "An omnidirectional electromagnetic absorber made of metamaterials", New Journal of Physics, Vol.12, No.063006, Jun. 2010

[28] L.Ran, J.Huangfu, H.Chen, Y.Li, X.Zhang, K.Chen, J.A.Kong, "Microwave solid-state left-handed material with a broad bandwidth and a ultra low-loss", Phys.Rev.B, Vol.70, No. 073102, 2004.

[29] Nikolay I. Zheludev, "A roadmap for metamaterials", OPN Optics & Photonics News, Vol.22, Issue 3, p.31, 2011

3 Systematic study of a narrowband multiple-layered ultrathin metamaterial-like absorber

3.1 Introduction

Metamaterial absorbers with multiple-resonances and a broader absorption bandwidth have been very much desired since the absorption capabilities of metamaterials have been proposed. Conventional absorbers have been required for different applications and frequency ranges, and within each frequency range they are required to operate at several frequencies at the same time. For many applications they have to cover relatively broad bandwidths, which represents a challenge for metamaterials that intrinsically have narrowband responses as a consequence of the resonant mechanisms involved in their operation. Several techniques have thus been repeatedly applied to try to achieve this, the use of multiple-layers of conductive and non-conductive material is one of them, with the aim of obtaining several resonant peaks adjacent in frequency ([2],[3],[6]).

In this chapter a quite innovating approach in the field of periodic absorbers is studied. Rather than trying to design an "optimal resonator", this topology is analyzed in a systematic way, in order to point out the sensitivity of the topology to its design parameters.

A unit cell of the complete periodic structure is taken into consideration for the analyses, as well as a rather unitary approach is used for measurements, where a sample made of two unit cells is fabricated. This has been done in the past in other experiments, a good example of which is [7], defined as metamaterial absorber by its authors. Analyzing only a unit cell of a periodic structure is already a rather standard practice in the field, with its foundations in Floquet's theorem "For a given mode of propagation at a given steady-state frequency, the fields at one cross section differ from those one period away only by a complex constant"[30] (normally realized by e^{-jkd}, using the Bloch vector wave number k and being d the vectorial position). Hill's, Floquet's, Bloch's and Lyapunov's theorem all expose the same basic idea from a mathematical point of view [31], and in general a different nomenclature is used specifically for different fields. A Bloch state –also Bloch wave or Bloch function- is a plane wave multiplied by a periodic envelope function, thus it is modulated by a periodic function. In solid-state physics it defines the energy eigenstates for electrons in a crystal structure. Thus a wave –or particle in this case- will be described by a Bloch function, having the periodic function in it the same periodicity as the (periodic) structure of the crystal.[32] According to [4] in chapter 1, a plane wave propagating in a periodic lattice can be seen as a plane wave propagating in free-space, modulated by a periodic function. If we take a structure with discrete periodicity, such as one made by periodically arranged unit cells, Bloch states differing in a multiple of this discrete periodicity are identical, and the wave numbers that differ in the same way are not different from a physical point of view. So are electromagnetic modes. When this is translated to photonic crystals, the eigenvalue problem to be solved - subject to periodic boundary conditions- can be regarded as "being restricted to a single unit cell of the photonic crystal". Analogously, this can be translated to periodic structures subject to periodic boundary conditions, which are made of unit cells, and spaced by a discrete

[30] G.V.Eleftheriades, K.G.Balman, "Negative-Refraction Metamaterials-Fundamental principles and applications", IEEE Press, John Willey and Sons, Inc, 2006

[31] The concept of Bloch states is described in Felix Bloch's "Über die Quantenmechanik der Elektronen in Kristallgittern", Z. Physik 52, pp. 555–600, 1928.

[32] For further theory and more detailed derivations see C. Kittel, "Introduction to Solid State Physics", Wiley, New York, 1996

periodicity that conforms a periodic lattice, as is well known. Additionally, through the presence of unit cells, periodicity in periodic structures and metamaterials is more clearly defined than in the structures of several photonic crystals.
In this way, in more general terms, a periodically arranged structure can be characterized by a unit cell with periodic boundary conditions.

Also, standard CST configuration for periodic structures' simulations is used: it is possible to set different boundary conditions' configurations in CST, among them "unit cell", available from CST 2012 version. This configuration enables 2D-periodicity and imposes periodic boundary conditions; Floquet modes are used. By using the unit cell boundary condition the modelled structure is virtually periodically repeated in a maximum of two directions up to infinity. Additionally, this configuration has proven reliable in previous simulations with known metamaterial resonators, such as SRRs, in results that have had perfect agreement with expected publication results and even with a second solver: MAGMAS.
From this chapter on, all periodic structures are analyzed using this feature in CST, unless a different configuration is specified.

In section 2 we give a theoretical background and framework to better understand and assess the main part of the work. In section 3 we explain the extensive study carried out. Then we expose the study separately for variations in the dimensions of the structure (geometrical parameters section 4) and when the characteristics of the dielectric material used are changed (section 5). In section 6 we present the results of a validation of the sensitivity analysis, carried out by means of an experimental validation and the use of a second electromagnetic solver. Section 7 contains the general Conclusions.

3.2 Topologies proposed for addition of adjacent frequency peaks

Among the structures proposed to obtain multiple-resonant or broadband absorbers the following two have been some of the most effective and frequently used.

3.2.1 Multiple-layers

The concept of this kind of topologies is to stack several layers of structures that generally have absorption capabilities on their own and are frequently made of metallic resonators and dielectric material. In several publications it has been shown that these topologies can manage to effectively merge resonant peaks closely positioned in the absorption spectrum [2] and have therefore become a good candidate to design metamaterial absorbers with a wider absorption bandwidth.
To achieve this, the resonators of the different layers have different sizes to obtain resonances at different frequencies closely positioned in the spectrum, as the size of the resonator is directly related to it resonant frequency.
Then the thickness of each layer should be responsible for impedance-matching of the structure to free-space at each resonant frequency corresponding to the resonator on top of each layer, extending the principles applied to design a metallo-dielectric one-layer structure. Then when a structure has to be tuned towards certain specifications, the principle generally applied is that the change in the size of a metallic resonator is expected to control fundamentally the frequencies of the resonances, while the variation of the thickness should modify mainly the impedance-matching of the structure to free-space

$$Z_{in} = \eta_0 (1 + S11) \Big/ (1 - S11) \qquad (1)$$

with Z_{in} the surface impedance of the absorber as in [7]. Thus the modification of thickness should be of both parameters the one that affects the absorption stronger.
The thickness of each layer is often tuned to have resonant peaks with similar absorption levels, positioned as close as possible in the spectrum when a creating a broad bandwidth absorber is the aim.
The resonator on the top layer is usually the smallest accounting for the high frequency resonance, the one on the layer below is larger, accounting for a lower frequency resonance, and so on (depending on the number of layers of the complete structure). As indicated in [2] and [6] then usually the electric and magnetic resonances at each frequency are mainly localized in the layer upon which the resonator for the corresponding frequency is. Still in [6] the dielectric layers in between the metallic patches change their side-length, while in [2], where a double and triple-layered absorber are presented, the side-length is constant. In [2] though, as we go from the lowest to the highest frequency resonance, the more layers and the more all of them contribute to the resonance. In the double-layered structure at the lowest frequency the bottom layer is mainly the one that contributes to the resonance, while at the high frequency the resonant contribution is more distributed among both layers. It is mentioned that the highest frequency resonances can be regarded as hybridized modes. This is one way to explain the absorption capacity of a multiple-layer metamaterial absorber.
A possible drawback in this kind of structure is that the thickness may become less interesting as more layers are added(which would be a straightforward way to add more resonant peaks and thus eventually enlarge absorption bandwidth at the end).
90% is a level of absorption that this kind of structures are frequently able to achieve in each resonant peak.
A ground-plane is also commonly used in this kind of structures to avoid transmission.

3.2.2 Adjacent resonators

In these kind of structures, generally also metallo-dielectric, the resonators are distributed on top of dielectric material in an only one-layer structure. This is, several resonators with different sizes are placed in the same geometrical plane on top of the dielectric. It has been observed that in this way the resonant modes can also be hybridized and absorption peaks closely positioned in the spectrum obtained. These structures are potentially thinner (due to the one-layer geometry) absorbers, if the sizes of the resonators, their geometrical distribution and dielectric thickness are properly adjusted.
Once again a ground-plane is commonly used in this kind of structures to avoid transmission.

3.3 Characteristics of the structure and analysis carried out

We analyze how the performance of a structure evolves with the tuning of specific parameters, namely we analyze how it specifically affects absorption and absorption bandwidth of the response obtained. Although the behaviour can be partly predicted by electromagnetic equations, and some parameters in concrete structures with fixed and defined dimensions have been varied in publications up to some extent, it is not common to carry out a systematic and extended analysis such as the one presented here, neither has one been systematically registered. As mentioned before, inspiration comes from the structures designed to have multiple-peaks and a broader bandwidth, and the objective of these analyses

is in part to validate the mechanisms frequently used to tune metamaterial absorbers and observe whether new ones can be proposed.
Primarily the geometrical parameters of the structure are extensively modified to observe the effect this has on performance and then using the same geometrical parameters the dielectric material is changed to observe the influence of the different changes in the absorber's performance.

For our analysis only normally incident electromagnetic waves are considered, results are equal for TE and TM polarizations.
As we use a metallic ground plane in our topology, there is no transmission and thus it is only necessary to study the reflection from the structure in order to determine the absorption it is yielding.

$$A(\omega) \equiv 1 - T(\omega) - R(\omega) = 1 - R(\omega) = 1 - \left|S_{11}(\omega)\right|^2 \qquad (2)$$

Thus it is only necessary to study reflectivity S_{11} .

3.3.1 Analysis and topology

For the analysis and all of the simulations presented in this chapter we choose a very simple structure as reference to see how different sensitive variations of parameters affect its performance. The structure has two layers of metallic and dielectric material and a ground plane. The metal used is always copper and as substrate FR4 with two different loss tangents (the standard one for FR4, tg(δ)=0.025, and tg(δ)==0.04) and a different dielectric constant and same standard loss tangent of FR4 are used in both layers. The shape of the metallic resonator is a square patch.

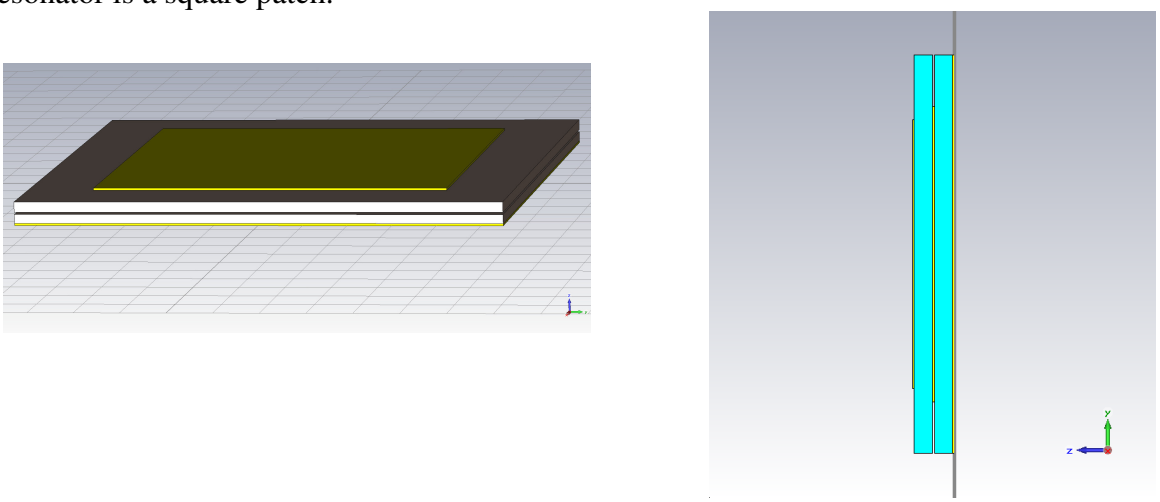

Fig. 1. Unit cell considered and analyzed.

The geometrical parameters we modify are the thicknesses of both dielectric layers and the size of the metallic resonator on top of the upper dielectric layer. The unit cell of the periodic array has a fixed side-length of 11mm , the size of the resonator on the bottom layer is also fixed (side-length of 8.2 mm), the thickness of the copper used is kept fixed as well (standard 0.05mm-check). The dielectric used for the geometrical parameters' variations is standard FR4 with the values specified in the previous paragraph.

The thickness of the top layer varies between 0.1 and 0.5 mm and is increased in steps of 0.1mm., the top layer's patch side-length goes from 7.40 to 8.52 mm and is increased in steps of 0.04 mm.

3.3.2 Numerical analysis simulated and processing of results

We use CST Microwave Studio for the numerical analysis of the several sets of parameters of the structure, obtaining the complex parameter S_{11} as a function of frequency for each one of them, which is the main source of our studies.
In this way we can determine the reflectivity level and bandwidth of the absorptive response for each set of parameters.

As expected most of the S_{11} frequency responses show two peaks evidencing a double-resonant behaviour originated by the two metallic resonators, but as the top layer's patch size is increased, for some bottom and top layer thicknesses only one peak instead of two separated resonances can be distinguished:

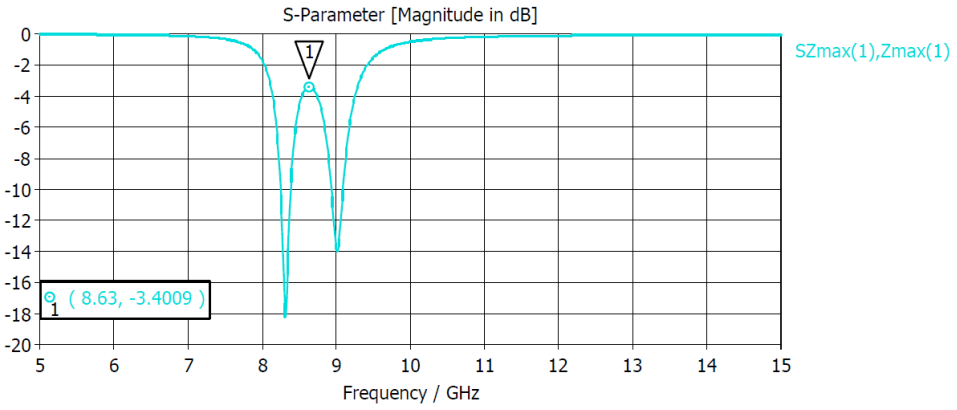

Fig. 2. Example of S11 plot for a patch size of 7.60mm and thickness of 0.4mm.

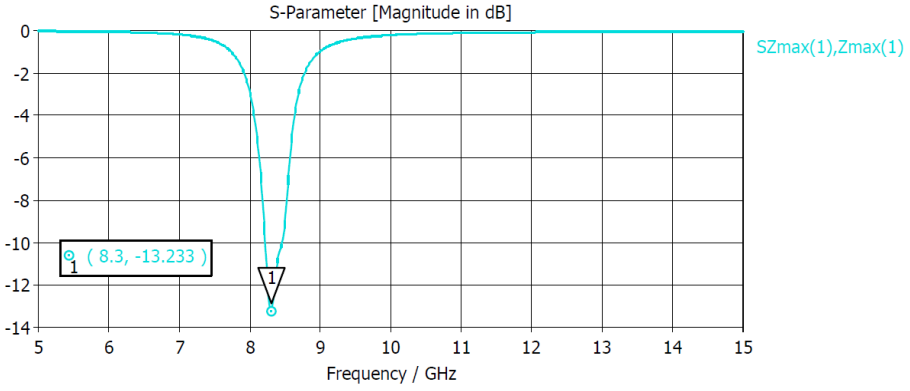

Fig. 3. S11 plot for patch size 8.20mm and thickness of 0.3mm.

Therefore the point where the reflectivity is defined is not necessarily trivial: it is registered at the point where both resonant peaks "merge" in the S_{11} graph (marked with pointer "1" in Fig.2), when two clearly separated peaks can be distinguished, and as the minimum

reflectivity dip (marked with pointer “1” in Fig.3) when two peaks can no longer be distinguished.
In order to characterize absorption, we introduce the notion of continuous spectrum absorption level. This differs from the way most publications consider the absorption capacities of their multiple-resonant structures when resonances are clearly discrete, which is by giving the absorption of each discrete frequency peak. Here instead we always evaluate the absorption capacity of the structure in terms of the maximum width of frequency spectrum it can cover (with a noticeable level of absorption), and not how much it can absorb at specific discrete frequencies.
The concept of continuous spectrum can also be explained as follows: in Fig.2 at -8dB the frequency response occupies a bandwidth of approximately 1GHz but it is not continuous because there is a “gap” in the band; for frequencies in that gap the response does not reach the -8dB level (reflectivity at these frequencies is -3.4, -6, etc). Therefore at -6dB we would have two continuous bandwidths or spectra. But at -2dB from 8-9.5GHz a continuous spectrum can be measured, at -6dB from 8.8-9.2GHz another one can be identified, etc. If we would like to have a material capable of absorbing at a continuous range of frequencies and not only at specific frequencies (a rather typical absober-like behaviour), with the parameters set as in Fig.2 we would be able to ensure an absorption of about 54% (reflectivity =-3.4dB) in the complete range of 8.1-9.3GHz.This is the kind of capacity we are primarily evaluating, the one demanded from a typical absorber. On the other hand the material would have much more absorption at around 8.4 and 9GHz, around which the two minima of S_{11} are observed.

Consequently also only continuous spectrum is considered when registering absorption bandwidth, thus for the parameters corresponding to Fig.2 at -6dB we would have “two absorption bandwidths” (two continuous absorption bandwidths), as mentioned in the previous paragraph, whereas at -2dB we would be able to register a continuous absorption bandwidth of about 1.5GHz. In principle, the bandwidth of each frequency response is registered for reflectivity levels-6,-8,-10 and -16 dB. Therefore in the graphs displaying the variation of bandwidth , for certain sets of parameters and reflectivity levels we will have two bandwidths and for others one bandwidth.
When for a specific reflectivity level the two bandwidths transform into one bandwidth, many times sudden steep increases can be observed in the curves as they can be considered one and thus the values of each one separated are added, this enhances any increase in bandwidth. When the increase is not so steep many times is because one of the two separated bandwidths (at one of the separated resonant peaks) is too small or inexistent. Thus the variation of absorption has an important influence in the variation of bandwidth for separated resonant peaks and single peaks.
For instance it is responsible for making peaks "detectable" at certain reflectivity levels or not (if we can say whether there is a bandwidth at -10 or -16dB or not, depending on the absorption level of the peak or peaks).

3.4 Variations in the geometrical parameters

3.4.1 Results for a bottom layer thickness of 0.2mm

The detailed analysis and conclusions for a bottom layer thickness of 0.2mm are also valid in general terms for other bottom layer thicknesses when different top layer thicknesses are used.

When the bottom layer has a fixed thickness of 0.2mm and the size of the top patch and thickness of the top layer are varied as explained in the topology's description, we observe that for all top layer thicknesses simulated a single peak is achieved. The result of registering the reflectivity and absorption bandwidth for each set of parameters as explained in the previous section is depicted in the following graphs:

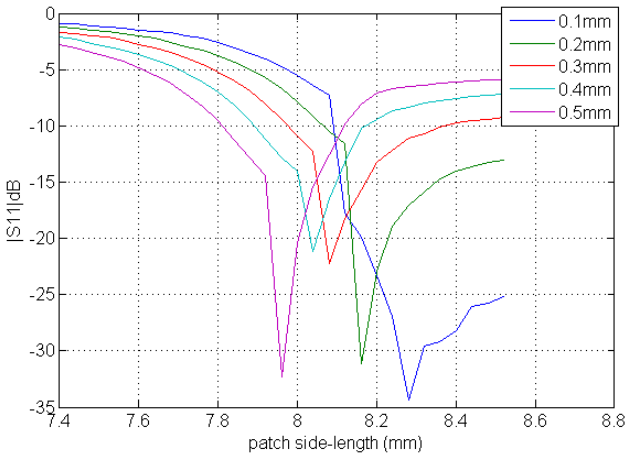

Fig. 4. Refelectivity of each new set of parameters plotted as a function of the top layer's patch size.

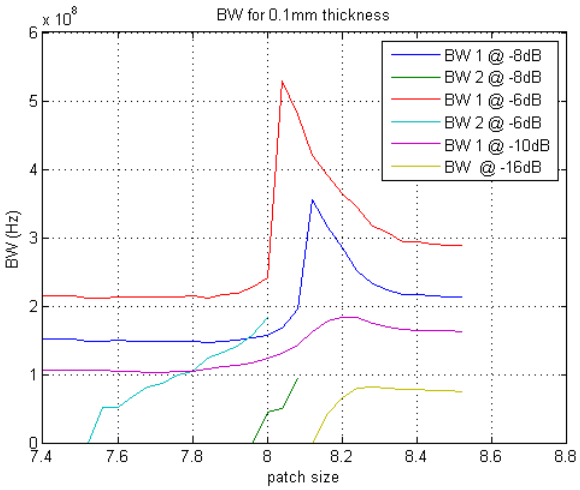

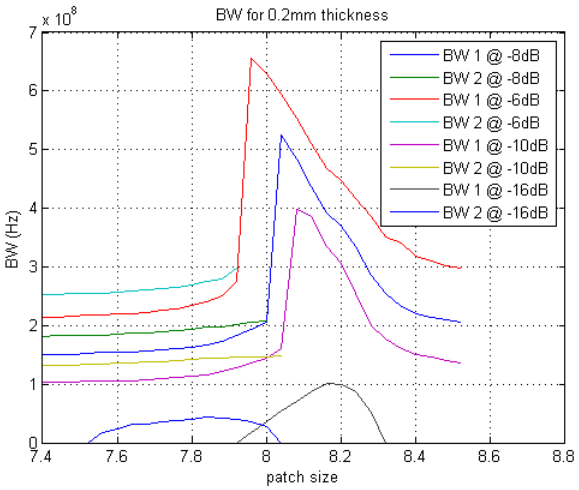

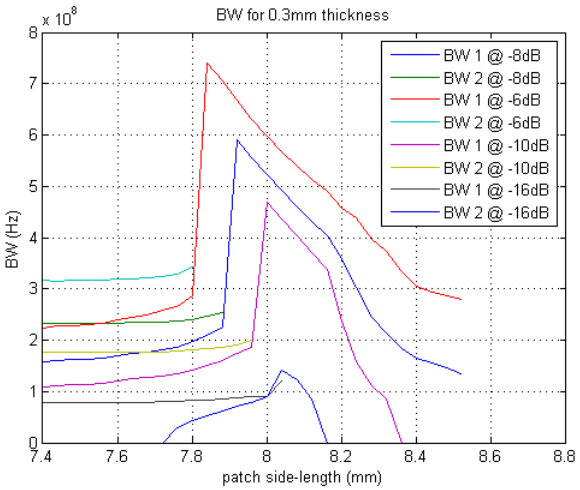

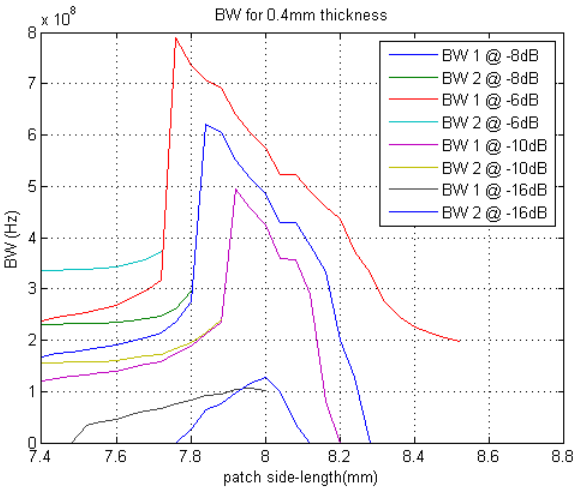

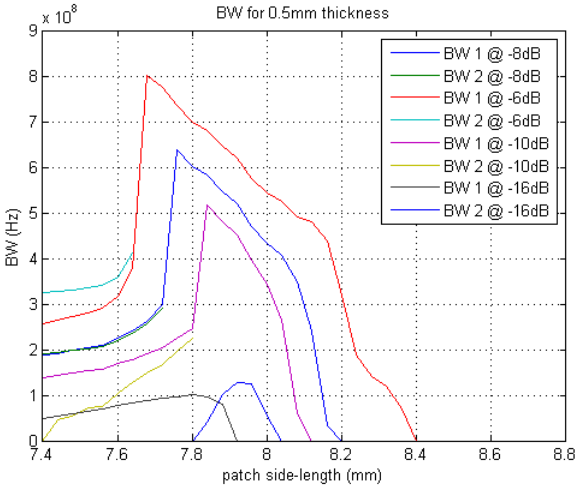

Fig. 5. Bandwidths for each thickness are plotted separately . Some artefacts observed are attributed to CST's calculations, particularly for thickness 0.4mm where two simulations have a similar bandwidth. CST is still a simulator, thus the numerous calculations are not always accurate nor physical (do not reflect what would happen in nature). Also,it cannot offer infinitely continous frequency dependant calculations (the frequency point calculated is not exactly at -10dB, for instance).

Given the method used to register reflectivity, there is a sudden decrease of reflectivity when nearly one peak can be observed , when no longer the "merging point" but the minimum is registered. For some sets of parameters an even smaller reflectivity level is reached in the frequency response once the one peak can be distinguished.
Also a steep sudden increase is observed in bandwidth for most reflectivity levels and many sets of parameters, due to the how the bandwidth is registered, when no longer two continuous bandwidths but only one can be observed for the different reflectivity levels. The change from two to one bandwidth is generally observed with patch size increase, as the resonant peaks will typically shift closer in frequency and the reflectivity level will decrease (this will be further commented in the next paragraphs). The two bandwidths that we had at a certain reflectivity level will be one continuous bandwidth at the same level with a larger patch size (for a top layer's thickness of 0.1mm, at -6dB, we have a continuous spectrum at a patch size of around 8.12mm but with smaller patch sizes we have two bandwidths).
The same sudden increases in the general graphs that show the variation of reflectivity and bandwidth obviously will also be observed for other sets of parameters in the following sections, as the method for registering reflectivity and bandwidth is always the same.
The presence of recordable bandwidth at -16dB shows that each peak individually reaches reflectivity levels lower than -16dBs and beyond for several patch sizes.

3.4.1.1 Separated double-resonant response

When we only change the size of the top patch leaving the rest of the parameters unchanged, the corresponding higher frequency resonance of the structure changes as expected (its frequency decreases as the size increases, see Fig.6).

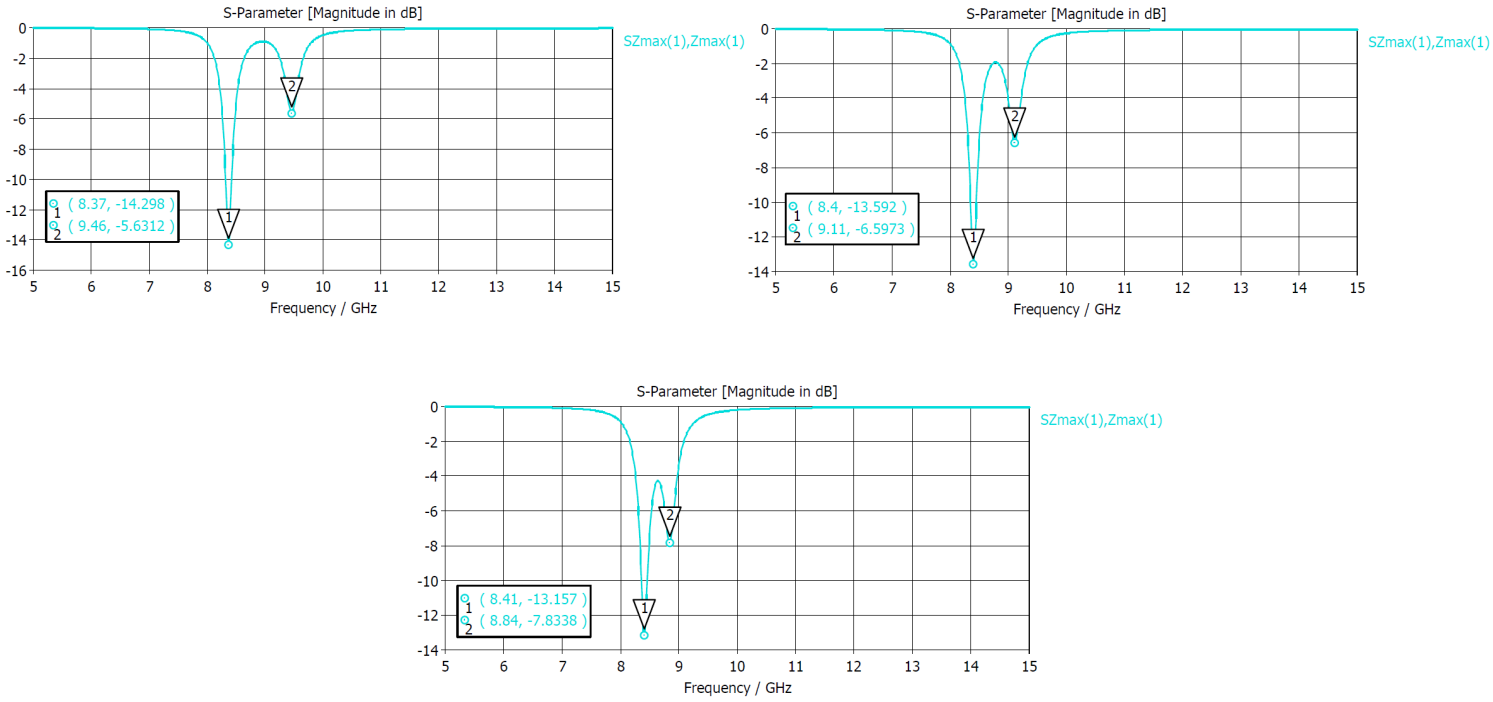

Fig. 6. The high frequency peak (always marked as "2") decreases with patch size.The change is comparatively larger than the one observed in the low frequency resonance.The resonance responses are plotted for patch sizes of 7.40 mm first, 7.72 mm and 7.96 mm, respectively at a thickness of 0.1 mm.

Additionally, as impedance-matching to free-space is mostly dependable on thickness, with each new patch size impedance-match will not necessarily be the best at that higher frequency resonance (best-matching would be at a different thickness for each patch size and the top layer's thickness remains fixed). As a result the absorption of the higher frequency resonance will also be variable. The effect on the matching conditions of the other patch and layer have to be taken into account as well. It is once again confirmed that for a multi-layer structure the multiple resonances are not easily controlled independently by the elements of each layer.

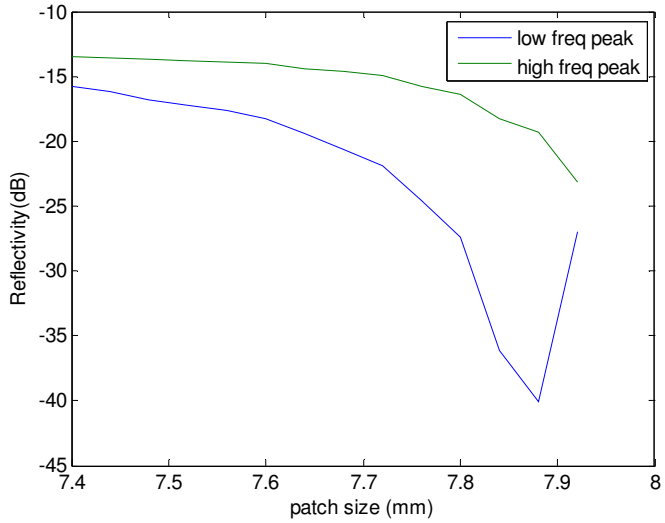

Fig. 7. Reflectivity for each peak as a function of patch size at 0.4mm-thickness while two separated peaks can be clearly distinguished.

As a consequence of the above mentioned variations and the continuous decrease of the higher resonance's frequency (both resonant peaks come closer in frequency), the reflectivity of the continuous spectrum decreases with the increase of the patch size alone (Fig.4).

Obviously impedance-match variation is also observed with changing thickness for a fixed patch size. As expected the tuning of thickness affects absorption more significantly than the one of patch size. Additionally both peaks are more strongly affected and the increase of the top layer's thickness continuously increases the absorption of the structure. And once again it is confirmed that both resonances are affected when a parameter on only one layer is changed.

The effects of top patch size and top layer's thickness increase combined result in the increasing slope observed in the reflectivity curves (Fig.4).Thus for an increase of only 0.4mm in the total thickness of the structure its reflectivity is reduced from around -2.5 dB to almost -10dB (about 90% absorption), for a top patch size of 7.8mm.

The bandwidth of each resonance changes consequently, as it can be seen on the curves (Fig.5), experiencing in general an increase with thickness and an increase of the slope with patch size. It is though a very slight increase indicating that it can be mainly attributed to the increase of absorption.

It is not necessary then to tune the parameters on each thickness separately, as it is the classic approach in order to increase the absorption of the continuous spectrum, by linearly increasing only one or two parameters in one of the layers, absorption and bandwidth can be effectively enhanced. This could be very useful when there are limitations that allow modifications on only one layer of the structure.

3.4.1.2 Single peak

After only one peak can be appreciated, the situation and thus tendencies change almost completely:
One peak is observed when the size of the top patch approaches the size of the fixed one, but it is when both resonances are close enough in frequency with the proper absorption levels that nearly one peak can be distinguished. Either one of the peaks is very small in comparison with the other one and the larger one will be mainly responsible for the unified resonance or both resonances are well matched at almost the same frequency (different matching for each different thickness).

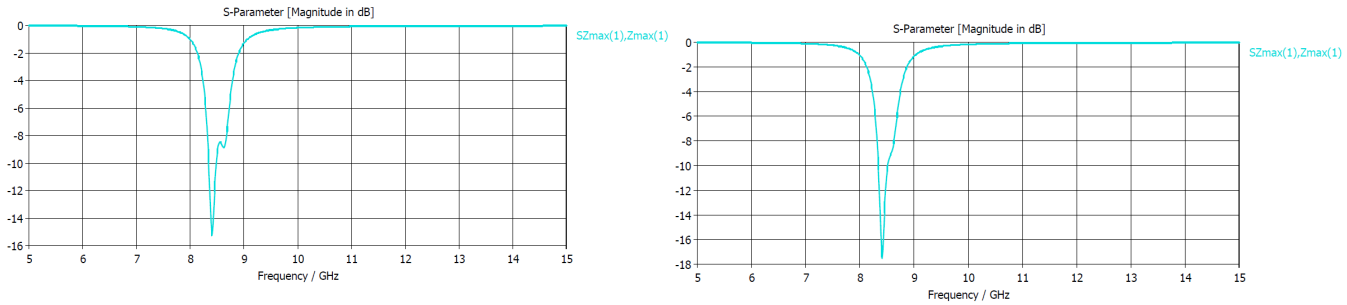

Fig. 8. One peak is much smaller than the other one.(8.12mm and 8.16mm–patches respectively for a thickness of 0.1mm).

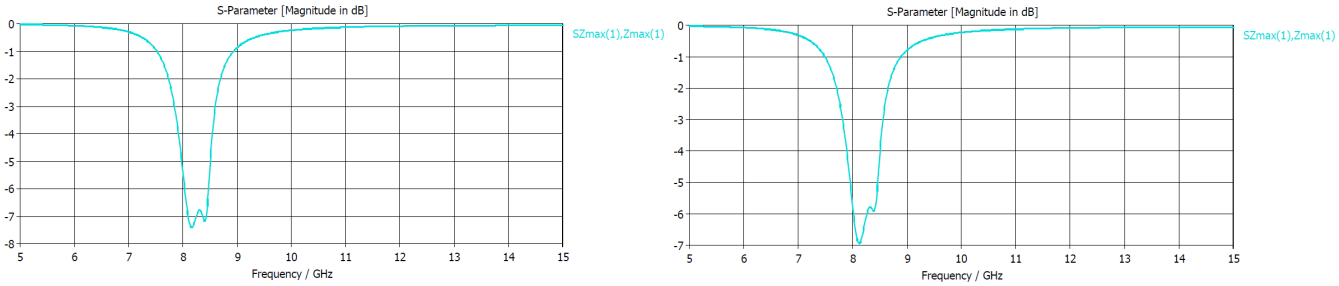

Fig. 9. Peaks have a more similar absorption (8.16mm and 8.20mm-patches for a thickness of 0.5mm).

The influence of each resonance upon the other is stronger after this point and in part can be explained by the fact that as the patch size keeps increasing over the fixed patch dimension it "takes over the task of ground plane" as the bottom layer's patch did before [16]. This shows once again that basic principles applied to patch antennas (electromagnetic radiation) are applicable to periodic structures. Therefore also for the last and largest patch sizes, once the absorption has been reduced drastically for most thicknesses, it tends to maintain the same value even with a growing top layer's patch size. This means that for a thickness of 0.2 mm absorption is kept at around -13dB and at around -25dB for 0.1mm, with a changing patch size (Fig.4).

As the absorption for a double-peak response grew with thickness, one peak is observed for a smaller patch size when the thickness is larger. Consequently the maximum absorption is found also with smaller patch sizes (Fig.4 again). For a fixed top layer's thickness, once the maximum absorption is reached, it decreases nearly exponentially with the increase of the top layer's patch size, as opposite to the tendency observed for the double-peak response. As a result of all these, the absorption decreases with thickness, also contrary to the previous double-peak resonance behaviour.

The observation of one peak is possible due to the dimensions we have chosen and the consequent matching of the structure.
The transformation into one peak is however not maintained in all top layer thicknesses: for thickness 0.4 and 0.5mm with the increasing patch size two peaks can be distinguished at some points and then one peak is observed again (see Fig.9).Again the possibility of having one peak with two metallic resonators is proved to be dependant on the structure's parameters.

The slope in the decrease of the bandwidth is smaller with thicker top layer thicknesses (Fig.5).

3.4.1.3 Singularities of bandwidth from one through two peaks

Because the absorption increases with patch size and thickness while we are in the double-peak region, the patch size at which a continuous spectrum can be identified is also smaller with thickness (comparatively at all reflectivity levels registered, see Fig.5) and consequently, because the resonances will be more separated in frequency, the maximum absorption bandwidth is larger with an increasing thickness.
The bandwidth of the single peak is for many sets of parameters larger than the one of each individual peak when resonances are separated in frequency. This occurs even when all reflectivity levels are comparable (for instance in 0.2mm-thickness, for a patch size close to 8.3mm, who's reflectivity is -16 or -17dB, and any patch size between 7.5 and 8mm)

3.4.1.4 Some conclusions for variation of parameters with a fixed bottom layer thickness of 0.2mm

The tendencies of absorption performance were practically reversed when a natural limit in the size of resonators was trespassed (for instance less absorption with a thicker substrate), which could be used for special needs in periodic materials applications. Also the tendency towards stabilization of the absorption value in this region could be utilized for applications that need to maintain an absorption level with a patch size that can only change within certain limits. There was no reversion for the interval chosen to vary the top layer's thickness. In fact we performed some isolated simulations with a top layer thickness of 0.7mm for some bottom layer thicknesses and the tendency of growth in absorption was still observed.

Also with a very simple and thin multiple-layer structure, while well matched, we can still obtain very high absorption levels (99% and more for -20dB , -30dB). The trade-off for those peaks is a low bandwidth, as it drops generally towards the -20dB. While we find high absorption levels, overall bandwidth levels are not high, being the best one around 800MHz at -6dB for thickness 0.5 mm (9.63% for a mean resonant frequency of 8.3GHz) among the maximum bandwidths found for each thickness, as mentioned in the last section. The highest bandwidths can be found generally around the patch sizes where the single peak can be distinguished and for reflectivity level -6,-8 and -10dB.

3.4.2 Results for a bottom layer thickness of 0.5mm

These are the results when the bottom layer thickness is 0.5mm and the top layer thickness and patch size are varied in the same way as for a bottom layer thickness of 0.2mm in section 4.1:

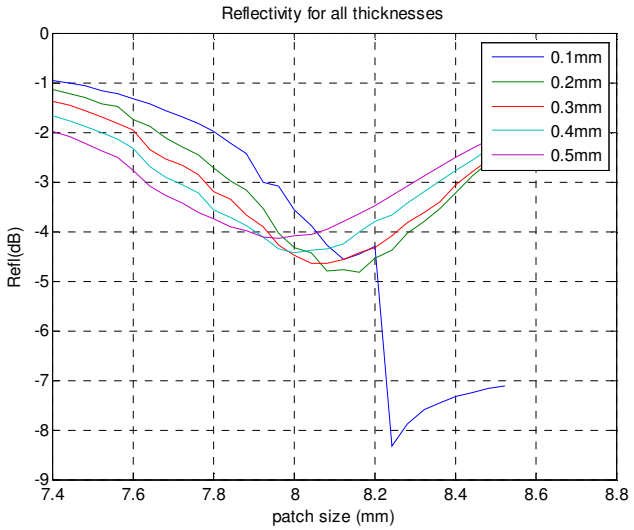

Fig. 10. Reflectivity for the same variation of parameters with bottom-layer thickness 0.5mm.

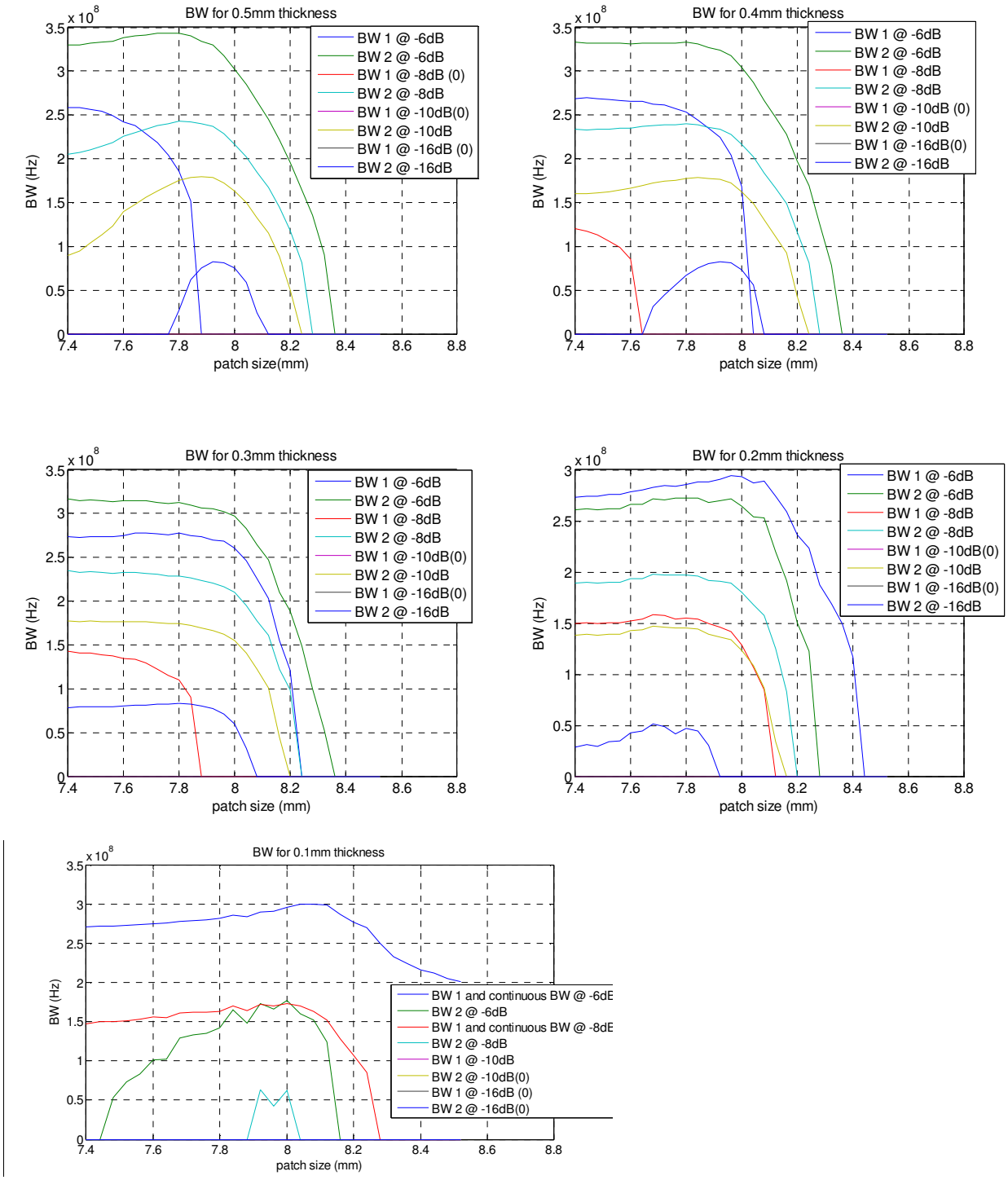

Fig. 11. Absorption bandwidth for some top layer thicknesses with a bottom-layer thickness 0.5mm.Colours indicated with zero actually correspond to peaks that do not reach a detectable bandwdith at the reflectivity levels referenced.

The first difference that we observe with respect to a bottom layer thickness of 0.2mm just by observing the absorption capability of the structure is that a single peak is not achieved with all top layer thicknesses, only for a top layer thickness of 0.1mm.The reflectivity levels of each separated resonant peak and their proximity in frequency do not achieve reflectivity levels in the "merging point" as low as with other bottom layer thicknesses and thus a single peak is not easily achieved in this case. This is reflected in the fact that reflectivity levels are never lower than -8dB as opposite to reflectivity levels with a bottom layer of 0.2mm, this is, the overall absorption decreases with bottom layer thickness of 0.5mm.In general terms an

overall increase in the absorption capabilities could have been expected with the thicker bottom layer, as a thicker top layer leads to an increase in absorption capabilities for the double-resonant response. Still the absorption's behaviour follows tendencies analogous to the ones with a bottom layer thickness of 0.2mm with patch size and top layer thickness increase. However the "stabilization region" identified for bottom layer 0.2mm for the last and largest patch sizes cannot be clearly identified here.

The bandwidth is not increased either, bandwidth levels are in general all smaller than with a thinner bottom layer thickness (less than 400 MHz). As with a bottom layer thickness of 0.2mm they all tend to decrease at the end but the slopes are very different, there are no sudden increases as the single peak is barely present. Still the tendency of the bandwidth levels for patch sizes that are far smaller than the bottom layer's fixed patch size is the same for bottom layer 0.2mm and 0.5mm, the slopes of the curves indicate very slight increases.

3.4.3 Results for a bottom layer thickness other than 0.5mm

For bottom layer thicknesses of 0.1 and 0.3 mm, with patch size and top layer thickness' increase, absorption's behaviour tends to be analogous to the one observed with bottom layer thickness 0.2mm again, although for bottom layer thickness of 0.3 mm absorption levels are in general lower after the single peak is reached with respect to the ones of bottom layer 0.2 mm.
With a bottom layer thickness of 0.1 mm all top layer thicknesses reach the single peak. Also for all top layer thickness absorption again increases and decreases after the patch side-length approaches 8.2mm and reaching the single peak.

3.4.4 Further comments for variations in geometrical parameters

The increase in bandwidth level is larger with the single peaks (when single peaks are reached for the different top layer thicknesses), this is, for all the patch sizes where the single peak has been reached, as the bandwidth increase for both resonances is added. The increase of bandwidth in individual peaks, this is when both resonant peaks are clearly separated, is not so notorious, being their bandwidth levels more comparable and increases sometimes of only 50MHz.

Regarding absorption, coherently as bottom layer thickness increases there are less single peaks achieved and its maximum value also decreases. It can clearly be appreciated that with a thinner bottom layer the number of top layer thicknesses or parameter sets for which a single-peak can be observed increases. It is confirmed that indeed the single peak with two resonators is not observed for all thicknesses.

There is a clear change of tendencies when the bottom layer thickness 0.5mm where with only one top layer thickness the single peak is observed. The fact that with only one top layer thickness the single peak is reached indicates that absorption levels are really much smaller than with other bottom layers and if the bottom layer is increased more than 0.5mm the single peak will not be observed at all. It is as expected, another limit as it happens when patches are almost equal in size.

Differences in performance tendencies between top and bottom layer thicknesses can be attributed to the physical mechanisms underlying absorption mentioned in [1] and in the

"Multi-layer" section. They indicate that with a double-layer structure, for a higher frequency both layers instead of only one contributed to a greater extent to resonance. Both layers contribute differently to resonance and absorption, thus changes in one or the other layer can affect the performance of the absorber differently. And obviously the fact that the patch in only one of the layers is varied has a major influence.

3.5 Variations in the characteristics of the dielectric material

Next we will consider an increase of the losses and of the dielectric constant in the dielectric material. Geometrical variation of the parameters has been maintained for comparison purposes with variations with standard material characteristics. We intend to observe changes on the performance of the absorber when its material parameters are changed and whether the geometrical changes affect the performance similarly when different materials are used.
We will display and comment results obtained with a bottom layer thickness of 0.5mm and 0.2mm. We chose one bottom layer thickness in the limit of the variation interval and a bottom layer thickness inside the limits of the interval as reference. With standard material parameters at a bottom layer thickness of 0.5mm a limit could be established in the increasing tendency of the structure's performance, above all in bandwidth. It would be interesting to see whether it is possible to increase the presence of single peaks with this bottom layer thickness and the limit in performance extended.

3.5.1 Change in the loss tangent

As mentioned before the loss tangent chosen was tg(δ)==0.04, almost twice the standard loss tangent of FR4.This is the only parameter changed in the dielectric material.
Overall levels of absorption do not show a considerable increase with the larger loss tangent, this is observed above all in the maximum values with the current and the standard loss tangent.
With a bottom layer thickness of 0.2mm the absorption indeed does not strike as increased with respect to levels obtained with a loss tangent of 0.025 above all because the maximum values are not larger with tg(δ)=0.04, but the slope in the region where the two resonant peaks are separated is slightly larger (due to closer positioning of the peaks in frequency or larger absorption of each peak). For a top layer thickness of 0.5mm the slope with patch size is notably smaller with respect to tg(δ)=0.025, thus absorption levels are higher for the largest patch sizes.

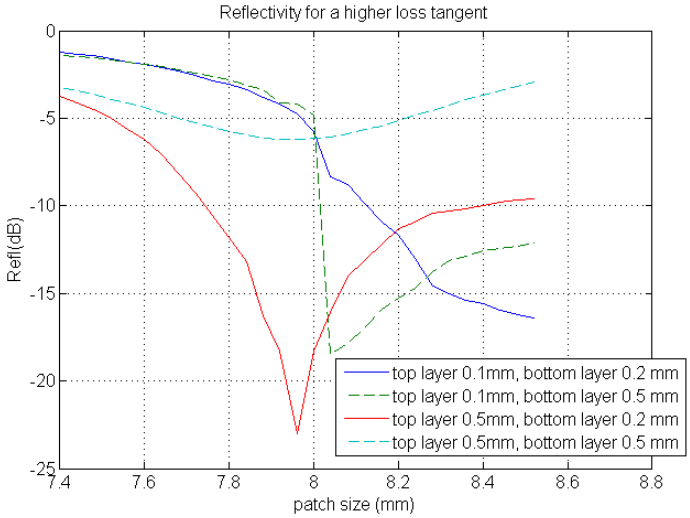

Fig. 12. Reflectivity curves with a more lossy dielectric with loss tangent=0.04 for the indicated top/bottom layer thicknesses.

With a bottom layer thickness of 0.5mm the variation of reflectivity is very similar to the one observed with tg(δ)=0.025.With a top layer thickness of 0.5mm the single peak is not observed, as well it could not be observed with a loss tangent of 0.025.
Only with a top layer thickness of 0.1mm after the single peak has been reached is absorption really considerably larger (about twice the value with loss tangent 0.025) and also the slope in the separated double resonant region is larger, causing the patch size where the single peak is reached to be smaller.

It is observed that the bandwidth varies in a quite similar way with the new loss tangent than it does with loss tangent 0.025, that is, with patch size increase both resonant peaks increase, decrease and shift in frequency in a quite similar way. This accounts for having again two bandwidths -one for each peak- that become one bandwidth at a certain patch size.

It observed that the bandwidth levels increase with the larger loss tangent in the dielectric, and again above all after the single peak is observed, as it happened with a larger thickness when only geometrical parameters where varied. With the larger loss tangent the increase is enhanced, as expected, with increases of nearly 200MHz with respect to the levels with tg(δ)=0.025 at the maximum values of reflectivity levels of -6 and -8dB , with top layer thickness of 0.5mm.

The bandwidth variation with bottom layer thickness of 0.2mm and top layer thickness 0.5mm is very similar to the one with loss tangent 0.025, but the bandwidth levels are considerably higher with loss tangent 0.04. For the maximum values at -6 and -8dB the increase is of nearly 200MHz.

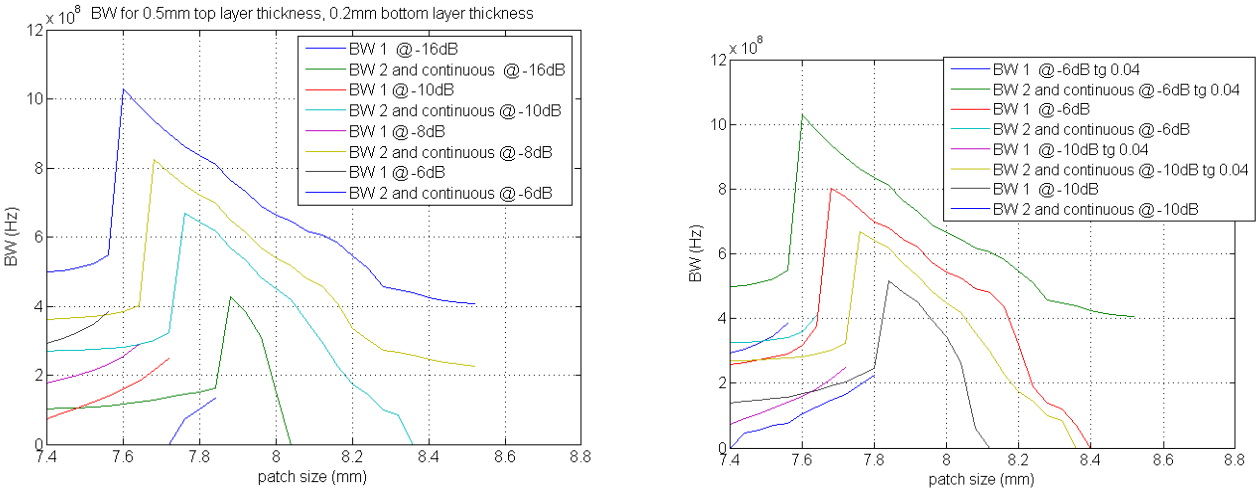

Fig. 13. Left: Absorption bandwidth for the referenced top and bottom layers. Right:Comparative graph at the indicated reflectivity levels with a loss tangent of 0.04 and a loss tangent of 0.025. It shows that almost the same difference in bandwidth levels is maintained for all reflectivity levels registered.

With a top layer thickness of 0.5mm bandwidth variation is quite similar too in comparison with a loss tangent of 0.025, except for the sudden steep increase and decrease at-6dB, and there is again an increase in bandwidth, which in the case of -6dB is of about 100MHz. The absence of a single peak as in past cases is probably causing the increase not to be very large with respect to a loss tangent of 0.025.

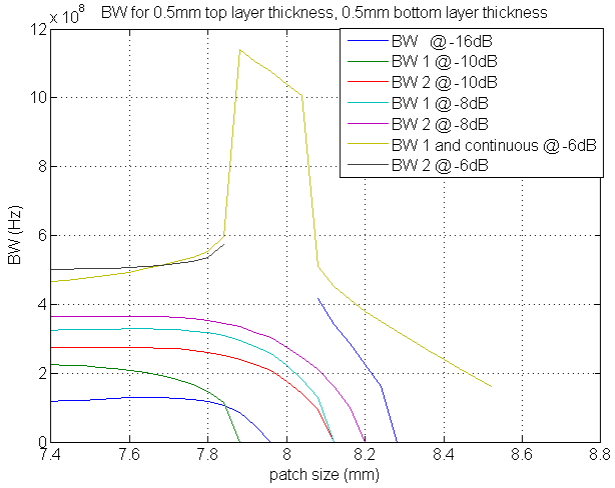

Fig. 14. Absorption bandwidth for top and bottom layer thickness of 0.5mm, with loss tangent=0.04.

The sudden steep increase and decrease mentioned before are to account for the absorption being slightly larger than the one of loss tangent 0.025 at and around the maximum value of the absorption curve for this top layer thickness. For the patch sizes in this region, where the bandwidth suddenly increases, there is a single peak only at -6dB (instead of two bandwidths there is only one).Then the absorption decreases and we have two bandwidths again.

3.5.2 Change in the dielectric constant

A new dielectric constant epsilon=7.8 higher than the standard one of FR4 (epsilon=4.3) is chosen for the dielectric substrate of both layers. Standard FR4 loss tangent tg(δ)=0.025 and the rest of the electrical parameters are left unchanged. We chose a higher dielectric constant with the expectation of observing some of the effects achieved by the nowadays very much used high-k dielectrics. 7.8 is comparatively higher than the standard FR4 dielectric constant. Dupont substrates are offered with a permittivity of 7.8 but in many cases measured at lower frequencies than the permittivity of FR4.
The frequency responses of S11 shift their operational frequency considerably with respect to the one obtained with epsilon=4.3, from a range of approximately 7-9 GHz for epsilon=4.3 to 5-7GHz for epsilon=7.8.

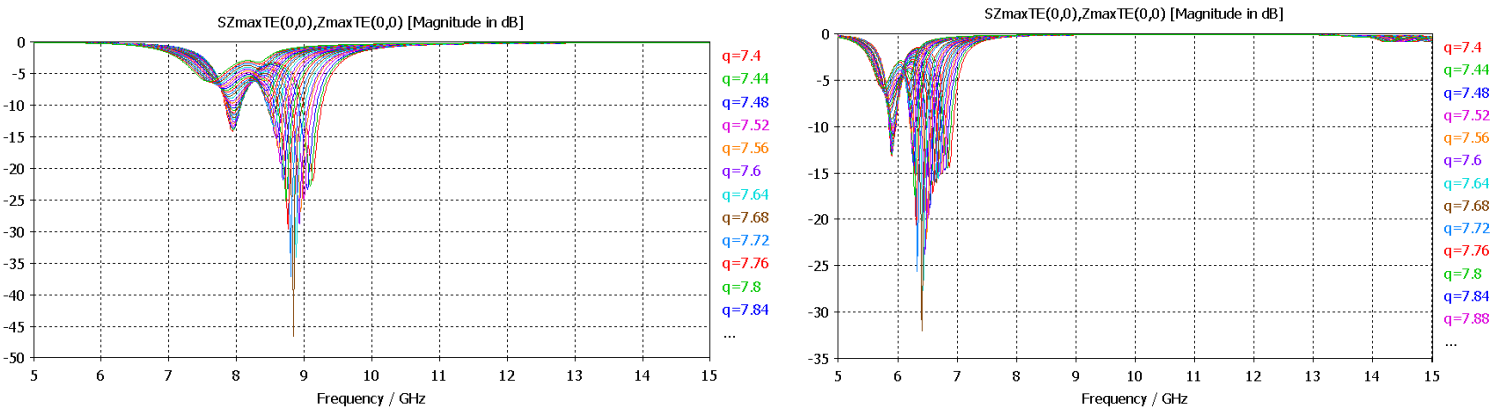

Fig. 15. S11 graphs for top and bottom layer thickness 0.5mm .Left:.for loss tangent 0.04. Right: for permittivity 7.8.

It is easy to observe that reflectivity curves with the higher epsilon vary again in a comparable way with respect to the curves with a loss tangent of 0.04, and absorption levels are lower. For a bottom layer thickness of 0.5mm again only with a top layer of 0.1mm the single peak can be observed. The patch size where the single peak can be observed is again similar to the one with loss tangent 0.025 but the absorption after this point is specially larger than with this loss tangent. For a top layer thickness of 0.5mm absorption levels are very similar.
With respect to a loss tangent of 0.025, with a bottom layer thickness of 0.2mm and a top layer thickness of 0.5mm, before the single peak is reached the slope of the curve is smaller and the patch size where the single peak is reached is larger. After this point the absorption with a higher epsilon is again slightly larger, particularly for the last patch sizes. With a top layer thickness of 0.1mm absorption is overall smaller in comparison with the absorption using a loss tangent of 0.025.

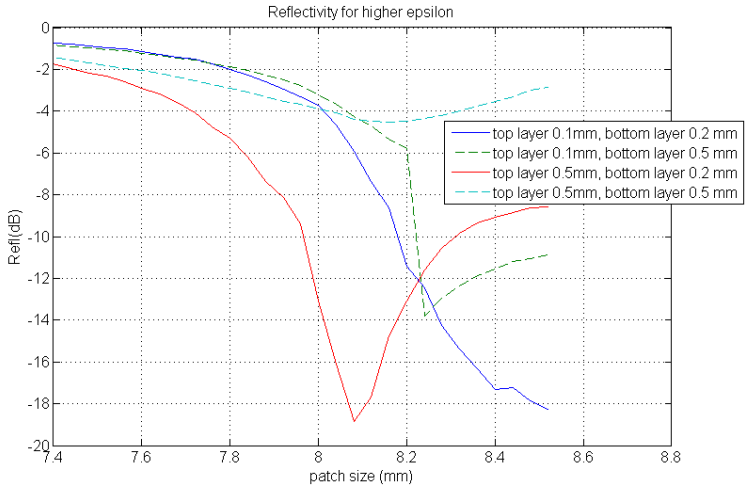

Fig. 16. Reflectivity curves for a dielectric with a higher permittivity (=7.8) for the indicated top/bottom layer thicknesses.

As opposite to what was observed with tg(δ)=0.04, with a higher dielectric constant the bandwidth is not increased in general: The variation of bandwidth is again similar to what has been observed with loss tangent 0.025 and 0.04, but bandwidth levels with the higher dielectric constant are in general considerably smaller than with loss tangent 0.025. This is observed with a bottom layer thickness of 0.5mm, although the decrease in bandwidth levels is not so strong with higher absorption levels. With a top layer thickness of 0.5mm the sudden large increase of bandwidth at -6dB observed with a loss tangent of 0.04 is not present with the higher epsilon, as the absorption level is comparably lower. And again with lower absorption levels the decrease in bandwidth is more evident with this top layer thickness**.**

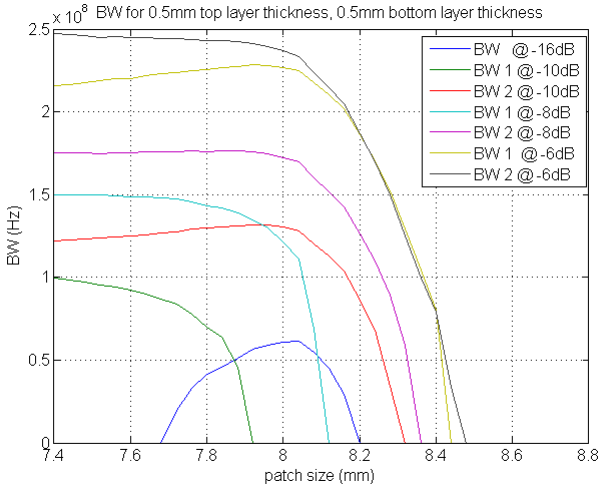

Fig. 17. Absorption bandwidths for bottom layer thickness of 0.5mm, top layer thickness 0.5mm, with permittivity =7.8.

With a bottom layer thickness of 0.2mm and a top layer thickness of 0.5mm at -6dB the decrease with respect to the levels with loss tangent 0.025 is more than 200MHz at the maximum value. The slightly different behaviour and increased values of absorption for the

single peak in the results with the higher epsilon and loss tangent 0.025 are to account for the peaks in -16dB to be detectable with the higher epsilon.

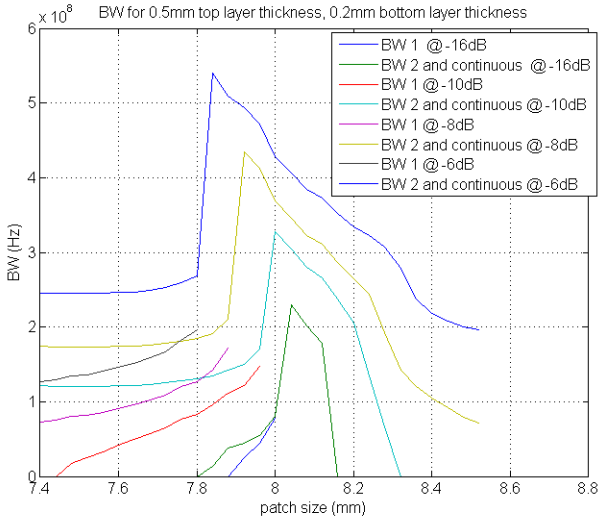

Fig. 18. Absorption bandwidths for bottom layer thickness of 0.2mm , top layer thickness 0.5mm, with permittivity =7.8.

3.5.3 Comments and conclusions for changes in the dielectric material

The same tendencies of bandwidth and absorption increase and decrease could be observed with the variation of geometrical parameters and the changed material parameters, in comparison with the original material parameters, for fixed bottom layer thicknesses and in general different bottom layer thicknesses (this is within the same top and bottom layer thickness variation limits).
For the limit parameters of top and bottom layer thicknesses of 0.5mm the peaks did not merge together in a single peak but the bandwidth increase was noticeable and considerable with the higher loss tangent although there were only separated resonant peaks. Also with a top layer thickness of 0.5mm the slight increase of absorption causes the "single peak" at -6dB to be observed, but besides this there are no dramatic changes on the tendencies for this combination of parameters at the limit of the variation interval.

While the absorption levels with a higher loss tangent were not always clearly higher, although increases in some regions can be confirmed, bandwidth is clearly and interestingly higher with more losses in the dielectric, as it was expected. For instance with bottom layer thickness of 0.2 mm, top layer thickness 0.5mm with a patch size of 8mm absorption with a higher loss tangent is even smaller (less than 20dB in absolute value) but bandwidth is about 200MHz larger at reflectivity levels of -6dB and -8dB.
For most cases there is no clear trade-off bandwidth-absorption (more bandwidth is at the expense of less absorption).

Results with a higher dielectric constant evidence a decrease of about 2GHz in range in the operational frequency of the structure. The use of a material with a higher permittivity in a parallel plate capacitor would increase its capacitance without modifying the distance between the plates (or thickness of the dielectric material). Thus the effect on the electrical system analyzed would be the same as if we reduced its thickness. Our structure, at least in a one-layer case, could be compared to a parallel plate capacitor model. We did observe a slight

decrease in operational frequency with thinner top layer thicknesses and as reducing thickness would have the same effect on the system as an increase of the dielectric constant, the shift of operational frequency observed could partly be caused by the increased dielectric constant. The frequency shift observed with decreasing top layer thickness was small but only one layer was modified, here both layers have a material with a higher dielectric constant, thus two series capacitors which would enhance the effect.
Also and more directly, the resonance frequency f_m for such a patch structure would be $f_m = 1/\sqrt{LC} \sim \frac{1}{a}$ with *a* the side-length of the patch (from [23]), thus indeed if we increase the capacitance of the structure, the resonance or operational frequency would be reduced.
This could also be consistent with the decrease in bandwidth observed, that will be commented next (we observed a decrease in bandwidth when substrate thickness was decreased), but the decrease in operational frequency has to be taken into account also for the calculation of relative bandwidth (we would not be able to center the frequency at 8.3GHz anymore for this purposes, as it would be outside the new range).

As mentioned before, bandwidth does not increase in absolute levels but rather decreases in most cases , but also the operational frequency decreases. So for instance if we take the maximum bandwidth level at -6dB for a top layer thickness of 0.5 mm and bottom layer thickness of 0.2mm., which is around 550MHz, with a reference centered frequency of 6.3GHz, the relative bandwidth would be of 8.7%, whereas for the same top and bottom layer thicknesses at the same reflectivity level and maximum value with a dielectric constant of 4.3 and a loss tangent of 0.04 we would have a bandwidth of nearly 1GHzwith a centered frequency of 8.5GHz, thus 11.7%. With permittivity 4.3 and loss tangent 0.025 the comparable value would be 800MHz at 8.3GHz, thus 9.6%.Thus bandwidth is still relatively smaller, although not as much as it would be with a higher operational frequency.

Absorption is in general lower than with loss tangent 0.04 or at least comparable with a loss tangent of 0.025 (and permittivity of 4.3 in both cases), although for top layer thickness of 0.1mm, bottom layer 0.5mm after the single peak has been reached absorption is much larger with the higher permittivity in comparison with permittivity=4.3, loss tangent=0.025.
For the bottom layer thickness of 0.5mm (a limit parameter) no special dramatic changes could be observed, there is only an increase with top layer thickness 0.1mm, but still no single peak was observed with a top layer thickness of 0.5mm, as it was coherent and expected.

3.6 Validation of previous simulations

Previous simulations with CST were validated by means of a second solver, HFSS, and measurement of two samples corresponding to two different kinds of responses.

3.6.1 Experimental validation: measurements

It was requested to fabricate and measure the response of two samples of our configuration. We fabricated and measured a sample with parameter values corresponding to a single-resonant response and one with parameter values corresponding to a double-resonant response.
Basically an open or a closed system (sample is measured inside the waveguide) could be used to measure the absorption capacity of the samples. A closed system as the one used in [7] was chosen, presumably less losses would occur in such a system and less noise should be

present in the measurements. This kind of measurement setup determines considerably the characteristics of the sample, for instance restricting its size (thus number of unit cells). Also smaller samples are typically used in closed systems. In our case this meant that the sample had to have a size of exactly two unit cells, once the side-length of our unit cells was reduced from 11 mm to 10 mm. This did not affect the simulations' results in a perceivable way. It is worth mentioning that the unit cell side-length of 11 mm is less than one third of the wavelength, thus a periodic array of these unit cells could be considered as effective media.
The samples fabricated have thicknesses that are sub-wavelength: a 0.8 mm-thick sample in the case of the double-resonant response, thus less than a sixth of the wavelength, and a 1.6 mm-thick sample for the single-resonant response, around a third of the wavelength.

In our case only a closed waveguide -instead of two- connected to the available Network Analyzer (PNA-X) to measure the S11 response was necessary. Most waveguides available in our research group could be used in the range 8-12 GHz and this was compatible with the responses of our configuration. A standard waveguide with its corresponding dimensions for X band ([24]) was used, suitable for the responses of our designs. The waveguide is directly connected to the flexible test port cables (2.4 mm, 85133-60016) of the Network Analyzer through a 2.4 mm to 3.5 mm connector.

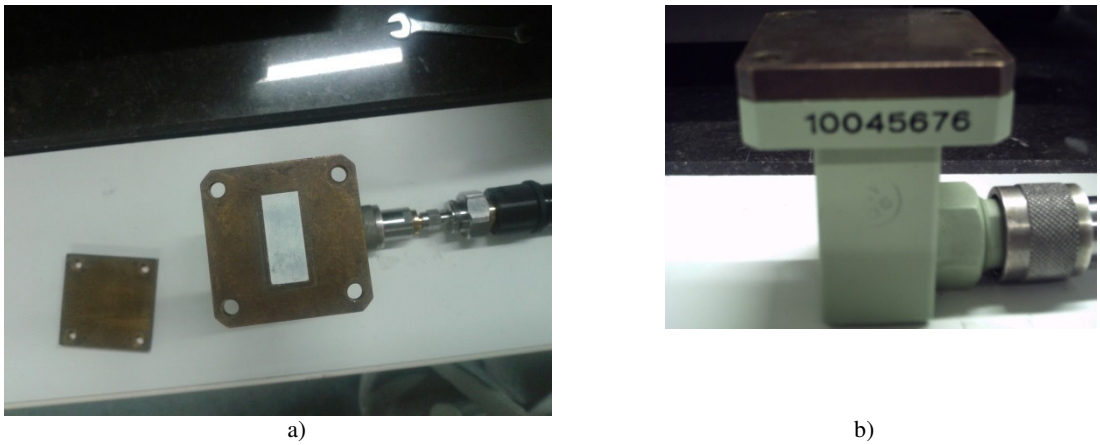

a) b)

Fig. 19. a) Photograph of the measurement set-up , showing the waveguide opened viewed from above, so that the sample inside it can be appreciated.The connector and part of the cable connecting to the network analyzer can be seen as well. b) Waveguide viewed from the side.

Due to the fact that our configuration has a metallic back-plane that prevents transmission (T=0), only S11 parameters had to be measured to observe the absorption performance of the samples.

For the double-resonant response the set of parameter values originally selected is a 0.5 mm-thick layer of FR-4 dielectric with a square copper patch of 7.4 mm-side length on top. Both of them are on top of a 0.2 mm-thick layer of FR-4 dielectric with a square copper patch of 8.2 mm-side length on top of this second layer. For the single-resonant response both FR-4 dielectric layers are 0.8 mm-thick, with the copper patch on top of all layers having a side length of 7.88 mm and the copper patch on bottom having a side length of 8.2 mm. The copper used is 0.03 mm–thick.
The previous originally selected values had to be modified due to fabrication and measurement set-up restrictions, being the final nominal values for the double-resonant

sample a top patch side-length of 7.40mm, a bottom patch side-length of 8.2mm, a top layer thickness of 0.523 mm and a bottom thickness of 0.163 mm. This design was fabricated in Eurocircuits, silver plated copper was used for the patches (Eurocircuits) and the standard dielectric for multi-layer PCBs (laminate and prepeg). For the single-resonant sample fabricated at CDE the top patch side-length was of approximately 7.80 mm, the bottom patch side-length of approximately 8.07 mm (see clarifications in next paragraphs), and top and bottom layer thicknesses of 0.8 mm.
The sample's design can be seen in figure 20.

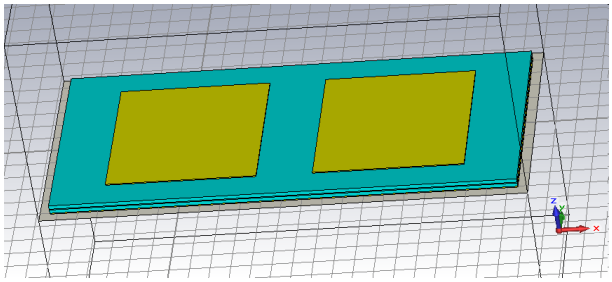

Fig. 20. Scheme of the sample's design to be fabricated.

It is also worth noticing that the fabrication of the double-resonant sample was outsourced and manufactured in one piece, while the single-resonant sample (in-house manufacturing) was fabricated in two pieces, which offered more difficulties when mounted in the measurement set-up. The resulting sample that was outsourced had a much better finishing in comparison with the fabrication of the single-resonant sample (non-square patches with varying side-length, unparallel patches and PCB's edges as depicted in figures 21 and 22, irregular finishing of edges only slightly improved with sanding).

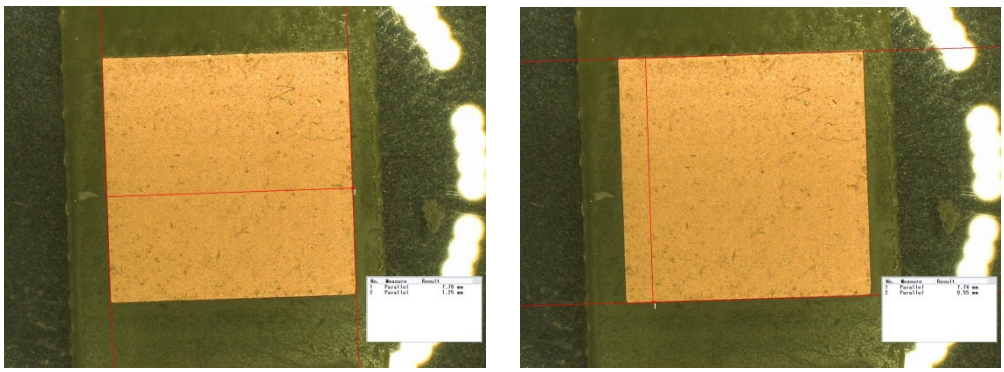

Fig. 21. Microscope photographs of the top patches fabricated by in-house manufacturing. Variation of side-length was from 7.78 to7.74 mm.

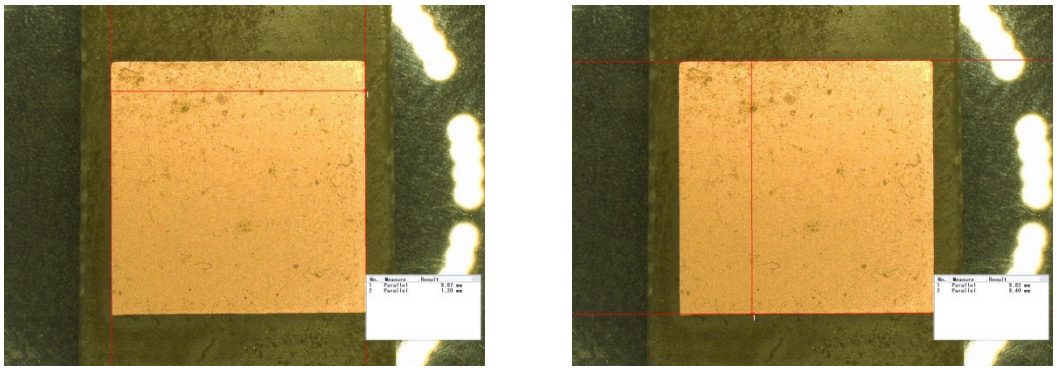

Fig. 22. Microscope photographs of the bottom patches fabricated by in-house manufacturing. Variation of side-length was from 8.02-.8.07 mm.

The results for the double-resonant response are shown in figure 23.

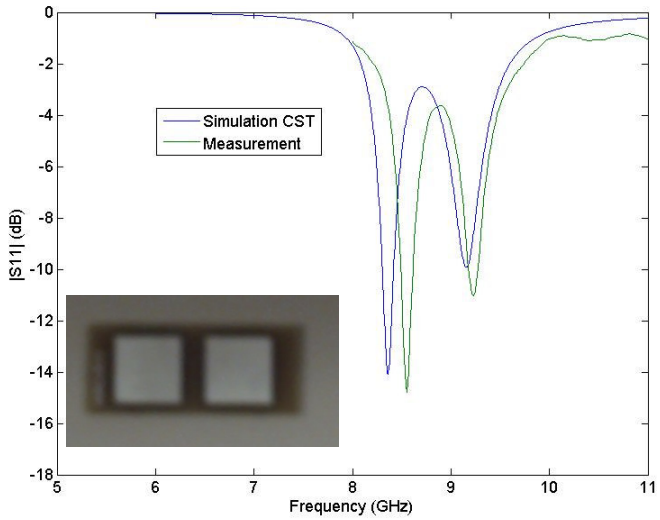

Fig. 23. Simulation and measurement results for a top patch size 7.40mm, bottom patch size 8.2mm, top layer thickness 0.523, bottom layer thickness of 0.163 mm,. Fabricated in Eurocircuits.

We obtain both resonances predicted in the simulations, with absorptions close to 97% and of more than 90%, at frequencies that were very close to the ones predicted in the simulations as well.

The results for the single-resonant response are shown in figure 24.

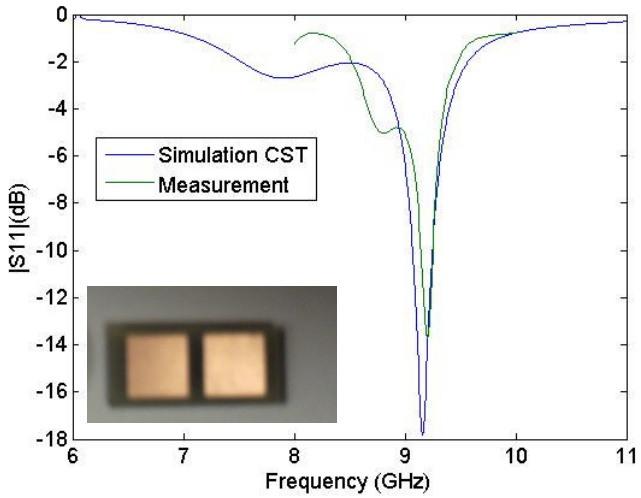

Fig. 24. Simulation and measurement results for a top patch size approx. 7.80 mm, bottom approx.8.07, top and bottom layer thicknesses 0.8 mm. In-house fabrication at CDE.

The result for the single-resonant response has an absorption close to 96% and the resonant frequency is again very close to the one predicted.
Results observed were as expected nearly noiseless, very precise, highly absorptive and polarization-insensitive for normally impinging waves. The essential features of the frequency responses were validated.
Through these results it was possible to observe that two different types of responses observed in the simulations could indeed be obtained.
In addition to this we can say that the agreement between measurement and simulation for the double-resonant response is very good and limitations in the manufacturing of the single-resonant response sample did not seem to have had a relevant negative effect in its measurement results.

3.6.2 Benchmarking with second electromagnetic solver

Before running simulations in HFSS, the electromagnetic model of our configuration was built in this solver as similarly as possible with respect to CST.
More than 100 parameter sets (samples) distributed over the original range of simulations were ran in HFSS and these simulations' results processed.

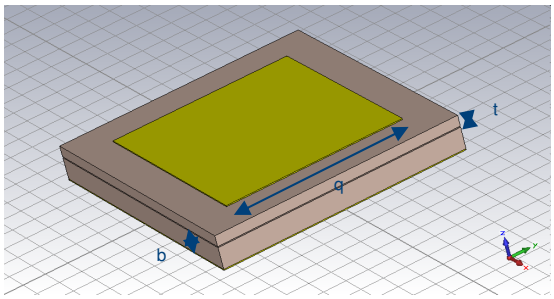

Fig.25 Configuration of the unit cell used and the variable parameters in it: top patch side-length q, top layer thickness t, bottom laver thickness b.

The S11 responses of both solvers were compared one by one. Next, part of the total amount of responses is shown comparatively in both solvers, for the thinnest and thickest top layer thicknesses (1st and 2nd column respectively) and the smallest and largest patch sizes (1st and 2nd row respectively) of our original range of variations.

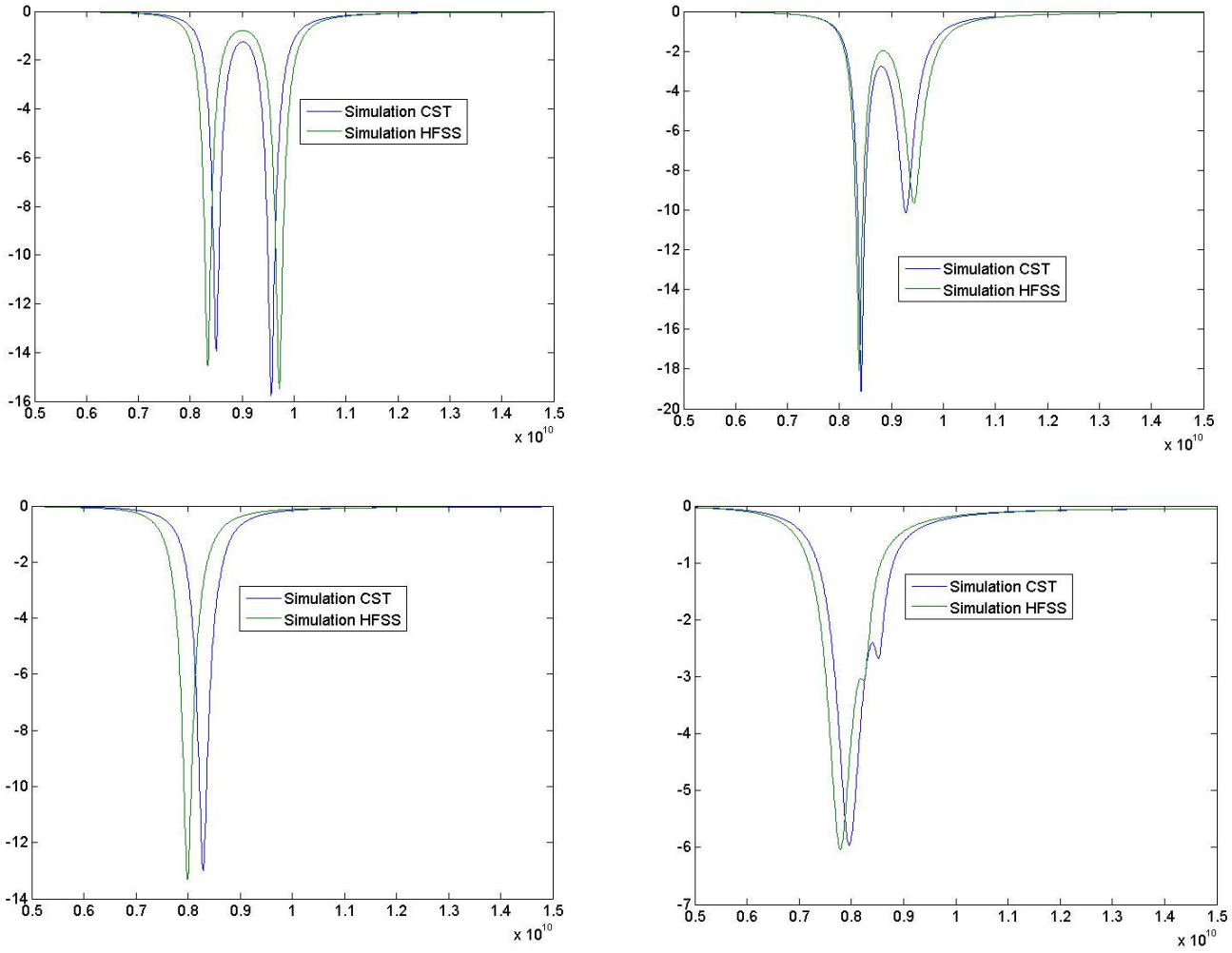

Fig. 26. Samples for a bottom layer thickness of 0.2 mm. 1st column corresponds to top layer thickness of 0.1 mm, 2nd to 0.5 mm. In both columns the figures on top correspond to top patch side-length=7.40 mm, figures on bottom to a top patch side-length=8.52 mm. Coordinate axis (S11 response) is shown in dB, frequency (abscissa) is shown in Hertz.

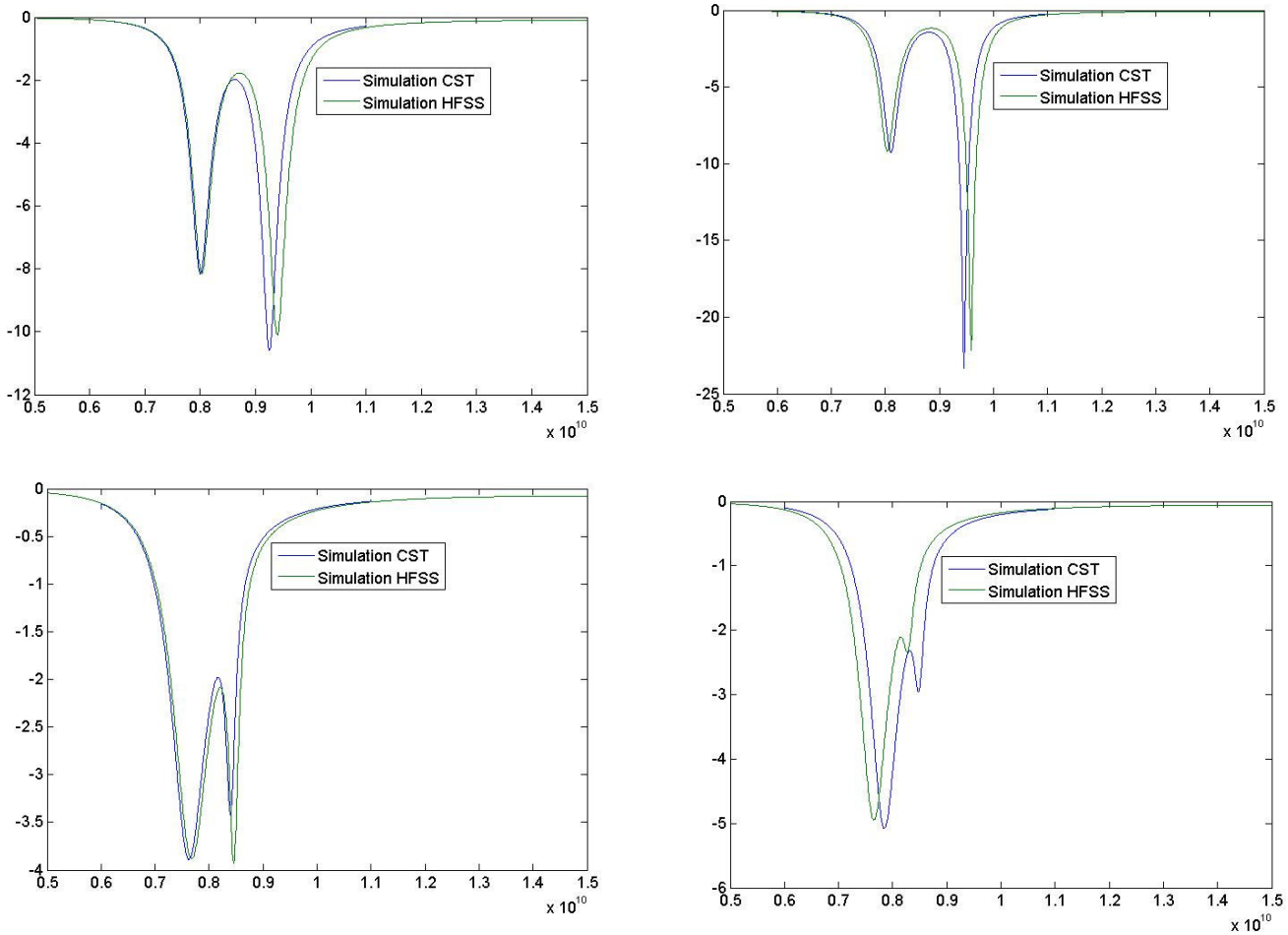

Fig. 27. Samples for a bottom layer thickness of 0.5 mm. 1st column corresponds to top layer thickness of 0.1 mm, 2nd to 0.5 mm. In both columns the figures on top correspond to top patch side-length=7.40 mm, figures on bottom to a top patch side-length=8.52 mm Coordinate axis (S11 response) is shown in dB, frequency (abscissa) is shown in Hertz

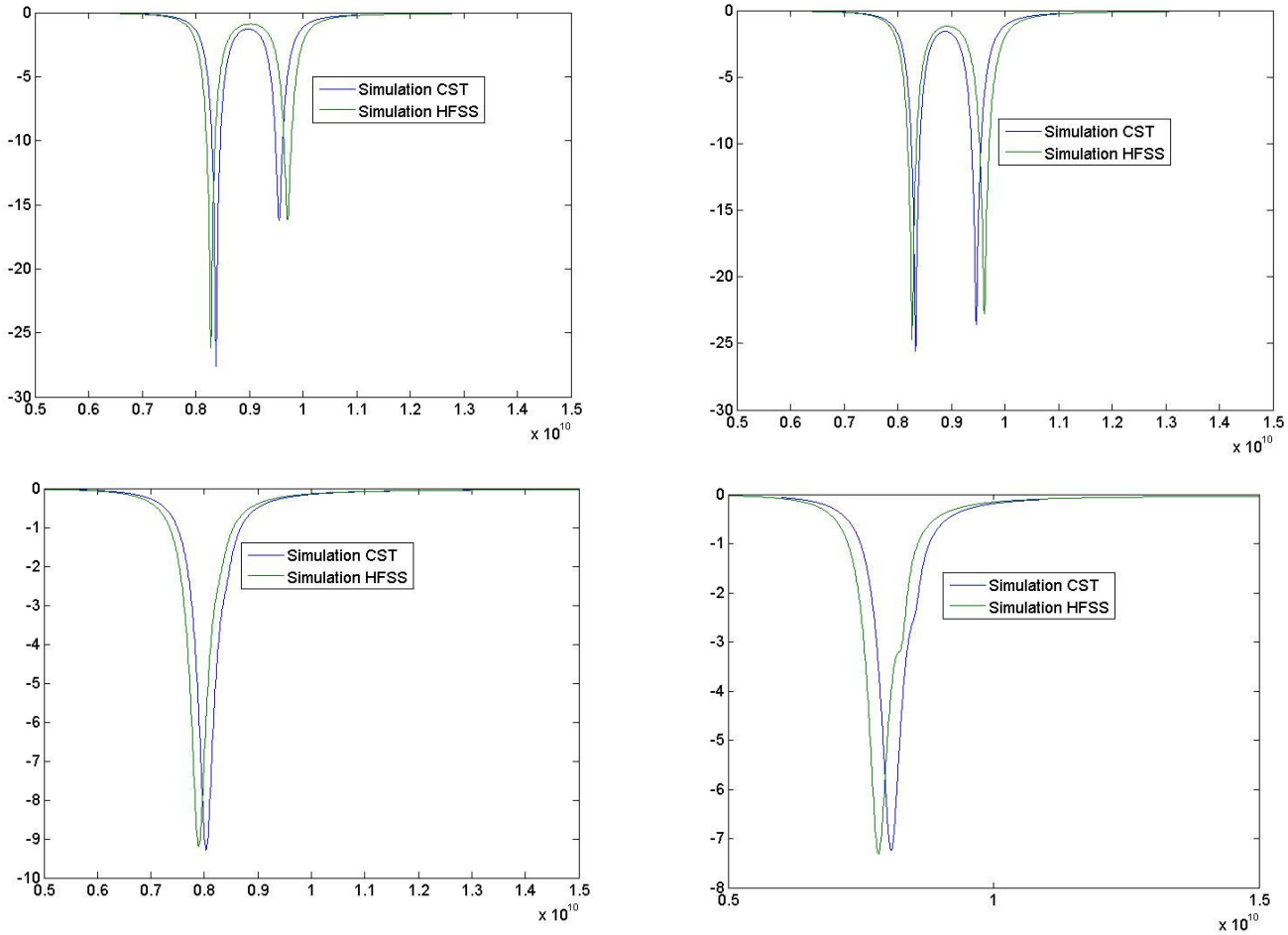

Fig.28. Samples for a bottom layer thickness of 0.3 mm. 1st column corresponds to top layer thickness of 0.1 mm, 2nd to 0.5 mm. In both columns the figures on top correspond to top patch side-length=7.40 mm, figures on bottom to a top patch side-length=8.52 mm Coordinate axis (S11 response) is shown in dB, frequency (abscissa) is shown in Hertz

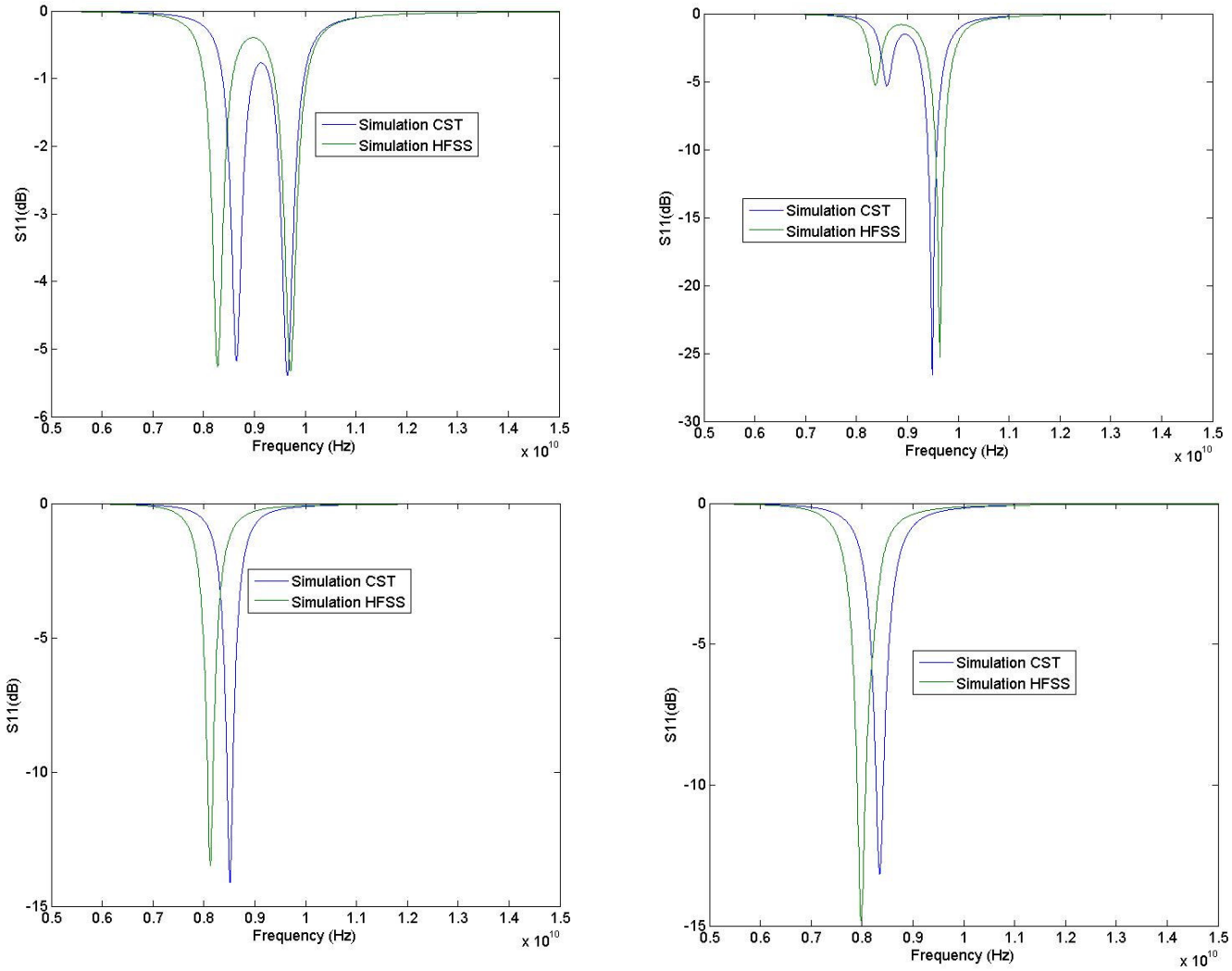

Fig.29. Samples for a bottom layer thickness of 0.1 mm. 1st column corresponds to top layer thickness of 0.1 mm, 2nd to 0.5 mm. In both columns the figures on top correspond to top patch side-length=7.40 mm, figures on bottom to a top patch side-length=8.52 mm Coordinate axis (S11 response) is shown in dB, frequency (abscissa) is shown in Hertz.

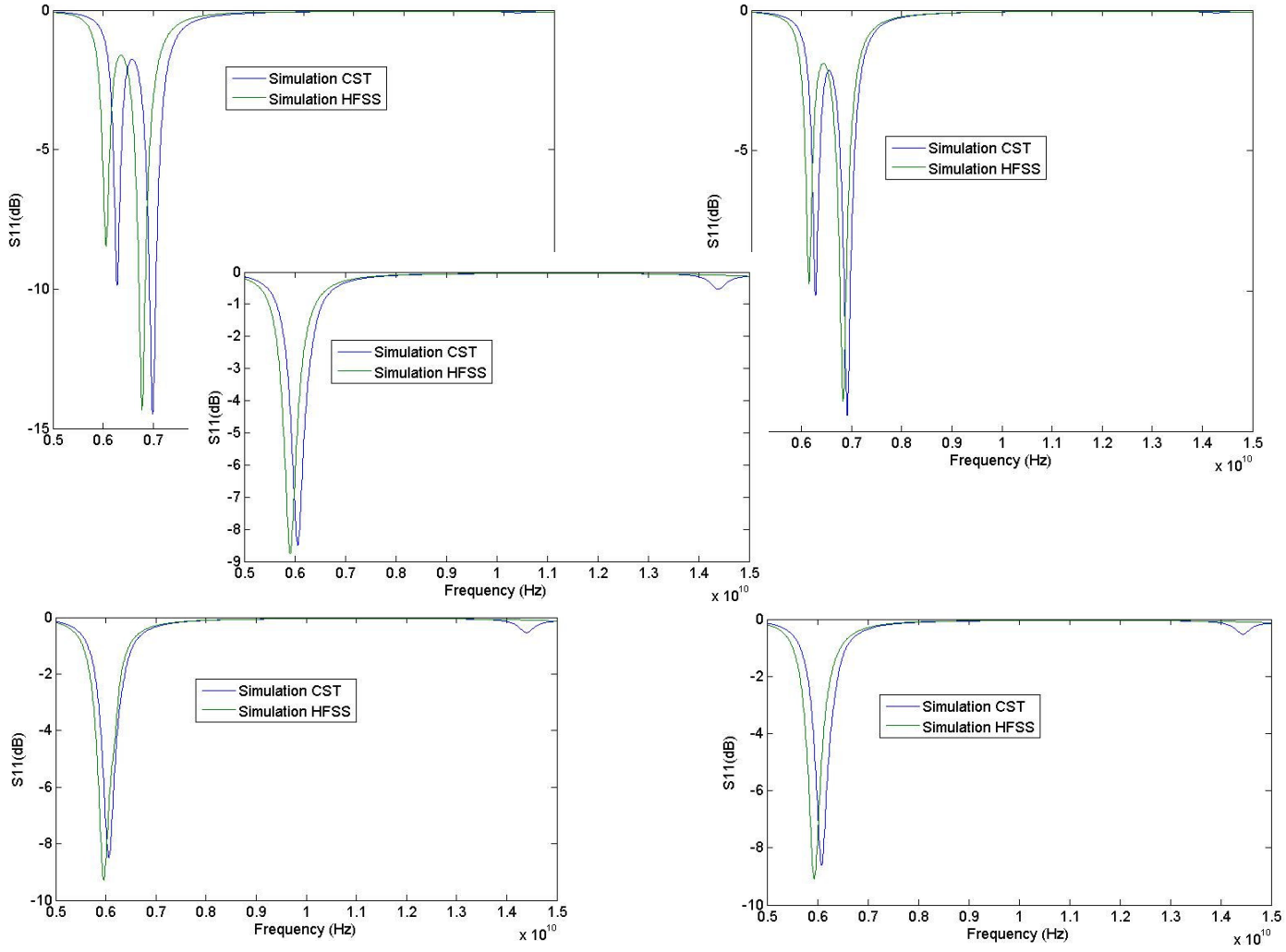

Fig.30. Samples for a dielectric with higher dielectric constant epsilon =7.8. Coordinate axis (S11 response) is shown in dB, frequency (abscissa) is shown in Hertz.

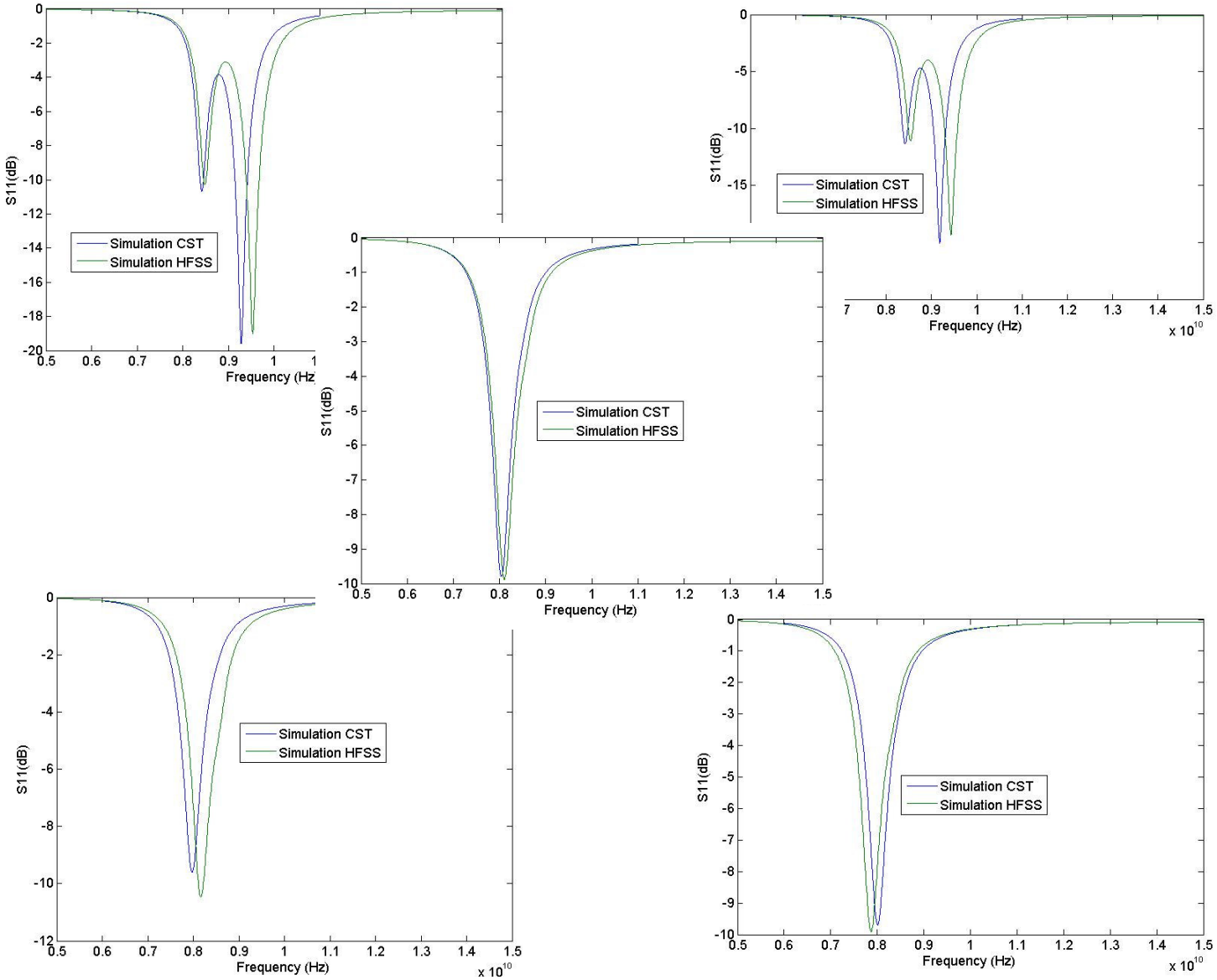

Fig.31. Samples for a dielectric with a higher loss tangent tgδ=0.04. Coordinate axis (S11 response) is shown in dB, frequency (abscissa) is shown in Hertz.

It could be observed that the agreement between both solvers was very good. Shifts between both solvers results are very small in general, to account for different solvers and consequent slightly different calculation of each parameters' combination. This provides a further validation of our previous simulations.

Additionally it has to be born in mind that a big number of current wireless technologies have operating frequency bands that are narrowband, for instance LTE bands are typically 0.1 GHz wide, ISM 2.4GHz spectrum is also typically divided in 0.1 or 0.4 GHz at the most, Bluetooth operates between 2.4 and 2.4835 GHz, among other technologies. Therefore the designs presented here, with narrowband absorption capabilities, would find good applications with these technologies, preventing radiation at very specific frequency ranges. For these specific bands our designs should be scaled first. As all planar metamaterials its small and tunable size and small –particularly small in this design- thickness makes it very suitable for the planar antennas intensively used in the previously mentioned applications, also required to be small and thin.

Eventually several layers of our designs could be added to increase the number of resonant frequencies towards a multi-band or a broader bandwidth design and as with any metamaterial, our designs could also be further scaled to fit further specific applications.

3.7 General conclusions

By only changing the multiple-layer structure's thicknesses within dimensions below 1 mm a relatively wide spectrum of variation in performance can be observed. It is interesting to observe the added effect of several simultaneous geometrical variations and the changes in the systematic tendencies of the performance they can induce.

The logical trade-off bandwidth-absorption is still maintained as calculated bandwidth diminishes for larger levels of absorption.

Also the singularities of the contribution from each layer in the performance of a multiple-layer structure are evidenced, given the physical interactions of the conductive and non-conductive between layers.
Although the use of metamaterials provides more flexibility in terms of tuning and adaptability of a structure to specific requirements, in metamaterial absorbers the characteristics of the non-conductive material still plays an important role in the general performance of the structure, above all on absorption bandwidth.

It could be also worth mentioning that with a very simple and thin multiple-layer structure, while well matched, we can still obtain very high absorption levels (99% and more for -20dB, -30dB). This can be observed for instance at a top and bottom layer thickness of 0.2 mm with top patch size 8.16 mm and 8.24. Maximum bandwidth levels are around 800MHz at -6dB, for instance for a top layer thickness 0.5 mm, bottom layer thickness 0.2 mm, top patch size 7.68 mm at -6 dB (relative bandwidth of 9.63% for a mean resonant frequency of 8.3GHz).

Besides this, the outcome of the validations provides further confidence in the results. It was important to experimentally confirm the essential features of the frequency responses produced by our configuration. Additionally the fabricated designs' very small thicknesses should provide a good angular stability as mentioned in [1] and [26], so a fairly wide-angle absorption should be observed if measured. Samples are additionally rather simple to fabricate, with fairly standard technology, which could make them more readily available and easier to acquire than conventional absorbing material. Multi-layered prototyping would be highly recommended based on these experiments' experience.

Further developments based on the designs proposed here could be very good selective filters, moreover being its small size and thickness an advantage for current electronic components that are continuously downscaling in size. Furthermore, multiple absorption or filtering can be relevant to a current need for wireless multi-band and broadband applications.

3.8 References

[1] N.I.Landy, S.Sajuyigbe, J.JMock, D.R.Smith, W.J.Padilla, "Perfect metamaterial absorber", Physical Review Letters, Vol.100, No.207402

[2] Yu Qian Ye, Jin, and He, "Omnidirectional, polarization-insensitive and broadband thin absorber in the terahertz regime",Journal of the Optical Society of America B, Vol. 27, Issue 3, 498-504, 2010.

[3] Sun, Liu, Dong, Zhou; “An extremely broad band metamaterial absorber based on destructive interference”; Optics Express,Vol.19 , No.22, 21155,2011

[4] Mias, Yap; "A varactor-tunable high impedance surface with a resistive-lumped-element biasing grid"; IEEE Transaction on Antennas and Propagation, Vol.55, No.7,2007

[5] Li, Yuan, Zhou et.al, "Ultrathin multiband gigahertz metamaterial absorbers",Journal of Applied Physics Vol.110, No.014909,2011

[6] Ding, Cui, Ge, Jin, He; "Ultra-broadband microwave metamaterial absorber", Applied Physics Letters; Vol.100; No.103506,2012

[7] Li, Yang, Liang; "A wide -angle polarization-insensitive ultra-thin metamaterial absorber with three resonant modes "; Journal of Applied Physics;Vol.110; No.063702,2011

[8] Gu, Barrett, Hand, Popa, Cummer; "A broadband low-reflection metamaterial absorber", Journal of Applied Physics700MHzol.108, 064913,2010

[9] Cheng, Wang, Nie, Gong, Xioing, Wang; "Design fabrication and measurement of a broadband polarization-insensitive metamaterial absorber based on lumped elements"; Journal of Applied Physics; Vol.111 ; No.044902,2012

[10] Shen, Cui, Zhao, Ma, Jiang, Li, "Polarization-independent wide-angle triple-band metamaterial absorber", Optics Express, Vol.19, No.10,2011

[11] Xu, Zhou, Zhang, Chen, Deng, "A wide-angle planar metamaterial absorber based on split ring resonator coupling"; Journal of Applied Physics; Vol.110; No.044102,2011

[12] Alici, Bilotti, Vegni, Ozbay; “Experimental verification of metamaterial based subwavelength microwave absorbers”; Journal of Applied Physics, Vol.108, No.083113,2010

[13] Costa, Monorchio, Manara ; “Analysis and Design of Ultra Thin Electromagnetic Absorbers Comprising Resistively Loaded High Impedance Surfaces”; IEEE Transactions on Antennas and Propagation; Vol.58; No.5,2010

[14] Pang, Zhou, Wang; “Equivalent circuit method analysis of the influence of frequency selective surface resistance on the frequency response of metamaterial absorbers” ; Journal of Applied Physics, Vol.110; No.023704,2011

[15] Lee,Lim;"Bandwidth-enhanced and polarization-insensitive metamaterial absorber using double resonance"; Electronic Letters; Vol.47; No. 1,2011

[16] Vandenbosch G.A.E, Van De Capelle A., “A study of the effect of the top patch in rectangular dual patch microstrip antennas”,Annales des Telecommunications,47,n°3-4,1992

[17] Alves, Kearney, Grbovic, Lavrik, Karunasiri; “Strong terahertz absorption using SiO2/Al based metamaterial structures”; Applied Physics Letters,Vol.110, No.111104,2012

[18] Chen, Cheng, Yang, Li, Duan, Gu,Tian; "Polarization insensitive and omnidirectional broadband near perfect planar metamaterial absorber in the near infrared regime"; Applied Physics Letters; Vol.99; No.253104,2011

[19] Landy, Bingham, Tyler, Jokerst, Smith, Padilla; “Design, theory and measurement of a polarization-insensitive absorber for terahertz imaging”;Physical Review B ,Vol.79, No.125104,2009

[20] Hao, Wang, Liu, Padilla, Zhou, Qiu; “High performance optical absorber based on a plasmonic metamaterial”; Applied Physics Letters, vol.96, No.251104,2010

[21] Tao, Bingham, Strikwerda et.al; “Highly flexible wide angle of incidence terahertz metamaterial absorber: Design, fabrication, and characterization”;Physical Review B, Vol.78, No.241103,2008

[22] Huang, Chen; "Multi-band and polarization insensitive metamaterial absorber", Progress in Electromagneics Research, Vol.113, 103-110, 2011

[23] Luo, Chen, Gong;"Numerical study of metamaterial absorber and extending absorbance bandwidth based on multi-square patches", The European Physical Journal B, Vol.81, 387-392, 2011

[24] "Agilent RF and Microwave Test Accesories" available at www.keysight.com/upload/cmc_upload/All/Agilent_Waveguide_Overview1.pdf (agilent.com/find/accesories)

[25] Herrera C., Vandenbosch G.A.E., “Systematic study of double-layered ultra-thin stacked patch absorbers”, Proc.EMC Europe 2013, (p.998), Brugge, Belgium, Sep.2013

[26] F.Costa, S.Genovesi, A.Monorchio, G.Manara; “A circuit-based model for the interpretation of perfect metamaterial absorbers”; IEEE Transactions on Antennas and Propagation; Vol.61; No.3; 1201-1209; Mar.2013.

4 E-shapes as resonating elements in periodically structured absorbers

4.1 Introduction

The narrow bandwidth nature of the responses from most metamaterial structures due to its underlying resonant mechanisms is known in the field, and is the origin of the intrinsically narrow bandwidth absorption in metamaterial absorbers ([7]-[14]), as has been mentioned in previous chapters. In this particular sample of publications [7]-[14], relative absorption bandwidth is not more than 9% at absorptions beyond -10 dB (approximately 90% of absorption), for designs operational in the microwave range. In the terahertz range, [10] presents a bandwidth is not more than 14.6% at FWHM (approximately 50% of absorption), but 9.7% at -10 dB and [12] 13% also at FWHM. While wide bandwidth behaviours have been achieved, often by adding the resonances of multiple resonators in a single- or multiple-layered structure (in the microwave range [4]-[6]), single resonators that can widen this narrow bandwidth absorption have not been frequently reported. For instance in [4] a 38% of absorption bandwidth in the terahertz range is reported but even at FWHM, not at 90% of absorption or beyond. In [21] approximately 30% is reached but again at FWHM and using resistors and capacitors that make the design very bulky, the same kind of design is presented in [22] although here around 50 % is reached, still at FWHM. In [23] multiple nested CRR resonators are used, but not more than 4.3% is reached and in [24] where multiple ELC resonators are used not more than 5.4%.

Besides this, in the commercial scope, with non-metamaterial absorbing material, very wideband absorbing material can be found but often with an absorption that is smaller in comparison with the ones presented in this chapter. For instance the FGM absorber from Emerson & Cuming, who's response is shown in figure 1, yields a reflectivity below -10dB approximately in the band of 4 -12GHz and barely reaches -15dB.

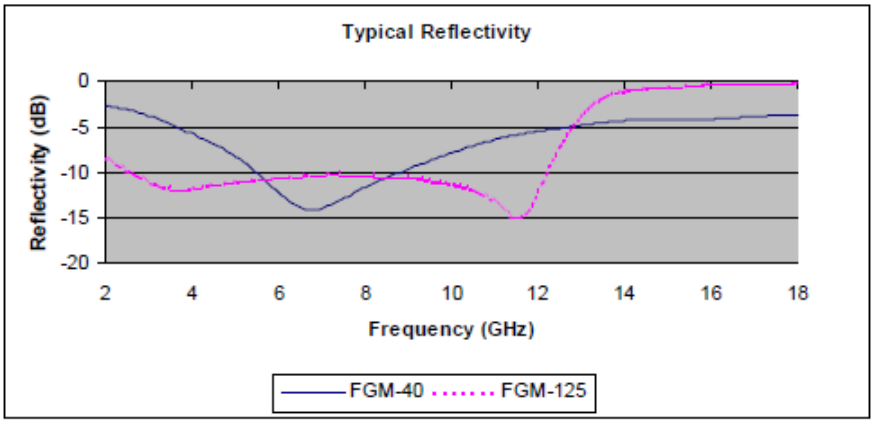

Fig. 1. Reflectivity of an FGM absorber from Emerson and Cuming.[33]

On the other hand the SF narrowband absorber from Emerson and Cuming is more absorptive but for a smaller band of frequencies, dependable on the operational frequency of the absorber (see response depicted in figure 2).

[33] Image extracted from an FGM absorber datasheet ("FGM Tech Bulletin") at http://www.eccosorb.com/products-eccosorb-fgm.htm (http://www.eccosorb.com/Collateral/Documents/English-US/FGM.pdf).

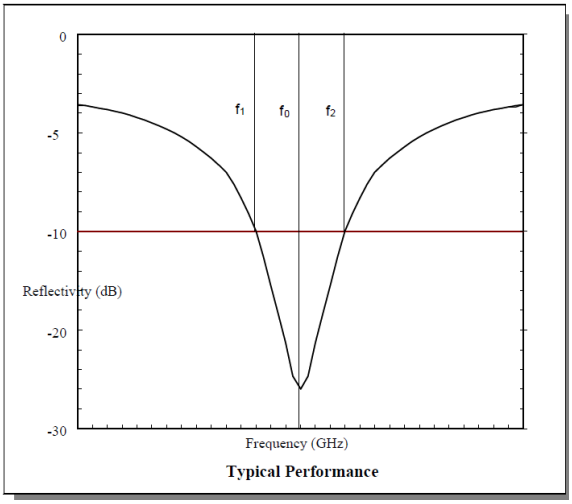

Fig. 2. Reflectivity of an SF narrowband absorber. The bandwidth is f0 ±5%, thickness depends on frequency f0.[34]

An absorbing material with a response that could be classified in between the above mentioned narrow- and wideband absorbers –with an absorption bandwidth wider than the one of the SF absorber but smaller than the one of FGM, with more absorption than the last one and less than the first one- is not so often found and could also be considered as an interesting option in the commercial scope. It could prove less probable to be able to design a metamaterial absorber -that does not use multiple resonators or multiple layers- or even a periodically structured absorber with a wideband response as the one of FGM Emerson and Cuming, but one with a narrower band could be realizable.

Antennas designs including E-shapes have been used in the past with resulting broadband responses ([1]-[3]). The relatively large bandwidth obtained with this shape in the antennas field was a good motivation to investigate the performance of these shapes as metallic resonators for periodically structured absorbers. This investigation could add a new contribution to the research of broadband periodic absorbers or even metamaterial absorbers.
The E-shape has so far not being studied as metallic resonator in unit cells of metamaterial or periodic absorbers, to the best of our knowledge.

Therefore in our first simulations we try to explore the promising capabilities of the E-shape as resonator with a wideband response. Our objective is in fact double: not only performing a basic exploration of this resonating element as absorbing material in a metamaterial structure but simultaneously also trying to obtain a response that approaches the wide bandwidth-like one observed in [1], [2] and [3]. With this in mind we try different strategies up to a certain extent (change of basic shape, change of dimensions). Performing these further variations also allowed us to know better how to achieve our ultimate aim and the effect of each variation on the design.
The main changes in parameter values and results of the above described exploration are summarized in section 2. A motivation for the research carried out in the following sections is also given.

[34] Image extracted from an SF absorber datasheet ("SF Tech Bulletin") at http://www.eccosorb.com/products-eccosorb-sf.htm (http://www.eccosorb.com/Collateral/Documents/English-US/SF.pdf).

In section 3 we address and increase losses in non-conductive materials and try to further optimize the first wide-band result obtained. In 4 we add a substantial change in the unit cell's layer structure. In section 5 the sensitivity study performed on our design is exposed. Section 6 describes adjustments made on the design for fabrication, fabrication and measurement process and corresponding results. Section 7 contains the general conclusions.

4.2 Initial simulations

In our initial simulations we performed different kinds of variation in the structure of the unit cell in order to investigate which of them could approach the response of our topology to a wider band behaviour. We try to obtain the same kind of response as for the last configuration in [3] without deviating excessively from the initial parameters and shapes, meaning changes in the parameter values should not be of more than 80% , for example.

4.2.1 The initial structure

As inspiration and starting point for our research and optimizations we took one of the first E-shapes used in antennas ([3]) and the parameter values corresponding to the last configuration presented in [3]:

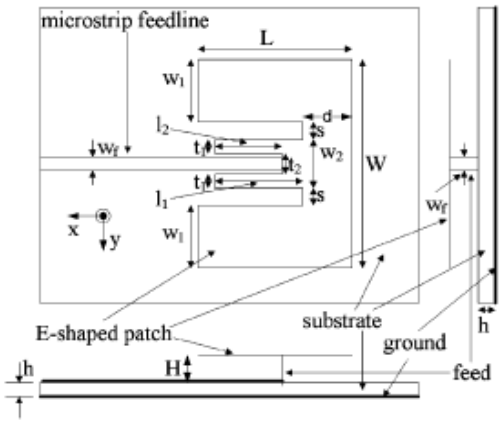

Fig. 3. Design of antenna prototype used in the last configuration presented in [3]

Parameter name	Value [mm]
L	22.2
d	7.4
l1	12.3
s	2
W	33.2
w1	10.6
w2	8

Table 1 - Paramater values corresponding to E-shape shown in figure 1.

For this last configuration, where the antenna was fed via a microstrip line, the dielectric substrate's thickness was 0.8 mm and the E-shaped antenna was mounted 2.5 mm above the substrate's surface. In our metamaterial, which finally resulted in a periodic absorber design, the feed cannot be used and a unit cell size has to be defined or tuned. From the structure shown in figure 3, initially we only take then the metallic E-shape, without the slot in its middle-branch and with its corresponding initial parameter values shown in table 1 and

indicated in the sketch of figure 3.The resulting E-shape used for our unit cell is depicted in figure 4.
The corresponding frequency response is centered around 5.5GHz, thus with a unit cell size of for instance 40 mm we would have a sub-wavelength structure (<λ/2). The material initially chosen as substrate for our periodic absorber was lossy FR-4 dielectric, with ε=4.3, loss tangent =0.025.
Thus for our unit cell, we initially choose a layer structure composed by the copper E-shape using exactly the same parameters indicated in table and figure 1 -with the exceptions previously mentioned referring to the slot in the central branch and microstrip feedline- as metallic resonator, a substrate layer with initial thickness=0.8 mm and copper back-plane (refer to figure 4).

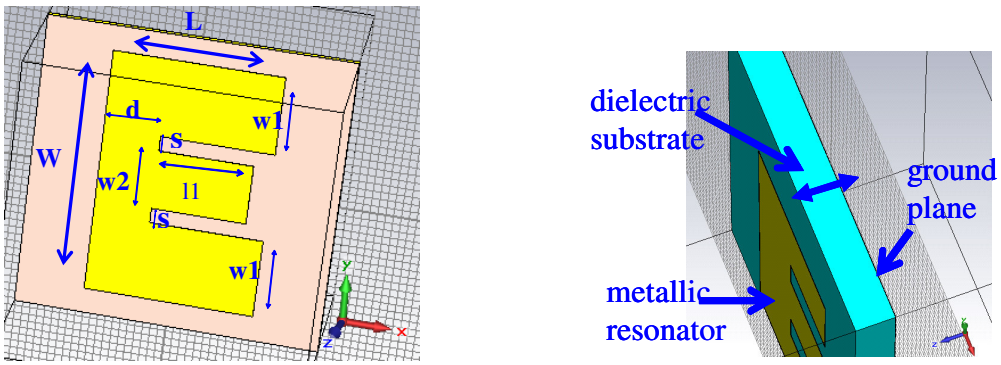

Fig. 4. a) (Left) Structure of the unit cell built for a periodic absorber, with correspondance to parameters of table 1 indicated in the metallic resonator. b) (Right) Layer structure of the unit cell.

Plane waves are impinged with normal incidence on the structure, thus with TE polarization the E-field is directed in the positive direction of the y axis and with TM polarization in the positive direction of the x axis. This results in the following incidence on the structure:

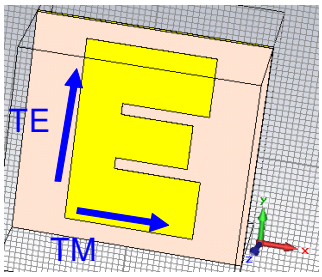

Fig. 5. How TE and TM polarizations impinge on the structure with normal incidence.

With TE polarization double-resonant responses were observed, as will be seen in all the following sections (from figure 9 on), while with TM polarization in general only single-resonant responses were observed, when the same frequency range as with TE polarization was selected.
With TM polarization results had a fairly large absorption in most cases. A typical response of this kind can be observed in figure 6:

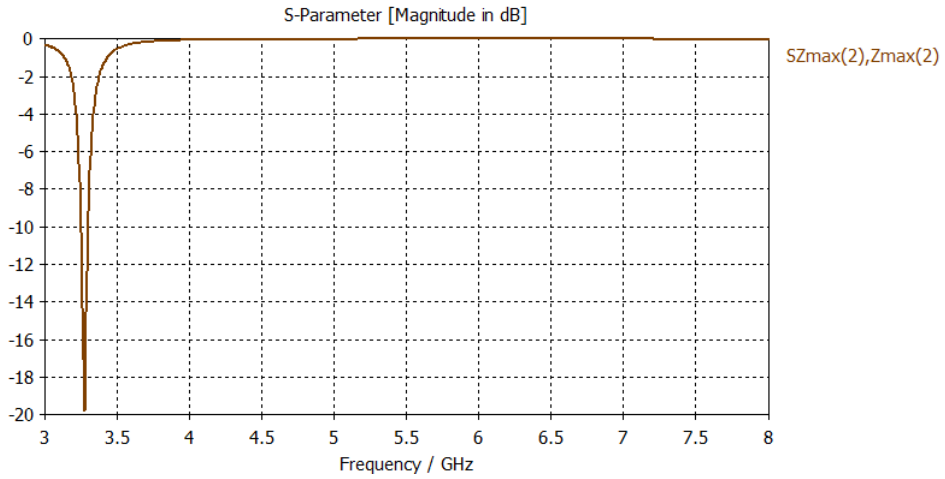

Fig. 6. Initial frequency response obtained with TM polarization. Unit cell size is 40 mm, substrate's thickness 0.8 mm.

Thus as for most results TM responses do not deviate much from this typical response, the majority of results shown correspond to TE polarization, unless the opposite is indicated.

4.2.2 Initial variations and changes

Starting from the initial parameter values (unit cell side-length of 40 mm, substrate's thickness 0.8 mm and values of table 1) and according to initial simulations and optimizations with varying values of unit cell size and substrate thickness, a unit cell side-length of 34 mm and a substrate's thickness of 3.5 mm showed to be the most promising values in order to obtain an absorptive response that approaches a wideband behaviour.
Results were still very distant from a really wide-band response and only acceptable in terms of absorption. An example of the responses obtained during the process can be seen in figure 7.

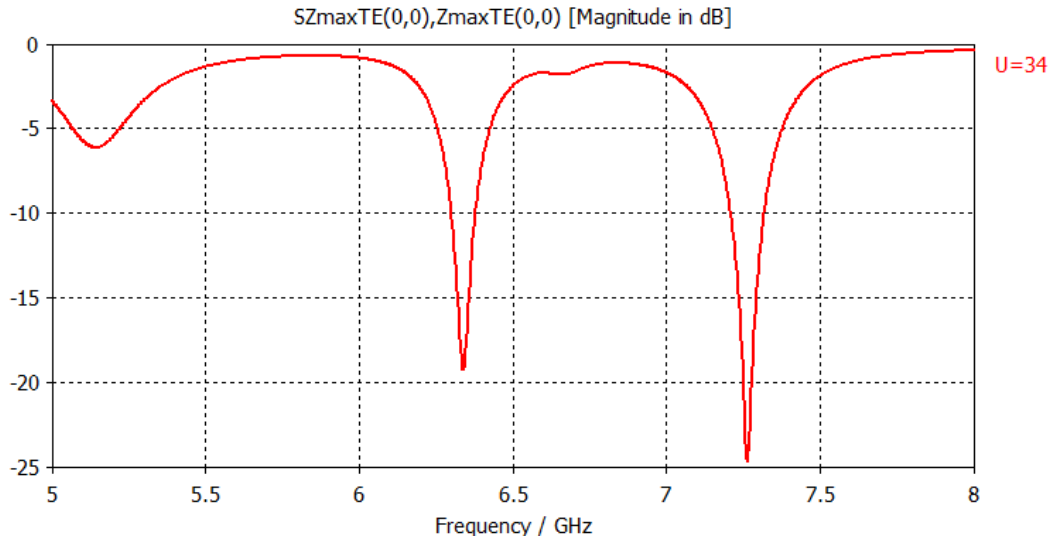

Fig. 7. S11 response for a unit cell size of 34 mm, substrate thickness 3.5 mm.

Therefore further simulations were performed, choosing the best results in terms of absorption and approximation towards the wide-band response in order to further progress in the simulations. Again we are trying to approach a frequency response similar to the one referenced in [3] or a wider band response

Different variations on the basic form of the E-shape were introduced , some of which are shown in figures 8 and 9 (the shape in figure 9 was inspired by [3], the one in figure 8 was inspired by [1] and [2], where wider band results were obtained). In figure 9, a slot is made in the central branch with l_2, t_1 and t_2 of figure 3 having the same values as in [3]. The E-shape of figure 8, where the three branches are equally long (L-d=l1), was the one that yielded comparably better results.

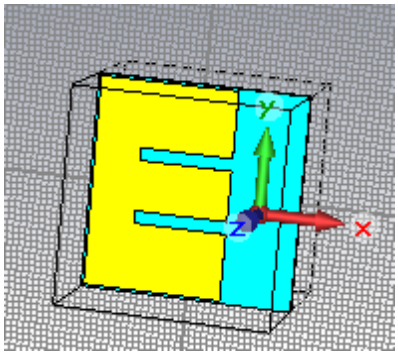

Fig. 8. E-shape with its three branches equally long, thus L-d=l1.

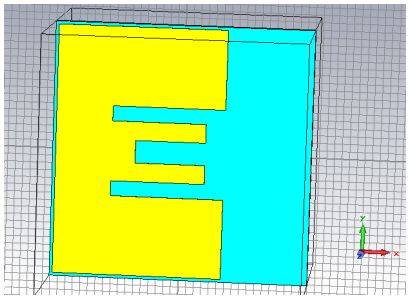

Fig. 9. E-shape with slot in the middle branch, as the original shape used in the antenna with a microstrip feed.

Then using the shape of figure 8**,** the shape's dimensions were further varied. The best result was obtained with w1=w2= 8.6 mm, substrate's thickness of 3.5 mm and unit cell size of 34 mm again.

During these initial simulations and exploration of the E-shape as resonator, it was possible to obtain strong resonances, high absorptions and multiple-resonant responses but not yet towards the same kind of responses obtained in antennas ([1]-[3]) that could be classified as of a more wide bandwidth kind, or even closely positioned multiple-resonant peaks.

We think that the relatively small loss of FR4 might be limiting the performance of our designs.

4.3 Introduction on the effect of changes in the dielectric material over an absorber's properties

There are few materials readily available with more intrinsic losses than FR4.
Still some materials slightly improved the response, mainly in terms of absorption, despite being equally or even less lossy than standard FR4. The method that proved to be more effective to start to observe some considerable improvement was to increase loss tg.

4.3.1 Different dielectric materials for substrate

Next some typical effects observed with the change of the material on the dielectric substrate of our structure illustrated with a unit cell size of 34 mm, variable substrate's thicknesses depicted as "thick_d1" in figure 10 and with slots in the shape corresponding to w1=w2= 8.6 mm.
We also re-examined the influence of thickness to increase losses in a material. Then simultaneously we used a loss tangent of 0.07 (almost three times the original loss tg value of standard FR4).

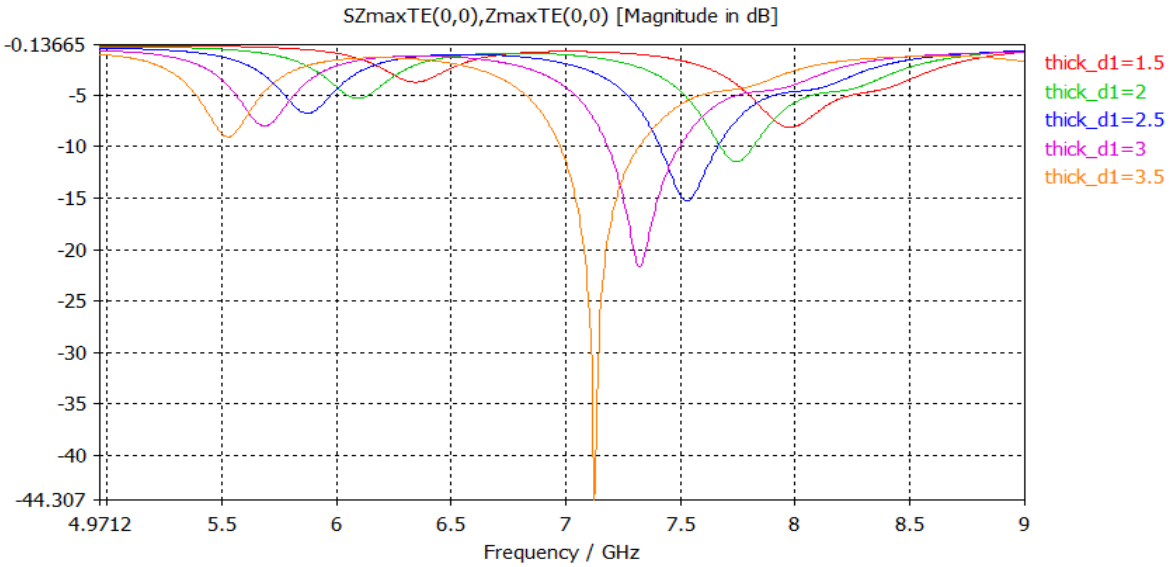

Fig. 10. S11 response for a unit cell size of 34 mm, substrate thicknesses thick_d1 and with wider slots in the shape, corresponding to w1=w2= 8.6 mm in this case. Dielectric material used for the substrate was standard FR4 with loss tg =0.07.

An increase in substrate's thickness also indicated increase in absorption, as expected.

Although Isola IS415 does not have a loss tg (loss tg ~0.0127 at 5 GHz, ~0.0125 at 10 GHz) that is larger than the one of standard FR4 , in this case it increases the absorption capacity of the structure, in addition to shifting its frequency response towards higher frequencies.

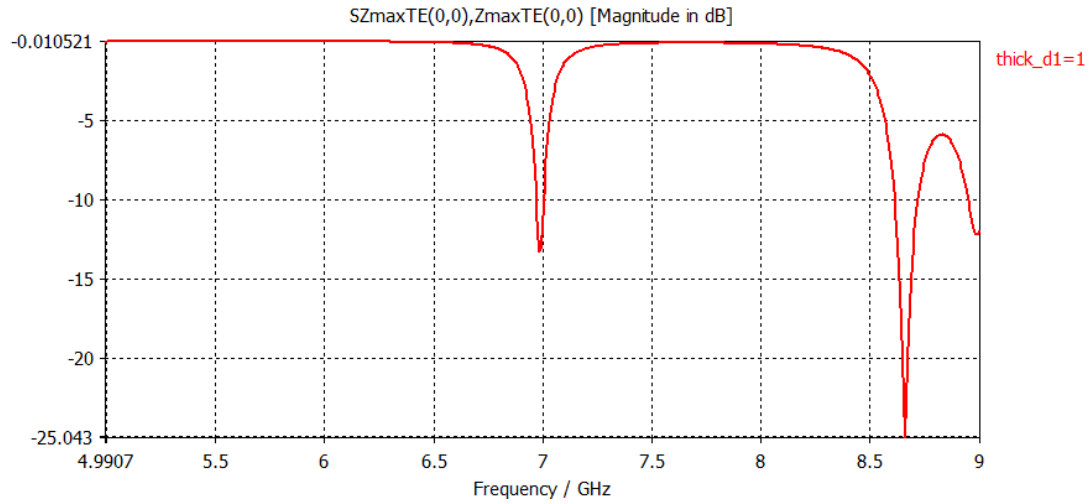

Fig. 11. S11 response for a unit cell size of 34 mm, substrate thicknesses thick_d1 and with wider slots in the shape, corresponding to w1=w2= 8.6 mm in this case. Dielectric material used for the substrate is IS415 from Isola.

When using G10 as dielectric material for the substrate there was very little difference in the response with respect to standard FR4, as expected.

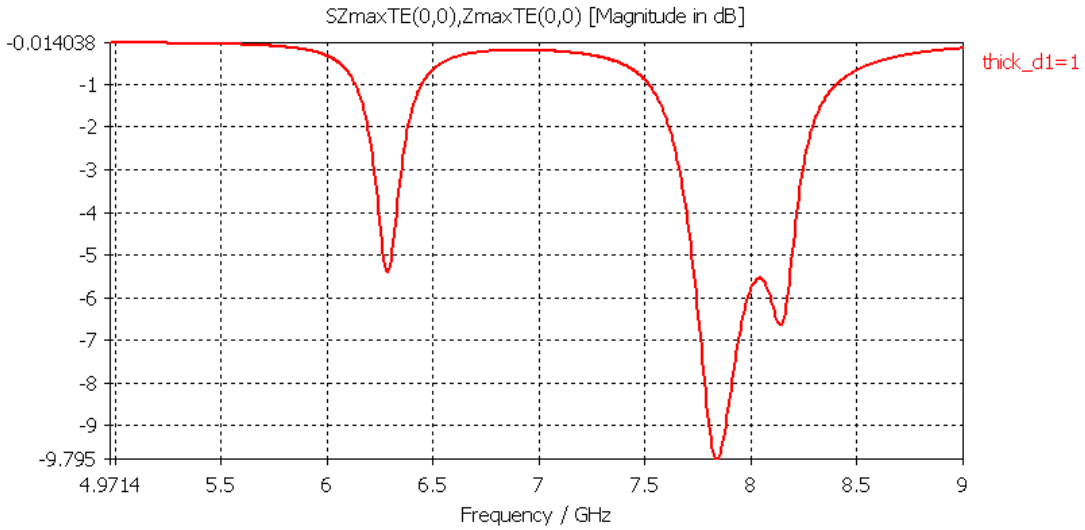

Fig. 12. S11 response for a unit cell size of 34 mm, substrate thicknesses thick_d1 and with wider slots in the shape, corresponding to w1=w2= 8.6 mm in this case. Dielectric material used for the substrate is G10.

4.3.2 Simultaneous further changes in unit cell dimensions and high increase in substrate's losses

In addition to investigating whether the sole increase of intrinsic losses in the dielectric of our structure could approximate its response to the desired one, we made further changes in the dimensions and boundary values of our unit cell's parameters and in its basic shape.
Specifically in one of the parameters optimizations –CST's Genetic Algorithm was used- we used a rectangular unit cell instead of a square one, increased the maximum value of the substrate's thickness up to 4.5 mm and simultaneously used a fixed value of FR4's tg loss =0.07.

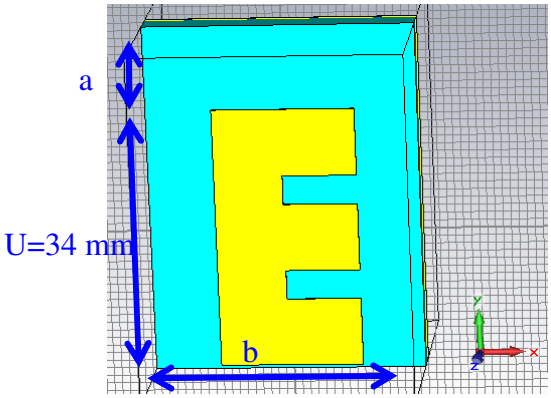

Fig. 13. Unit cell structure used in this set of simulations.

Parameter name	Value[mm]
L	17.9
d	8.6
s	3.7
W	33.2
w1	8.6
w2	8.6

Table 2- Paramater values corresponding to the E-shape depicted in figure 13.

For our optimizations, the length L of the unit cell dimension was composed of L= U+a, with U fixed in 34 mm and a ranging from 0 to 25 mm and the width b of the unit cell ranged from 34 to 60 mm. Substrate's thickness varied from 0.5 to 4.5 mm in steps of 0.5 mm.

A very good result in terms of its approximation to a very wide bandwidth and highly absorptive response, and similarity to the ones obtained in [1], [2] and [3] was obtained with a=10.4 mm, b=34 mm and a substrate's thickness of 4 mm.

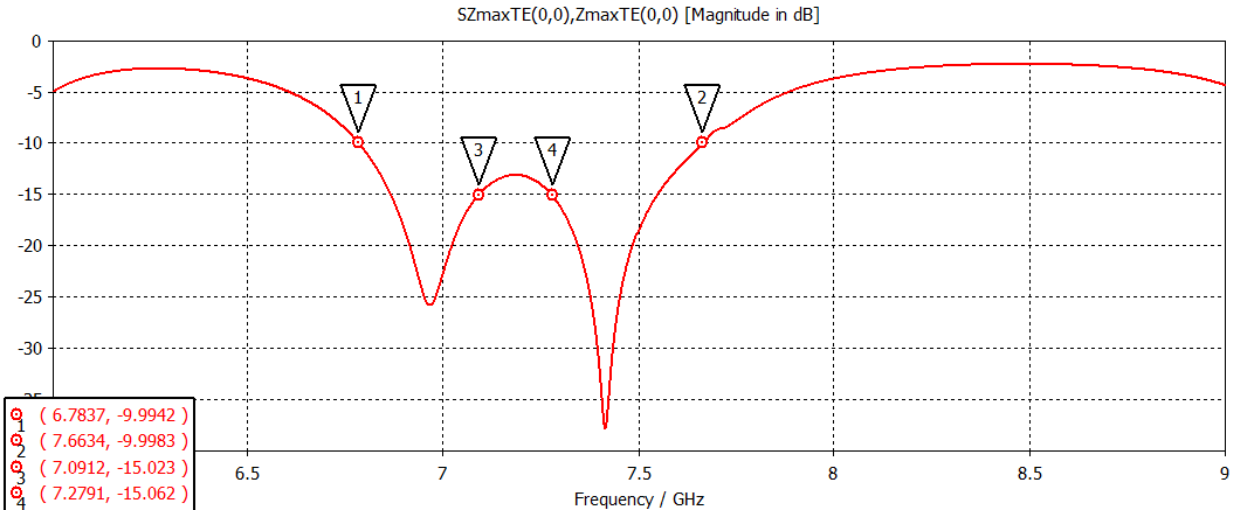

Fig. 14. S11 response for a=10.4 mm, b=34 mm mm, substrate thicknesses of 4 mm and loss tangent=0.07.

The relative bandwidth is of approximately 12.24 % at -10dB with respect to a central frequency of 7.19 GHz .This is a very good result taking into account the average relative bandwidth frequently obtained as a result of continuous bandwidth (as opposite to bandwidth obtained as a result of adding multiple resonant responses).
At -15dB the relative bandwidth is of approximately 9.5%, although the bandwidth is not fully continuous.
It is also a result that is much closer to the one obtained with an antenna topology at [3] than previous ones and more importantly it approaches the desired behaviour of bandwidth absorber.

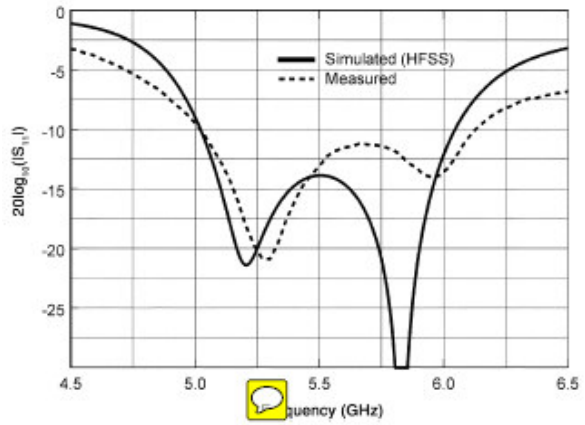

Fig. 15. S11 response corresponding to the last antenna configuration in [3], using a microstrip feed.

4.3.3 Optimization of best result

In order to optimize this particular result we first increased the loss tangent up to 0.41 in steps of 0.068 (0.41 is a value around the ones found in regular absorbing material, for instance loss tg =0.37 at 8 GHz for Eccosorb DSF-8). Substrate thickness and the rest of the parameters where left unchanged.

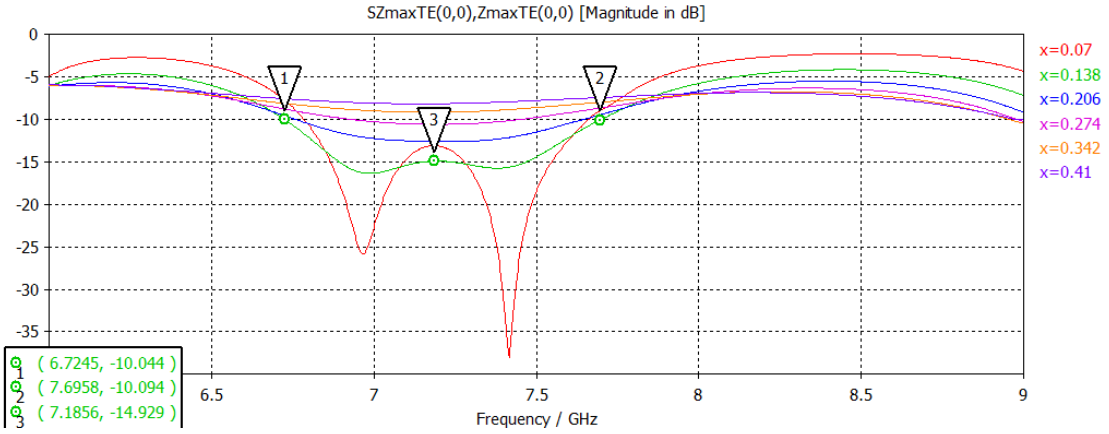

Fig. 16. S11 responses with the loss tg = x as only variable parameter.

A maximum absorption level with a fairly large bandwidth and in TE polarization could then be found between a loss tangent of 0.07 and 0.138. Still with loss tg=0.138 the response at the central frequency is almost at -15dB, which is already a very good level for an absorber, although the bandwidth is smaller than the one obtained with loss tg =0.07, and as expected the bandwidth is larger than with loss tg =0.07 at -10 dB, ranging from 6.72-7.70 GHz (a relative bandwidth of 13.6%).

With a loss tangent ranging from 0.07 to 0.13 in steps of 0.0075, the best results in terms of absorption and bandwidth could be set at 0.0925 or 0.1 (see figure 18). The optimal result with tg loss=0.1, as it provides the widest absorption bandwidth and is effectively entirely below -15 dB (then absorption bandwidth at -15dB is really continuous).

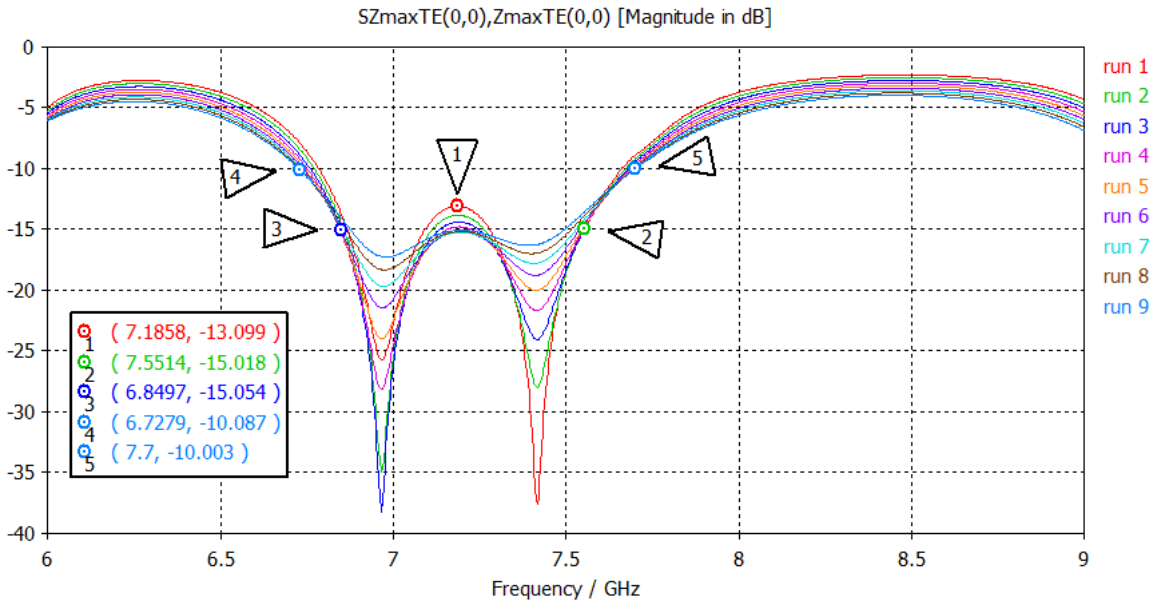

Fig. 17. S11 responses with the loss tg as only variable parameter for a substrate thickness of 4 mm. Each run corresponds to a different value of loss tg, being the first value 0.07 and last one 0.13 in steps of 0.0075 in ascending order (corresponding to run 1..run 9 respectively).

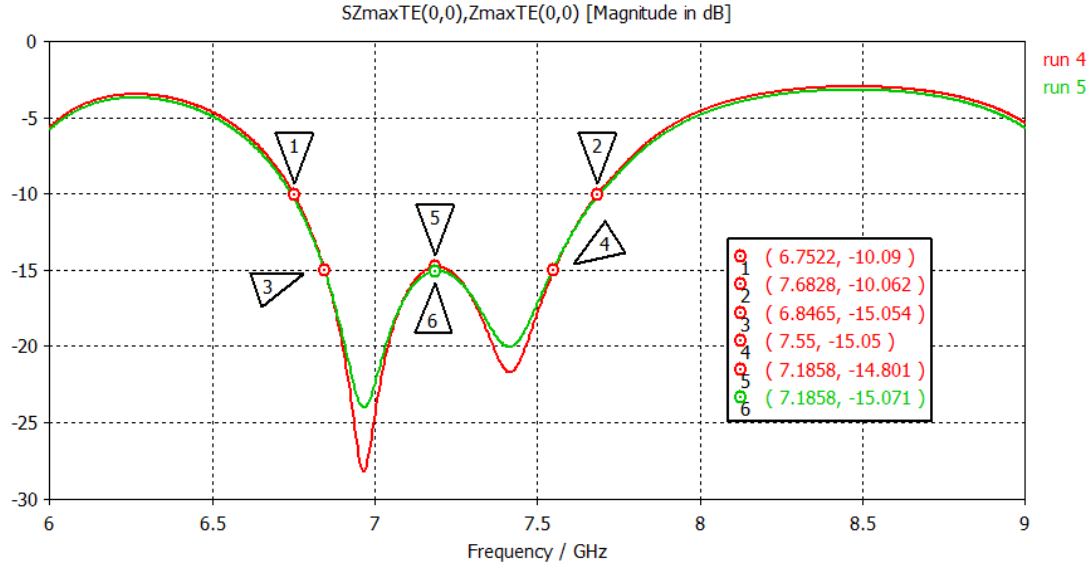

Fig. 18. S11 responses with the loss tg as only variable parameter for a substrate thickness of 4 mm. Each run corresponds to a different value of loss tg, being the first value 0.0925 and last one 0.1 (run 4 and 5 respectively).

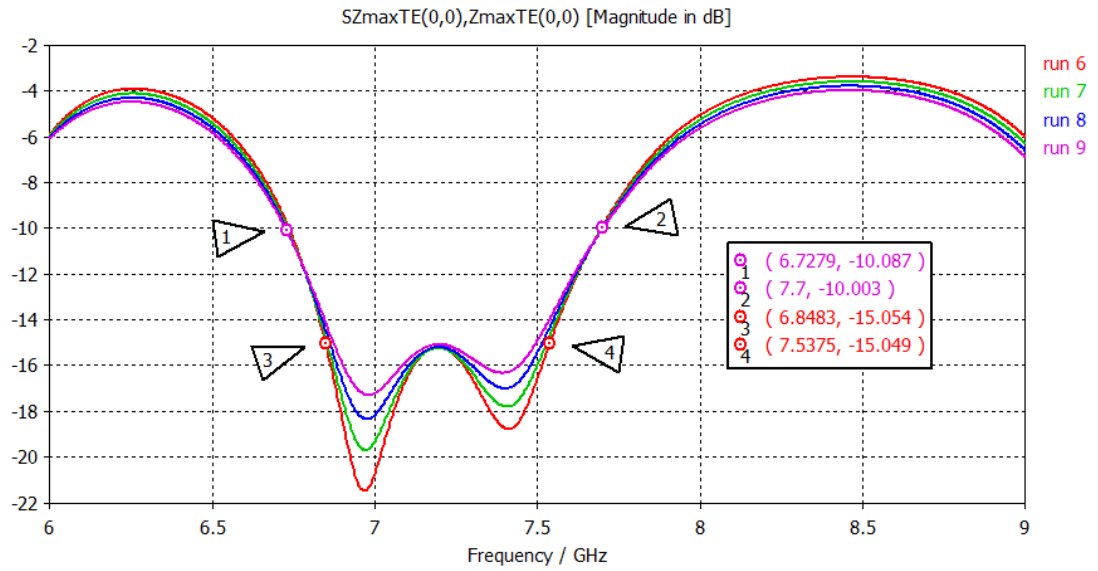

Fig. 19. S11 responses with loss tg as only variable parameter for a substrate thickness of 4 mm. Each run corresponds to a different value of loss tg, being the first value 0.1075 and last one 0.13 in steps of 0.0075 in ascending order (corresponding to run 6..run 9 respectively).

It is also worth showing the results obtained with TM polarization in the same loss tangent change range, as they also reach large absorption levels of more than -25dB, with optimum at loss tg =0.274. However the width of the responses is not as large as by TE polarization at -15dB (less than 0.5GHz) and slightly smaller at -10dB as well
(smaller than 1GHz).

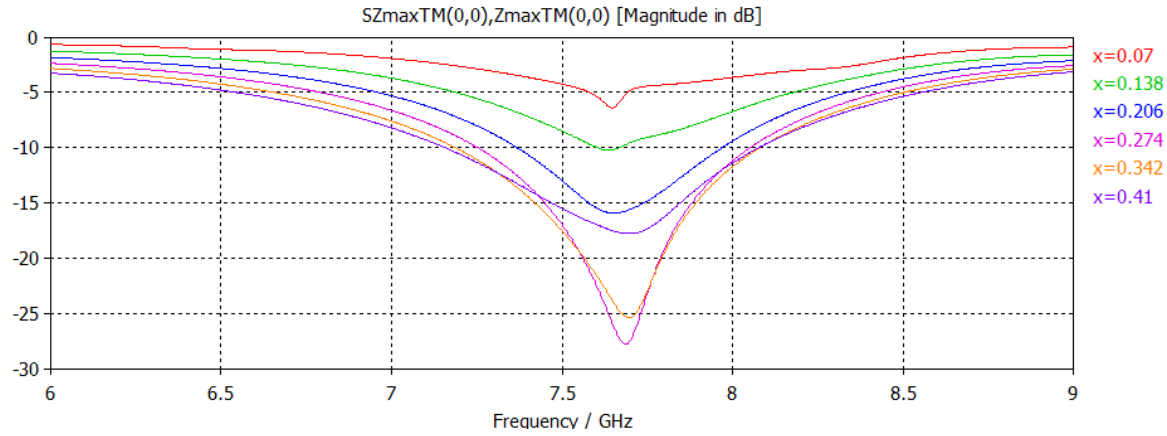

Fig. 20. S11 responses with the loss tg = x as only variable parameter for TM polarization.

4.3.3.1 Further increase of the substrate's thickness

We also further increased the substrate's thickness simultaneously with the increase in losses. The increase ranged from 4.5 to 6.5 mm, bearing in mind that a thick absorber is not very much desirable. Responses -for TE polarization- slowly shifted towards lower frequencies, which increases the relative bandwidth. The wide bandwidth-like response was kept in most cases.

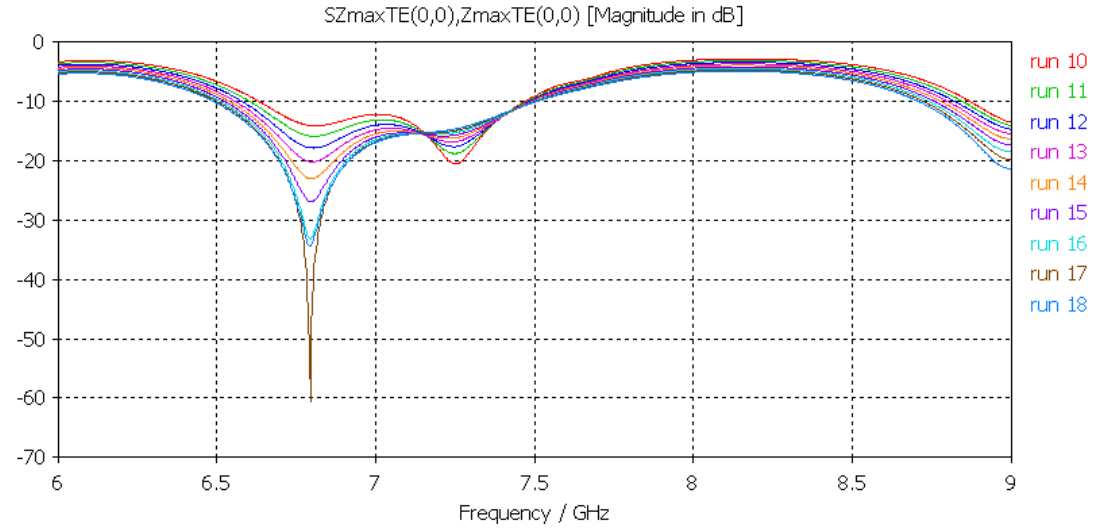

Fig. 21. S11 responses with loss tg as only variable parameter for a substrate thickness of 4.5 mm. Each run corresponds to a different value of loss tg, being the first value 0.07 and last one 0.13 in steps of 0.0075 in ascending order.

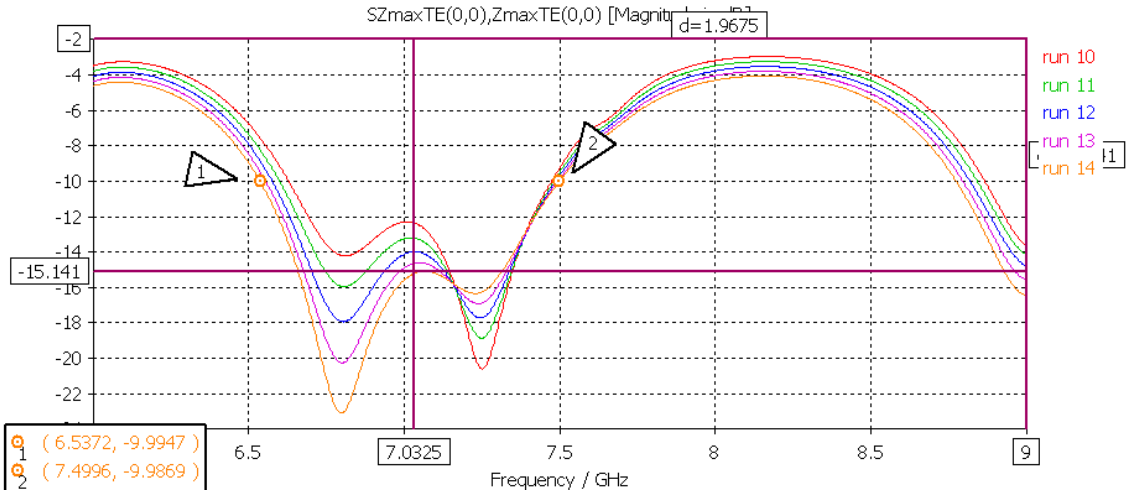

Fig. 22. S11 responses with loss tg as only variable parameter for a substrate thickness of 4.5 mm. Each run corresponds to a different value of loss tg, being the first value 0.07 and last one 0.1 in steps of 0.0075 in ascending order.

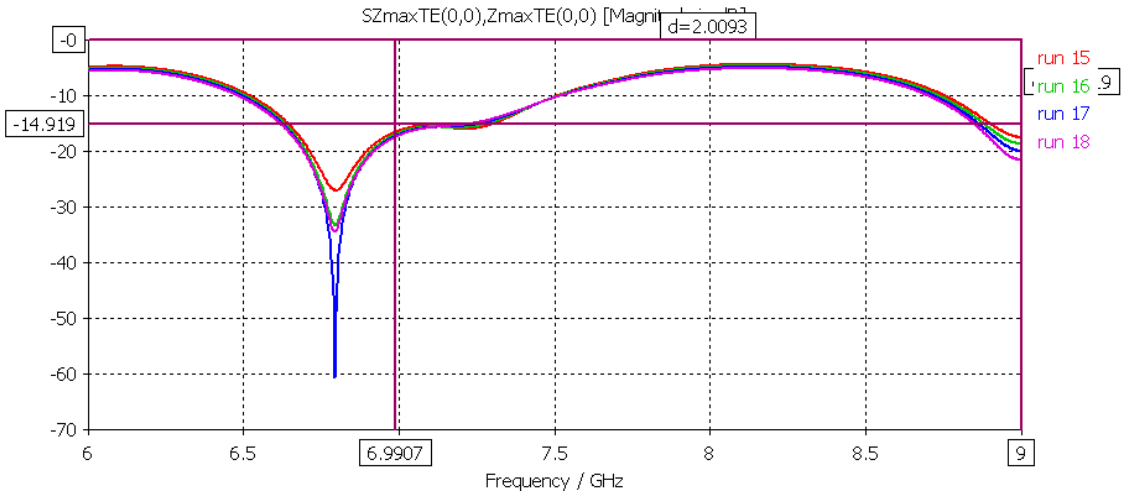

Fig. 23. S11 responses with loss tg as only variable parameter for a substrate thickness of 4.5 mm. Each run corresponds to a different value of loss tg, being the first value 0.1075 and last one 0.13 in steps of 0.0075 in ascending order.

For a substrate thicknees of 4.5 mm the maximum absorption level was found at a loss tg=0.1225. At loss tg=0.1 the effective frequency range of absorption is already just below -15dB.

For thicknesses from 5 to 6.5 mm the optimum response seemed to be beyond loss tg =0.13, maximum absorption levels were smaller than in previous results in the wideband frequency spectrum. Thus the bandwidth is less than 1GHz at -10dB and progressively diminishes.

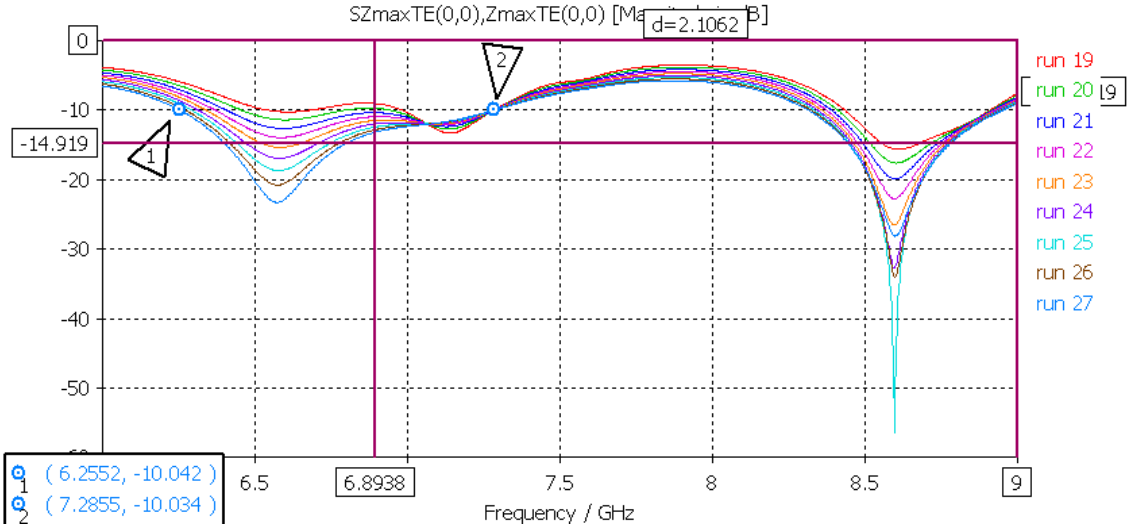

Fig. 24. S11 responses with loss tg as only variable parameter for a substrate thickness of 5 mm. Each run corresponds to a different value of loss tg, being the first value 0.07 and last one 0.13 in steps of 0.0075 in ascending order.

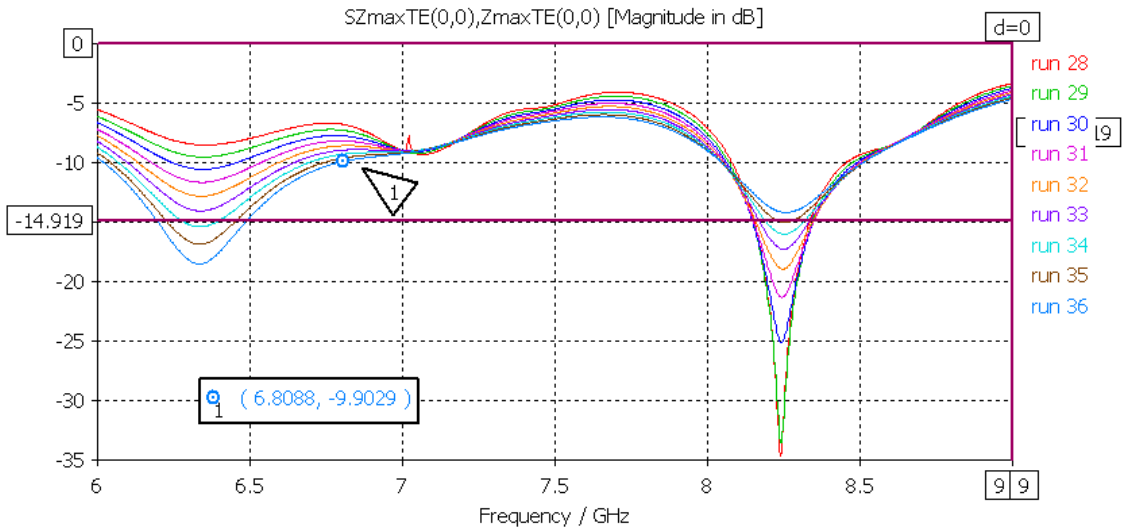

Fig. 25. S11 responses with loss tg as only variable parameter for a substrate thickness of 5.5 mm. Each run corresponds to a different value of loss tg, being the first value 0.07 and last one 0.13 in steps of 0.0075 in ascending order.

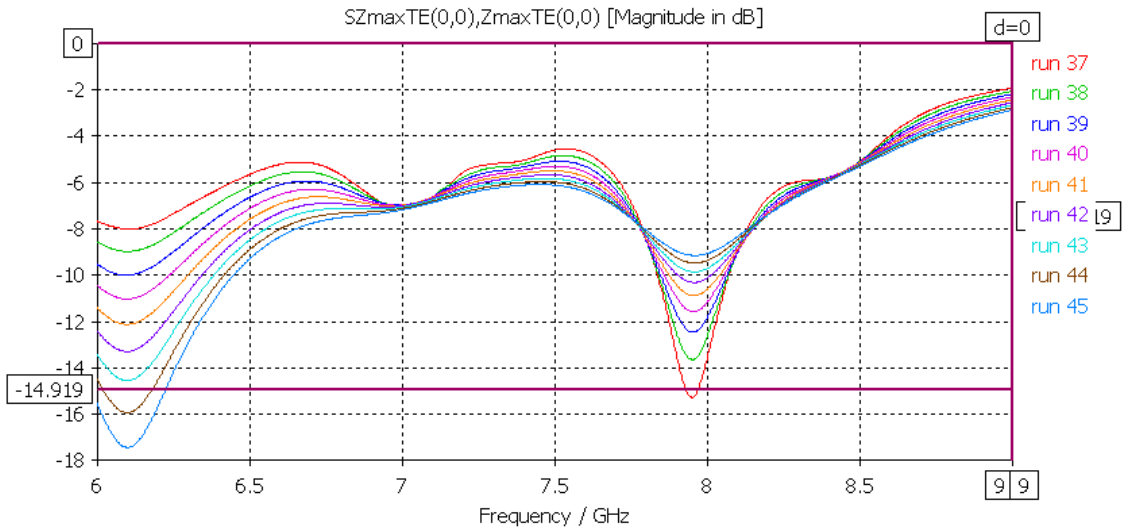

Fig. 26. S11 responses with loss tg as only variable parameter for a substrate thickness of 6 mm. Each run corresponds to a different value of loss tg, being the first value 0.07 and last one 0.13 in steps of 0.0075 in ascending order.

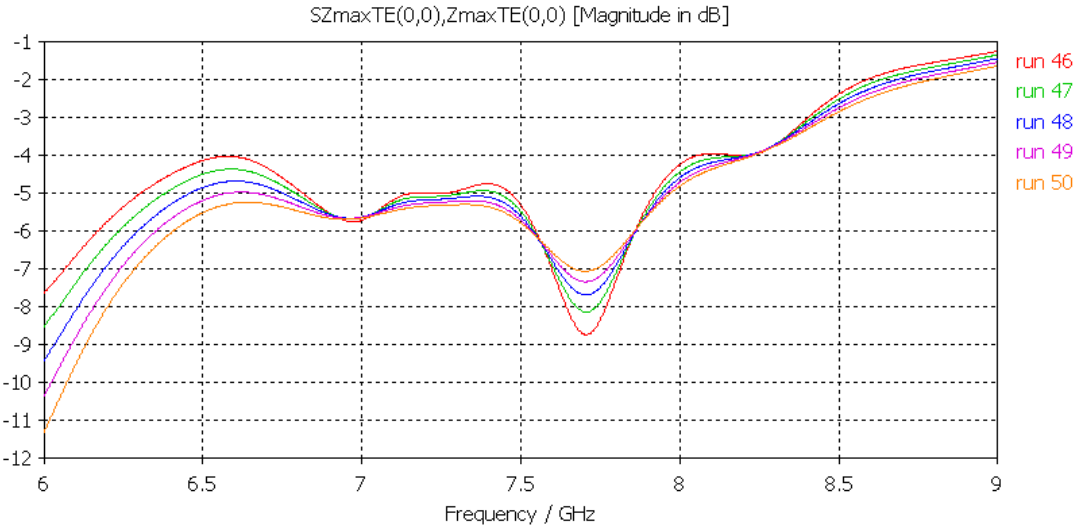

Fig. 27. S11 responses with loss tg as only variable parameter for a substrate thickness of 6.5 mm. Each run corresponds to a different value of loss tg, being the first value 0.07 and last one 0.0925 in steps of 0.0075 in ascending order.

The best results were then found with a substrate's thickness of 4.5 mm.

4.4 Introducing an air-gap to enlarge the bandwidth

With the specific aim of enlarging the bandwidth even more, a gap or an air layer was sandwiched between the ground plane and substrate in our unit cell, as depicted in fig.41.

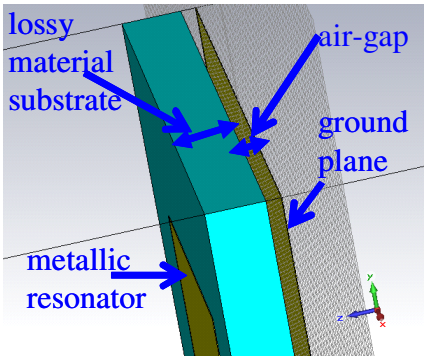

Fig. 28. Unit cell structure used in this set of simulations.

The introduction of air layers has been widely used in antenna technology. An air-gap in an antenna topology can typically enlarge the bandwidth of its response for some resonances in a determined structure. The increase is not necessarily linear with air-gap thickness.

Thus again a combination of progressive parameter variations and optimization were used to find a suitable air-gap thickness (that maximized bandwidth while minimizing a reduction in the absorption level with respect to the response without an air layer).
The first results with several air-gap thicknesses for a substrate's thickness of 4 mm and tg loss=0.1 (unit cell size unchanged: 44.4 by 34 mm) showed a noticeable widening of the bandwidth with air-gap thicknesses of 0.5 mm and 1 mm, at the expenses of a general reduction in absorption. With an air-gap of 1 mm the reduction of absorption in the central

band of the frequency response was smaller. There is then a possibility of finding a response with a wider bandwidth and minimal reduction of absorption capabilities with an air layer of around 1 mm.

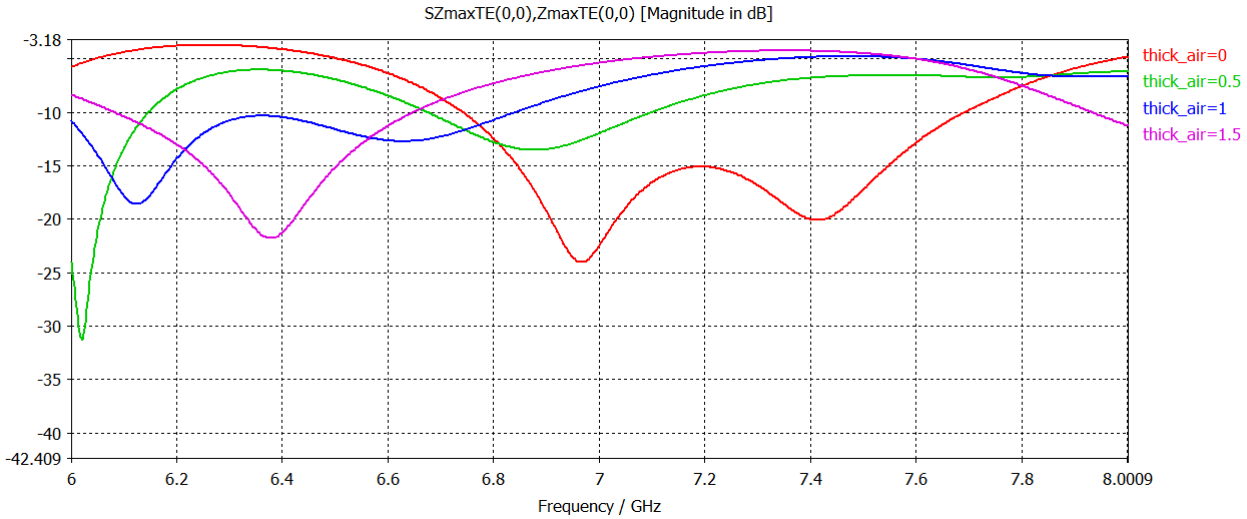

Fig. 29. S11 responses for a substrate's thickness of 4 mm, tg loss=0.1, u.cell 44.4 by 34 mm and thickness of air layer "thick_air".

The results using the same parameter values and larger air-gap thicknesses (≥3 mm) yielded much lower absorptions, not interesting for our purposes (figure 43):

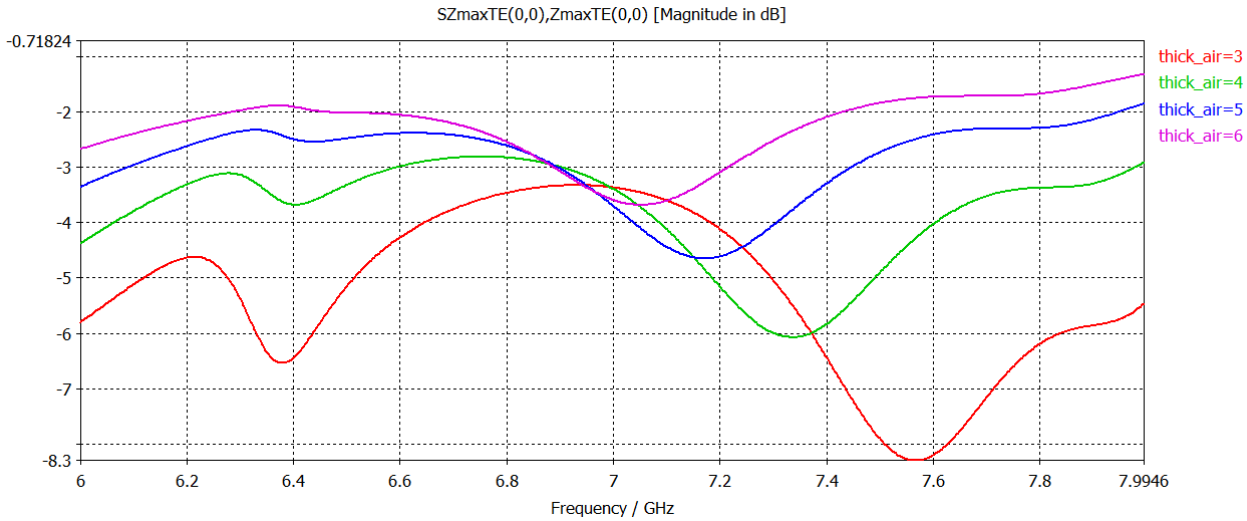

Fig. 30. S11 responses for a substrate's thickness of 4 mm, tg loss=0.1, u.cell 44.4 by 34 mm and thickness of air layer "thick_air".

With a larger tg loss = 0.138 of the susbtrate, the absorption at a 1mm-air-gap was larger than with a tg loss = 0.1, as expected, but it was also larger in comparison with an air-gap tickness =0 mm. Although the absorption bandwidth with air-gap=1 mm is not continuous and with air-gap=0 mm it is continuous, the reduction in absorption -when the air-gap is introduced- is far smaller than the reduction for a tg loss =0.138 (see figure 44)

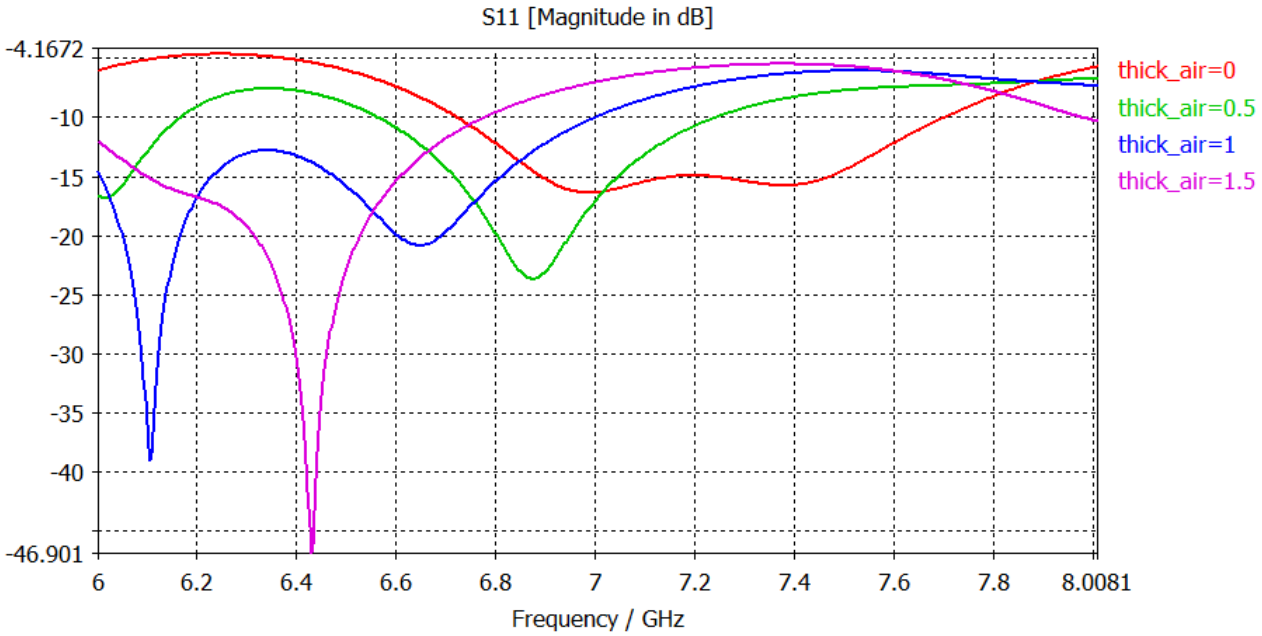

Fig. 31. S11 responses for a substrate's thickness of 4 mm, tg loss=0.138, u.cell 44.4 by 34 mm and thickness of air layer "thick_air".

In order to try to increase the absorption of the responses and achieve a really continuous bandwidth at -15dB, while further broadening the bandwidth until optimum performances are reached, the air-gap's thickness was further tuned, substrate's tg loss further increased in small steps and substrates' thicknesses other than 4 mm taken into consideration (figures 45, 46 and 47).

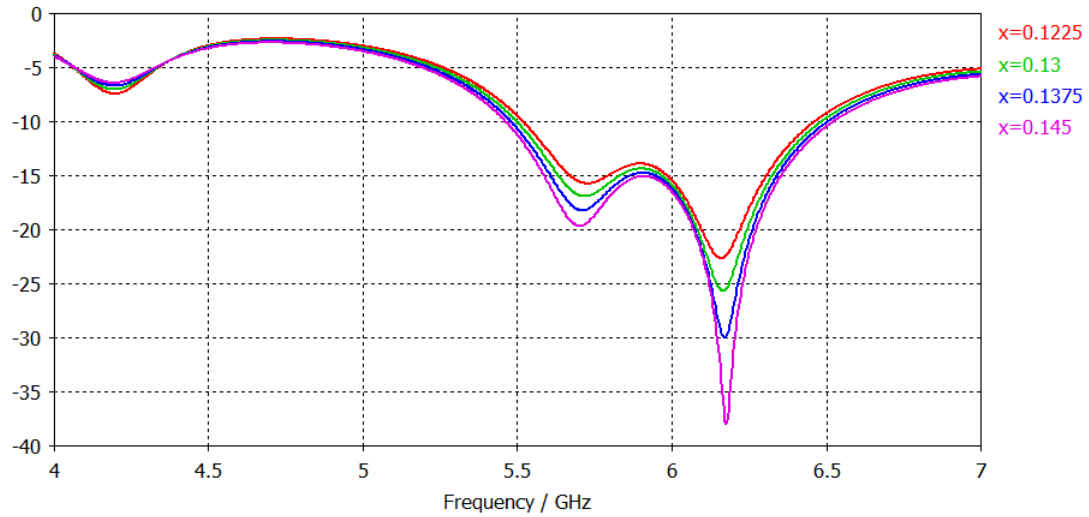

Fig. 32. S11 responses for a substrate's thickness of 5 mm, tg loss=x, u.cell 44.4 by 34 mm and thickness of air layer thickness =1 mm

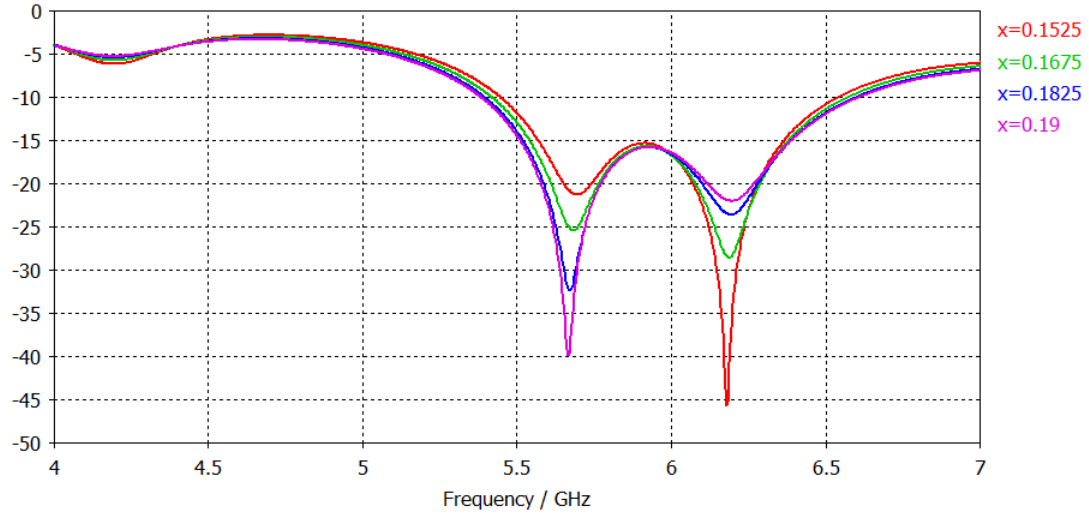

Fig. 33. S11 responses for a substrate's thickness of 5 mm, tg loss=x, u.cell 44.4 by 34 mm and thickness of air layer thickness= 1 mm.

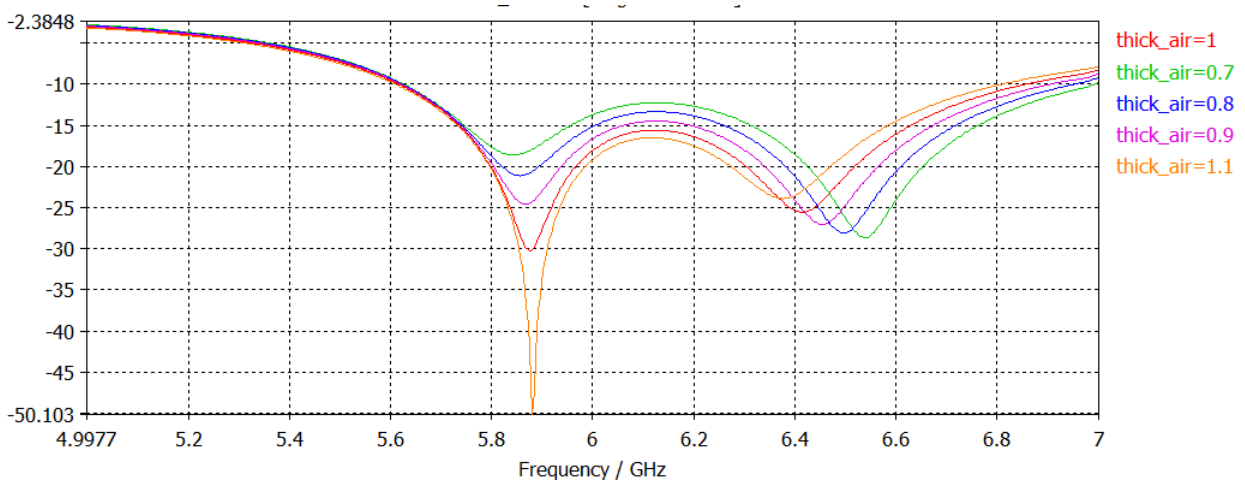

Fig. 34. S11 responses for a substrate's thickness of 4.5 mm, tg loss=0.19, u.cell 44.4 by 34 mm and thickness of air layer "thick_air".

It is worth mentioning that for a substrate's thickness of 4.5 mm tg loss=0.19, and air-gap = 0.7 mm, the relative bandwidth at -10 dB is around 22.2 %.

Finally a target of reaching 15% of relative bandwidth at -15dB was set. Now air-gap thickness and to some extent substrate's thickness and tg loss of the substrate were optimized in order to approach this target. Two of the best resulting responses are shown in figures 35 and 36, with a substrate's thickness of 4.5 mm and air-gap= 0.94 mm and substrate's thickness of 4.7 mm and air-gap= 0.94 mm respectively. The configuration with substrate's thickness 4.5 mm is slightly above -15 dB in its most reflective point, as observed the simulation. The E-shape parameter values remained unchanged with respect to the ones used to obtain the first optimal response shown in table 2.

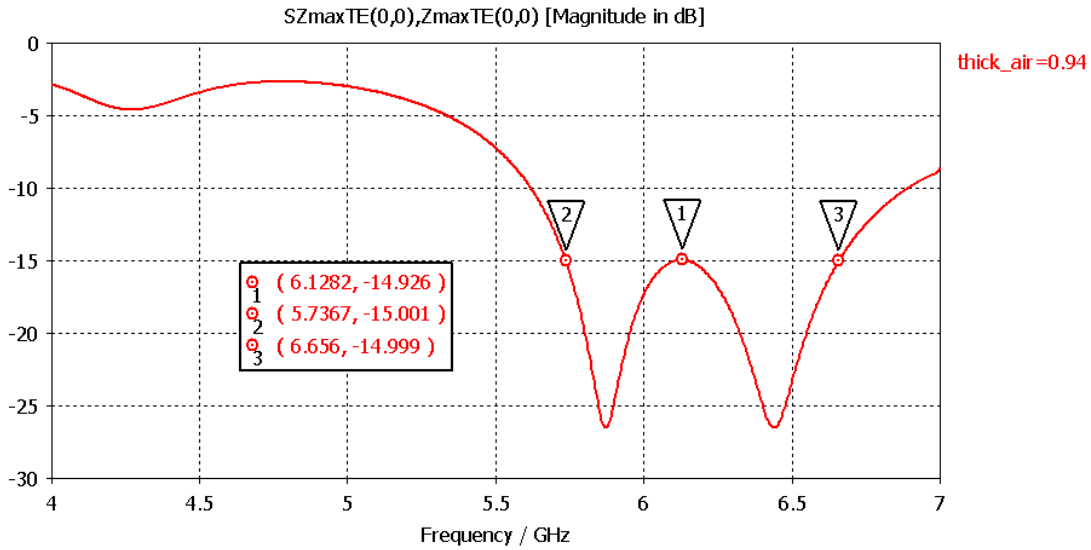

Fig. 35. S11 responses for a substrate's thickness of 4.5 mm, tg loss=0.19, u.cell 44.4 by 34 mm and thickness of air layer= 0.94.

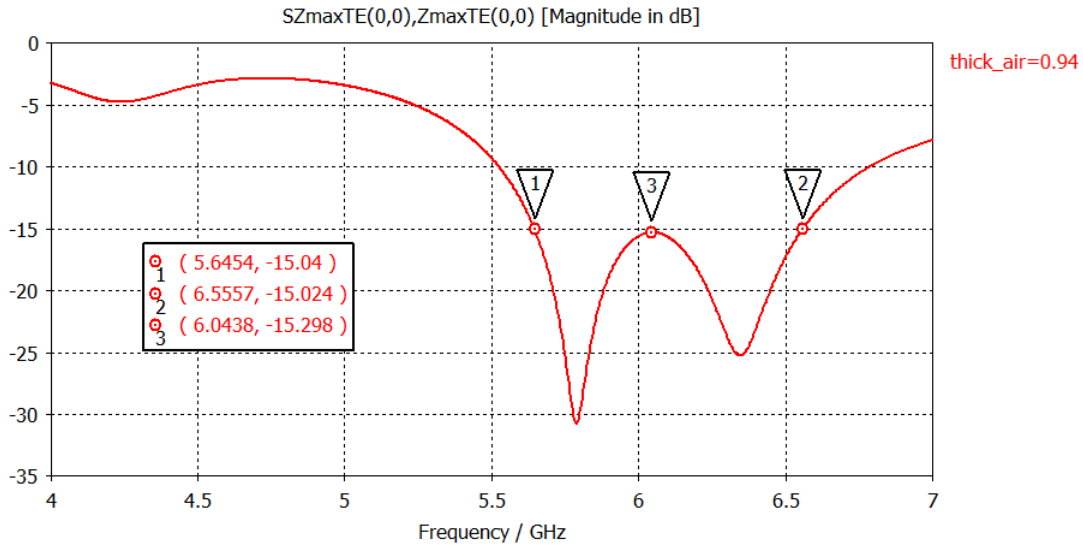

Fig. 36. S11 responses for a substrate's thickness of 4.7 mm, tg loss=0.19, u.cell 44.4 by 34 mm and thickness of air layer= 0.94.

The final optimum reached that could be considered to have the parameter values corresponding to the results in figure 36 has a relative bandwidth of 15.3% at -15 dB and 20.5% at -10 dB.
When the air-gap's thickness was tuned we could observe that there was a trade-off between the bandwidth and the absorption in the central frequency of the band.

4.5 Sensitivity Study

In addition to the theoretical study we decided to investigate whether the optimum design with a relative bandwidth of around 15% at -15 dB could also be fabricated, in order to see the results obtained reflected in real measurements as well.

The loss tangent of our substrate's material that achieved the best optimum in the simulations does not correspond to a specific existent material. Indeed no material with similar electric permittivity and loss tangent could be found in order to fabricate the sample.
Therefore it was important to perform a sensitivity study in order to establish the pertinent tolerance values before any further consideration. We were also able to confirm that in our final optimum result the actual optimal - or very close to optimum- combination of parameter values for this design were found. The simulations used for the study were performed again with CST. We expose results for permittivity and loss tangent of the lossy material used as substrate, substrate's thickness and air-gap's thickness. While one of these four parameters is varied, all others remain unchanged. Absorption in the most reflective point defines at which absorption level is the bandwidth observed:

TABLE III.

Permittivity	**BW [GHz]**	**~BW%**	**absorption in most reflective point (approx)**
3.9	1.024	16.2% (fc 6.3266)	-13.34
4	0.994	15.9% (fc 6.269)	-13.93
4.1	0.967	15.6% (fc 6.2115)	-14.47
4.2	0.939	15.3% (fc 6.1561)	-14.93
4.3	0.911	14.9% (fc 6.1010)	-15.3
4.4	0.881	14.6% (fc 6.0449)	-15.58
4.5	0.855	14.3% (fc 5.9915)	-15.73
4.6	0.825	13.9% (fc 5.9374)	-15.78
5	0.694	12.1% (fc 5.7176)	-15.07

Table 3 summarizes relative bandwidth values and absorption level at the most reflective point of the absorbing band (generally also the central frequency of the bandwidth) for permittivity values varying at around 10 % of the original permittivity. We observe that with a variation of only four decimals, performance falls out of the 15% bandwidth and absorption power at the band's central frequency is below -15dB (-13.339 at 3.9 for example, with relative bandwidth of 16%).
In figure 37 we can see S11 responses corresponding to several different permittivity values.

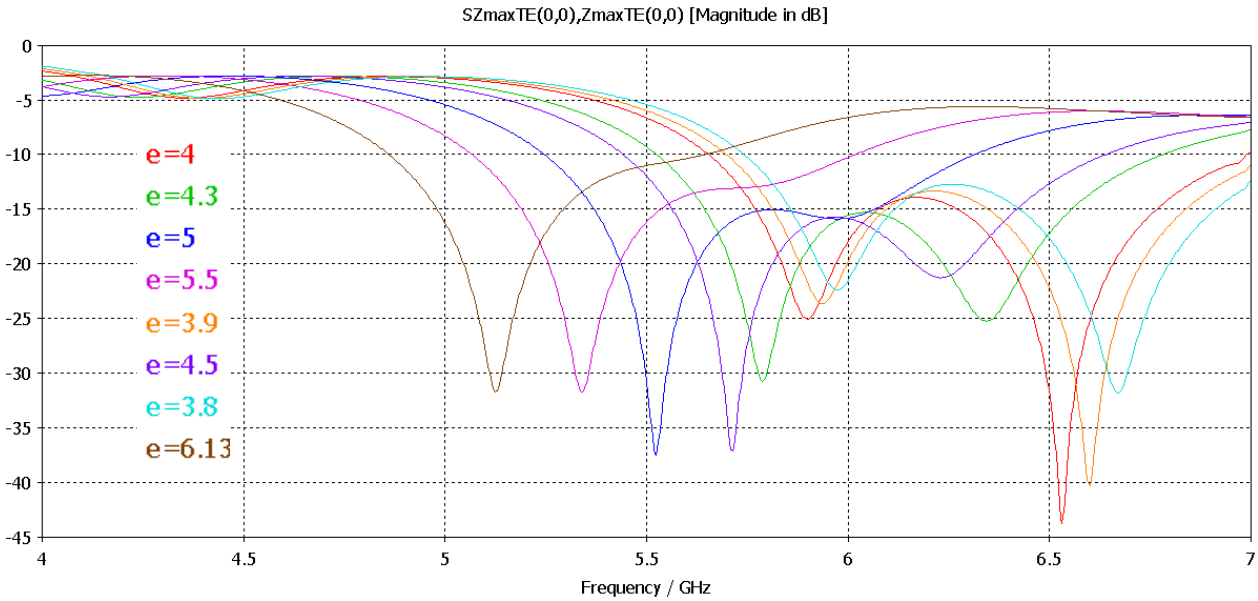

a)

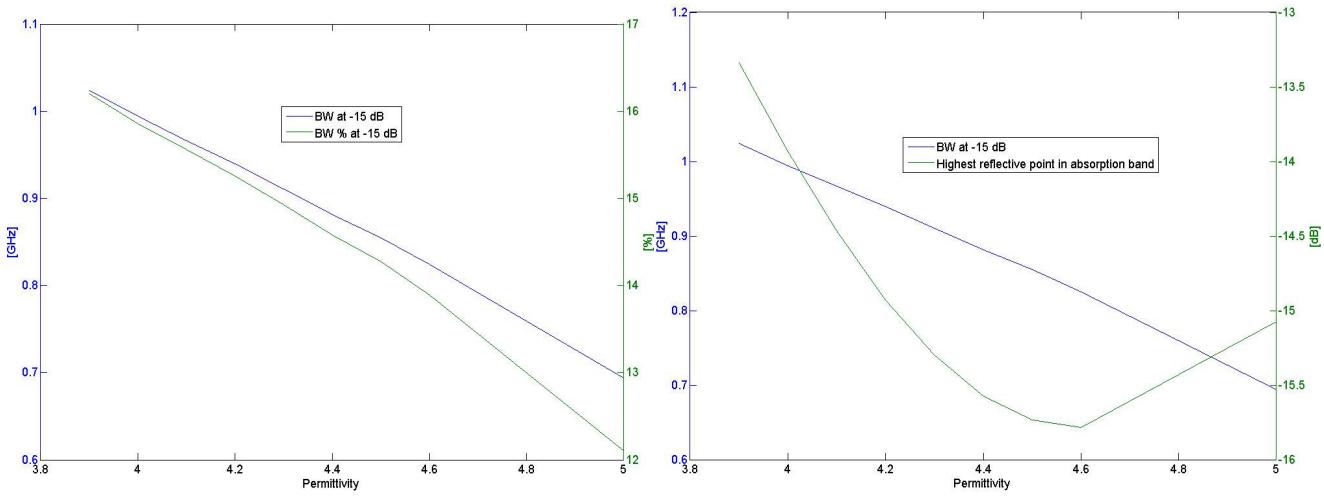

b) c)

Fig. 37. a) S11 responses for several permittivity values around the original optimum of 4.3, with all other parameter values unchanged. b) Plotted sensitivity values of relative absorption bandwidth and correlative bandwidth percentage as a function of selected permitivitty values, as exposed in table 3. c) Plotted sensitivity values of relative absorption bandwidth and correlative highest reflective point in absorption band as a function of selected permitivitty values, as exposed in table 3.

We observed a similar sensitivity with respect to loss tangent. As table 4 shows, with an increase of less than 10% from the original value of our optimum design, the relative bandwidth is already 14.26% at around-14.5 dB.

TABLE IV.

Loss tangent	**BW [GHz]**	**~BW%**	**absorption in most reflective point (approx)**
0.17	0.880	14.4% (fc 6.0936)	-15.16
0.18	0.899	14.7% (fc 6.1032)	-15.27
0.19	0.911	14.9% (fc 6.1013)	-15.30
0.2	0.919	15.1% (fc 6.0982)	-15.27
0.21	0.921	15.1% (fc 6.0935	-15.19
0.23	0.906	14.9% (fc 6.0811)	-14.89

0.25	0.864	14.26% (fc 6.0602)	-14.49

In the interval taken for table 4 we can observe how different is the sensitivity variation with respect to permittivity: relative bandwidth reaches a maximum at a loss tangent of 0.21 and then decreases (whereas the maximum absorption in the least absorptive point is reached with a loss tangent 0.19). When permittivity is increased beyond 3.9, relative bandwidth decreases continuously and the optimum point in terms of the trade-off relative bandwidth with absorption is reached at 4.3. In figure 38 we can observe the sensitivity of our design with respect to loss tangent on a more graphic way, where the response "flattens" as loss tangent is increased and thus bandwidth starts to increase, but the absorption level quickly diminishes and so does the bandwidth, as we can observe after a loss tangent 0.23.

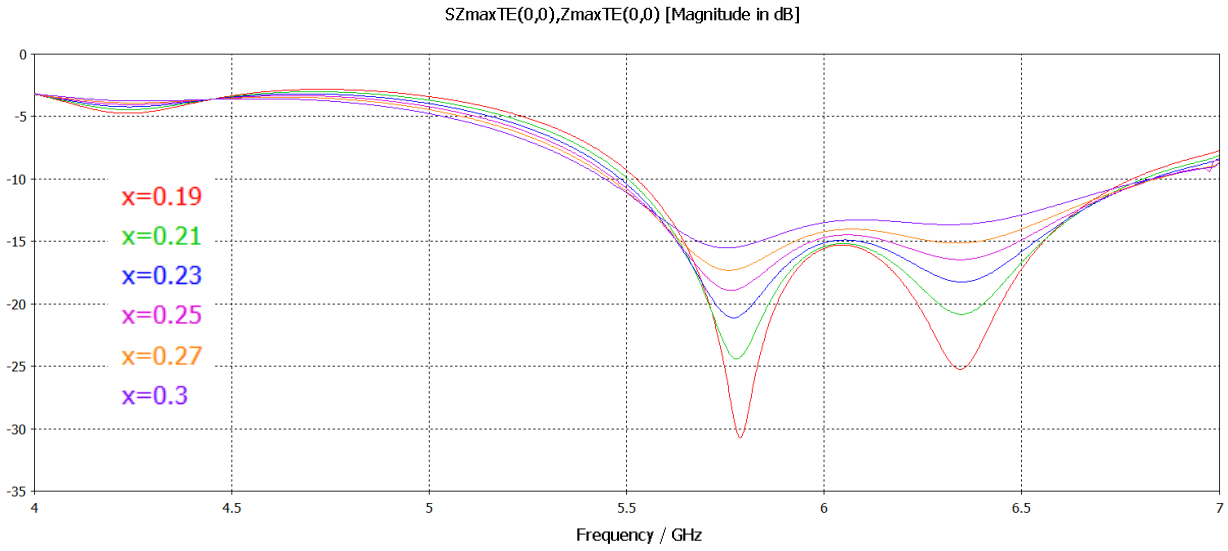

a)

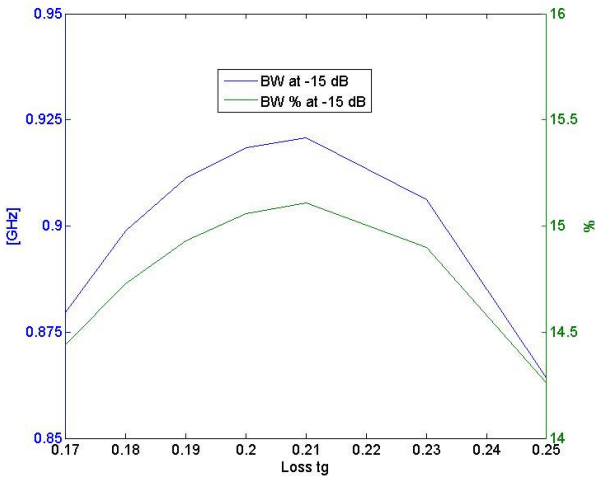

b)

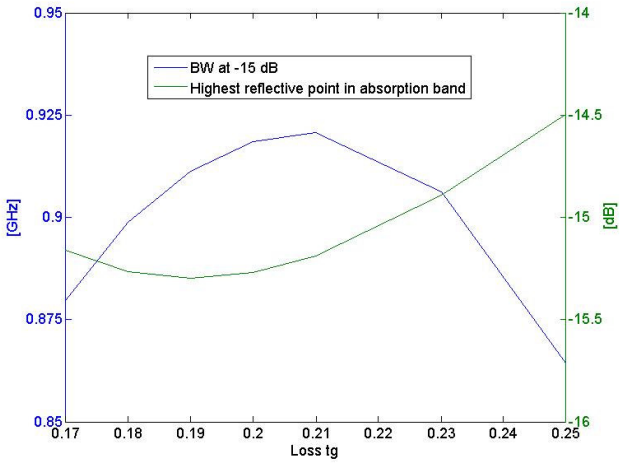

c)

Fig. 38. S11 responses for several loss tangent values, with all other parameter values unchanged. b) Plotted sensitivity values of relative absorption bandwidth and correlative bandwidth percentage as a function of selected loss tangent values, as exposed in table 4. c) Plotted sensitivity values of relative absorption bandwidth and correlative highest reflective point in absorption band as a function of selected loss tangent values, as exposed in table 4.

For the substrate's thickness the effect is easier to observe with several frequency responses again, as depicted in figure 39, in addition to the information summarized in table 5.

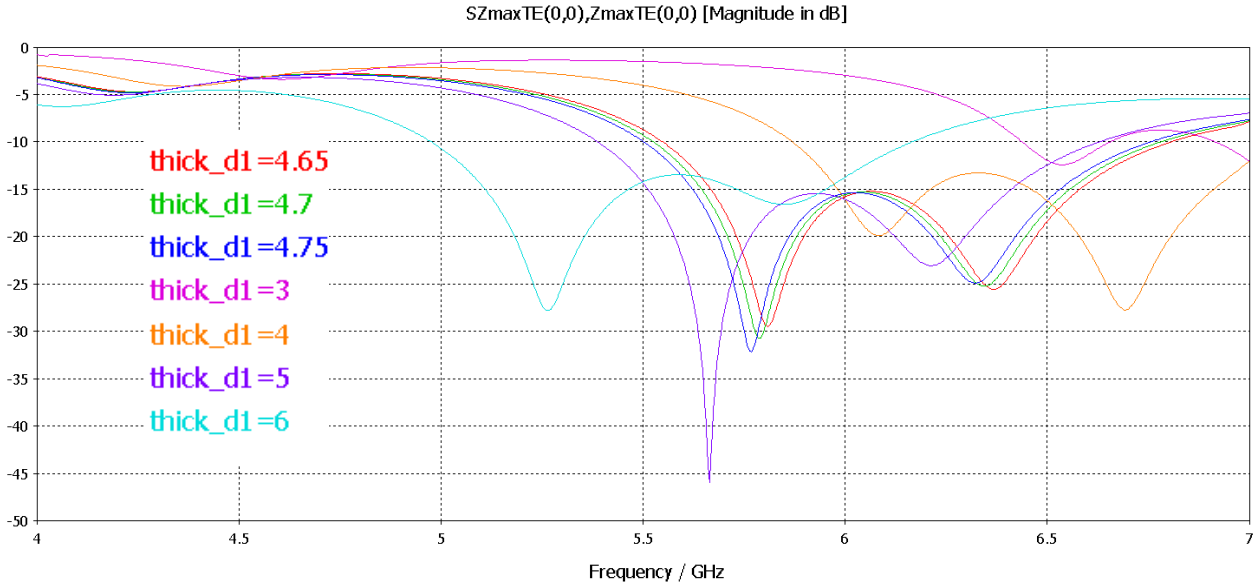

a)

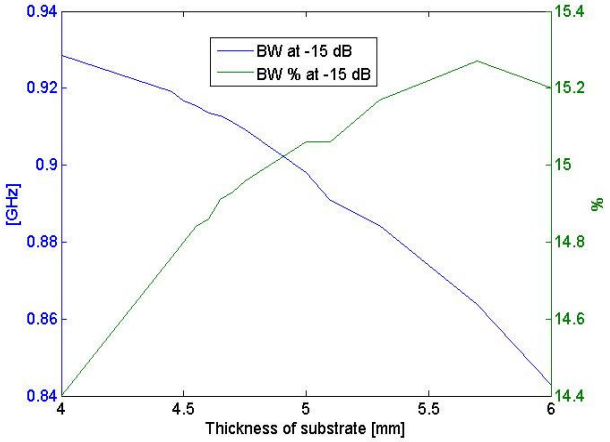

b)

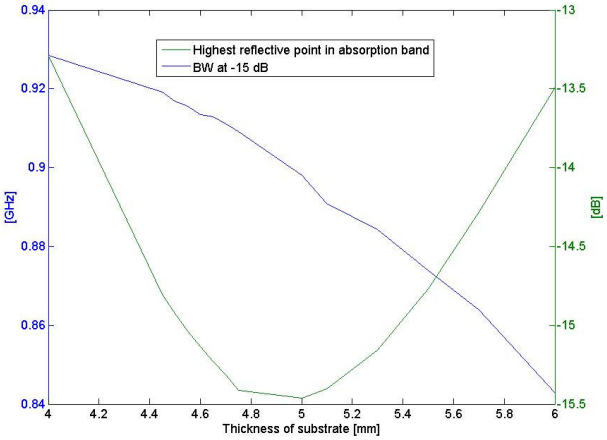

c)

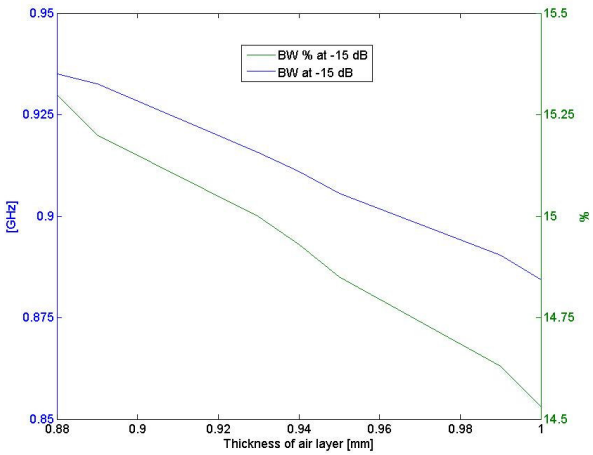

d)

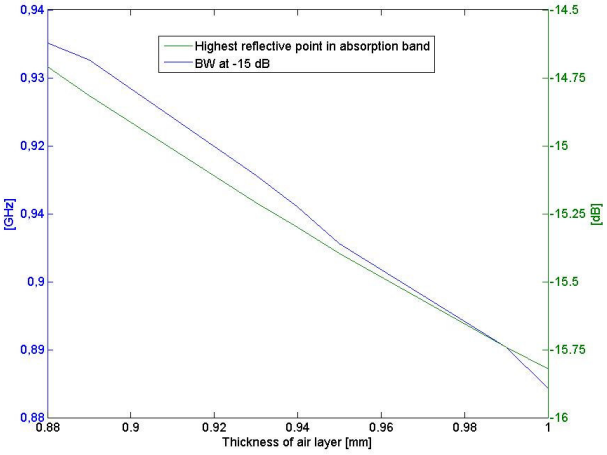

e)

Fig. 39. S11 responses for several substrate's thicknesses, with all other parameter values unchanged. b) Plotted sensitivity values of relative absorption bandwidth and correlative bandwidth percentage as a function of selected substrate's thicknesses, as exposed in table 5. c) Plotted sensitivity values of relative absorption bandwidth and correlative highest reflective point in absorption band as a function of selected substrate's thicknesses, as exposed in table 5. d) Plotted sensitivity values of relative absorption bandwidth and correlative bandwidth percentage as a function of selected air-layer's thicknesses, as exposed in table 6. e) Plotted sensitivity values of relative absorption bandwidth and correlative highest reflective point in absorption band as a function of selected air-layer's thicknesses, as exposed in table 6.

TABLE V.

Thickness of substrate [mm]	**BW [GHz]**	**~BW%**	**absorption in most reflective point (approx)**
4	0.929	14.4%	-13.29
4.45	0.919	14.8%	-14.80
4.5	0.917	14.8%	-14.93
4.55	0.916	14.8%	-15.04
4.6	0.914	14.9%	-15.14
4.65	0.913	14.9%	-15.23
4.7	0.911	14.9%	-15.31
4.75	0.909	15.0%	-15.41
5	0.898	15.1%	-15.46
5.1	0.891	15.1%	-15.40
5.3	0.884	15.2%	-15.16
5.5	0.874	15.2%	-14.77
5.7	0.864	15.3%	-14.28
6	0.843	15.2%	-13.49

For the thickness of the air-gap (see table 6), the optimum is reached between 0.93 and 0.94 where we have the maximum bandwidths with the maximum absorption level beyond -15 dB. In this interval increase in absorption is directly proportional to increase in thickness and inversely proportional to bandwidth increase. Sensitivity is less than with material parameters, especially in comparison with loss tangent were bandwidth decreases very steeply after a certain value.

TABLE VI.

Thickness of air layer [mm]	**BW [GHz]**	**~BW%**	**absorption in most reflective point (approx)**
0.88	0.935	15.3% (fc 6.1138)	-14.71
0.89	0.933	15.2% (fc 6.112)	-14.86
0.93	0.916	15.0%(fc 6.1028)	-15.21
0.94	0.911	14.9% (fc 6.1003)	-15.30
0.95	0.906	14.9% (fc 6.0975)	-15.40
0.99	0.890	14.6% (fc 6.089)	-15.74
1	0.884	14.5% (fc 6.0870)	-15.82

So indeed the sensitivity of our design to the material parameters of the substrate was slightly more important than to substrate's thickness.

4.6 Implementation of optimum design at -15 dB -fabrication and measurement of a sample

4.6.1 Considerations for fabrication of the sample

Even taking into account the tolerance values there was no material that matched permittivity and loss tangent and that was possible for us to acquire. So we decided to combine two different materials to conform the substrate. Even so it was not possible to find any solid available material that matched the tolerance values, nor was the purpose of this investigation to chemically combine different substances in order to create a new material. There are equivalent permittivity models for stacked layers of two different kind of materials ([16]-[18]). However, to the best of our knowledge there are no models for an equivalent loss tangent of a stacked layer structure. The strategy followed was the following: 1) Select the materials which come closest to the materials that are actually needed. 2) Based on these materials, realize two designs with the best possible performance, that are buildable and measurable. 3) Realize and measure these designs. 4) If there is a good agreement for these designs, it is reasonable to expect that the theoretically optimal design also can be fabricated and measured with the same accuracy, once the proper material would become available.

The materials that were used to conform the substrate in a two-layer structure were electromagnetic absorber Eccosorb DSF-U from Emerson & Cuming and the fluoroplastic Dyneon THV220 GZ from 3M (provided by the company without cost through collaboration). Fluoroplastics typically have a loss tangent close to 0.1 at around 10 GHz. The Dyneon is slightly flexible and soft, and according to specifications, it has a loss tangent of 0.08 and an electrical permittivity of 2.66 at 9.4 GHz. We must say that the originally chosen absorber was DSF instead of DSF-U. DSF-U has urethane as binder instead of the original silicone of DSF, but due to availability reasons of the manufacturer DSF-U had to be finally used. Anyway, this should not affect significantly the electrical parameters of interest, as it was also confirmed by the manufacturer. Its loss tangent is of around 0.3, a permittivity of around 13 and permeability 1 at 10 GHz. According to specifications, thickness could vary from 1.65 to 1.85 mm.

The performance obtained in simulation results was not very close to the optimum achieved in the theoretical study, as we can see in figure 40.

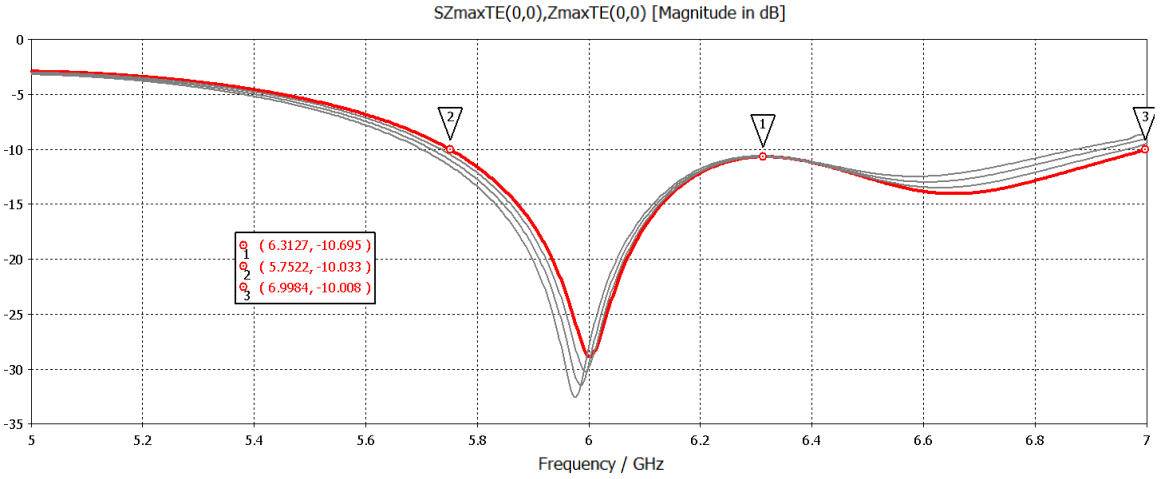

Fig. 40. Simulated S11 response of the new adapted design. Total thickness of lossy substrate= 4.7 mm. Thickness of fluoroplastic top layer 2.35 mm, thickness of absorber (bottom) layer 2.35 mm, adjusted air-gap thickness 1.1 mm

It is also worth mentioning that the air-gap's thickness had to be adapted to the new constituting materials, from 0.94 mm to 1.1 mm, the thickness of the absorber from 2.35 mm to 1.85 mm and the thickness of the fluoroplastic from 2.35 mm to 3 mm.
In order to actually fabricate the sample, it was necessary to introduce a new layer in order to be able to print the metallic resonators in it, as it is not possible to do this in the Dyneon plastic material with the resources available. A layer of PCB (FR4) had to be introduced into the design, with the consequent effects on performance.

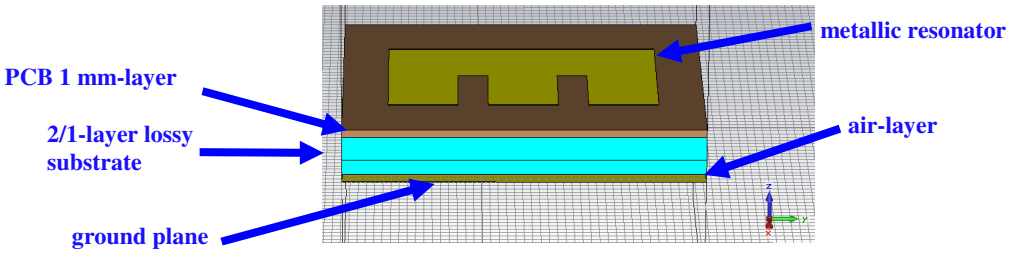

Fig. 41. Unit cell of the modified layer structure including the PCB layer. The lossy substrate is conformed by fluoroplastic and absorber for our first design.

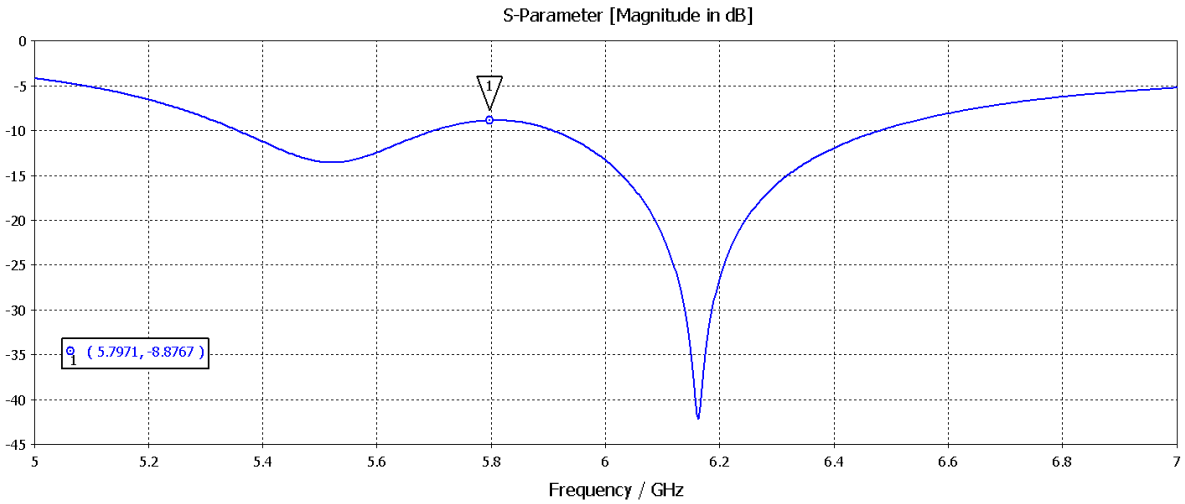

Fig. 42. Simulated S11 response with a 1mm-thick FR4 board, on top of 3mm-thick Dyneon layer and standard DSF-10 absorber with 1.85 mm thickness.Total thickness is then 4.85 mm.

The second design, inspired in the first optimum depicted in figure 14, did not include an air-gap in its layer structure, which was an advantage from the manufacturing or building point of view (see figure 43).

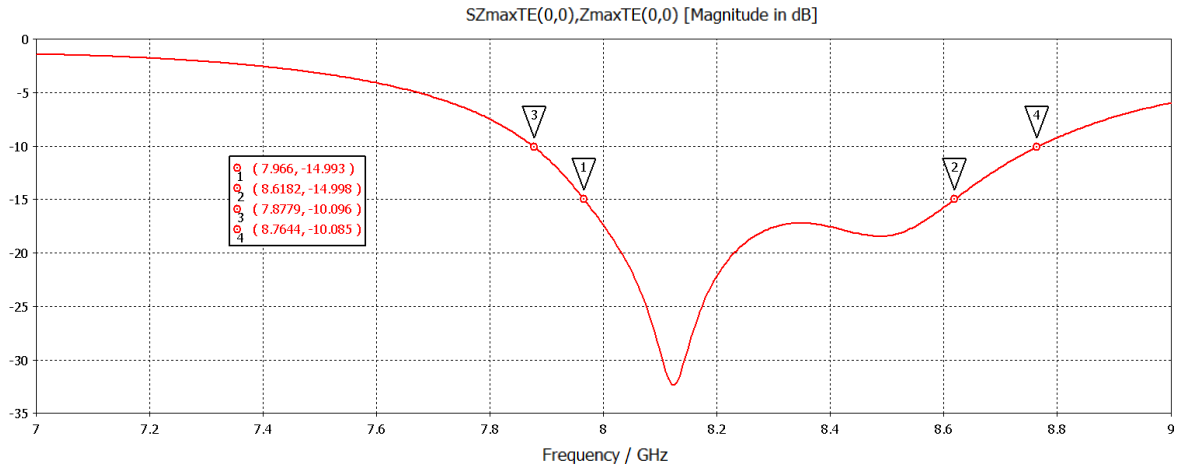

Fig. 43. Simulated S11 response for design using only Dyneon and FR4.Total thickness of lossy substrate is 4.3 mm. Thickness of Dyneon (top) layer 2.34 mm, thickness of FR4 (bottom) layer 1.97 mm, no air-gap.

The addition of a PCB layer in the model affected the original response in such a way that the main features of the original response (relatively wideband absorption beyond -15dB) were not clearly observed anymore (see figure 44).

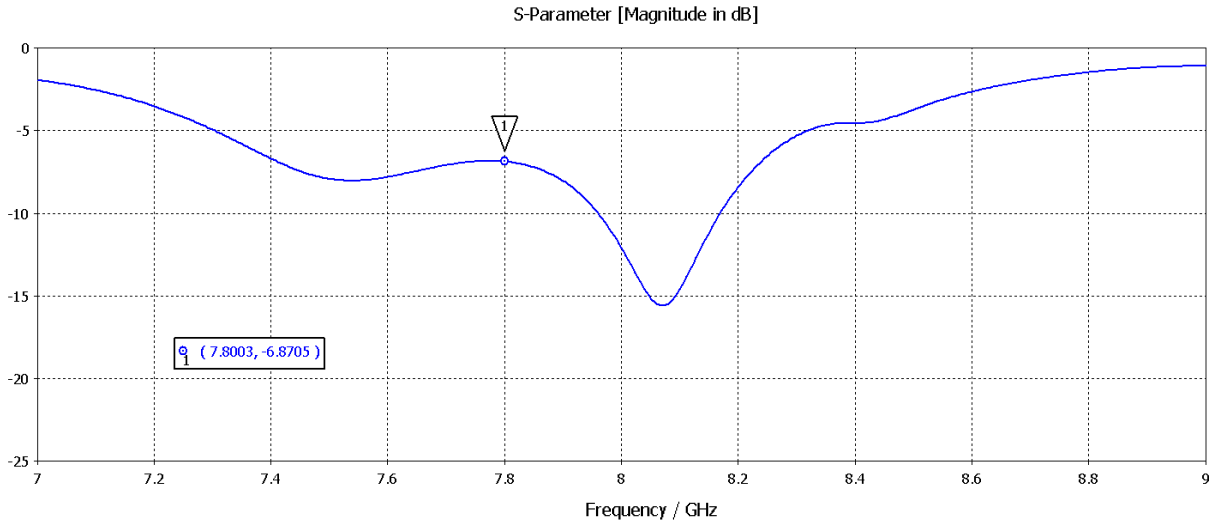

Fig. 44. Simulated S11 response of the design referred in figure 43 after adding a 1-mm -thick layer of PCB material on top.

4.6.2 Measurement set-up and considerations related to it

Given the size of the unit cell of our design (comparable to a wavelength of the operational frequency), we were not able to use waveguides to make the measurements: The operational frequency of the unit cell , when scaled to the size of standard waveguide adapters fell out of the operational frequency range of the waveguides. So if we scaled our design in order to fit the waveguide's size, we were not going to be able to see its response. Thus we had to use an open system to make the measurements, involving horn antennas. In our case, as our design has a back metal plane, only reflection (S11) needs to be measured and thus only one horn antenna is necessary. We used the set-up shown in figure 45 connected to a network analyzer, where the distance of the horn antennas with respect to the reference plane can be adjusted.

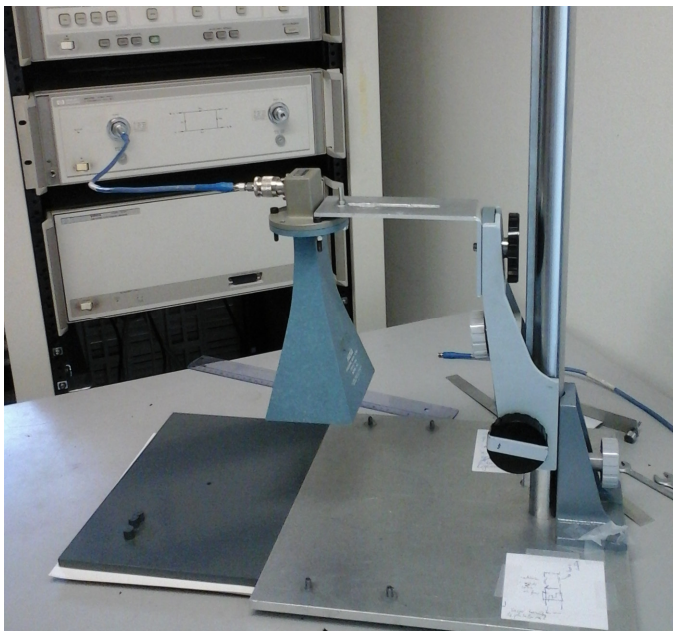

Fig. 45. Measurement set-up used, with adjustable distance to the sample (modified by the black and grey round handle).

The open system set-up implies more leakage (electromagnetic radiation that is not transmitted to the sample and is lost in free space, also finally contributing to reflections) in the measurement and multiple reflections between sample and horn. For very close distances, the system starts even to resemble a cavity topology.
The open system also implied the use of a large sample, but then for the unit cell it was also possible to use the same dimensions as in our original design (it was not necessary to scale it). Making the sample as large as possible is intended to reduce the effect of the edges as much as possible.

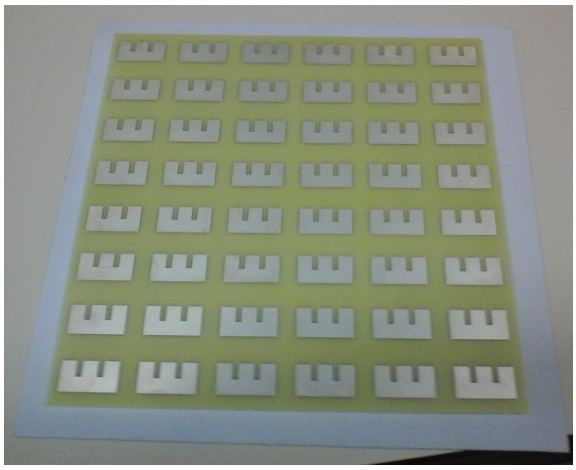

Fig. 46. Photo of the assembled sample.

Whereas the dimensions of the absorber and PCB board were similar (maximum size of absorber was one sheet of around 305 mm by 305 mm, maximum size of PCB board slightly large, thus the dimensions of one sheet of absorber were taken as reference and final size of the PCB board was 266.4 mm by 272 mm), Dyneon plastic could only be delivered in round plaques of 200 mm diameter. Therefore, square pieces had to be cut from the plaques and 4 of them were necessary to reach the dimensions of the board and the absorber. Its thickness is of 3 mm. The thickness of the absorber sheet was of 1.85 mm.

Due to the small thickness of the air-gap the best possible option was to use spacers of 1 mm to implement this air-gap. It was not possible to cut such a thin layer of air-mimicking foam within our facilities. The use of plastic screws, besides being mechanically unpractical in a real application, could also damage the layers of absorber and plastic and again it was nearly impossible to do it for these two materials with the infrastructure available. The screws should transverse all the layers to hold the sample together and keep the air-gap of 1 mm constant. It has to be born in mind that the absorber is very flexible and soft. Thus if the screws were used only at the edges of the sample the absorber would bend in the center -also because of the large dimension of the sample- making the thickness of the air-gap highly inconstant.

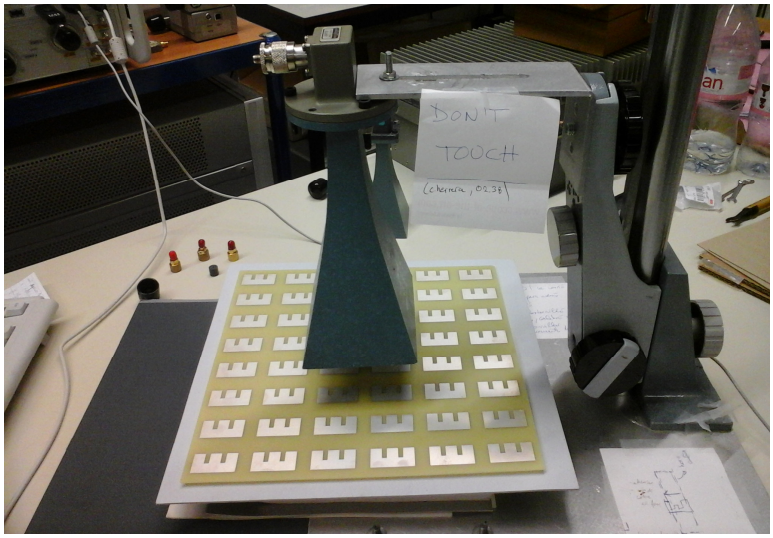

Fig. 47. Sample in the measurement set-up.

4.6.3 Measurement Results

We used a measurement technique previously utilized in our research group for transmission and developed for open measurement systems [15]. It mainly consists in making several measurements with the horn antenna at different distances and averaging the results. Calibration was also performed and reflection in free space and different distances with respect to the reference plane were taken into account. This should also partly mitigate the contribution of multiple reflections in the measurements.

The fact that electromagnetic waves are less planar as they are closer to the excitation source, and the increased presence of leakage or losses when the horn antenna is at the largest distances from the sample, should be taken into account as well.

The result of measuring from a distance of 4 cm to the sample to a distance of 7.5 cm to the sample, after performing the processing [15], can be seen in figure 48. This was done in a minimum of 7 steps, thus 7 measurements.

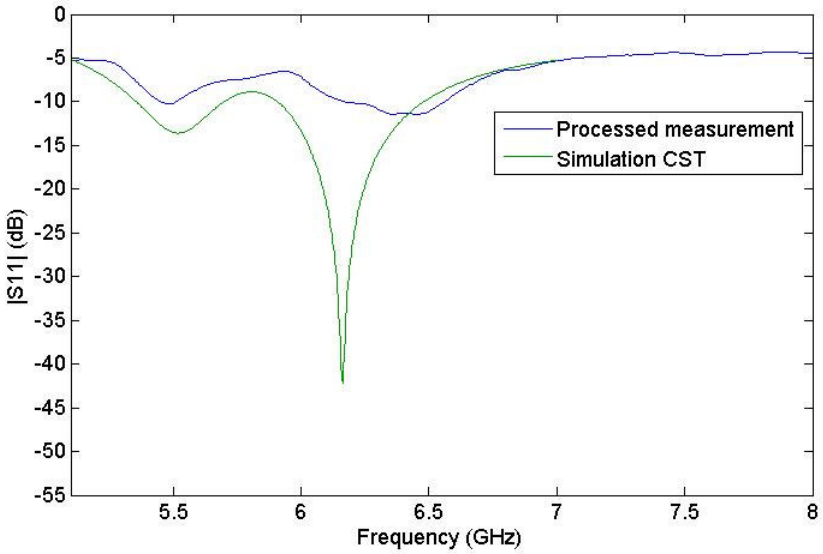

Fig. 48. Processed measurement results compared with simulation of the design with addition of PCB board, as shown in figure 42. However here air-gap's thickness is of 1 mm in the simulation, instead of 1.1 mm, as available spacers were 1 mm-thick.

It has to be born in mind that this technique [15], previously used in our research group, which in most cases consists in making an average of several measurements -as it was the case here- not only can reduce the noise in the measurements, but very likely to do it also with the magnitude of the resonances in the response. It thus reduces the absorption, in our case. Thus it is also responsible for "smoothing" very sharp or high absorption values, which have actually been produced by the sample.
The technique can reduce noise specially originated by the edge effect of using a finite sample, effect which should be increased with smaller samples that are not many λs-long.

In figure 48 the measured result is shown in comparison with the simulation performed using the manufacturer's specifications and standard thicknesses, simulation result that is also shown in figure 42. The high absorptive peak at around 6.16 GHz could be considered as "non physical", meaning it is very unlikely that the absorption level reached would be so high in real measurements.
However, taking into account the sensitivity of the original design we directly measured the thicknesses of the constituting layers and the permittivity values of the absorber and fluoroplastic, in order to have a reference. These values are updated in the simulation and the compared result is shown in figure 49. Table VI summarizes and better highlights the differences between the original and updated values.

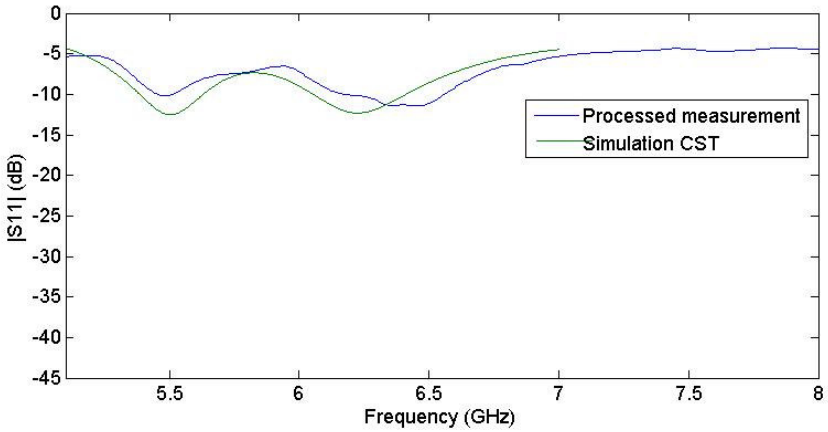

Fig. 49. Processed measurement results compared with the simulation of figure 48 but with permittivity=11.9, loss tangent=0.3 at 10 GHz for Eccosorb absorber and permittivity =2.7, loss tangent=0.08 at 10 GHz for Dyneon plastic. Eccosorb absorber's thickness is 1.81 mm, Dyneon plastic 3.24 mm and air-gap is of 0.7 mm.

TABLE VII.

Nominal and measured values of material parameters

Materials parameters	**Datasheet and component's nominal values**	**In-house measured values**
Permittivity of Dyneon fluoroplastic	2.66	2.7
Permittivity of Eccosorb absorber	13	11.9
Eccosorb-layer thickness	1.85 [mm]	1.81 [mm]
Fluoroplastic-layer thickness	3 [mm]	3.24 [mm]
Air layer thickness	1 [mm]	0.7 [mm]

Although the level of absorption obtained is not very interesting in terms of applications or prototyping, the results were fairly broadband, thus an intrinsically wideband behaviour can still be observed in the fabricated structure, which was also one of the original objectives in this periodic absorber design. The substrate's material was probably the most harmful issue in this respect, together with the kind of system that had to be used.

Given the operational frequency of our optimum design, centered around 5.5 and 6 GHz, it could find different wideband applications in the 5.4 GHz band. If the proper material for substrate is found, a single-layer instead of the here implemented two-layer structure could have more practical usability in a myriad of applications, including:

-a wideband absorber attached to walls, for instance of a building that needs to be secured from wireless radiation (a secure wireless environment) in a specific frequency band, as proposed in [19] for graphene, but using a less expensive alternative to this material. In [19]

the broad bandwidth presented is not really continuous (absorption periodically fell to nearly 50% in the absorption bandwidth, unless five or more layers of graphene were used. Still with five layers, absorption was not larger than 90% for the whole frequency band), as opposite to the bandwidth of our design. Our designs could be used in the microwave band.

-as isolator between elements of an antenna array (a MIMO array is an example), if a wide bandwidth of absorption is required. Metamaterial and periodically structured absorbers are specially adequate for small antenna arrays, like the ones often used with MIMO, where small sized, planar and thin –at least thin as the antennas themselves- materials are required [20].

4.7 General conclusions

Although it was not possible to fabricate the optimum design, it represents, as a new design, an interesting contribution to the field of periodic absorbers and absorbers themselves:

A metallic resonator previously used in antennas has been introduced and studied to investigate its performance in metamaterial absorbers. To our knowledge this has not been done before with this specific resonator and this is why it should represent a contribution to the field of periodic absorbers and the work performed should have a certain level of originality.
Interesting bandwidths of around 15% and even 20% have been achieved at levels of absorption of -15dB (97% absorption) and -10 dB (90% absorption). This is relevant taking into account that the scientific state of the art for topologies for which only one resonator in a single-layer structure is used, bandwidths are typically of around 12% at the most. Larger bandwidths can be achieved but typically by using multiple resonators and or multiple layer-structures, where several resonances in different frequencies are added, whereas it is more difficult to find a topology where the addition of multiple resonances is not used and only one resonator is necessary to reach a continuous bandwidth. Although multiple-layer structures do not necessarily lead to thick absorbers single-layer structures (or structures with few layers) are valuable to try to avoid thickening and more complex fabrication technology -multiple-layer structures and multiple resonators, which can have different dimensions, usually require more costly fabrication technologies-. The shape used for our metallic resonator is not excessively complex, which could be an advantage if we bear in mind fabrication. No lumped elements such as resistors or diodes are used either, which can also be an advantage in terms of complexity or compactness of the design for applications.
Commercially the responses obtained are interesting as their bandwidths are wider than typical narrowband absorbers, at absorption levels that although smaller could be regarded as similar (commercial absorbers can reach -20dB, 99% absorption, our configuration can reach with a continuous bandwidth around -15dB, 97% absorption). Commercial broadband absorbers typically have bandwidths that are wider than the ones achieved in this work, but are not more absorptive than -10dB (90% absorption). Thus our configuration could be regarded as more than narrowband but less than wideband, in terms of commercial absorbers. Additionally its frequency dependence with thickness has not proven to be as strong as in some current commercial absorbers. It might be also worth mentioning that although the material used for the substrate in our configuration is not a low-loss dielectric, its loss tangent is however smaller than the ones that can be found in currently commercial absorbing materials (0.31, 0.41, 0.71 for instance).
Not to mention the fact that metamaterial and periodic absorbers with a fully wide or at least not-narrow band absorption are desired, as absorbing material is often required to cover a wide spectrum of frequencies as fully as possible.

4.8 References

[1] Z.Ma, G.A.E.Vandenbosch, “Low-Cost wideband microstrip arrays with high aperture efficiency”, IEEE Transactions on Antennas and Propagation, vol.60, no. 6, pp. 3028-3034, Jun. 2012.

[2] Z.Ma, V.Volskiy, G.A.E.Vandenbosch, “Optimal design of a highly compact low-cost and strongly coupled 4 element array for WLAN”, IEEE Transactions on Antennas and Propagation, vol.59, no. 3, pp.1061–1065, Mar. 2011.

[3] Y.Ge, K.P.Eselle, T.S.Bird, IEEE Transactions on Antennas and Propagation, Vol.52, No. 12, December 2004.

[4] Yu Qian Ye, Jin, and He, “Omnidirectional, polarization-insensitive and broadband thin absorber in the terahertz regime”,Journal of the Optical Society of America B, Vol. 27, Issue 3, 498-504, 2010.

[5] Sun, Liu, Dong, Zhou; “An extremely broad band metamaterial absorber based on destructive interference”; Optics Express,Vol.19 , No.22, 21155,2011

[6] Ding, Cui, Ge, Jin, He; "Ultra-broadband microwave metamaterial absorber", Applied Physics Letters; Vol.100; No.103506,2012

[7] N.I.Landy, S.Sajuyigbe, J.JMock, D.R.Smith, W.J.Padilla; "Perfect metamaterial absorber", Physical Review Letters, Vol.100, No.207402

[8] Li, Yang, Liang; "A wide -angle polarization-insensitive ultra-thin metamaterial absorber with three resonant modes "; Journal of Applied Physics;Vol.110; No.063702

[9] Lee, Lim;"Bandwidth-enhanced and polarization-insensitive metamaterial absorber using double resonance"; Electronic Letters; Vol.47; No. 1

[10] Alves, Kearney, Grbovic, Lavrik, Karunasiri; “Strong terahertz absorption using SiO2/Al based metamaterial structures”; Applied Physics Letters,Vol.110, No.111104

[11] Alici, Bilotti, Vegni, Ozbay; “Experimental verification of metamaterial based subwavelength microwave absorbers”; Journal of Applied Physics, Vol.108, No.083113

[12] Landy, Bingham, Tyler, Jokerst, Smith, Padilla; “Design, theory and measurement of a polarization-insensitive absorber for terahertz imaging”;Physical Review B ,Vol.79, No.125104

[13] Hao, Wang, Liu, Padilla, Zhou, Qiu; “High performance optical absorber based on a plasmonic metamaterial”; Applied Physics Letters, vol.96, No.251104

[14] Tao, Bingham, Strikwerda et.al; “Highly flexible wide angle of incidence terahertz metamaterial absorber: Design, fabrication, and characterization”;Physical Review B, Vol.78, No.241103

[15] S. Yan, G.A.E. Vandenbosch, "Compact circular polarizer based on chiral twisted double split-ring resonator", Applied Physics Letters, vol. 102, No. 10, 103503, March 2013.

[16] D. J. Bergman, "The dielectric constant of a composite material - a problem in classical physics", Physics Reports, Vol. 43, No. 9, 377, 1978.

[17] Alabaster, C.M, "The Microwave properties of tissue and other lossy dielectrics", PhD dissertation, Department of Aerospace, Power and Sensors, College of Defense Technology, Cranfield University, 2004.

[18] T.Nakamura, K.Ogawa and R. Sato, "Electric Characteristics of a Dipole Near the Boundary between Two Media", Electronics and Communications in Japan, Part 1, Vol. 89, No. 9, 2006

[19] Wu, Tuncer, Naeem,Hao et.al.; “Experimental demonstration of a transparent graphene millimetre wave absorber with 28% fractional bandwidth at 140 GHz”; Scientific Reports, Vol.4, No.4130, 2014

[20] Sharawi,Numan,Aloi; “Isolation improvement in a dual-band dual-element MIMO antenna system using capacitively loaded loops”; Progress In Electromagnetics Research, Vol. 134, 247-266, 2013.

[21] Gu, Barrett, Hand, Popa, Cummer; "A broadband low-reflection metamaterial absorber", Journal of Applied Physics, Vol.108, No.064913, 2010.

[22] Cheng, Wang, Nie, Gong, Xioing, Wang; "Design fabrication and measurement of a broadband polarization-insensitive metamaterial absorber based on lumped elements"; Journal of Applied Physics; Vol.111 ; No.044902, 2012

[23] Shen, Cui, Zhao, Ma, Jiang, Li, "Polarization-independent wide-angle triple-band metamaterial absorber", Optics Express, Vol.19, No.10, 2011.

[24] Li, Yuan, Zhou et.al, "Ultrathin multiband gigahertz metamaterial absorbers",Journal of Applied Physics Vol.110, No.014909, 2011

5 L-shapes and combinations of L and E-shapes as resonating elements in periodically arranged absorbers

5.1 Introduction

Inspired by the E-shape and using our previous experience with the E-shape resonator, we decided to analyze the effect of using L-shapes as resonators for a metamaterial absorber –an L-shape can be seen as an E-shape with two missing branches. Instead of changing the length of the branches, they were suppressed-, which finally resulted in periodic absorbers designs. Double L-shaped resonators have been used in the past in metamaterials to seek for a negative index of refraction, but not often one single L-shaped resonator is used in the microwave frequency and not for a metamaterial absorber [1]-[12]. In plasmonics L-shapes have been frequently used –it is the "basic noncentrosymmetric shape"- and are known to produce multiple resonances [3]. This motivated the introduction of the L-shape as another resonator for wideband absorbers, as it could also possibly produce wideband responses.

The initial objective is to improve or enhance any feature of the results achieved with our most wideband absorption results obtained with the E-shape: either keeping the performance achieved with the E-shape resonator but use a substrate material with lower losses or that is more easily available –and thus more easily manufacturable-, or achieving polarization insensitive results with a wideband absorption, or finally achieving better absorption bandwidths with equal or larger levels of absorption.

In the end a number of designs were found with a total absorption performance that, in numerical calculations, was simply better than the one of the E-shape and a design that in addition to this is polarization insensitive. The relevance of a wideband and continuous absorption has been already illustrated in previous chapters, as well as the merit of using a single metallic resonator instead of multiple to meet this aim. The bandwidth levels achieved in this chapter's analysis are interesting for the state of the art, where wide bandwidths are reached at a 90% of absorption, or more often at smaller absorption levels (at full wave half maximum, FWHM), instead of the 97% (-15 dB) reached here. Just one example of many is [12], where a 38% is achieved at FWHM, thus at less than 50% (-3dB) of absorption and with three resonators in a three-layer structure. The relative absorption bandwidths are large with respect to the state of the art, as can be seen from the performance of the absorbing structures presented in chapter 1 of this thesis. Also a single resonator instead of multiple, as is often the case, is used to achieve this, neither lumped or active elements are used as opposed to what has been several times presented in the state of the art.

As in many other structures in the state of the art, all designs presented in this chapter are planar structures with metallic ground plane.

Nevertheless, the resonant responses of the designs presented in this chapter rather rely on second or third order resonances, while metamaterial absorbers were originally inspired in losses generated by the resonances of sub-wavelength structures. Thus in structures where the size of its unit cells and inclusions is one order smaller than the wavelength at the operational frequency range, and then where first order resonances are responsible for the losses. Consequently in the state of the art of metamaterial and periodically arranged absorbers it can be easier to find structures which dimensions comply with the effective medium theory and that rely on first order resonances, these will also be more highlighted.

Besides their lossy resonances, the typical characteristics of sub-wavelength metamaterials that motivated their use as absorbing structures -and made them very different from most conventional absorbers- were adaptability and tunability, in particular tunability to the operational frequency of the application, low profile or small thickness and more

independency of thickness to establish their broad operational frequency range. These characteristics are mostly shared by our wideband designs.

Finally it was also desired to use a metallic resonator different from the one previously investigated and if possible original for the state of the art as well.

Our approach to the results presented in this chapter uses as start point the same layer structures -and sometimes parameter values- as the ones used in the optimal designs obtained with the E-shape, followed by further investigation and tuning until a phase of fine tuning and optimization of the designs is reached. Further investigation, tuning and optimization is only done with the combinations and resonators' shapes that show promising results above all in the initial phases.
More specifically, for the designs that use a single L-shape as resonator, investigation started by using longer L-shaped resonators as the one introduced in section 5.3.1, with a layer structure that was then progressively optimized. Shorter resonators in different structure configurations were studied, the most wideband structures were further optimized, and finally the most wideband results selected.
A deeper explanation and further criteria are given in subsection 5.1.1.

Using the same approach as with the single L-shape and inspired by [13], we finally intended to add the absorption capabilities of both L and E-shape resonators, by locating them adjacently in the same unit cell, in a coplanar configuration. Our objective is to enhance the previous results with the L-shape even further and observe the effect of adding the E and L-shape resonators. Very strong absorption performances were also obtained from this new configuration.

In section 2 a design that uses the L-shape and is polarization insensitive and wideband is presented.
In sections 3 and 4 several selected cases are presented, which have actually been part of the investigation preceding and resulting in the obtainment of the optimum polarization insensitive design presented in section 2. In the designs presented in these 2 sections, absorption bandwidth is significantly improved with the use of L-shapes, with respect to the E-shape design of chapter 4: Section 3 presents the results of using a design with a layer structure that includes an air-gap. In section 4 the air-gap is removed.
In section 5 we try to use the experience of both L and E-shaped resonators. Section 6 contains the general conclusions.

5.1.1 Design process, components' influence and criteria in an absorbing structure's performance

In a general design cycle of a planar grounded structure typically using only a single metallic resonator, with ultimate focus on absorption bandwidth, some important issues are:
If we have only the substrate -material parameters and thickness, for example- determined we can eventually further optimize the resonators' design, the parameter values of the resonator's shape. If impedance of the resonating shape is known, then the relationship between its parameters and impedance match, and finally its influence in absorption level is easier to establish. In any case as there is a trade-off between absorption level and bandwidth, the last one can be modified. The tuning of any metallic resonator can also create more resonant responses and modify the existing ones, which can finally also affect absorption bandwidth. The slight adjustment of unit cell dimensions can also contribute to better match absorption

level and could in turn finally also have an effect on bandwidth. Thus resonator's parameters and unit cell's dimensions can also further optimize an absorption bandwidth result. Obviously if we have a determined substrate but the metallic resonator is not determined, the election of a resonator -and dimensions- will have a clear influence in the bandwidth, as each resonator will have a characteristic frequency response, with one or multiple resonances, that will change or have a different influence with each different substrate -or even layer-structure-. Thus the response of the resonator and substrate will couple. This will create different absorptive responses and bandwidth, depending on the addition of resonances and absorptive properties of the structure's components.
If the thickness of the substrate is not determined, it can be increased or decreased to improve the structure's performance after the rest of the parameters of the structure have been determined. The influence of substrate's thickness on absorption level through impedance matching (see Introduction of chapter 3), as well as that of total thickness of an absorbing structure in bandwidth is known. According to our previous experience, there are also boundary values for a substrate's thickness, when all other parameters in the structure are determined, beyond which absorption bandwidth starts to decay.
Analogously when substrate's material parameters are changed, there are values for which the maximum bandwidth absorption is reached, when all other parameters in the structure are defined. This is the case with loss tangent of a material, for instance.
When a specific absorption bandwidth wants to be reached, anyhow typically the absorption level is first addressed, as the bandwidth will be required for a defined absorption level, then the bandwidth is address, but the trade-off between both has to be born in mind.
There are losses in the metallic resonator and the substrate -ohmic and dielectric losses-, so both contribute to the absorption in different combinations of proportions for each design. This is why typically both have to be taken into account for tuning and optimization.

Optimization comprises at least the use of optimization algorithms in an electromagnetic solver, but also previously using electromagnetic and geometric criteria, and further simulations including parameter sweeps.

A circuit model is typically used to better match or to find a perfect match between the structure and free-space, in order to reach perfect absorption (a more detailed explanation is provided in the Introduction of chapter 3. The dimensions of the resonator will ultimately determine its resonant frequency, as is well known). It is not sufficient however when also a wideband absorption is required and specially if rather absorption bandwidth and not perfect absorption is the focus.
There is an intrinsic trade-off between absorption level and absorption bandwidth, already mentioned in section 4.4 in chapter 4. Typically when absorption increases in a resonant response, its absorption bandwidth decreases and vice versa, to an increase of absorption bandwidth, the absorption level of a particular response decreases.
Full scaling of a design or structure shifts its resonant response to higher or lower frequencies, there is no direct relation between the size of a structure and its performance.
What makes a structure "sub-wavelength" is the frequency range chosen as operational frequency of that structure. The size of the structure is then compared to the wavelength corresponding to that operational frequency.

Anyhow the design procedure can differ depending on the structure, specifications and requirements to it other than the absorption bandwidth - this is why each publication describes the design procedure used -, but all the previously mentioned criteria are taken into account for the design process.

5.2 Polarization insensitive response with the L-shaped resonator

In this section we tried to make a polarization insensitive response from previous wideband results obtained with one L-shape resonator. This would be an important improvement with respect to previous absorption performances with the E-shape as well.
We use the most optimum design of the L-shape with the geometry made symmetrical (resonator and unit cell), as depicted in figure 1. The largest absorption bandwidth was obtained with a loss tangent = 0.21 and substrate's thickness=4.4 mm. The fully polarization insensitive version obtained is shown in figure 2.
The dimensions of the symmetrical L-shape resonator are shown in table 1, substrate's material permittivity is 4.3.
Except for a slight adjustment on the value of the permittivity, the optimum parameter values used were a result of the sensitivity study presented in section 2.1.

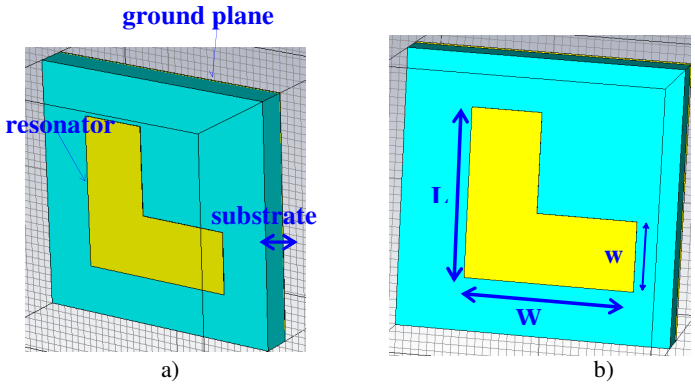

Parameter name	Value [mm]
L =W	20.9
w1	8.6

Table 1- Symmetrical L-shape dimensions

Fig. 1. a) Unit cell size is 34 by 34 mm. No air-gap is used in the layer structure of the unit cell. b) New symmetric unit cell.

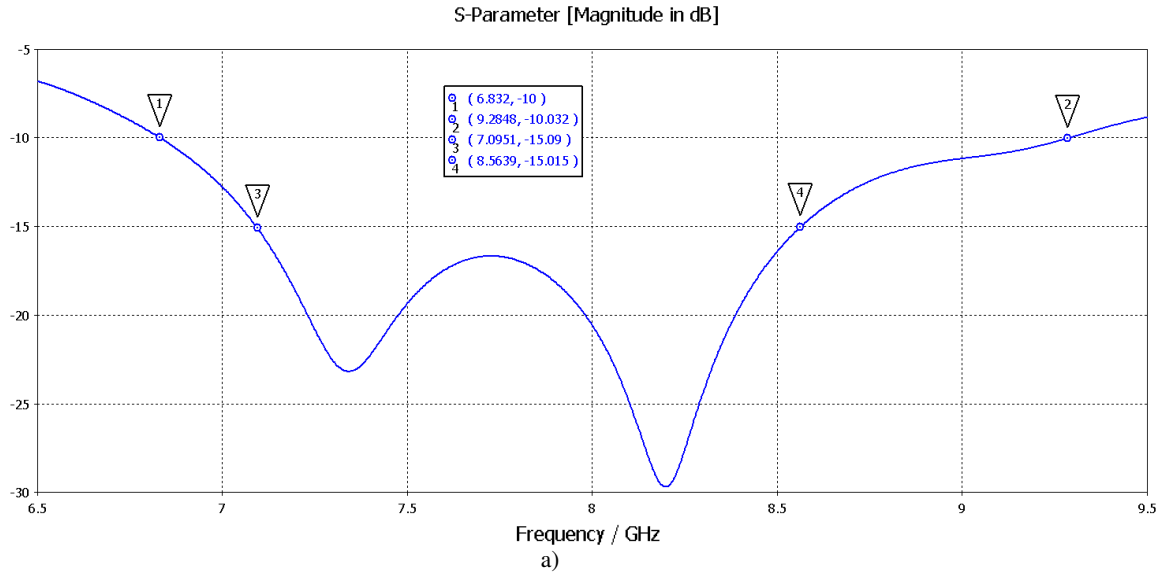

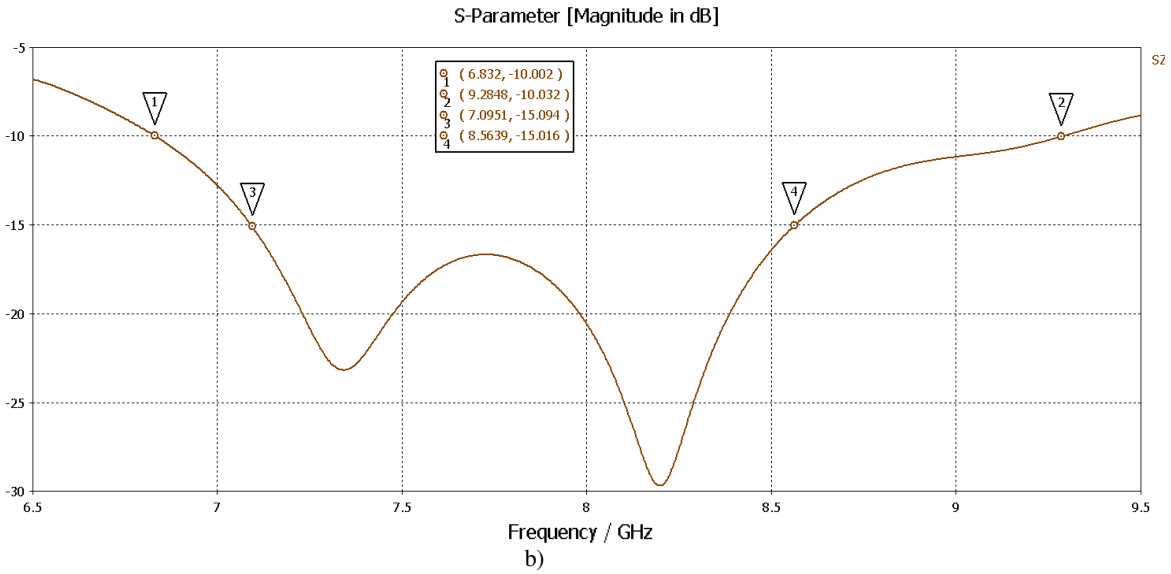

b)

Fig. 2. Results for a layer structure with air-gap=0 mm, a symmetrical short L-shape, substrate's thickness=4.4 mm and substrate's loss tangent=0.21 for a) TE polarization. b) TM polarization.

For both polarizations, absorption bandwidth at -15 dB is around 1.5GHz, a relative bandwidth of 18.8%. At -10 dB absorption bandwidth is 2.5 GHz, around 30.9% relative bandwidth.
As can be observed the relative bandwidth at -15 dB is smaller than the maximum obtained so far with TM polarization, 27%, but it is still high and larger than the one obtained with the E-shape.

5.2.1 Sensitivity study

The sensitivity study presented in this section confirms that the parameters used in the polarization insensitive design are close to the optimum, except for the permittivity, that was initially kept as close as possible to the value of standard PCB substrate.

In figure 3 the resulting S11 responses when only the loss tangent of the substrate is varied are shown and in table 2 the corresponding variation in absorption bandwidth is detailed. The resulting sensitivity is as expected.

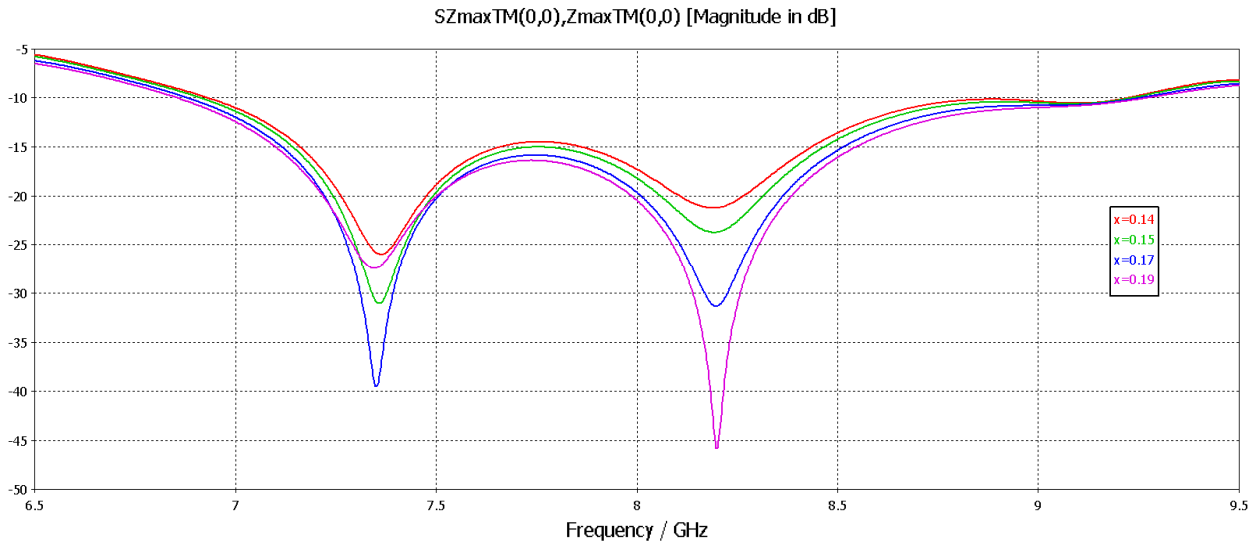

a)

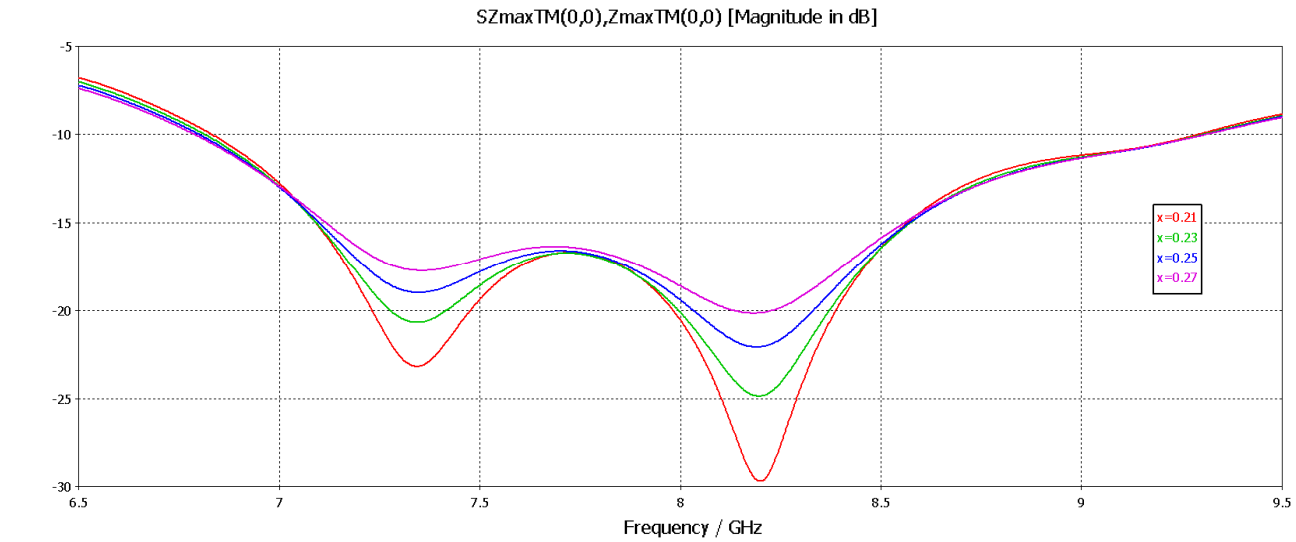

b)

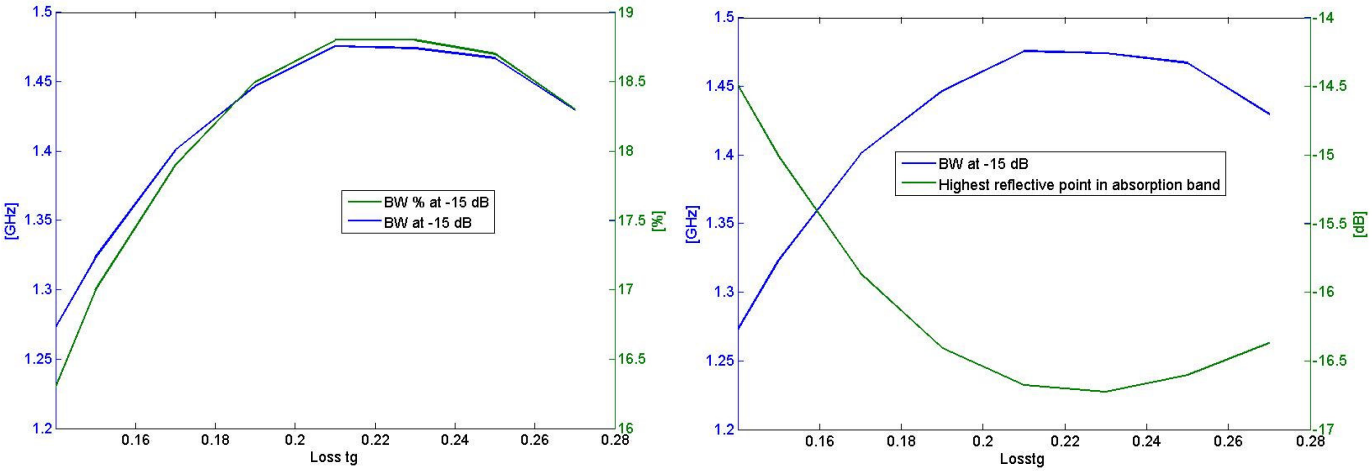

c) d)

Fig. 3. S11 results for the polarization insensitive design of figure 1 when only the loss tangent of the substrate's material is variable a) from a loss tangent of 0.14 to 0.19 b) from a loss tangent of 0.21 to 0.27. c) Plotted sensitivity values of relative absorption bandwidth and correlative bandwidth percentage as a function of selected loss tangent values, corresponding to table 2. d) Plotted sensitivity values of relative absorption bandwidth and correlative highest reflective point in absorption band as a function of selected loss tangent values, corresponding to table 2.

Loss tangent	**BW [GHz] at -15 dB**	**~BW%**	**absorption in most reflective point of BW (approx)**
0.14	1.27	16.3	-14.49
0.15	1.32	17	-15.01
0.17	1.40	17.9	-15.86
0.19	1.45	18.5	-16.41
0.21	1.48	18.8	-16.68
0.23	1.47	18.8	-16.73
0.25	1.47	18.7	-16.61
0.27	1.43	18.3	-16.37

Table 2- Absorption bandwidths for a variable loss tangent corresponding to the results of figure 3.

With a variation in the thickness of the substrate the absorptive responses shift to lower frequencies, as expected, when the thickness increases and also increase and subsequently decrease absorption levels.

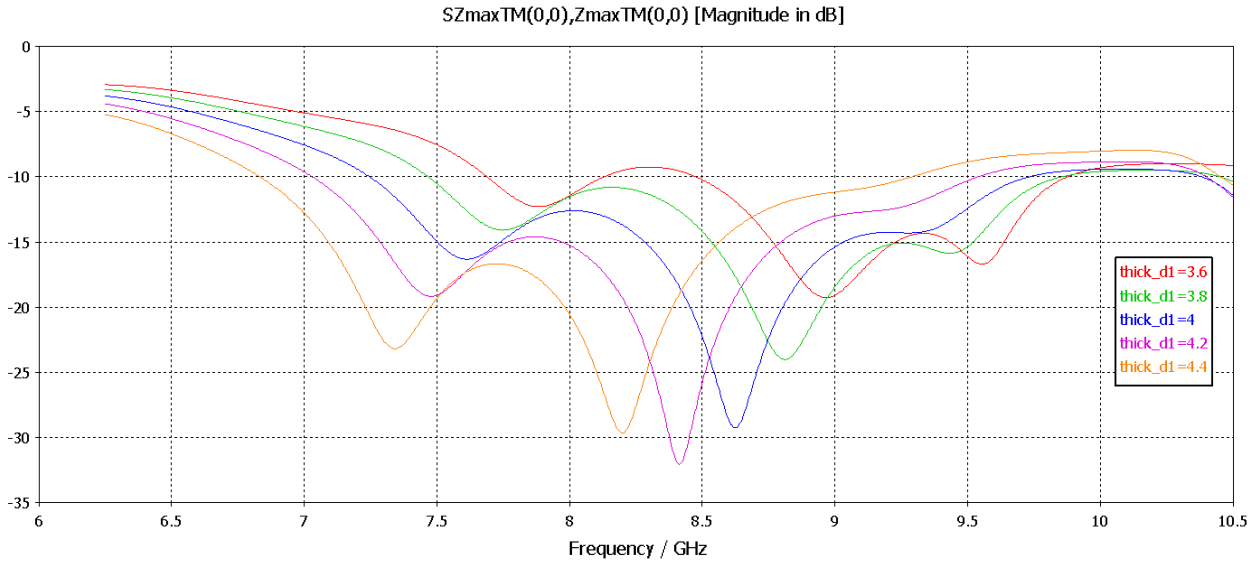

a)

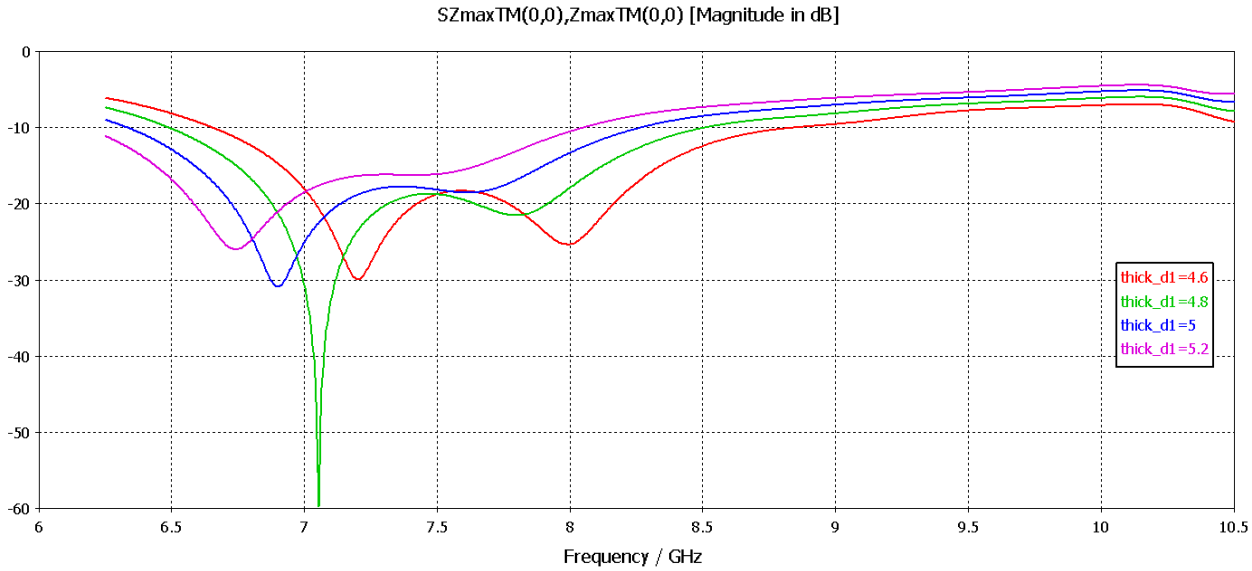

b)

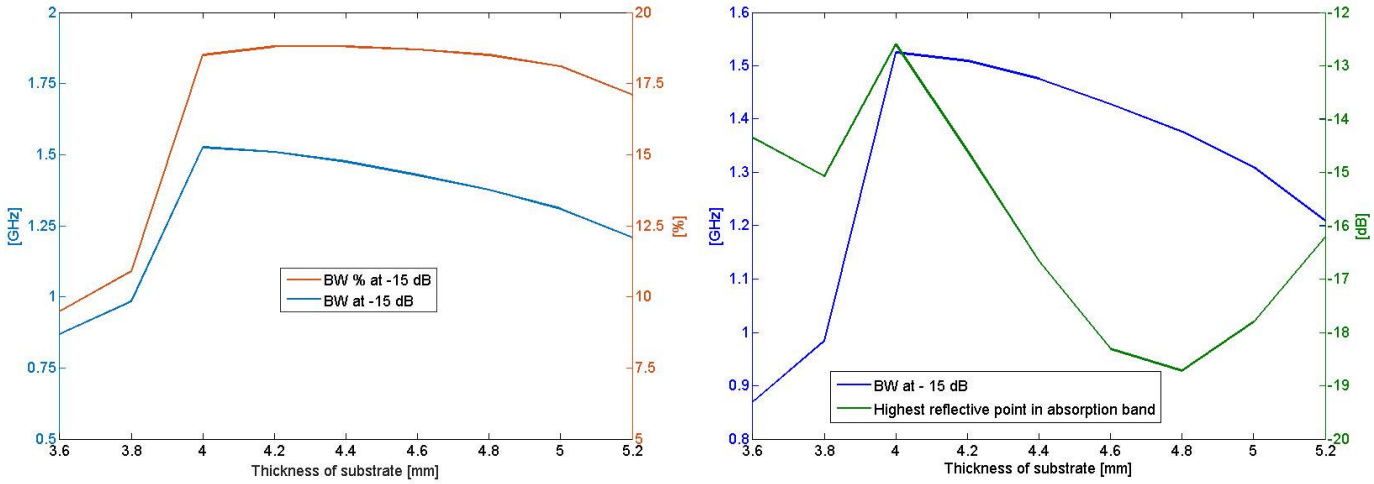

c) d)

Fig. 4. S11 results for the polarization insensitive design of figure 1 when only the substrate's thickness is variable a) from a thickness of 3.6 to 4.4 b) from 4.6 to 5.2. c) Plotted sensitivity values of relative absorption bandwidth and correlative bandwidth percentage as a function of selected substrate's thickness values, corresponding to table 3. d) Plotted sensitivity values of relative absorption bandwidth and correlative highest reflective point in absorption band as a function of selected substrate's thickness values, corresponding to table 3.

Thickness of substrate [mm]	**BW [GHz] at -15 dB**	**~BW%**	**absorption in most reflective point of BW (approx)**
3.6	0.87	9.5	-14.34
3.8	0.98	10.9	-15.07
4.0	1.53	18.5	-12.60
4.2	1.51	18.8	-14.60
4.4	1.48	18.8	-16.68
4.6	1.43	18.7	-18.31
4.8	1.38	18.5	-18.72
5	1.31	18.1	-17.81
5.2	1.21	17.1	-16.22

Table 3- Absorption bandwidths for a variable substrate's thickness corresponding to the results of figure 4.

With a variation in substrate's material permittivity the responses also shift towards lower frequencies, as expected and shown in figure 5 and table 4. At a permittivity of 2.5 absorption bandwidth decrease is much more significant.

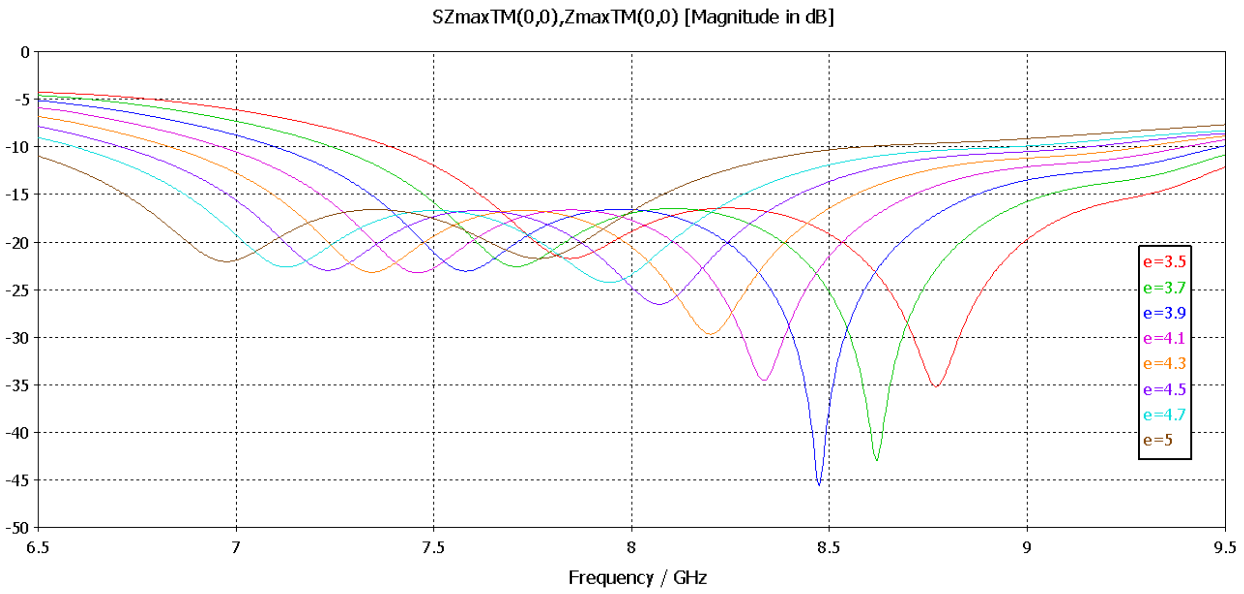
SZmaxTM(0,0),ZmaxTM(0,0) [Magnitude in dB]
0
-5
-10
-15
-20
-25
-30
-35
-40
-45
-50
6.5
7
7.5
8
8.5
9
9.5
Frequency / GHz
e=3.5
e=3.7
e=3.9
e=4.1
e=4.3
e=4.5
e=4.7
e=5

a)

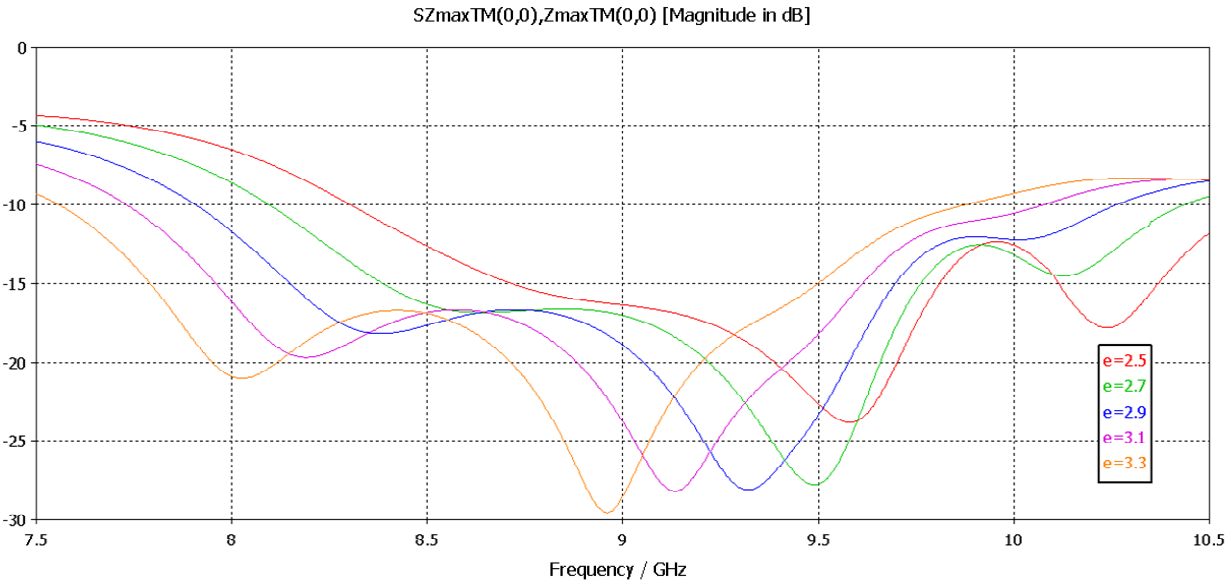
SZmaxTM(0,0),ZmaxTM(0,0) [Magnitude in dB]
0
-5
-10
-15
-20
-25
-30
7.5
8
8.5
9
9.5
10
10.5
Frequency / GHz
e=2.5
e=2.7
e=2.9
e=3.1
e=3.3

b)

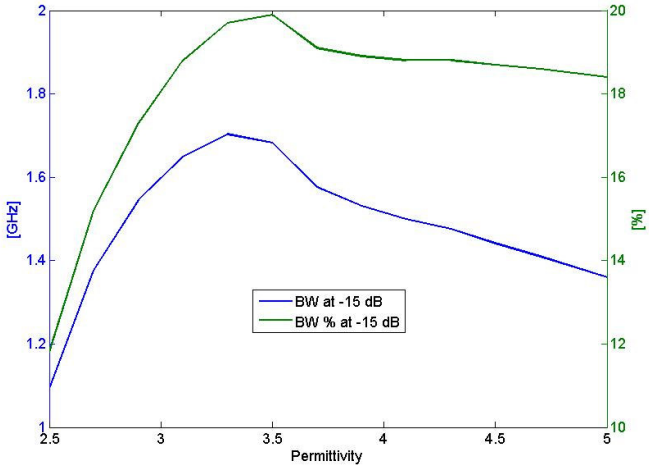
[GHz]
[%]
BW at -15 dB
BW % at -15 dB
Permittivity

c)

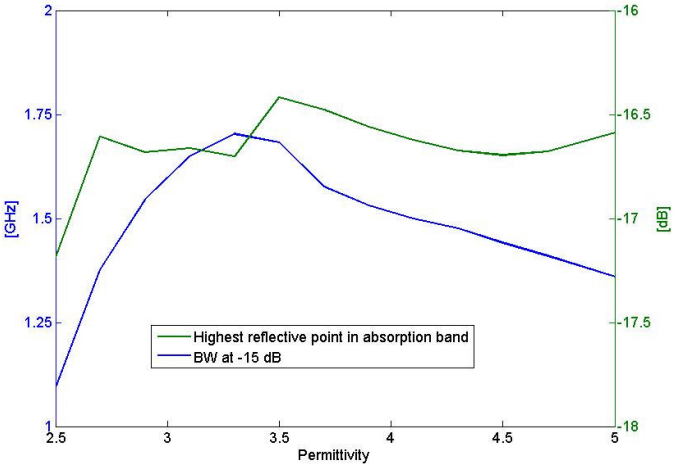
[GHz]
[dB]
Highest reflective point in absorption band
BW at -15 dB
Permittivity

d)

Fig. 5. S11 results for the polarization insensitive design of figure 1 when only the permitivitty of the substrate's material is variable a) from a value of 3.5 to 5 b) from a value of 2.5 to 3.3. c) Plotted sensitivity values of relative absorption bandwidth and correlative bandwidth percentage as a function of selected permittivity values, corresponding to table 3. d) Plotted sensitivity values of relative absorption bandwidth and correlative highest reflective point in absorption band as a function of selected values, corresponding to table 4.

Permittivity	**BW [GHz] at -15 dB**	**~BW%**	**absorption in most reflective point (approx)**
2.5	1.09	11.8	-17.19
2.7	1.38	15.2	-16.61
2.9	1.55	17.3	-16.68
3.1	1.65	18.8	-16.66
3.3	1.70	19.7	-16.70
3.5	1.68	19.9	-16.42
3.7	1.58	19.1	-16.48
3.9	1.53	18.9	-16.56
4.1	1.50	18.8	-16.62
4.3	1.48	18.8	-16.67
4.5	1.44	18.7	-16.70
4.7	1.41	18.6	-16.68
5	1.36	18.4	-16.59

Table 4- Absorption bandwidths for a variable permitivitty corresponding to the results of figure 5.

When the permittivity was also further optimized in the sensitivity study, it was observed that it was actually possible to increase the absorption bandwidth in approximately one percentage point. Namely with a design with a permittivity closer to a value of 3.5 an absorption bandwidth of nearly 1.7 GHz at -15 dB was achieved, instead of the around 1.5 GHz with a permittivity of 4.3. The corresponding new relative bandwidth is 19.9%.

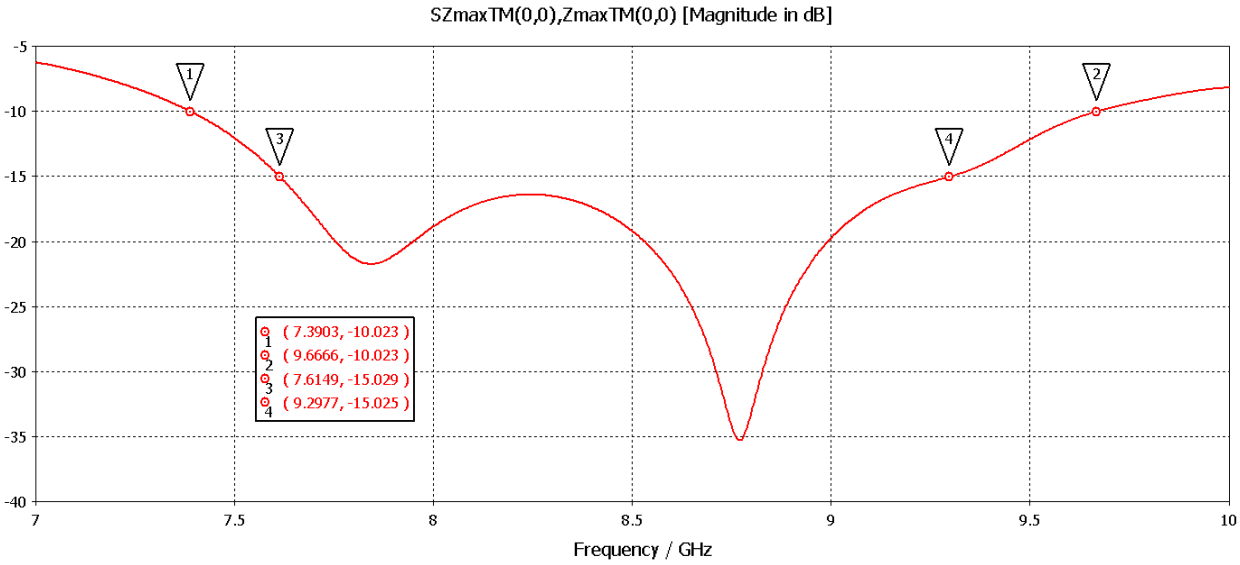

Fig. 6. S11 response for a layer structure with air-gap=0 mm, a symmetrical short L-shape, substrate's thickness=4.4 mm, substrate's loss tangent=0.21 and substrate's permitivitty of 3.5.

At -10 dB absorption bandwidth is around 2.3 GHz, relative bandwidth of around 26.7 %.

It can also be observed that sensitivity with the susbtrate's permittivity is not as high as with the other parameter values of the design, neither as it was when permittivity was varied in the E-shape design of chapter 4.

5.3 Design with an L-shape as resonator and an air-gap in the layer structure

5.3.1 Design with a Long L-shaped resonator

An L-shape with the same dimensions of our optimal E-shape design in its longer and shorter branches was used for the first results shown in figure 8. Unit cell dimensions and thickness are also the same as in the original optimal E-shape design (chapter 4, figures 26 and 41): unit cell's width is 34 mm, length is 44.4 mm, thickness 4.7 mm and air- gap 0.94 mm. Loss tangent of the substrate's material is 0.19 and permittivity 4.3. L shape dimensions are detailed in Table 3.

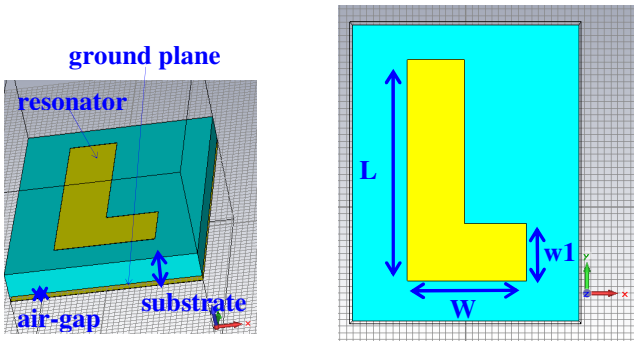

a) b)

Parameter name	Value [mm]
L	33.2
W	17.9
w1	8.6

Table 5- Large L-shape dimensions

Fig. 7. a) Unit cell with L-shaped resonator considered. b) L-shape's dimensions indicated.

When plane waves imping normally in the structure, a wide bandwidth at -10 dB is obtained both with TE and TM polarizations. Although the design does not produce a polarization insensitive response, as this was not the objective in this section, absorption bandwidths are already more comparable with each polarization, as opposite to results obtained with the E-shape (only for TE polarization). With TE polarization the response is shifted approximately 1GHz to higher frequencies.

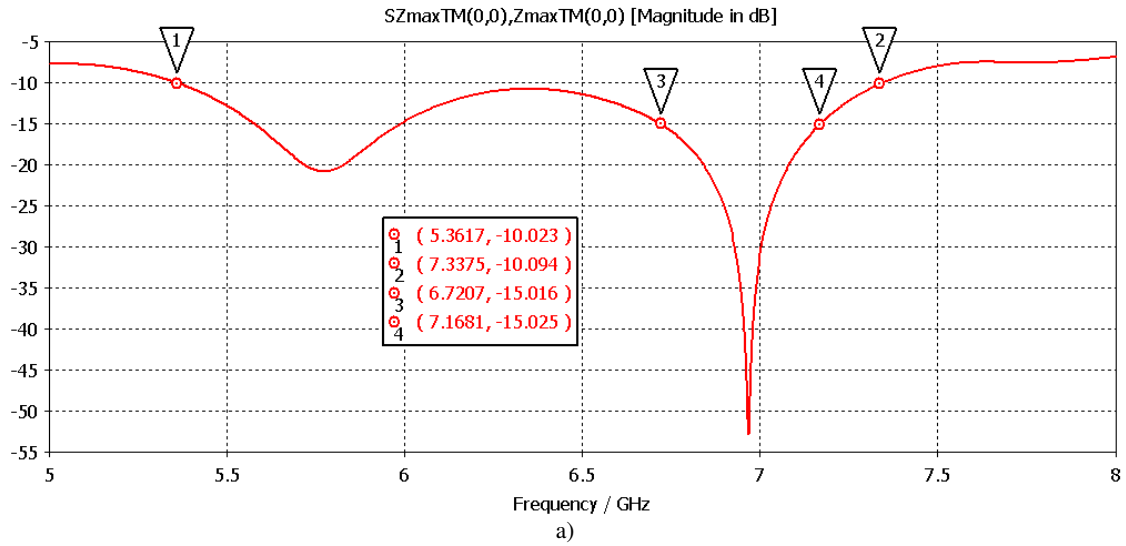

a)

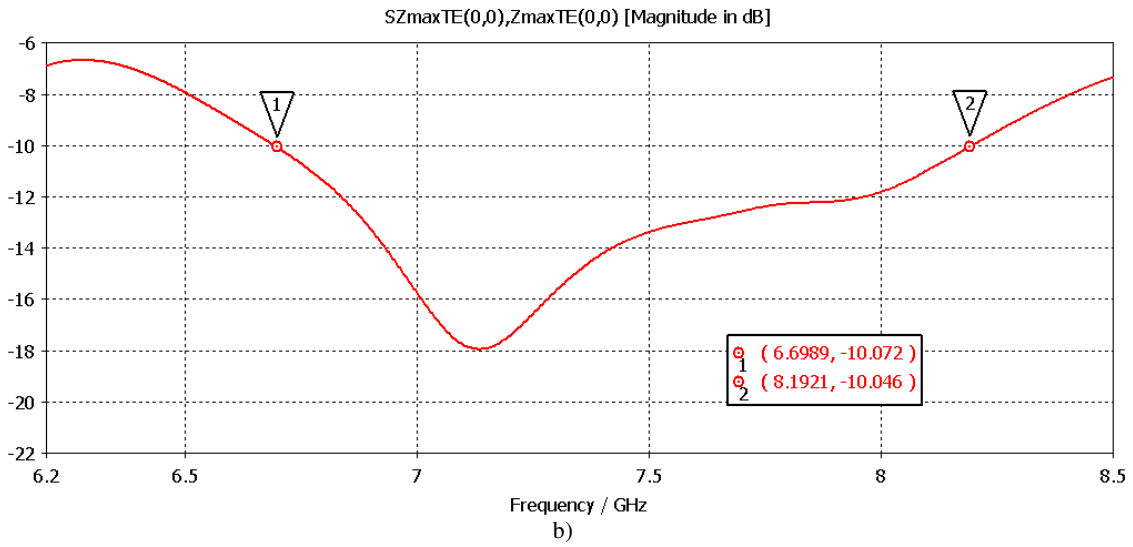

b)

Fig. 8. a) S11 result of impinging normally incident plane waves on the unit cell of figure 7 for TM polarization. b) Results for TE polarization.

With TM polarization absorption of -10 dB (around 90%) has a bandwidth of 1.98 GHz, with TE polarization bandwidth is 1.5 GHz. Relative bandwidths are 31.1% and 20.1%, respectively.

5.3.2 Design with a short L-shaped resonator

The layer structure and unit cell size of the previous subsection is kept but the L-shaped resonator is changed by a smaller one, with the dimensions detailed in Table 6 and resulting in the shape shown in figure 9.

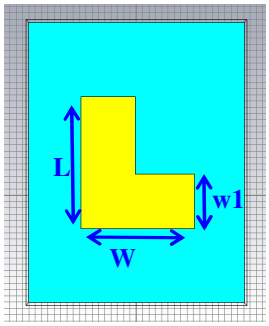

Parameter name	Value [mm]
L	20.9
W	17.9
w1	8.6

Table 6- Short L-shape dimensions

Fig. 9. L-shape's dimensions indicated.

Results obtained for both polarizations are shown in figure 10.

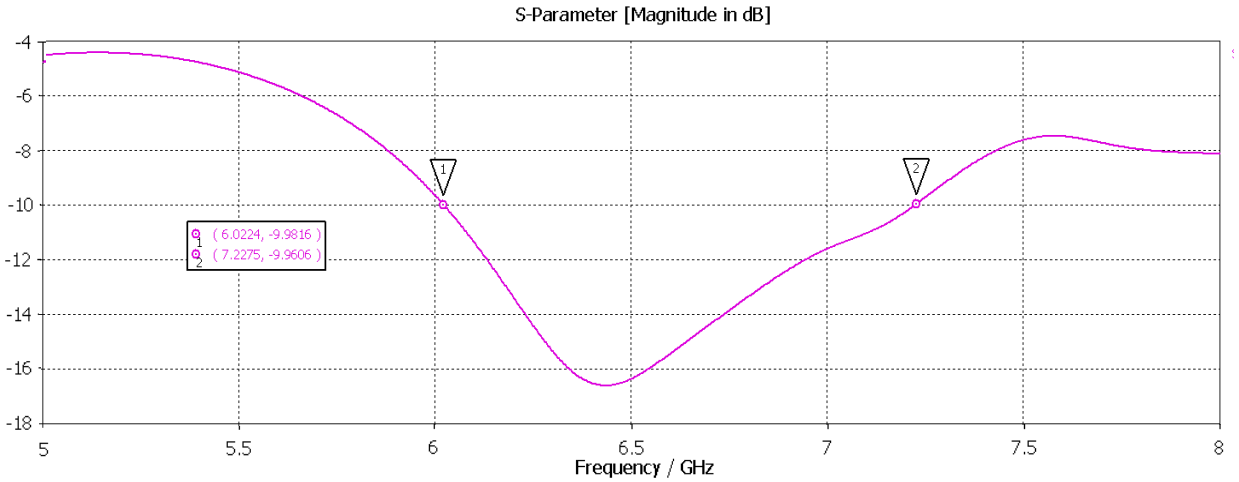

a)

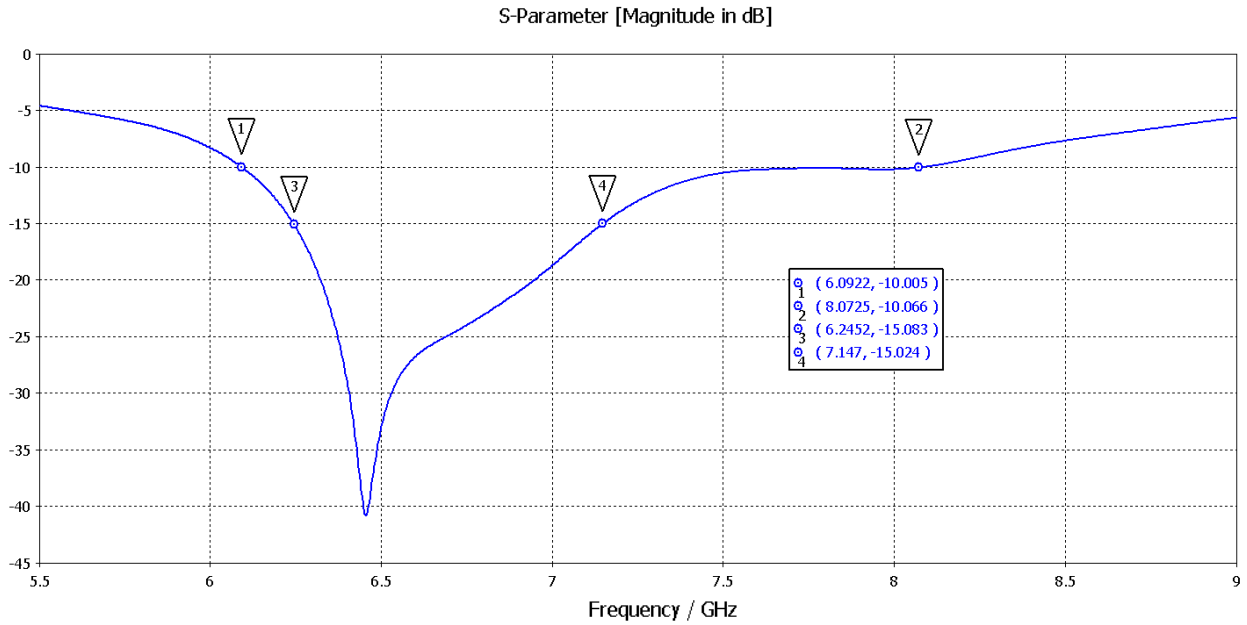

b)

Fig. 10. Results for configuration of figure 9 with susbtrate's thickness=4.7 mm with a) with TM polarization b) TE polarization.

The absorption bandwidth with TM polarization at -10 dB is 1.2GHz, thus a relative bandwidth of 18.1%.With TE polarization is 1.99 GHz at -10 dB and 0.9 GHz at -15 dB, relative bandwidths of 28.2% and 13.47% respectively. Thus the response is polarization sensitive, with the best performance found with TE polarization. These absolute and relative bandwidths are only larger than the ones obtained with the optimal E-shape design that did not include an air-gap in the layer structure (chapter 4, figure 27), of around 0.9 and 0.19 GHz, 12% and 9% at -10 and -15 dB respectively.

The optimum absorption bandwidth with this design that uses a short L-shape is obtained when the thickness of the substrate is reduced to 4 mm and the rest of the parameter values are unchanged, as shown in figure 11.
By using a smaller loss tangent value with any of the substrate's thicknesses only a lower absorption level and absorption bandwidth are obtained.

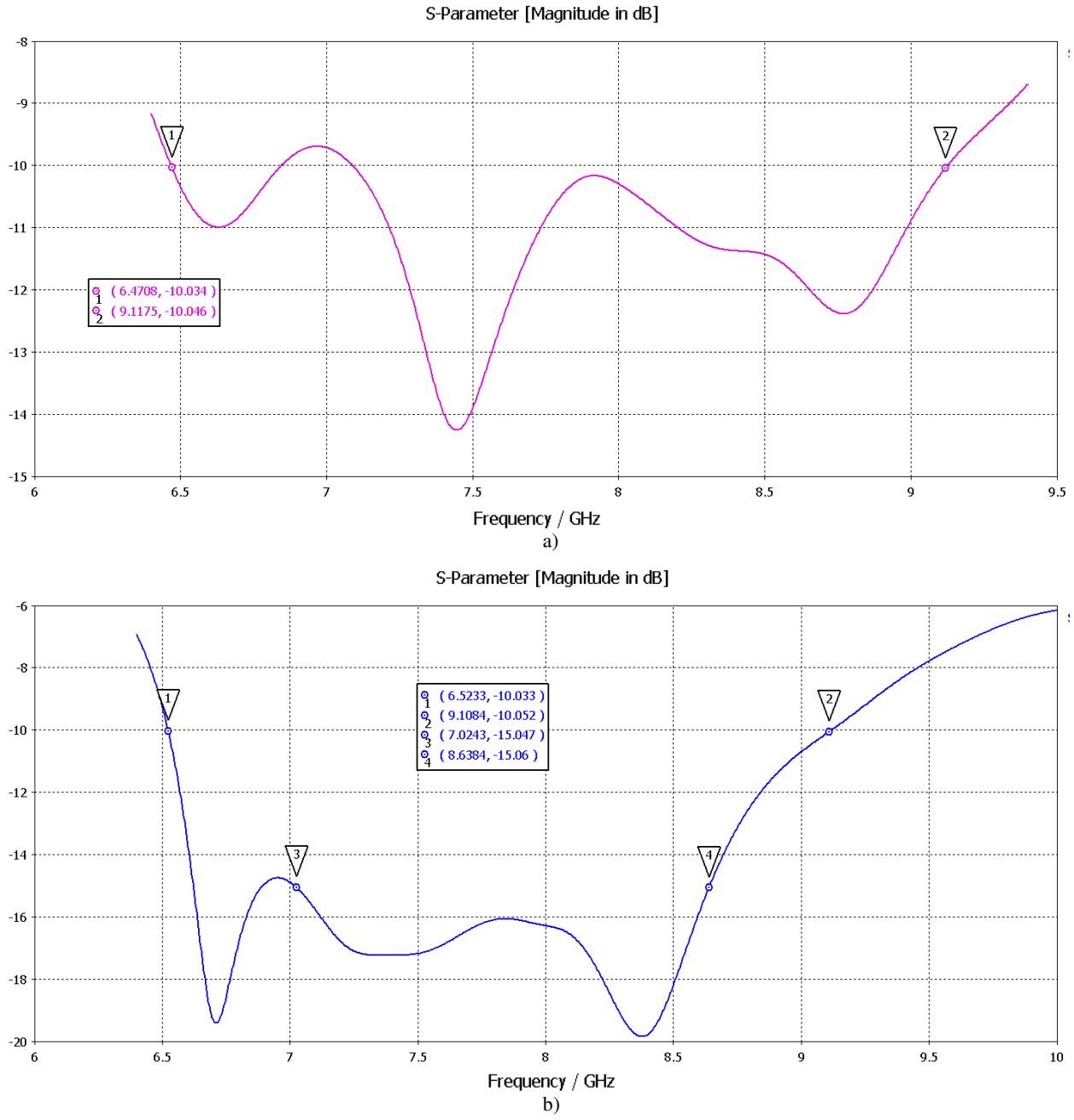

Fig. 11. Results for configuration of figure 9 with susbtrate's thickness=4 mm for a) TM polarization b) TE polarization.

For TM polarization, absorption bandwidth at -10 dB is 2.02 GHz, relative bandwidth is 24.9%. For TE polarization, absorption bandwidth at -10 dB is around 2.6 GHz, relative bandwidth of 33.2% and at -15 dB 1.6GHz, relative bandwidth of 20.4%. Thus the absorption bandwidths and relative absorption bandwidths are much larger than the maximum levels obtained with the E-shape (15.3% at -15 dB and 20.5% at -10 dB).

5.4 Design with an L-shape as resonator and no air-gap in the layer structure

The second layer structure previously used with the E-shape is introduced, namely the layer structure depicted in figure 7 a is now composed by no air-gap (air-gap=0 mm) and unit cell's

dimensions are unchanged with respect to previous L-shape design (width=34 mm, length=44.4 mm). Substrate's material permittivity is 4.3. If absorption bandwidths obtained in this section are comparable with the ones obtained in the previous one, the layers structure of this section would be more practical in terms of fabrication as it does not need to include a layer of air. This constitutes a motivation to investigate this layer structure that does not include a layer of air.

With this new layer structure, results with the larger L-shape introduced in figure7 b and the dimensions depicted in table 5 are not satisfying. In figure 12 the results for a substrate's loss tangent =0.08 and substrate's thickness = 4 mm are shown.

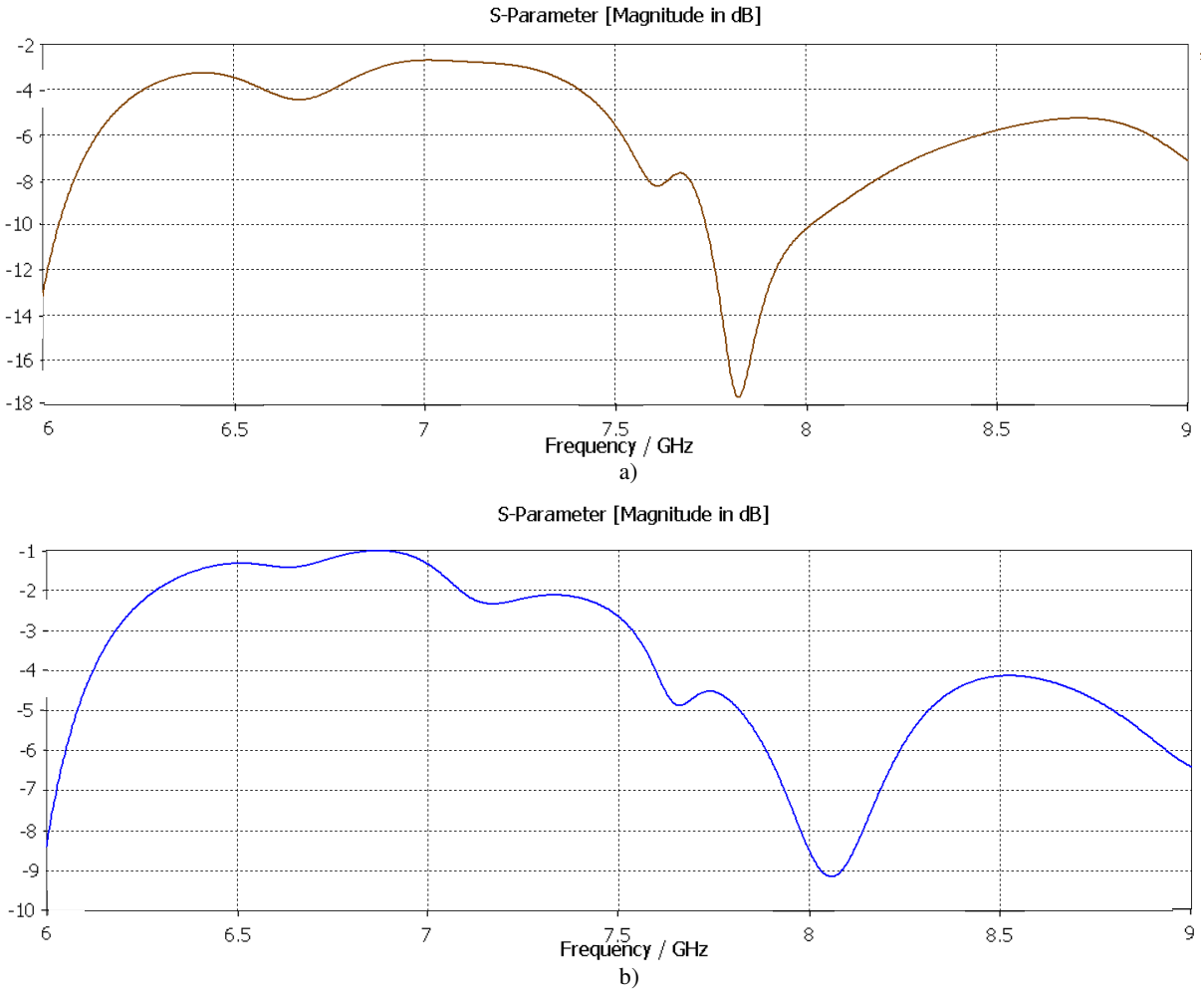

Fig. 12. Results for a layer structure with air-gap=0 mm, large L-shape resonator, substrate's thickness=4 mm and susbtrate's loss tangent =0.08 for a) TM polarization b) TE polarization.

In this way the relevance of a resonator's shape is also shown, as the size of the L-shape resonator in this case is exactly the same as the size of the E-shape used in previous chapters, the layer structure is the same used in the first optimum obtained with the E-shape, but the results are completely different.

More interesting results were obtained by using the shorter L-shape resonator with the dimensions specified in table 6 and layer structure unchanged.

In this case only in TM polarization are relevant results obtained, shown in figure 13 a. With TE polarization a lower absorption and absorption bandwidth were obtained.

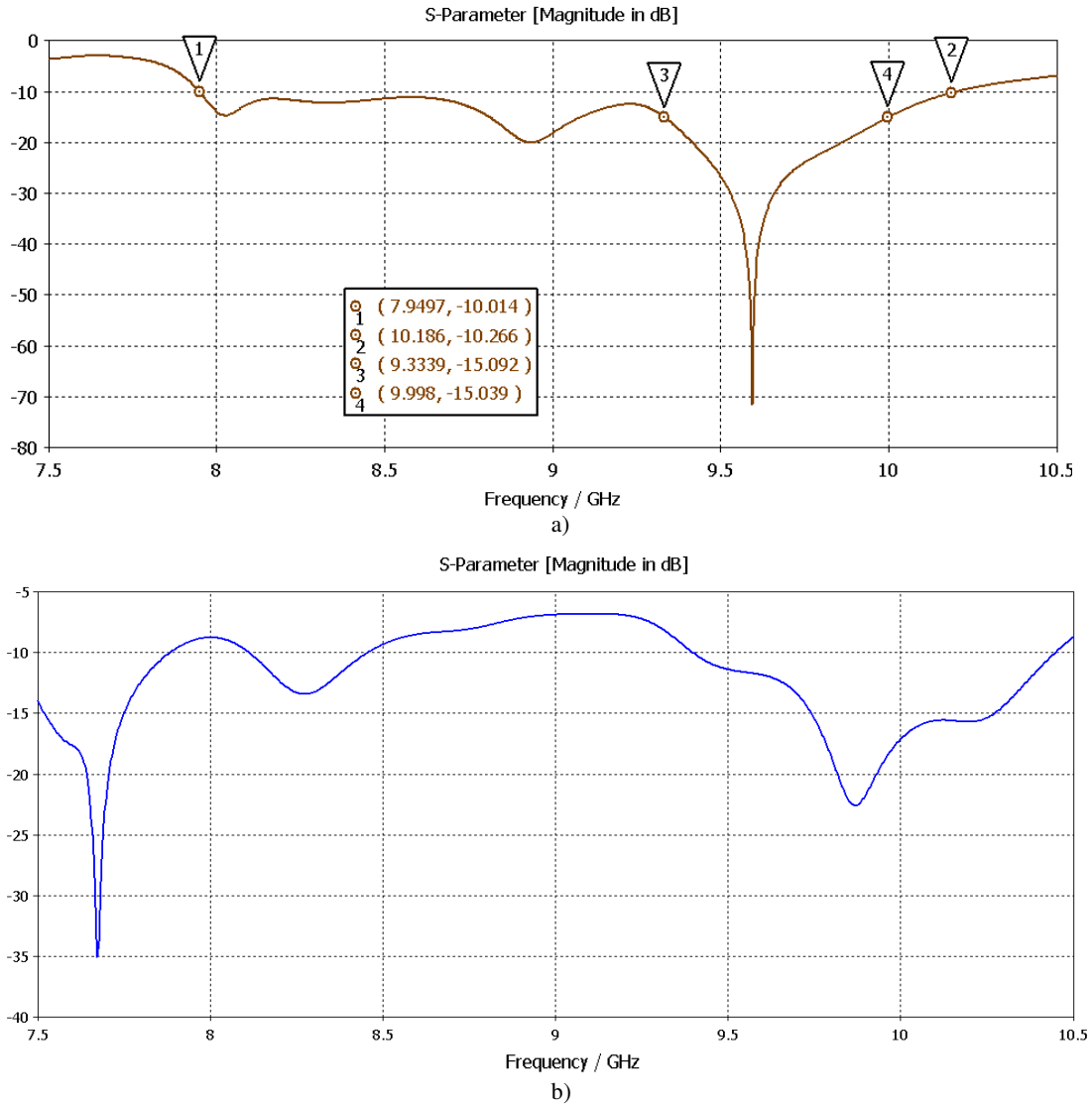

Fig. 13. Results for a layer structure with air-gap=0 mm and short L-shape, substrate's thickness=4 mm and susbtrate's loss tangent =0.08 for a) TM polarization b) TE polarization.

In terms of polarization these results are opposed to the ones obtained with E-shape, where the TE polarized radiation showed the best performance in terms of bandwidth and absorption. Here it is with TM polarization that the best results are obtained.

With TM polarization, the bandwidth obtained at -10 dB is significantly larger than previous ones obtained with E-shapes of around 1.5 GHz at -10 dB: approximately 2.24 GHz-wide. Corresponding relative bandwidth is 24.7%. In comparison to the previous layer-structure that included an air-gap, the -10 dB bandwidth is shifted by 1.4 GHz to higher frequencies. More importantly, by keeping the layer structure used for the E-shape optimum that did not have an air-gap and with a low loss tangent in the substrate material, we obtained more absorption bandwidth by using the L-shape than by using the E-shape.

At -15 dB the bandwidth is 0.7 GHz, also significant in comparison to previous results. Relative bandwidth in this case is 7.7%.
It could be fabricated using only Dyneon material previously utilized for the E-shape, with permittivitty of around 2.7 and loss tangent 0.08 at 9.4GHz, where again a PCB could be used to print the metallic resonators. Then a dielectric with very low losses, like Rogers, would be convenient to be used as PCB material to print the metallic resonators.

Given the interesting, wide bandwidth result obtained with a combination of parameter values already known, we further optimized the parameters.

With a loss tangent of 0.14, relative absorption bandwidths overtakes the maximum relative bandwidth obtained at -15 dB with the E-shape previously.
Substrate thickness of 4 mm or very close to this value yielded the optimum result with this loss tangent.

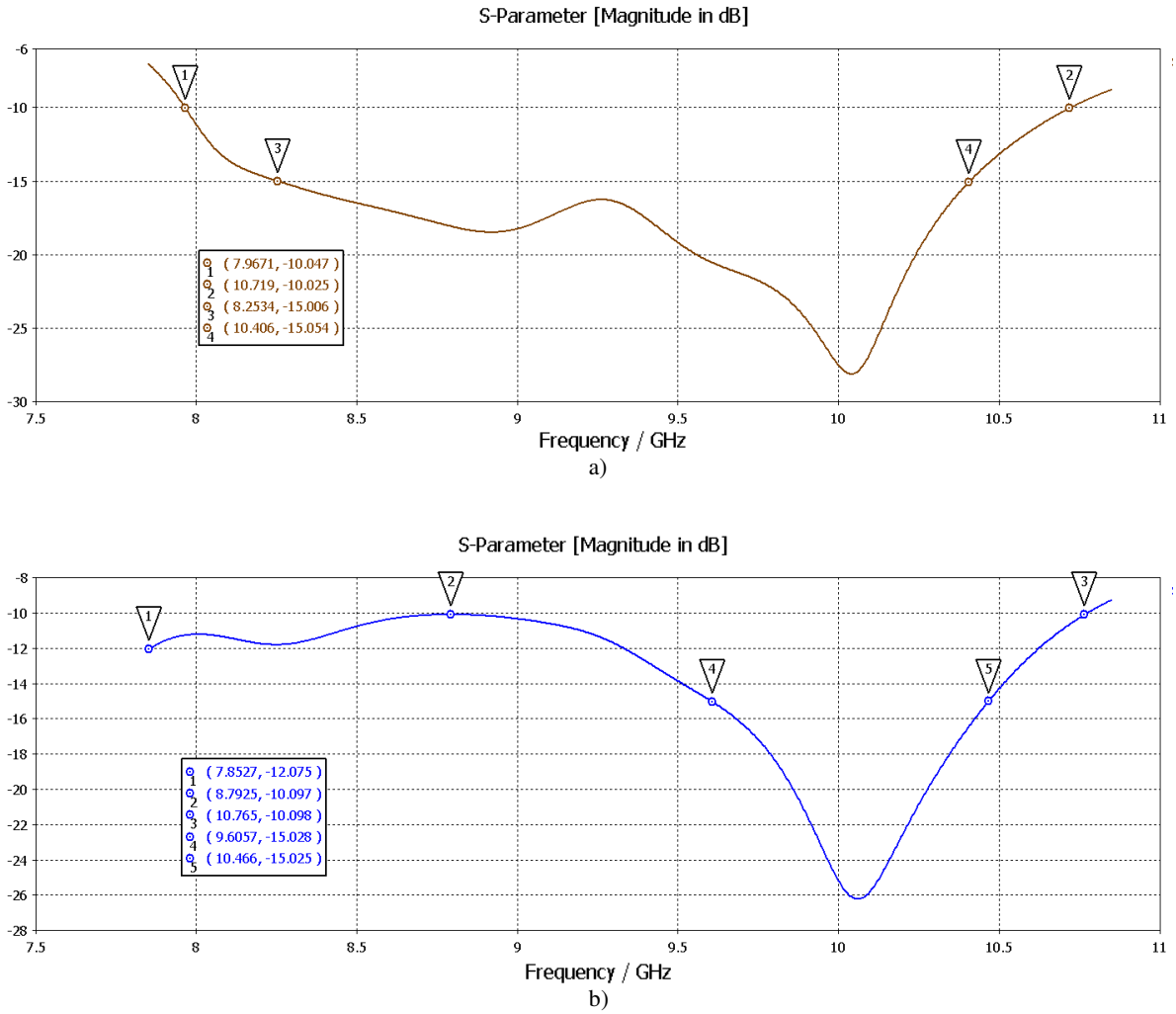

Fig. 14. Results for a layer structure with air-gap=0 mm, short L-shape, substrate's thickness=4 mm and substrate's loss tangent=0.14 for a) TM polarization b) TE polarization.

Thicker or thinner substrates yielded results that were more narrowband and with lower absorption levels, as depicted in figure 15 for substrate's thickness 4.7 mm.

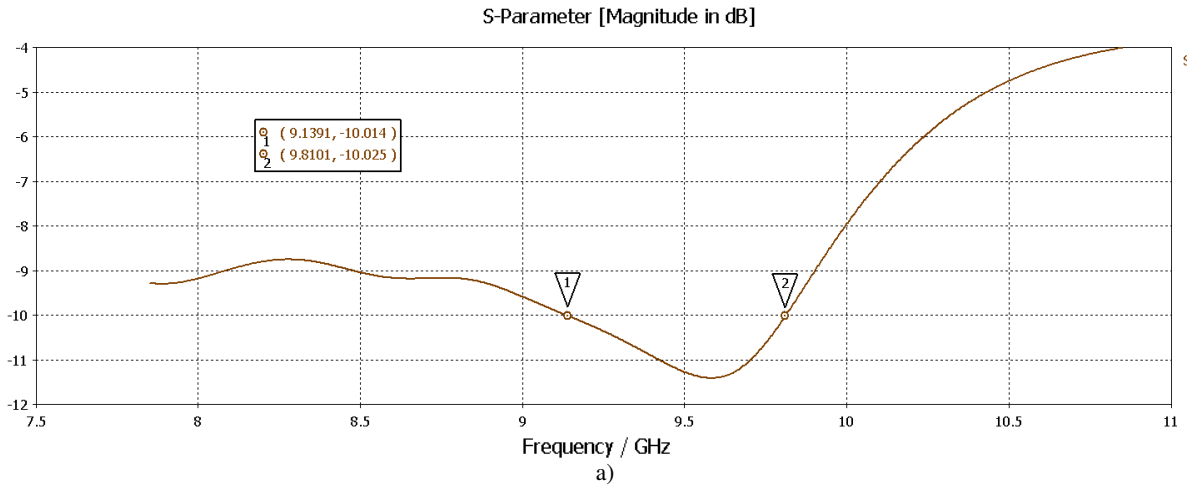

a)

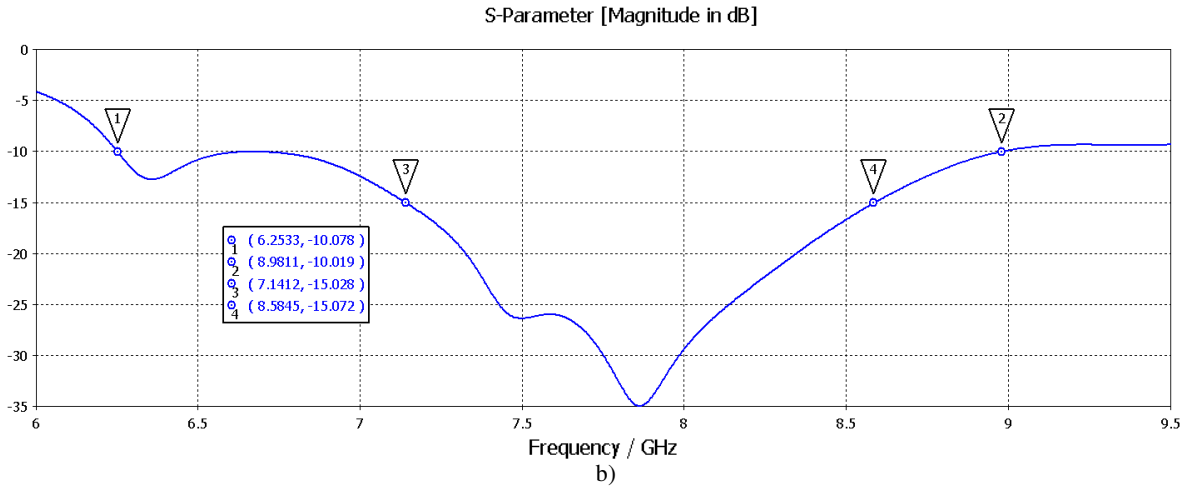

b)

Fig. 15. Results for a layer structure with air-gap=0 mm, short L-shape, substrate's thickness=4.7 mm and substrate's loss tangent=0.14 for a) TM polarization b) TE polarization.

The optimum or close to optimum result with this design –thus the result with the largest absorption bandwidth- was obtained with a loss tangent =0.21, rest of the parameter values unchanged. With TM polarization, absorption bandwidth at -15 dB is 2.5602 GHz , relative bandwidth of 27.1 %, at -10 dB is 3.1909 GHz, corresponding relative bandwidth is 33.5% . These absolute and relative bandwidths constitute a major increase with respect to the previously achieved 0.91 GHz, 15% at -15 dB and 1.5 GHz, 20.5% at -10 dB using the optimum design with an E-shape resonator in chapter 4. On top of it no air-gap was needed to reach this.

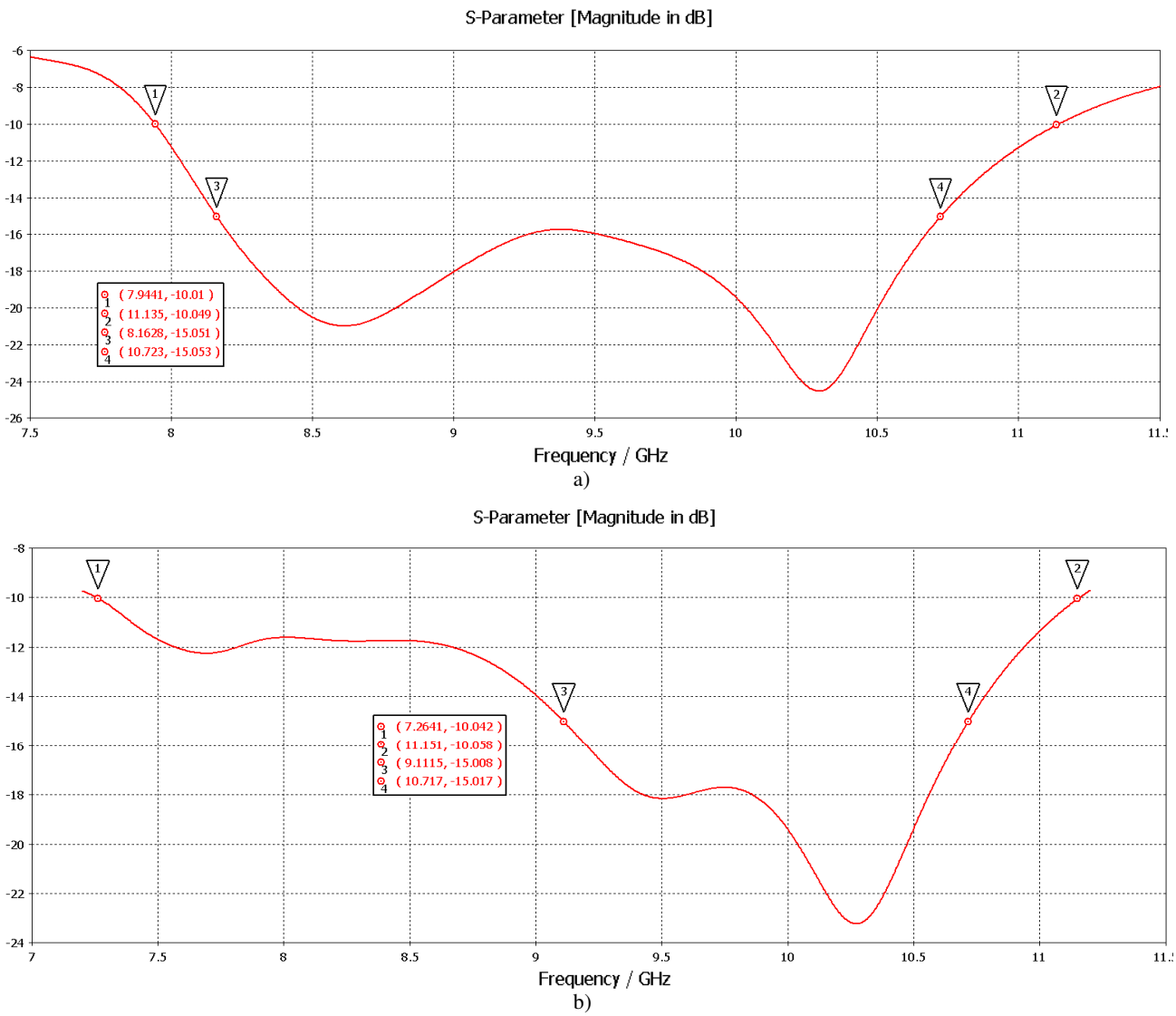

Fig. 16. Results for a layer structure with air-gap=0 mm, short L-shape, substrate's thickness=4 mm and substrate's loss tangent=0.21 for a) TM polarization b) TE polarization.

Anyway absorption bandwidths at -10 and -15 dB with loss tangent=0.18 or 0.19 do not diminish significantly: with TM polarization for loss tangent=0.19 at -15 dB, bandwidth is 2.5 GHz, relative bandwidth 26.3%. For loss tangent =0.18, it is 2.4 GHz, relative bandwidth of 25.8%. Thus if a substrate with a lower loss tangent of around 0.18 or 0.19 is needed the performance will not be significantly affected.

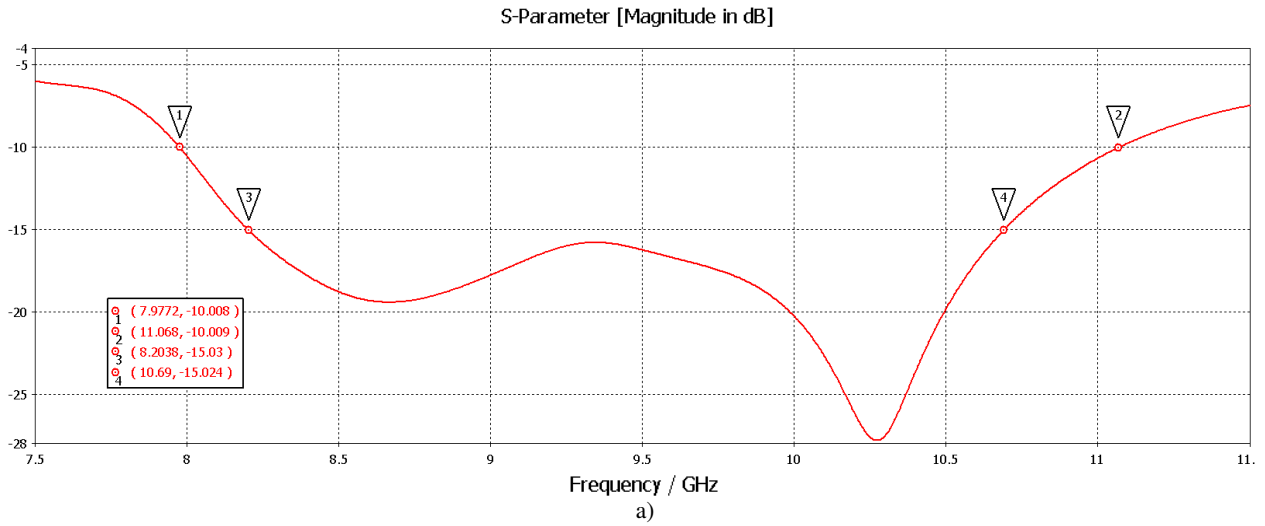

a)

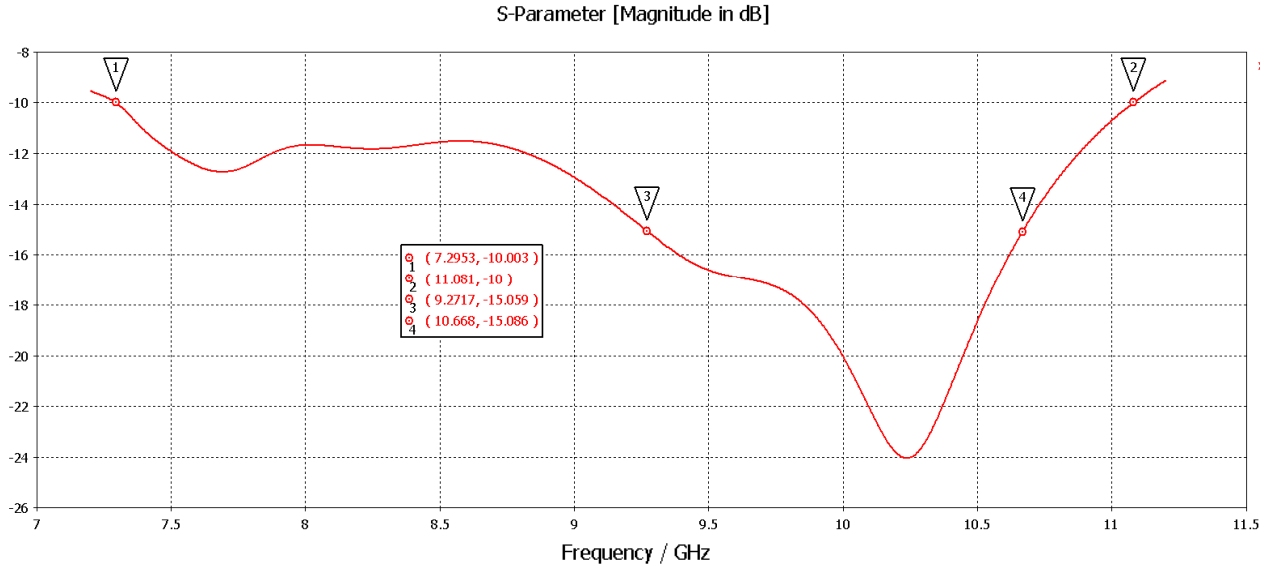

b)

Fig. 17. Results for a layer structure with air-gap=0 mm, short L-shape, substrate's thickness=4 mm and substrate's loss tangent=0.19 for a) TM polarization b) TE polarization.

With the present design, if the layer structure is modified by again introducing an air-layer as we investigated in section 3, absorption performance does not improve despite tuning of other parameters.

5.5 Physical insight on designs using single L-shapes

With the intention of giving a more physical insight, we can say that an L-shape is not necessarily a more wideband resonator than an E-shape nor has it proven to be the optimal wideband resonator, to the best of our knowledge. In fact when using an L-shape with the same dimensions in length and width as our optimum E-shape resonator (table 5), bandwidth performance was not better than the one of the E-shape (figure 8). Mainly a double-resonance with relatively wide absorption peaks around close frequencies originates the response of the L-shape in the absorbing frequency band. This double-resonant response can be already observed in the results of early simulations in figure 8, as it was also observed with the different designs using the E-shape exposed in chapter 4. The losses in the metallic L-shape are generated by resonances in it, as has been mentioned previously, and these losses are

responsible for absorption. When this is added to the losses in the substrate (non-metallic) material, the total absorption of the structure increases –and up to a larger extent in those resonant frequencies with higher resonances- and bandwidth can be increased by the addition of losses in several different frequencies.

As an example, in figure 18 we can see conductive current density plots for TE polarization at 8.189, 7.3 and 6.5 GHz for the polarization insensitive design of figure 1. Larger currents should indicate more resonance. At 8.189 GHz there is specially higher intensity in a small point in one of the edges of the of the lower branch of the L-shape, and also a spot of moderately higher intensity in the substrate (green area) relative to the same area at 7.3 GHz. It could be said that in general current intensity is moderately higher and there is also more contribution of losses from the substrate at 8.189 GHz with respect to 7.3 GHz. Thus the addition of losses in the metal and dielectric is stronger at 8.189 GHz, leading to a higher absorption. The difference with results at 6.5 GHz is even larger, as expected. This is consistent with the levels of absorption found in the corresponding S11 plot (figure 2, permittivity=4.3) for this frequencies. The current flows especially towards the edges of the L-shape for higher order modes.

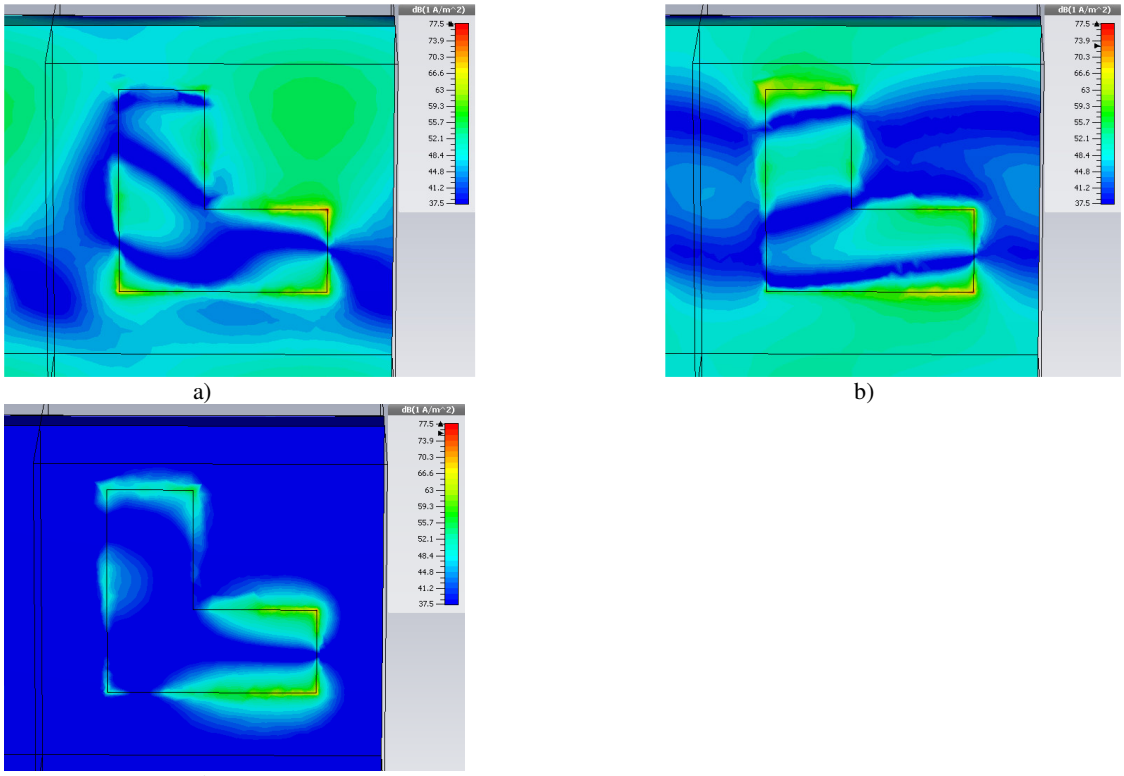

Fig. 18. Current density plots of the the polarization insensitive design in figure 1 for selected frequency within the absorption band a) 8.189 GHz approximately where the highest absorption point should be, b) 7.3 GHz around where the second largest absorption point should be found c) 6.5 GHz . Part of the edges of adjacent unit cells (periodic model) can be seen as well.

What has just been mentioned about the contribution of substrate and metal to losses is also observed when a transversal cut is made in the unit cell (plane z-y) and where the hot spot was found at 8.189 and 7.3 GHz (x=10.45). In figure 19 these plots are shown for all the same frequency points. The resonator is at the extreme left of the figure. At 8.189 GHz more intensity can be observed in the whole cut and there are also more green areas than at 7.3 GHz, where more blue areas -areas of much lower intensity- can be seen in the substrate. At 6.5 GHz the presence of blue areas is even larger. The differentiation of losses in the metal at

each frequency is much less as seen in the transversal view, in the top view perhaps only a very slight increase in differentiation can be seen. All this suggests that the contribution of the substrate has made a difference at the most absorptive frequencies, and we can see the differentiated contribution from the metal and the substrate to losses.

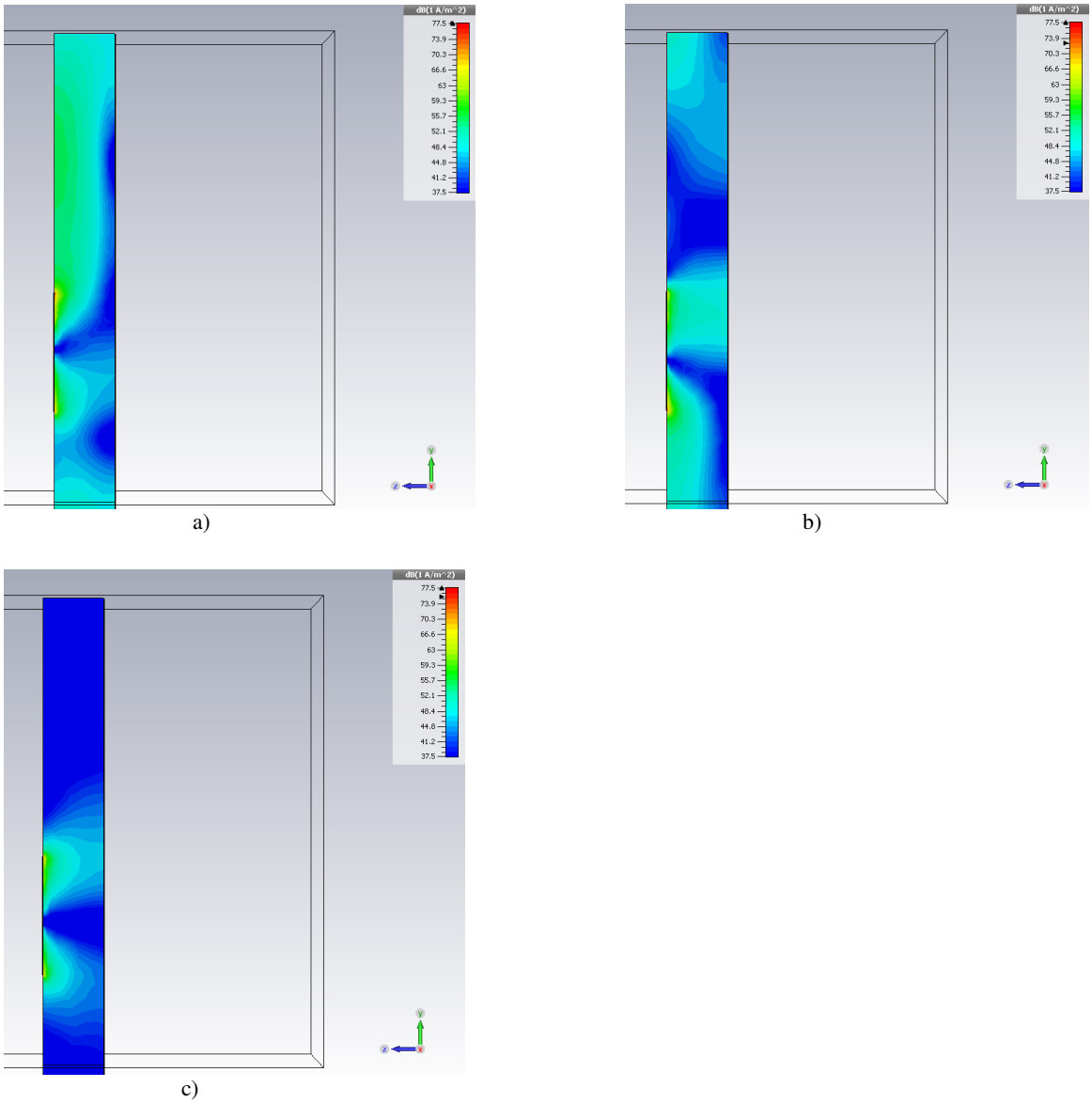

Fig. 19. Transversal view (plane z-y, cut at x=10.45) of current density plots for the the polarization insensitive design in figure 1 for selected frequency within the absorption band, a) 8.189 GHz approximately where the highest absorption point should be, b) 7.3 GHz around where the second largest absorption point should be found c) 6.5 GHz.

In figure 20 we can see plots of the unit cell, cut at different distances with respect to the ground plane, at 8.189 GHz. It can be observed that losses, and thus absorption, goes fairly deep in the substrate.

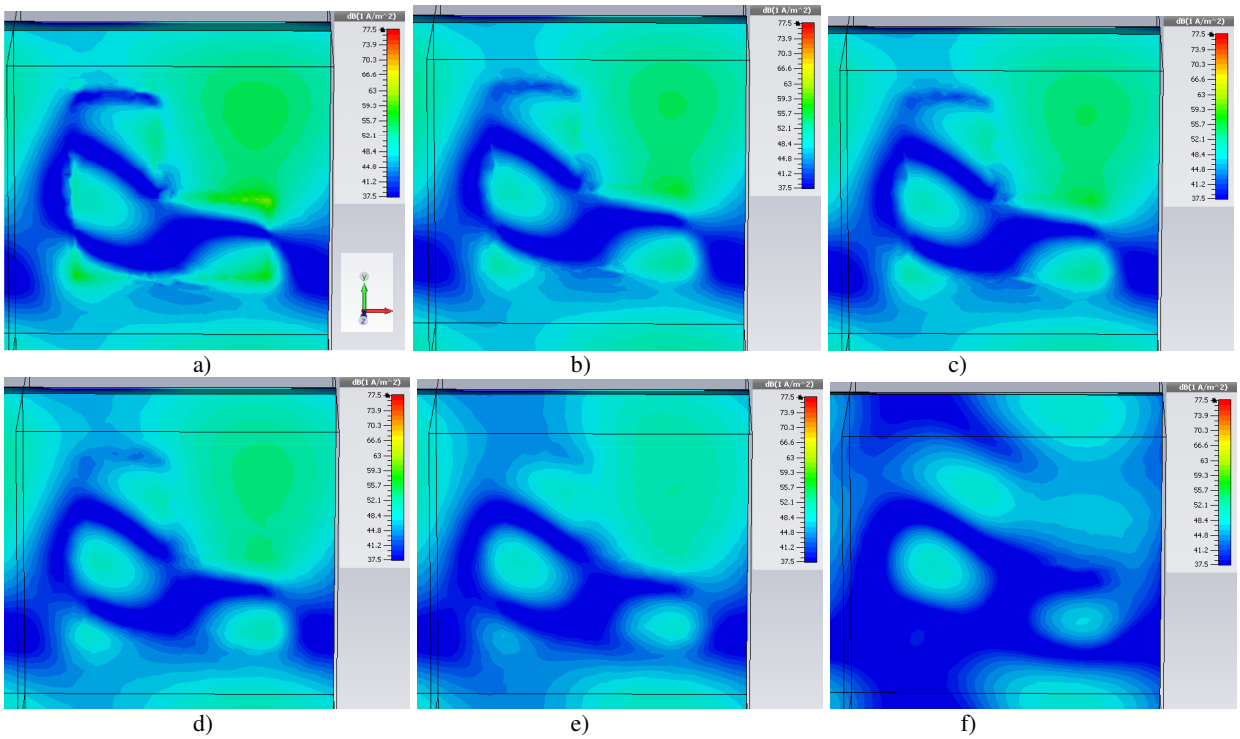

Fig. 20. Current density plots of the the polarization insensitive design in figure 1 at 8.189 GHz., with the unit cell cut at the unit cell cut at different distances with respect to the ground plane, thus different points in z with z=0 at the bottom side of the ground plane. In a) the reference coordinates' system is inserted. a) z = 4 mm, b) z = 3.45 mm, c) z = 3.4 mm, d) z = 3 mm, e) z = 2.25 mm and f) z = 1 mm, thus already close to the ground plane. Part of the edges of adjacent unit cells (periodic model) can be seen as well.

As the design is polarization insensitive, for TM the focal points in the metal shift symmetrically to the upper branch of the L-shape.

Thus the lossy substrate chosen, has probably shifted the total absorption to an increased level in the whole band. In some frequencies, such as 8.189 GHz, losses in the metal and substrate are both high and add up to absorption. We could risk saying that in others, if losses in the metal are smaller, losses in the substrate could have higher losses that compensate, which successfully manages to keep a constant relatively high absorption level in the whole band. So losses in metal and substrate either coincide or are complementary in several consecutive frequencies. This complementary coupling of both types of losses realizes the wide absorption band observed in the S11 plots, or in wider terms, losses in the metal and substrate coincide in frequency, they superpose in the same frequency band.

In the case of our best performing designs using a single L-shape resonator, these exhibit the highest and largest number of resonances, most widely spread in a frequency band in comparison with the other designs, and therefore they have the best performing results.
As in all our absorbing designs, a metallic back-plane as ground plane is used that neutralizes transmission, therefore by analyzing reflectivity the absorptive response of the designs is already known, as has also been explained in chapter 3.
Although the L-shape is not necessarily a more wideband resonator than an E-shape, when it is combined with the other components of the structure the resulting design is more wideband. This can be partly explained by the fact that the L-shape can be more flexibly modified than the E-shape: for example, while keeping the same microstrip width in both L and E-shape, the main branch in the E-shape has to be always slightly larger than three times the width of each

of its branches -in chapter 4, figure 4a), if w1=w2, W > 3w1-. The corresponding main branch in the L-shape can, on the other hand, be made smaller – in figure 7b, where L would correspond to W in previous E-shape, even L =W or L > W-. The microstrip width in these examples would be w1, with w1=w2. This will always happen in order to keep E-shapes's similarity to the letter "E", the E-shape will always have "two extra branches", while the L-shape has more "degrees of freedom". Then the L-shape, because of its geometry, would be easier to adjust to the rest of the parameters in the structure, in order to obtain a better result – in terms of bandwidth in this case-.
In fact, in this study, the L-shape made it possible to find a better combination of the structure's components, that lead to a result more optimal than previous ones. The whole structure was optimized, not only the resonator. It is the losses in both the metallic resonator and the substrate that achieve the optimal absorption bandwidth result. Physically we could say that we were able to obtain losses from the resonator and the substrate at very close frequency points.
Anyhow it can be observed that with the L-shape, in most of its configurations, it was possible to obtain a more wideband result with TM polarization, as opposed to designs using an E-shape. With this TM-polarized response shifted to higher frequencies. Also most of the designs proposed with an L-shape do not include an air-gap in their layer-structure.

Additionally, in order to obtain a polarization insensitive response, an E-shape could never be made completely "polarization insensitive" because it would never be completely symmetric as the L-shape can be, as shown in figure 1b in this chapter.
Also, we can observe that results with the L-shape were in general less polarization sensitive than with the E-shape, which is consistent with being the last one a shape with less symmetry.

5.6 L and E-shaped resonators combined in coplanar configuration

The analysis is started with the optimal E-shape resonator design obtained in previous chapters and corresponding best performing layer structure, in order to try to obtain the best combined resulting performance. Nevertheless the E-shape is combined both with a large and a short L-shape as the exact effect of adding both resonant responses is not known with precision. Operational frequency range and response type is different for each L-shape with TE and TM polarization.

The unit cell and layer structure is depicted in figure 21. The new unit cell has twice the length of previously used unit cell, thus its size is 88.8 by 34 mm.
Using an air-gap=0.94, loss tangent=0.19 and permittivity=4.3 for a 4.7 mm-thick substrate, an L-shape resonator with the dimensions specified in table 5 and an E-shape with the same dimensions of our previous optimum E-shape design (chapter 4, figure 13) and table 6: L = 33.2 mm, d = 8.6 mm, s = 3.7 mm, W= 17.9 mm, w1 = 8.6 mm and w2 = 8.6 mm), the absorption response shown in figure 23 is obtained.

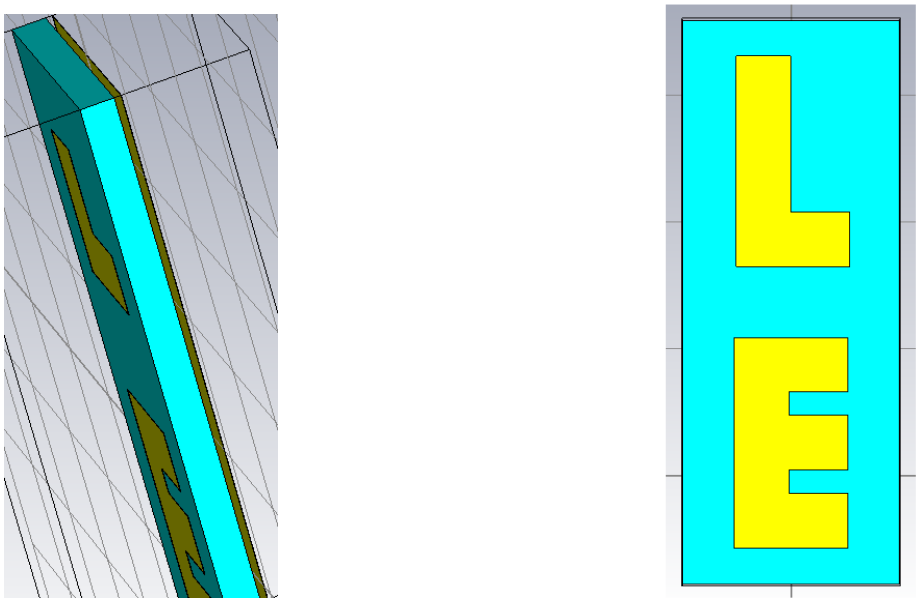

a) b)

Fig. 21. a) Layer structure of the new unit cell, twice as long as previous ones. b) Unit cell with L and E-shape resonators.

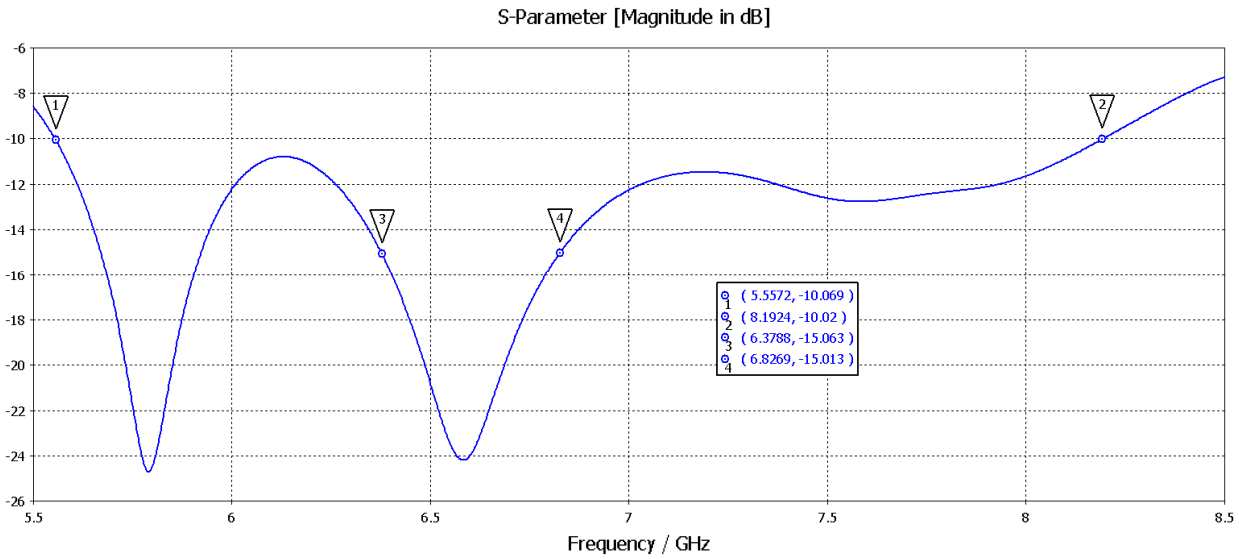

a)

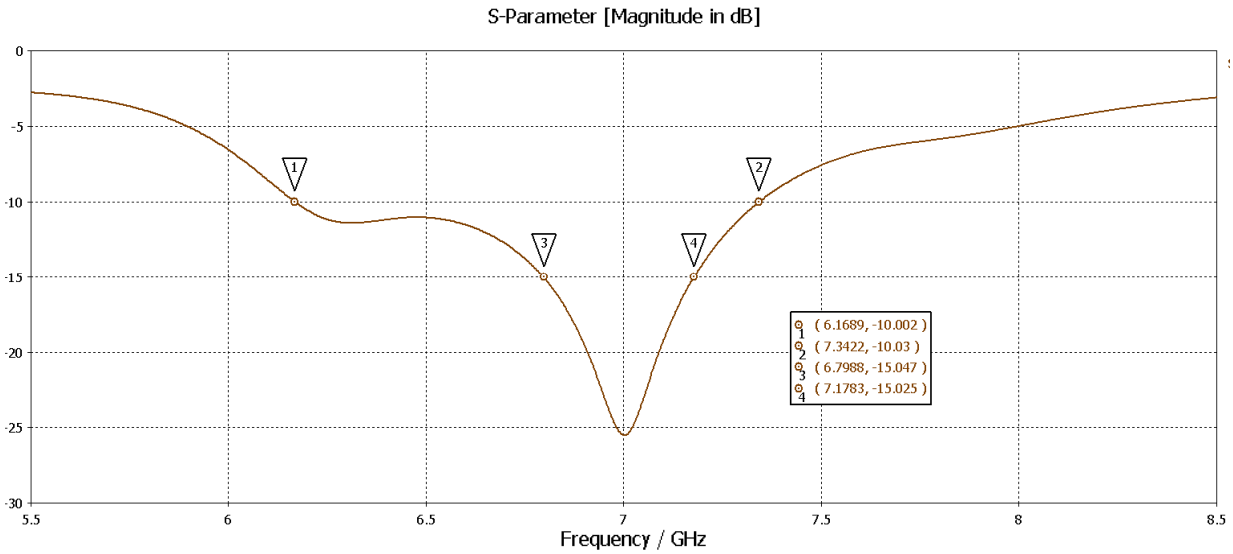

b)

Fig. 22. Results corresponding to the design of figure 21 for a) TE polarization b) TM polarization.

As expected the response is not polarization insensitive. With TE polarization the bandwidth at -10 dB is around 2.6 GHz, relative bandwidth 37.8%, at -15 dB there are two bands of around 0.25 and 0.5 GHz, relative bandwidths of 4.3% and 7.5% respectively. Thus at -10 dB the relative bandwidth is larger than the result shown in figure 15 (33.5%) for TM polarization. With TM polarization the bandwidth at -10 dB is around 1.2 GHz, relative bandwidth 17.2%, at -15 dB is 0.4 GHz, relative bandwidth 5.9%.

When an L-shape resonator with the dimensions specified in table 6 is used instead, the absorption response shown in figure 24 is obtained. The corresponding new unit cell is shown in figure 23.

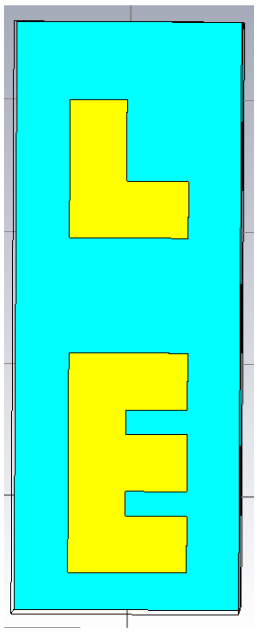

Fig. 23. Unit cell with L and E-shape resontors.

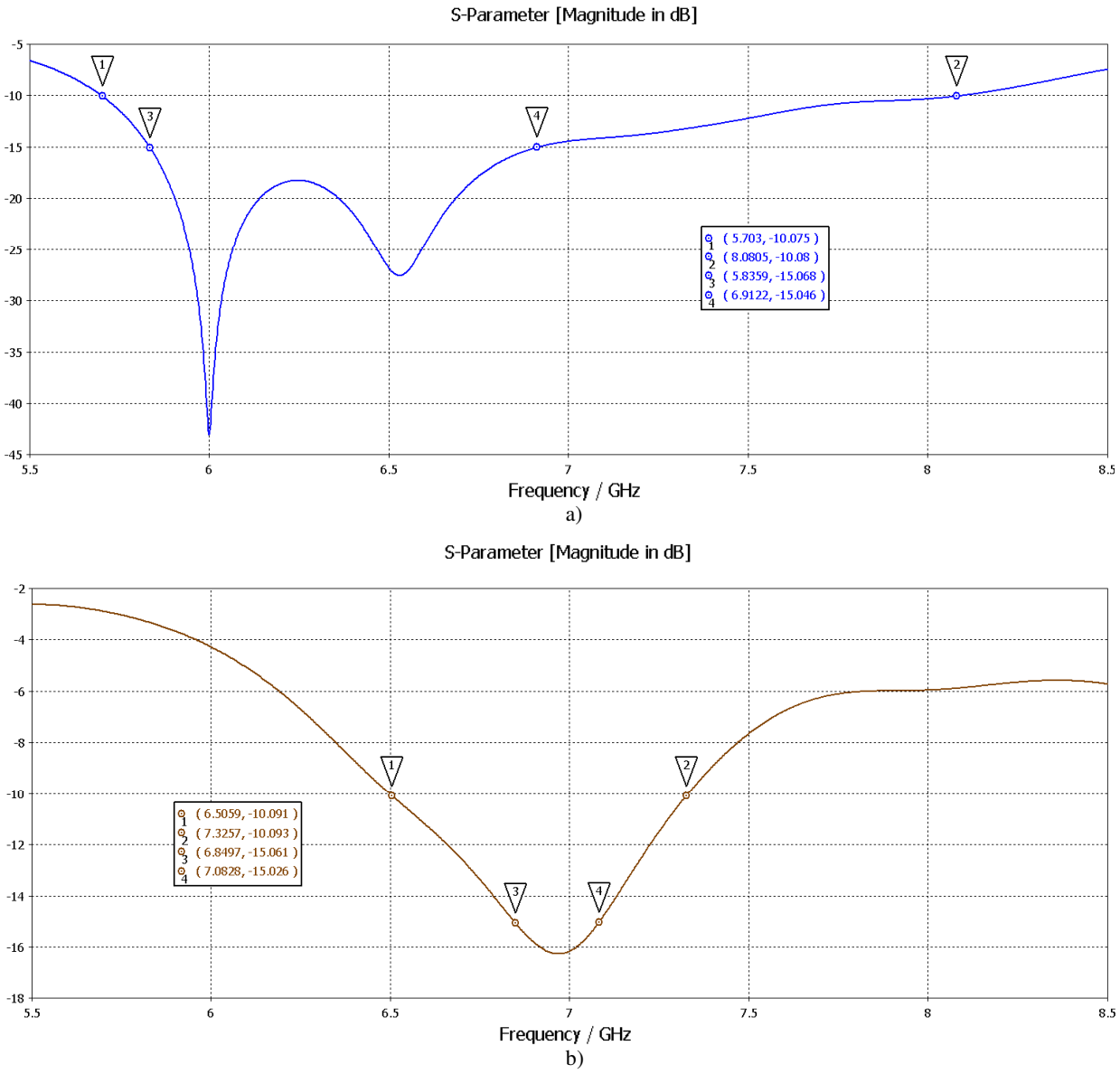

Fig. 24. Results corresponding to the design of figure 20 for a) TE polarization b) TM polarization.

Although the results of the previous design had a larger bandwidth at -10 dB with TE polarization, these results of figure 24 are notably better as there is a far larger bandwidth at -15 dB.

With TE polarization, absorption bandwidth at -15 dB is around 1.1 GHz, relative bandwidth 17.2%**,** at -10 dB is 2.4 GHz, corresponding relative bandwidth 34.5%. With TM polarization, bandwidth at -15 dB is around 0.8 GHz, relative bandwidth 11.9%, at -10 dB is 0.2 GHz, relative bandwidth 2.9%. It is another interesting polarization sensitive response, with a larger bandwidth than the one obtained with our optimum result using only an E-shape (15%), but with a smaller bandwidth than our previous optimum result with only an L-shape (23.6%).

An air-gap of 0.94 mm is the optimum or close to optimum value for the previous design, as shown in figure 25 an air-gap= 1.1 mm yields a smaller absorption bandwidth and smaller absorption level -except for the response with TM polarization, where absorption is slightly better with air-gap=1.1-. At -15 dB relative absorption bandwidth with TE polarization, which

yields the best result with this design, is 14.3%, at -10 dB absorption bandwidth is also smaller than with an air-gap=0.94.

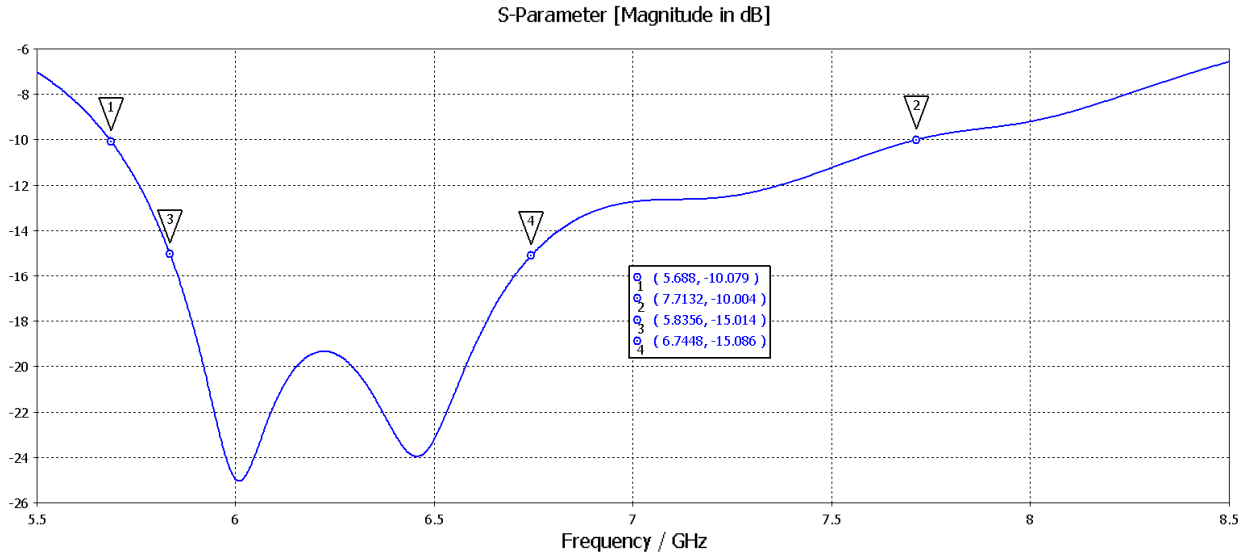

a)

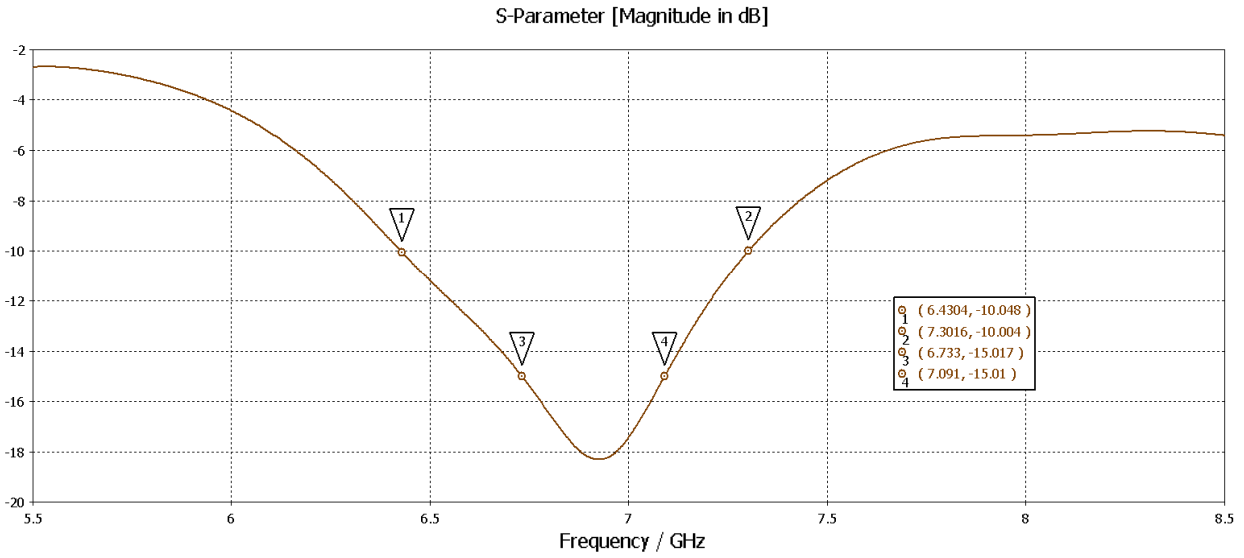

b)

Fig. 25. Results corresponding to the design of figure 23 when the air-gap=1.1 mm instead of 0.94 mm for a) TE polarization b) TM polarization.

When the previous design is used with the L-shape resonator made symmetrical as in figure 1 b), using the values of table 1 again, and an air-gap=0.94 mm, the response does not become more polarization insensitive, only absorption bandwidth decreases slightly and absorption levels have some increase, as can be seen in figure 26.

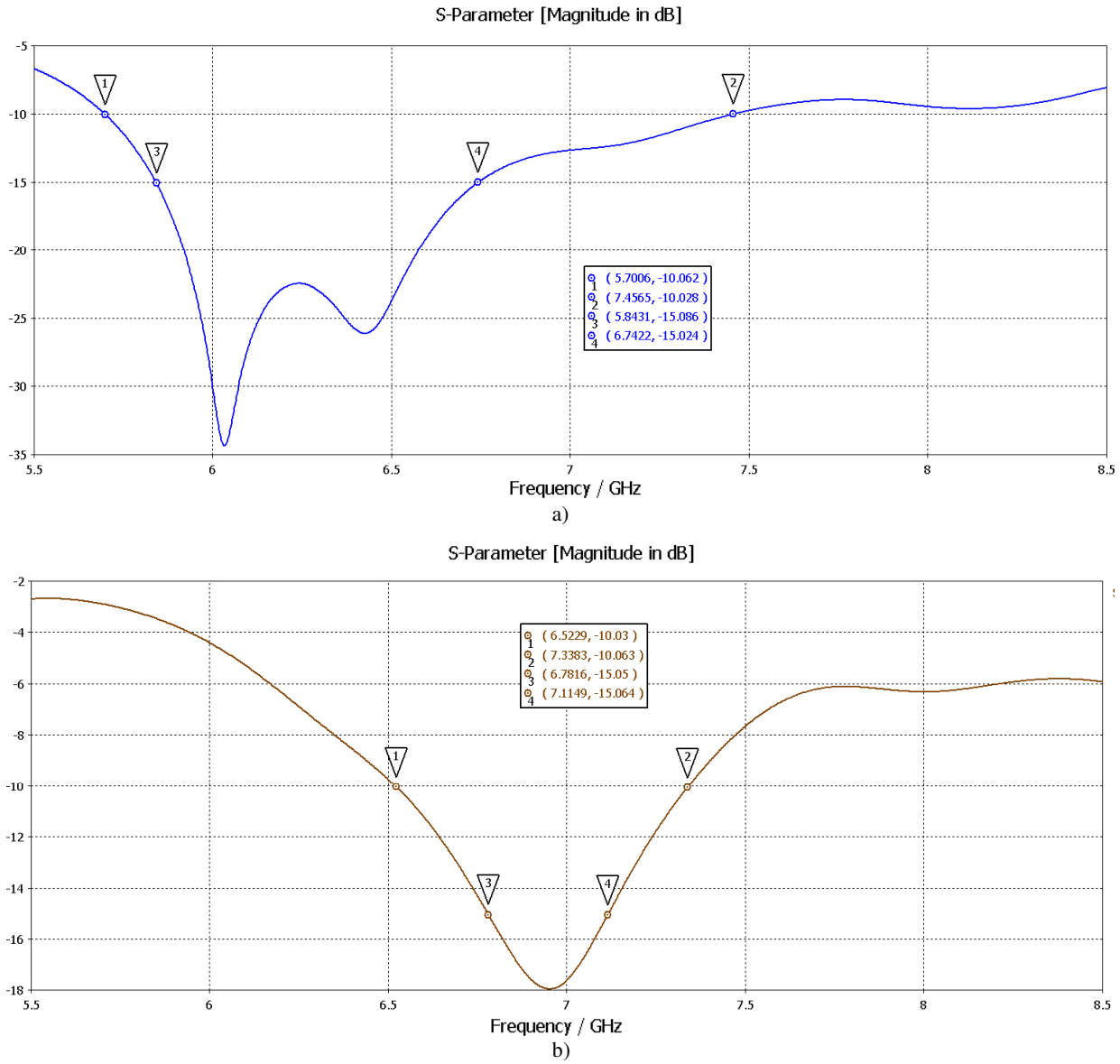

Fig. 26. Results corresponding to the design of figure 23 with a symmetrical L-shapes resonator for a) TE polarization b) TM polarization.

For TE polarization, absorption bandwidth is 0.9 GHz at -15 dB, corresponding relative bandwidth 14.3%, 1.8 GHz at -10 dB, relative bandwidth 27.4%. With TM polarization 0.3 GHz at -15 dB, corresponding relative bandwidth 4.8%, 0.8 GHz at -10 dB, relative bandwidth 11.5%.

5.6.1 Two sizes of L-shaped resonators combined in coplanar configuration

The combination of two of our previously utilized L-shapes, one of them with the values of table 5 and the second one with the values of table 6, also yields an interesting broadband response when a layer structure with the same parameter values used in the first design of this section are utilized (the layer structure that produced the results shown in figure 20, but using other resonators instead). Resulting unit cell is shown in figure 27 and corresponding response in figure 28.

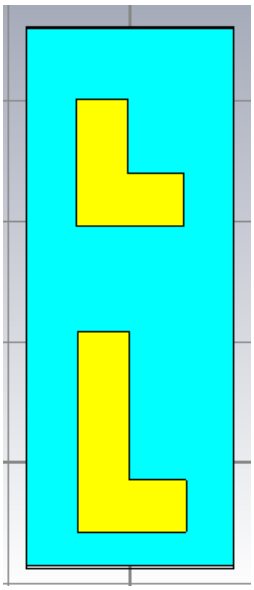

Fig. 27. Unit cell combining a large and a short symmetrical L-shape with L=33.2 mm, W=17.9 mm and w1=8.6 mm as summarized in table 5 and with L=20.9 mm, W=17.9 mm and w1=8.6 mm as summarized in table 6, respectively.

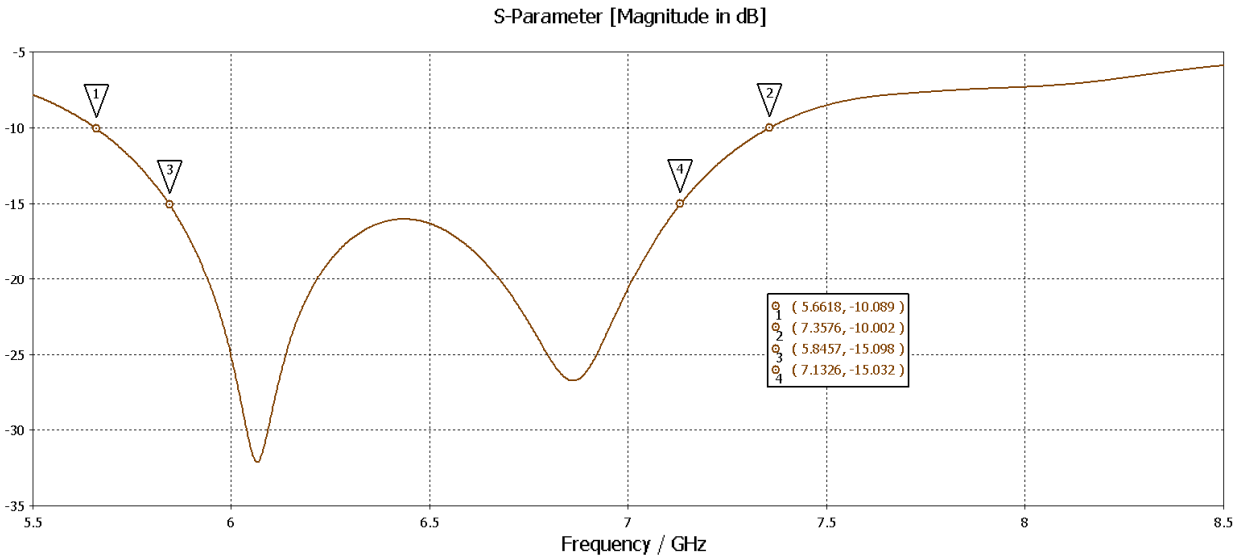

a)

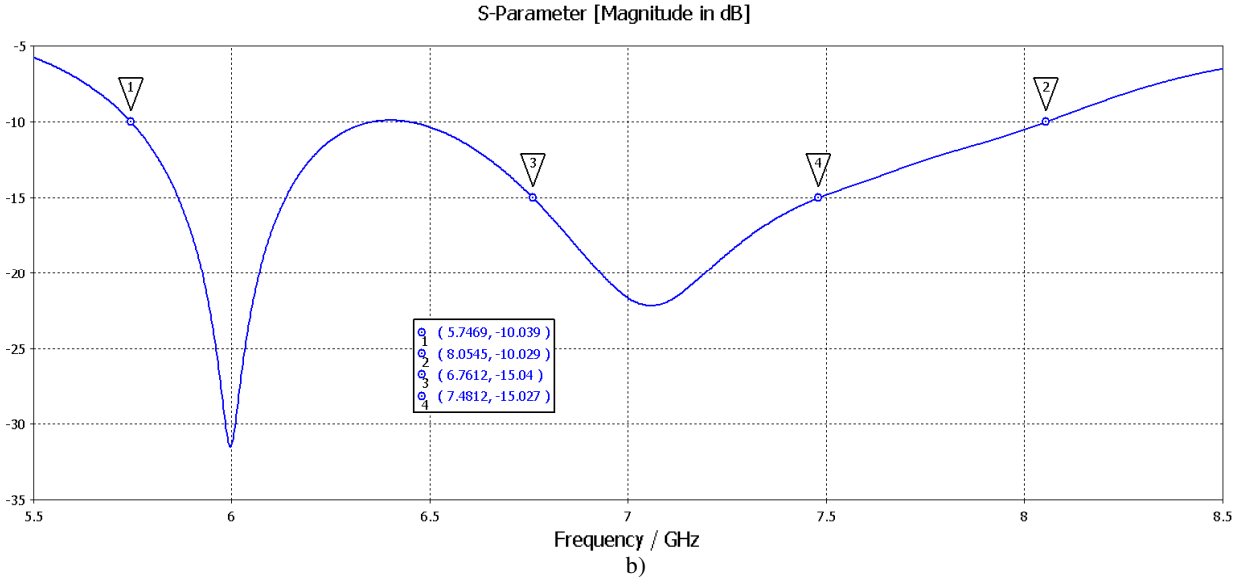

b)

Fig. 28. Results corresponding to the design of figure 27 for a) TM polarization b) TE polarization.

Responses are more polarization insensitive, although the absorption level is higher and beyond -15 dB with TM polarization. Absorption bandwidth for TM polarization is around 1.3 GHz at -15 dB, thus a relative bandwidth of 20%, and 1.7 GHz at -10 dB , relative bandwidth of 26.1%. With TE polarization there are two bands at -15 dB, absorption bandwidths are 0.27 and 0.72 GHz, corresponding relative bandwidths of 4.5% and 10.4% respectively, and 2.3 GHz at -10 dB, relative bandwidth 33.3 %. This more polarization insensitive response is expected due to the more symmetric double L-shape unit cell.
Thus at the maximum absorption level, the absorption bandwidth with TM polarization is also larger than the one obtained with our optimum E-shape design, which was a relative bandwidth of around 15 %.
This last design is thus the one that yields the best absorption bandwidths in this section and it has a more polarization insensitive response than our optimum result with only one L-shape.

5.7 Measurement of L-shape design prototype

For fabrication and measurement of an L-shape design prototype we had to face the same problem encountered in the fabrication of the E-shape designs regarding: size of the unit cell with respect to operational wavelength, and substrate material of the periodic absorber. The high loss tangent and low permittivity of the substrate do not match or correspond to any available material, and finally a substrate material with electrical and magnetic parameters close to relatively well performing values -as the ones exposed in the sensitivity analysis- could not be found.
It was requested to fabricate and measure the polarization insensitive L-shaped design, taking into account possible future polarization insensitive applications. In this particular case the smallest unit cell size is used (34 mm by 34 mm, figure 1), which is only slightly smaller than the wavelength at the central operational frequency, but size and operational wavelength are not compatible with available standard waveguides. This is illustrated in table 7, whereas it should be born in mind that for the polarization insensitive design 7.5-9.3 GHz is the approximate operational frequency range:

Waveguide name/type	Operational frequency [GHz]	Waveguide's size [mm]
J	5.85-8.2	34.85 by 15.80
G	3.95-5.85	47.55 by 22.15
H	7.05-10	28.50 by 12.62

Table 7- Standard waveguide sizes and corresponding nominal operational frequency ranges

Originated by the intrinsic physical response of the design of the absorber, this incompatibility cannot be overcome: even if for instance the absorber's permittivity is increased in order to shift the response to lower frequencies, absolute bandwidth will decrease even further, as observed in the sensitivity study of section 5.2.1, and frequency response will be increasingly and severely distorted. Relative bandwidth decreases even more significantly. As an example, with a permittivity of 6.2, operational frequency range reaches 7.3 GHz, thus still unmatched with G waveguide's range.
This incompatibility leads again to an open measurement system with consequences such as a large-scale sample, more presence of noise and possibly distortions in measurements.

A substitute design with available substrate materials has to be made, as it was the case with the E-shape design in chapter 4. As a result of this previous experience, as well as of a new investigation on further possible available materials for the polarization insensitive L-shape design and simulations, two materials were selected as the most suitable among the ones available: the same Eccosorb DSF-U absorber used in chapter 4 with the E-shape designs, and LS-16, another Eccosorb absorber with an approximate permittivity of 1.25 and loss tangent of 0.25 at 7.75 GHz, and 1.24 and 0.24 respectively at 8.25 GHz, according to values provided by the manufacturer itself. This new material thus is much closer than previous ones to the optimal loss tangent values found in the sensitivity analysis, but its permittivity is too small, distorting the optimal response of the design. Also therefore finding an appropriate second material that combined with LS -16 could issue an improved response was extremely difficult, and by means of simulations a second material with these characteristics could not be found.
According to its datasheet, LS-16 is said to be electrically conductive.
DSF material was used as substrate material in previous measurements with the E-shape designs, where also high loss tangent and low permittivity values similar to the ones required for the L–shapes designs were used. Therefore it is also suitable and can be reused in the L-shape designs, despite being far from configuring an optimal option. Additionally its mechanic characteristics make it adequate to build a prototype. As mentioned in chapter 4, the sheet of absorber is also large enough for samples built for free-space measurements.
Both materials were used in electromagnetic simulations before performing the measurements, as is usual practice.
Several other options were considered, like using a type of conducting ink from Dupont or even 3D printing, but either simulations results were even further away from the theoretical design than by using DSF and LS-16. Other reasons were that other materials were commercially not available, materials' parameters were undefined, as in the case of Dupont's ink, or implementation of the possible solution was out of budget and time scope. It was also sought to simultaneously shift the design's response to a standard waveguide frequency range, without success.

In order to print the metallic L–shaped patterns, there were at least two alternatives to the option of printing them on PCB, which had been implemented with the E-shape designs: spraying the patterns and using tape. Although both would be advantageous as they would not add FR4 to the structure of the periodic absorber, both could be less accurate, specially spraying which had proven to have a less regular and repeatable final result. Both could add more uncertainty to the process and be more problematic to implement. Also, taking into account the simulations' results, FR4 could actually be compensating some of the excessively high or low parameters of the absorbers' substrate material.

The layer-structure chosen for building the sample is composed as in previous designs by a PCB layer with the printed L-patterns, the lossy substrate and a ground plane. Then for the design that uses DSF as substrate, substrate layer's thickness is 1.81 mm as measured (DSF absorber's thickness), and PCB's thickness is 1.55 mm, using standard FR4.
In the design that uses LS-16 as substrate, standard available thickness of around 3.2 mm (0.125'=3.1496 mm) was chosen. Once the material was delivered, it could be observed that it was quite foamy, thus slightly depressible, therefore thickness had to be reduced to at least approximately 2.8 mm for simulations.
6mm-thick sheets were also available but its use would have taken the sample's thickness further beyond sensitivity tolerance values and worsen the design's result even further, as was

confirmed by much worsened simulation results. PCB thickness is also 1.55 mm, as the idea is to re-use the same piece of PCB for both designs.

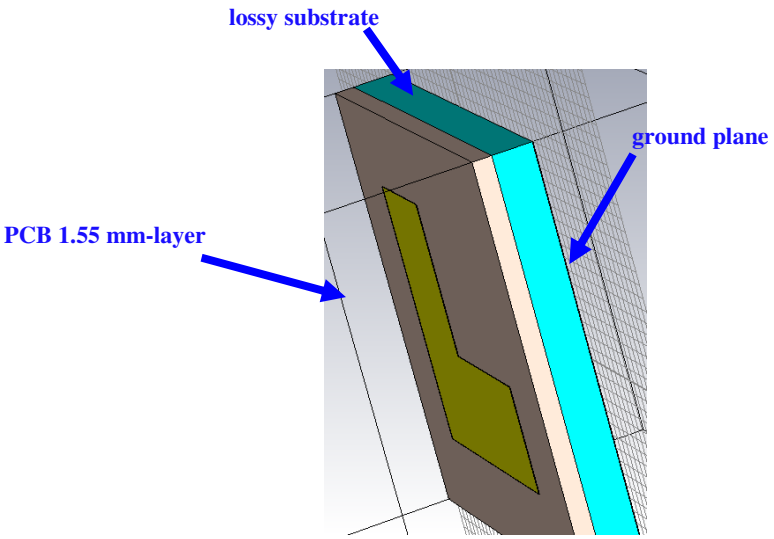

Fig. 29. Layer-structure of the unit cells conforming the periodic absorber to be built.

Adequate verifications on the measurements and checking of material parameters with measurements, that were duly performed in the case of DSF in chapter 4, could not be carried out with LS-16.[35] Due to this lack of adequate validation, results are not included here and can be found only as additional information in the Annex. However, in these preliminary results it could be well observed that the absorption bandwidth seems to be again shifted in frequency for around 1 GHz, as is the case with DSF.

For the substitute design including DSF, absorption bandwidth according to simulations at -15 dB would be 0.6 GHz and 1.84 GHz at -10 dB, relative bandwidths of 6.8% and 21 % respectively. In figure 30 the simulation result for this design is shown.

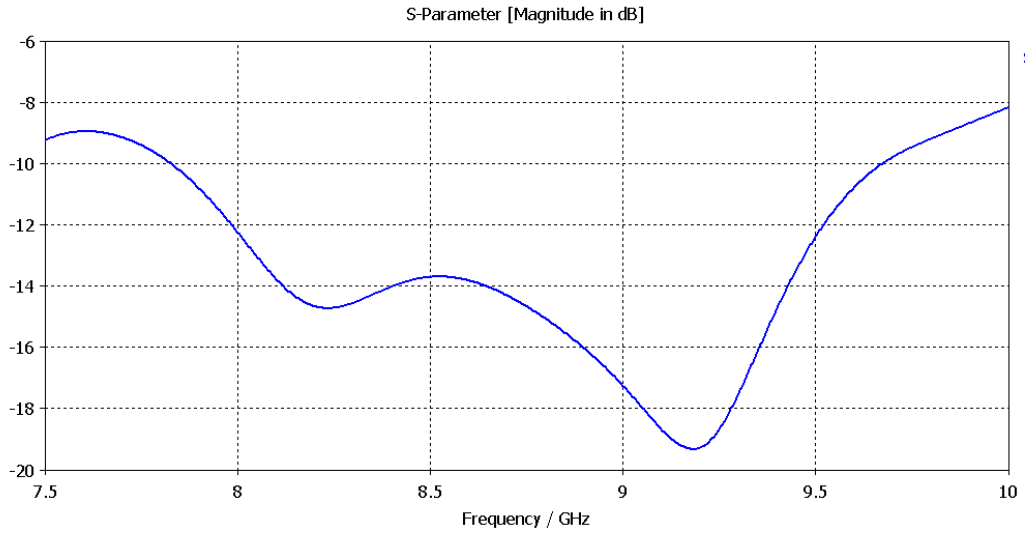

[35] There was no availability: LS-16 material finally arrived later than foreseen.

Fig. 30. Simulated S11 responses of the L-shaped polarization insensitive design to be built using a) DSF material b) LS-16 material.

The size of the sample was delimited by the one of the PCB, which is 238 mm by 238 mm thus 7 by 7 unit cells. This is comparable to the 8 by 7-unit-cell sample of the E-shape absorber. For the E-shape this resulted in a sample of around 5.26λ[36], for the L-shape design with DSF it corresponds to 7.3λ.

The technique used for the measurements is the same utilized for the measurements of E-shape designs in chapter 4. Again it is important to point out that as well as it can reduce noise in the measurements, it is highly likely to also smooth resonant responses and decrease their magnitude importantly with respect to its original value. Thus decrease absorption's magnitude.
The set-up used is thus the same as the one used for the E-shape absorber of chapter 4, the same device is used and connected to a Network Analyzer.

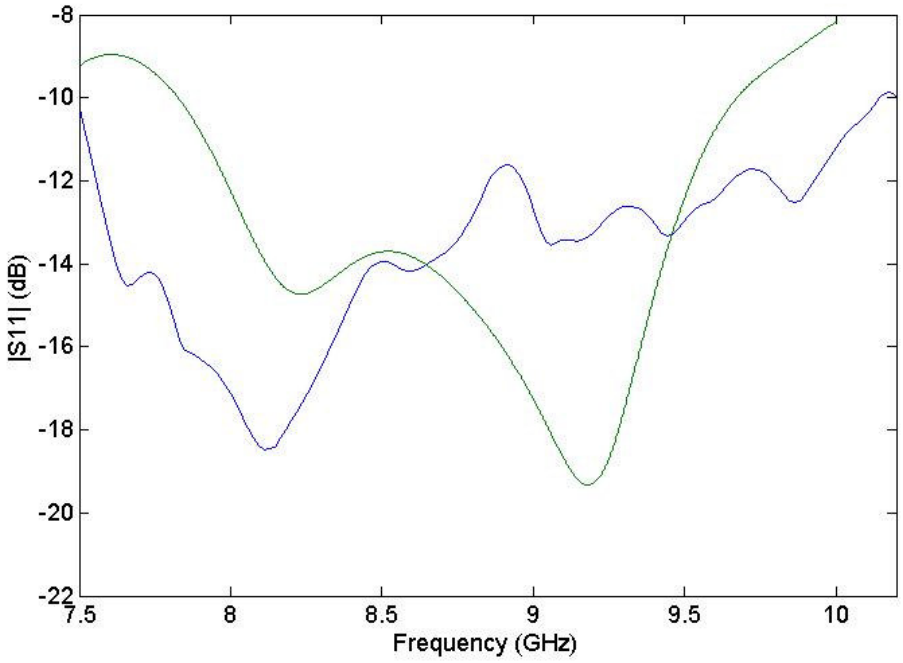

Fig. 31. Processed measurement results (blue line) and simulated results of the polarization insensitive L-shape design to be fabricated with DSF material as substrate (green line).

Although the bandwidth of the response measured is large and thus bandwidth's agreement with simulation is quite good, and even reflectivity levels in dB have a good agreement, at least in frequency agreement is not really good, with again a shift of around 1 GHz.

It is important to point out that for this prototype, unlike previous ones, a different finishing was used during the fabrication process of the PCB (outsourced), which reduced fabrication costs significantly. This finishing includes metals other than Copper, such as Tin (Sn) and

[36] Taking into account a central frequency of 5.8 GHz, according to simulations of fabricated sample.

Nickel. These components should be present only in the outer layer of the metallic patterns and its proportion should be very low, particularly the one of Nickel, which is a magnetic metallic alloy, due to the presence of Iron in it, among other metals. Magnetic materials would affect measurements, which is why we tried to avoid its presence in all prototypes' components. Although the proportion of these metals should be very small and it is not certain to which extent this should affect measurements, it is a difference with respect to previous prototypes, and it could be a possible source of the disagreement –frequency shift- previously mentioned. In fact in other very sensitive measurements performed by other colleagues in the group it has reported to have produced an important effect in measurements.
According to the provider of the finishing material, Felder Löttechnik, Nickel and Germanium are used and according to PCB manufacturer Eurocircuits, composition should be: Sn 99 %,, Cu 0,7%, Ag: 0,3, Rest: NiGe.
It is also often difficult to simulate Nickel in electromagnetic solvers and in fact the simulation crashed when it was used instead of Copper for the metallic patterns in the unit cell. With only Tin instead of Copper no significant distortions were observed in simulations' results.

The addition of some more measurements at more distances to the sample[37] should not have an important influence on frequency position of the full measurement.

Also the noise present in free-space measurements and edge effect have been mentioned previously as source of disturbance. Although they should have been significantly mitigated by the measurement technique used and the large size of the sample, their effect can be playing a not negligible role.

It was observed that the shape of some L-patterns in the PCB was slightly deformed as shown in figure 32, perhaps also due to the finishing. Again this is not expected to affect the measurements in an important way, nevertheless it is certainly a difference with respect to previous results. Also the fact that an open measurement system is used could make results more "sensitive" to small inaccuracies and disturbances, or it could be rather said that using this system could be "amplifying" their effect taking into account the multiple reflections, losses and noise present in such a system, that could add up to and interfere with several disturbances.
Anyhow these deformations should not cause directly a shift in frequency.

[37] Measurements at closer distances should be more relevant, according to previous group experience on the technique and despite the previously mentioned resemblance to a cavity topology.

a) b)

Fig. 32. a) and b) Sample picture's of the small deformations in the metal patter of the PCB board.

Nevertheless, as previously mentioned, a quite wideband behaviour can be observed in the measured results, comparable to the one of the simulation beyond at -15 dB (around 0.6 GHz) and larger at -10 dB, together with an overall good absorption level. Absorption levels in a wideband configuration have certainly increased with respect to previous cases.

It might be interesting to note that the DSF absorber used is designed to perform at a frequency range centred at 10 GHz (DSF-10), where it should also have its maximum performance. It can be observed that most of the absorption is measured at a lower frequency range and certainly the maximum performance is not found at or close to 10 GHz. Therefore we could dismiss the idea that only the DSF absorber is responsible for absorption, and that what is actually observed is its performance and not the one of the complete prototype.

5.8 Conclusions

By using a layer structure that is initially the same as the one of E-shapes, a better result in absorption and absorption bandwidth is achieved by using an L-shape resonator. The fact that with this resonator the substrate material necessary to reach the improved results has less losses than the one used with the E-shape, for some designs, it can be very interesting and desirable for future manufacturing. In the case of a loss tangent of 0.08, for the design that is not polarization insensitive, the previously used fluoroplastic Dyneon, with loss tangent=0.08, is an existent material that could be utilized in the fabrication.
We obtained not only much more wideband absorption results than the ones achieved with an E-shape in chapter 4 at -15 dB (97% absorption), being the maximum 27.1% , absolute bandwidth 2.5602 GHz -others in the order of 23% and 27 %- , but more importantly, also a polarization insensitive response with this new high absorption bandwidth (20% relative bandwidth at a high 97% absorption). No chirality was needed in the unit cell, a single resonator instead was sufficient. Additionally, this has been done with a shape that, as single resonator had not been used before in the design of periodic or metamaterial absorbers, to the best of our knowledge. More importantly, a relative bandwidth of around 27% is an interesting value for the state of the art, specially taking into account that this is achieved with an absorption of around 97%, a single resonator instead of multiple and without the need of

any lumped element such as resistors or capacitors. One drawback is that for this polarization insensitive result a substrate that was more lossy than the one used in the E-shape-design -loss tangent=0.21 instead of 0.19- had to be used, but for all the optimum results obtained with a single L-shape no air-gap had to be used. This is on the other hand a relevant advantage with respect to the single E-shape design,that can make the new design mechanically more practical for a future fabrication. Anyhow by using L-shapes, a substrate less lossy than the one used with the E-shape was sufficient to reach a larger relative bandwidth, namely 23%. The lower losses can give more merit to the structure itself rather than the substrate's material used. The importance of losses in the substrate for the most wideband structures coincides with the fact that the main loss mechanism for most published structures in the state of the art, in the microwave region, resides in the dielectric substrate [14],[15],[16].
Also, in the case of the polarization insensitive design, the unit cell's side-length is slightly smaller than the operational wavelength, as opposite to the unit cell size of the E-shape in chapter 4: 34 mm for a wavelength of 38.7 mm (with central frequency around 7.75 GHz). Anyhow it is not one order smaller than the wavelength or sub-wavelength.
All L-shaped structures in general are additionally relatively thin and their unit cells smaller than the wideband design on chapter 4, the E-shapes, which could be again an advantage, foremost for fabrication

Additionally also high absorption performances of around 20 % relative bandwidth with a 97% of absorption were reached by combining L and E-shaped resonators.

It is also interesting to verify that the resonant responses resulting from the use of different resonator shapes with the same total length and width dimensions, were indeed different with each different shape (L or E-shape). Thus it is not true that only the size of the resonator is what contributes to the final response of the design, meaning for these designs that using either a rectangle or a patch would produce equal responses, but actually the resonator's shape also plays an important role. Therefore it was interesting to use the parameter values of the E-shape-structure in chapter 4 -resonator and even layer structure- for some cases presented in this chapter.

Simulations are accompanied by free-space measurements of substitute designs. In the case of DSF material these yielded high absorption levels and medium to large bandwidth results.

5.9 References

[1] J.H.Ly, X.W.Hu, M.H.Liu, B.R.Yan, L.H.Kong, "Negative refraction of a double L-shaped metamaterial", J.Opt.A: Pure Appl.Opt., No.11, pp.085101-085104, May 2009.

[2] Y. Chang, S. Lu, H. Chung, S. Wang, T. Tsai, T. Guo, "High-Throughput Nanofabrication of Infra-red and Chiral Metamaterials using Nanospherical-Lens Lithography", Scientific Reports, Vol.3, No. 3339, Nov.2013

[3] H. Husu, J. Mäkitalo, J.Laukkanen, M.Kuittinen, M.Kauranen, "Particle plasmon resonances in L-shaped gold nanoparticles", Optics Express, Vol. 18, No.16, pp. 16601-16606, Jul.2010

[4] Y. Jing, Z. Jia-Sen, W. Xiao-Fei, G. Qi-Huang, "Resonant Modes of L-Shaped Gold Nanoparticles", Chin.Phys. Lett., Vol.26, No.6, p.067802, 2009

[5] B. Lamprecht, A. Leitner, F. Aussenegg, "SHG studies of plasmon dephasing in nanoparticles", Appl. Phys.B, Vol.68, No.3, pp.419–423,1999

[6] M. Kauranen, A. Zayats, "Nonlinear plasmonics", Nat. Photonics, Vol. 6, pp.737–748, 2012

[7] R. Czaplicki et al., "Enhancement of Second-Harmonic Generation from Metal Nanoparticles by Passive Elements". Phys Rev Lett, Vol.110, No.093902, 2013

[8] M.Li, L.Guo, J.Dong, H.Yang, "An ultra-thin chiral metamaterial absorber with high selectivity for LCP and RCP waves", J. Phys. D: Appl. Phys., Vol.47, pp.185102-185107, 2014

[9] J.Zhao,B.Xiao,X.Huang,H.Yang,"Multiple-band reflective polarization converter based on complementary L-shaped metamaterial", Mic. and Opt.Tec.Lett., Vol.57, No.4, April 2015

[10] D-J.Kim, J-H. Lee, "Broadband Left-handed Waveguide with Double L-Shaped Short Stubs and E-plane Posts", Proc. IEEE AP-S/URSI 2011, (p.2958), Jul.2011

[11] S.Bhattacharyya,S.Ghosh,D.Chaurasiya,K.V.Srivastava,"A broadband wide angle metamaterial absorber for defense applications", Proc.IEEE IMaRC 2014, (p.33),Bangalore, Dec.2014

[12] Yu Qian Ye, Jin, and He, "Omnidirectional, polarization-insensitive and broadband thin absorber in the terahertz regime",Journal of the Optical Society of America B, Vol. 27, Issue 3, 498-504, 2010.

[13] H. Luo, Y.Z. Cheng, R.Z.Gong., "Numerical study of metamaterial absorber and extending absorbance bandwidth based on multi-square patches", Eur. Phys. J. B, No.81, pp.387–392, Jun.2011

[14] C.M.Watts, X.Liu, W.J.Padilla, "Metamaterial Electromagnetic Wave Absorbers", Advanced Materials, Vol.24, No.23, pp.98-120, 2012.

[15] N.I.Landy , S.Sajuyigbe , J.J.Mock , D.R.Smith , W.J.Padilla , Phys.Rev.Lett.,Vol.100 , No.207402, 2008.

[16] C.G.Hu , X.Li ,Q.Feng , X.N.Chen , X.G.Luo, Opt.Exp.,Vol.18, pp.6598, 2010.

6 Conclusions and Outlook

6.1 Summary

As a general conclusive comment to the doctoral research carried out and what has been exposed in this thesis, we can say that not only wideband metamaterial absorbers or absorbing periodic structures are addressed, but a rather broader, global view intends to be offered, showing two most opposite structures above all in terms of the size of their unit cells with respect to the operational wavelength, and of the absorption bandwidth. With this global view we achieve the initial aim mentioned in chapter 1of performing a general research on metamaterial or periodically arranged absorbers. A more classical and often published kind of metamaterial absorber, like the one presented in chapter 3, is included, but it is also presented from an original point of view: a very simple kind of resonator is used, to which not much attention had been drawn in the past, and the effect on its performance after varying the structure of its unit cells is observed. Experimental results obtained with the fabricated prototype of these designs are very good and have an excellent agreement with numerical results, which additionally agree with two different solvers. Results obtained in both solvers also validate the previously exposed numerical study. The size of the unit cells for these designs is less than a third of the wavelength and minimum thickness less than a sixth of the wavelength.

Perhaps also a certain degree of originality can be given to the general approach to periodic absorbing structures, as we partly address intensively the issue of broadening the band of absorption, most difficult to achieve in the way it was done here, whereas other publications rather focus on polarization, flexibility of the sample, and increasing the level of absorption.

If we now focus in the wideband structures, presented in chapters 4 and 5, very large relative bandwidths of 15% and more interestingly beyond 27% at an absorption of more than 96% have been proposed. These are interesting bandwidths for the state of the art of non-multi-layer and multi-resonator designs that often need additional elements to reach bandwidths beyond 13%. Broadband responses are very difficult to achieve from resonating structures, as their frequency response is intrinsically narrowband.

A specific design that uses the L–shape achieves polarization insensitive absorption, which is required specially by some applications, but in general also demanded for a large number of absorbers. Again this is additionally reached with an interesting relative bandwidth of 20%. Achieving this with a single and simple resonator, instead of a chiral or geometrically more complex shape -that could offer more complications even when fabricated- is not commonly observed in other polarization insensitive designs for absorption, where sometimes much more complex shapes are necessary. Additionally just a single-layer of substrate was sufficient –and no air-gap had to be used- to achieve the performance of the best L-shaped absorbers with above 20% relative bandwidth, which could reduce in the first place a good number of complications in its fabrication. Also a substrate less lossy than the one used with the E-shape was sufficient to reach a larger relative bandwidth, 23%, as mentioned in chapter 5.

Again, achieving these wideband results by using only one resonator instead of multiple and neither by adding narrowband responses of multiple resonators can be of interest for applications and environments that require serious geometrical and structural constraints, for the first case, or a strictly uninterrupted bandwidth of high level absorption for the second case.

It is also worth mentioning that, to the best of our knowledge at the moment of starting our research with the E-shape, it had not been notoriously used as resonator in periodic or metamaterial absorbers, and not even in metamaterials. Thus its use in the field is definitely

original. The L-shape has been mainly used in plasmonics and to achieve the double-negativity of a material, and more than one L-shape combined in a metamaterial absorber has been reported [1], but the use of a single-shape for metamaterial absorbers or periodically absorbing structures has not been so often or notoriously reported, to the best of our knowledge.
These very wideband structures can have great potential and further research on them can add value to more complex applications and systems.
The sensitivity studies performed for the wideband structures could contribute to a future development of sensor applications or simply for necessary changes in the designs' implementation.
Besides this, the experience acquired by building our first piece of metamaterial –a first experience both for the author and in the research group- was of major importance to learn fundamental issues related to fabrication and experimentation with this special kind of materials. Almost the same applies to simulations first time carried out with metamaterials, where all related basic knowledge had to be learned. It also gave more insight and understanding to the literatures studies previously made.

Additionally the learning process developed and stages that took place are interesting, as we start from having no knowledge about metamaterials, which is why we initially address a classical double-negative material, to investigating a very specific kind of periodic structure or rather an application of periodic structures and metamterials such as absorbers. In this way we meet another initial aim mentioned in chapter 1. And finally we address a very specific issue of metamaterial absorbers and periodically structured –and even conventional- absorbers: the absorption band.

Some main issues that can be improved in the past work carried out are:

- find a better substrate material for the E-shape based absorber
- propose more specific applications or develop them more in detail for the proposed designs

It would be strongly advisable for the proposal of future designs, that their performance can be measured using the same technique applied to measure the double-patch structure, presented in chapter 3. This method is more simple and straightforward, does not need much further post-measurement processing and it typically involves less sources of error and uncertainty than an open system method or set-up. It can therefore facilitate clarity at the time of comparing simulations and measurements. Besides this, it is more likely to ensure that the structure manufactured will be sub-wavelength, due to the size restriction that the use of the waveguide imposes in the material samples to be measured in it.

6.2 Applications and future outlook

Multi-band and broadband operability is gaining increasing relevance in new materials and devices, because of all new communications' applications demanded by the industry and the society. Also absorbing capabilities are and will be demanded, specially taking into account the increasing use of wearable technologies and devices. Multi-band and broadband absorbers should thus find applications in this context.

We review some possible concrete applications specific to the absorbing structures presented in this thesis:

-a wideband absorber attached to walls, for instance of a building that needs to be secured from wireless radiation (a secure wireless environment) in a specific frequency band, as proposed in [2] for graphene, but using a less expensive alternative to this material. In [2] the broad bandwidth presented is not really continuous (absorption periodically fell to nearly 50% in the absorption bandwidth, unless five or more layers of graphene were used. Still with five layers, absorption was not larger than 90% for the whole frequency band), as opposite to the bandwidth of our design. Our wideband designs could be used in the microwave band.

-as isolator between elements of an antenna array (a MIMO array is an example), if a wide bandwidth of absorption is required. Metamaterial absorbers are specially adequate for small antenna arrays, like the ones often used with MIMO, where small sized, planar and thin –at least thin as the antennas themselves- materials are required [3].

Specifically for ultrathin, narrow-bandwidth absorbers like the ones presented in chapter 3, good applications could be found to current wireless technologies technologies that have narrowband operating frequency bands like LTE and Bluetooth, preventing radiation at very specific frequency ranges. LTE bands are typically 0.1 GHz wide, ISM 2.4GHz spectrum is also typically divided in 0.1 or 0.4 GHz at the most, Bluetooth operates between 2.4 and 2.4835 GHz. In addition to their thin profile, their small and tunable size would make them particularly suitable for the small and thin planar antennas intensively used in the previously mentioned applications.
This structural characteristics could also be an advantage for any of current electronic components, that are continuously downscaling in size.

Besides this, 5.8 to 7 GHz is part of a range where several radar applications operate[38] and our E-shape designs operating in this frequency range could then find numerous applications in this area. Our wideband L-shapes' designs could also be used in these applications and cover the frequency range at 7-8 GHz, uncovered by most of both E-shape and double-patch designs. As with any metamaterial, their unit cells can also be scaled to adapt to other operational frequency ranges required by an application. This makes any periodically arranged or metamaterial structure adaptable to many applications besides the ones it might have been designed for.

To the question whether metamaterial absorbers with narrowband absorption can still "have a future", the answer would be that they can still find applications, for example where very high but not necessarily broadband absorption is required - not all applications require a highly broadband absorption-, specially as filters, or combined with other narrowband absorbing structures to achieve multi-band absorption. Very high absorption levels or nearly perfect absorption can be reached by metamaterial absorbers, with additional advantageous geometrical or topological characteristics with respect to conventional absorbers. More applications and suggestions for further development have been proposed in publications of these narrowband structures, a good number of these publications have been mentioned in this thesis.
Also an initial typical approach with metamaterial absorbers in order to have a broader or wide bandwidth has been to add the response of several designs or rather single metallic resonators, use several layers of metamaterials or even other additional elements. This is why they continue to be investigated.

[38] Some important exceptions are Meteorological and Aeronautical radars –in moderate and long distance, 2.8 and 1.2 GHz-. Also Maritime radars: at frequencies allocated around 9 GHz.

It might only be difficult to find metamaterial absorbers that comply with the effective medium theory and that exhibit a broad bandwidth of absorption. As wideband absorbers with single resonators they have intrinsically problems do to their resonant nature, and this is the point, relative to absorption bandwidth, we tried to make in the thesis. As Costa, Genovesi et. al. say in [10], "the so-called perfect metamaterial absorber […] has been rarely used in the microwave regime due to the very limited operational bandwidth […]. However, the limited bandwidth does not impede the use of this type of configuration because, in many applications, signals are located within very narrow frequency bandwidths." .

To think about further applications for metamaterial absorbers and periodically arranged absorbing structures in general, we must realize that they can be used anywhere where electromagnetic radiation needs to be absorbed. In the first place, they can have the same applications as conventional absorbers, being additionally thinner -for many of the designs proposed in the state of the art- and more tuneable than conventional absorbers, as has already been mentioned throughout this work. Metamaterial and periodically arranged absorbers also have as general advantage over conventional absorbers that the first ones can be made much smaller than the second ones, due to their constitutive small unit cells, thus they are more suitable for small and even miniaturized antennas and electronic devices. Conventional commercial absorbers have traditionally being used for antennas and antenna applications and in wireless telecommunications in general (including waveguides and base stations), and are already required in the industry of electronic devices to reduce noise in electronic circuits, to be part of installations of GPS units in microwave transceivers, among others. Renowned manufacturers have claimed commercial absorbers are also used in the medical industry for different electronic appliances, in MRI and in radiation treatment. Thus in all these areas metamaterial and periodic absorbers can be used, with an advantage on size, tuneability and scalability and, in most cases, of thickness for planar metamaterials or planar periodic absorbers.

Regarding less "conventional" applications and going beyond the microwave range, metamaterial absorbers have been heavily proposed as detectors or sensors above all in the infrared and THz range [4]. Multiple-resonant absorbers, more of the kind of our double-patch structure presented in chapter 3, yielding multiple but narrowband absorption peaks, have been proposed to be used in detection of explosives as many of them have specific fingerprints in the THz range. In the mm-wave band their application in automotive radar (77GHz), in imaging (95,110GHz), radar sensors [7] and even for LAN networks (92-95GHz) has been suggested. Even their use in photonic circuits has been postulated [8].

Periodic absorbers and metamaterial absorbers could also find different applications in current wireless sensor networks, in all developments involving the Internet of Things (including RFID and smart tags) and again in increasingly growing wearable devices and systems. For this last field further development of flexible absorbers would be fundamental. Specifically wideband antennas are being requested, for instance for some special kind of wireless sensor networks based on radar sensors.
Also very interesting applications of metamaterial absorbers could be found in wireless transfer of electrical energy and energy harvesting, being a good starting point the work published in [9].

More extraordinary applications could constitute three-dimensional perfect absorbers, for systems and devices that involve radiation for instance, and eventually for invisibility in the optical range. And research in the microwave region has been so far much more extended

than in the optical region. Metamaterial and periodically arranged absorbers could even be used to minimize the effects of electromagnetic pulses and even to contribute in systems ideated for protection against solar storms.

As for applications for double-negative metamaterials, a large number has been proposed along this approximated 15 years of research on metamaterials, some already mentioned in this work, being again one of the most extraordinary invisibility cloaks. Also many double-negative metamaterials have been developed to cover the needs of very specific applications mentioned in the corresponding publications, thus the focus for applications is made in metamaterial absorbers and periodically arranged absorbers.

6.3 References

[1] S.Bhattacharyya,S.Ghosh,D.Chaurasiya,K.V.Srivastava,"A broadband wide angle metamaterial absorber for defense applications", Proc.IEEE IMaRC 2014, (p.33),Bangalore, Dec.2014

[2] Wu, Tuncer, Naeem,Hao et.al.; "Experimental demonstration of a transparent graphene millimetre wave absorber with 28% fractional bandwidth at 140 GHz"; Scientific Reports, Vol.4, No.4130, 2014

[3] Sharawi,Numan,Aloi; "Isolation improvement in a dual-band dual-element MIMO antenna system using capacitively loaded loops"; Progress In Electromagnetics Research, Vol. 134, 247-266, 2013.

[4] C.M.Watts, X.Liu, W.J.Padilla, "Metamaterial Electromagnetic Wave Absorbers", Advanced Materials, Vol.24, No.23, pp.98-120, 2012.

[5] N.I.Landy , S.Sajuyigbe , J.J.Mock , D.R.Smith , W.J.Padilla , Phys.Rev.Lett.,Vol.100 , No.207402, 2008.

[6] C.G.Hu , X.Li ,Q.Feng , X.N.Chen , X.G.Luo, Opt.Exp.,Vol.18, pp.6598, 2010.

[7] A. I. M.Ayala , Master of Science Thesis, Tufts University, USA, 2009.

[8] Y. Gong, Z.Li, J. Fu , Y. Chen , G. Wang , H. Lu , L. Wang , X. Liu , Opt.Exp., Vol.19 , No.10193, 2011 .

[9] Y.Xie, X.Fan, J.D.Wilson, R.N.Simons, Y.Chen, J.Q.Xiao, "A universal electromagnetic energy conversion adapter based on a metamaterial absorber", Sci.Rep., Vol.4, No, 6301, Sept.2014.

[10] F.Costa, S.Genovesi, A.Monorchio, G.Manara, "Low.Cost Metamaterial Absorbers for Sub-GHz Wireless Systems", IEEE Antenas and Wireless Propagation Letters, Vol.13, p.27, 2014

Publications and Curriculum Vitae

C. Herrera, G.A.E. Vandenbosch, "Analysis of stacked patch periodic absorbers", Proc. URSI Benelux Forum 2012, (p.45), Brussels, Belgium, Sep.2012.

C. Herrera, G.A.E. Vandenbosch, "Systematic study of double-layered ultra-thin stacked patch absorbers", Proc. EMC Europe 2013, Brugge, Belgium, Sep.2013.

C. Herrera, G.A.E. Vandenbosch, "Polarization sensitive wideband periodic absorber with E-shapes microstrip resonator", IEEE Transactions on Electromagnetic Compatibility, submitted in July 2015 (under review).

03/2003 - 29/05/2009: Engineer in Telematics, Universidad de Montevideo
This Electrical Engineering degree has its focus on Telecommunications and Computer Science Engineering/Informatics. As Thesis work to graduate I developed a security solution in a Linux environment, integrating -proprietary and open- routing and security devices (SNORT among them). The main part of this solution, which is the one that achieves integration, is a system developed by myself in Unix programming languages (bash scripting mainly). Virtual Machines were also used.
The career also includes specialized courses on Project management and Investment Projects courses, Quality control, Business Administration, Economy, Accountancy, Marketing and Costs systems instruction. CoBIT and ITIL were also included in the education.

03/2008 - 05/2010: National Bank of Uruguay -BROU
Position won in open, public competition and performed at the Telecommunications Department, Division of Technology and Operations, reporting to the Manager of the Telecommunications Department.
BROU's computer network is one of the largest in the country (core and satellite networks, with above 5.000 employees, more than 100 bank branches) and uses a wide variety of products, technologies and platforms. The latest technology coexists with older ones in this network. The Telecommunications Department administers, develops and optimizes this and the digital and IP telephonic network, carrying out departmental and divisional projects. Innovation is sought, as long as it brings benefits to the bank and its clients.

10/2006- 03/2008: IBM
Worked in the company's Networking department, focusing in IT Security for a particular project. The client this project is running for holds one of the largest computer networks in the country. Within support and administration of the client's information security network, tasks included monitoring, configuration changes, support and solving problems in a wide variety of network services and devices (among other a wide range of Cisco and IBM products, network security devices such as IDSs, firewalls, Content Filtering solutions and open source solutions). Periodic security reports, including SLA reports had to be documented and produced.

03-08/2005: PricewaterhouseCoopers - Universidad de Montevideo Development of a system programmed in Java language able to process forms designed in Excel spreadsheets. It produced statistical information based on the data processed. Project carried out under own deployment.

01/2005: Telmex S.A. Internship at its NOC (Networking Operations Center).

03/ 2003-02/2004: Universidad de Montevideo Internship at Department of Communication and Marketing

4/10/2002: CCNA -Cisco Certified Network Associate

03/2001-08/2002: Cisco Networking Academy Program CCNA 4 WAN Technologies: CNAp graduate (Networking Administrator).

2000:German School of Montevideo - German-Uruguayan Chamber of Commerce
Programmer I. First module: Fundamentals of Informatics. Structured Programming Principles. Basic Pascal Programming. Second module: Pascal advanced programming.

Languages

12-13/12/2002: Certificate of Proficiency in English, CPE (University of Cambridge) CEFR: C2
13-14,20/08/2002: Deutsches Sprachdiplom. Zweite Stufe der Kultusministerkonferenz CEFR: C2
Commercial and business English, technical and business Portuguese at the University.
Dutch CEFR: B1

Courses and Seminars

Dec. 2009.- BROU Training plan.- Building Scalable Cisco Internetworks (BSCI) v3.0.
17/09/2009.- ORT University. - Microsoft and Innovation. Applications in education: Robotics and videogames.
15/09/2009.- ORT University.- Advances in the comprehension of cellular behaviour and new therapeutic tactics in cancer.
08/09/2009.- ORT University.- CMMI for services, a new enterprise of SEI.
01/09/2009.- UCUDAL. Catholic University of Uruguay.- R+D+I Management system in Spain and the rest of Europe.
28/07/2009.- ORACLE DAY - TILSOR S.A.- Oracle trends and all about new products and technologies.
05-2009.- BROU Training plan.- BootCamp CCNA.
03-2009.- BROU Training plan.- Cisco Voice Gateways and Gatekeepers, VoIP course by Logicalis (Cisco partner).
05/11/2008.- IEEE- Catholic University of Uruguay.- Analog IC Design Methodology
03/09/2008.- ISACA- Universidad de Montevideo.- Web-application's security.
23/07/2008.- IEEE - ORT.- Economical principles in Telecommunication's Networks Control.
06/12/2007.- Arcanus - ISACA.- Arcanus Security Tour.
9-11/10/2007.- Universidad de Montevideo- ANTEL.- Days on Informatics and Information Security on Internet.
20/10/2006.- UNIT- ISACA – Datasec.- Fundamental bases for the implementation of information security management system. UNIT-ISO/IEC 27001 / UNIT-ISO/IEC 17799 standards.
19/10/2006.- ISACA - ORT University.- Security governance. Key element for corporate social management and responsibility.

02/10/2006.- RAB/TAB Tour 2006. IEEE RAB/TAB Group – Student's Branch IEEE Universidad de Montevideo-Sheraton Montevideo.-Introducing the IEEE Student's Branch from Universidad de Montevideo to IEEE directors

29/09/2006.- IEEE - ANTEL.- Telecommunications Projects Management. Project management activities under pressure for meeting successful results and in a demanding environment.

21/09/2006.- IEEE, Engineering Management Society – Universidad de Montevideo.- Work Breakdown Structure.

24/08/2006.- IEEE, Section Uruguay, Computer Society – Universidad de Montevideo.- Free Software and Software Development Tools.

23/08/2006.- ISACA Montevideo Chapter - Universidad de Montevideo.- Software measurement.

26/05/2006.- IEEE, Section Uruguay, Biomedics-Control - Solid State Chapter – UCUDAL.- Paradigms in Biomedical Engineering.

23/05/2006.- ISACA Montevideo Chapter-Universidad de Montevideo.- Security in Wireless Communications.

25/04/2006.- ISACA Montevideo Chapter-Universidad de Montevideo.- Cobit 4.0-An updated version.

10-2005.- TATA Consultancy Services.- TACTICS Iberoamerica. The first TCS Iberoamerica Technical Architects' Conference.

08-10/06/2005.- UDELAR Faculty of Science– Pro Ciencia – SBPC.- Regional Meeting of Science, Technology and Society.- Academic Communication Nets. Associations for Science and Inter-science Progress.

04-2003.- Work Breakfasts-COMMON Uruguay.- Telecommunications seminars.- Antel Data: Present technology of its services, technological platform, products y services. Ancel: Present technology, future ways, Use of the mobile phone net for data transmission and its applications. IP Telephony-The new era

20/09/2002.- IEEE- Section Uruguay-Communications chapter.- The future of the net and Quality of Service in multiservice nets.

Lectures given

02/10/2006.- RAB/TAB Tour 2006. IEEE RAB/TAB Group – Student's Branch IEEE Universidad de Montevideo.- Introducing the IEEE Student's Branch from Universidad de Montevideo to IEEE directors (Eng. Cecelia Jankowski, Peter Starker and Celia Desmond, among others).

Annex

CST Microwave Studio's limitations on large permittivity and permeability values

CST confirmed that indeed there was a problem when using relatively large permittivity and permeability values for a material and that this was a bug. Namely the mesh became extremely large and simulations with these values seemed to require at least 13GB of memory to be run. They first tried several different material and mesh settings but always with negative values without having success, but finally the problem was related to both permittivity and permeability and the larger the values, the worse it became. The case was reported to CST's developers and it remains open.

This partially explains why the simulation run out of memory when using the values of the reference dispersion equation even only in three frequency points around the theoretical resonant frequency 10.5GHz (which is the one taken into account to calculate far-field parameters), as they reach relatively large magnitudes close to this frequency as can be seen in table 1:

freq(GHz)	Re{ε(ω)/ ε_0}	Im{ε(ω)/ ε_0}
1.0480e01	-14.4392	0.0688
1.0500e01	-12.8820	0.0558
1.0520e01	-11.6079	0.0461

Table 1a)-Permittivity values of the function evaluated

freq(GHz)	Re{μ(ω)/μ_0}	Im{μ(ω)/μ_0}
1.0480e01	-1.1409	0.0040
1.0500e01	-1.0438	0.0037
1.0520e01	-0.9549	0.0034

Table 1b)-Corresponding permeability values around 10.5GHz

Much larger values are reached along the complete range (8-12GHz) making the meshing probably even larger when the whole range was taken into account in the first simulations. In table 2 an example is shown up to 10.46 GHz:

freq(GHz)	Re{ε(ω)/ ε_0}	Im{ε(ω)/ ε_0}
1.0240e01	47.8516	0.6196
1.0260e01	71.1936	1.3937
1.0280e01	141.0848	5.5684
1.0300e01	1.0000	3522.8539
1.0320e01	-138.8122	5.5683
1.0340e01	-68.9213	1.3937
1.0360e01	-45.5794	0.6196
1.0380e01	-33.9034	0.3485
1.0400e01	-26.8968	0.2231
1.0420e01	-22.2253	0.1549
1.0440e01	-18.8885	0.1138
1.0460e01	-16.3858	0.0871

freq(GHz)	Re{μ(ω)/ μ_0}	Im{μ(ω)/μ_0 }
1.0240e01	-3.9025	0.0207
1.0260e01	-3.4312	0.0170
1.0280e01	-3.0420	0.0141
1.0300e01	-2.7149	0.0120
1.0320e01	-2.4364	0.0103
1.0340e01	-2.1963	0.0089
1.0360e01	-1.9871	0.0078
1.0380e01	-1.8033	0.0069
1.0400e01	-1.6406	0.0061
1.0420e01	-1.4954	0.0055
1.0440e01	-1.3651	0.0049
1.0460e01	-1.2476	0.0044

Table 2a)- Permittivity values on other frequency points Table 2b)-Corresponding permeability values

CST support had also recommended to make some adjustments in the configuration of the frequency solver as measure to try to reduce the amount of memory and time required to run

the simulations: disabling the adaptive mesh refinement feature if necessary, reducing the number of frequency points in the calculation only to those that were of real interest and reducing the frequency range to a narrow frequency around the point of interest. This last configuration means that the solver does not "sweep" the whole frequency band set as a reference parameter in CST (in the last simulations, approximately 10.45-10.55GHz), instead it makes a calculation in a narrow band around sampled frequencies. This narrow band may be reduced to the frequency itself, as was done in our simulations and as showed in figure 1:

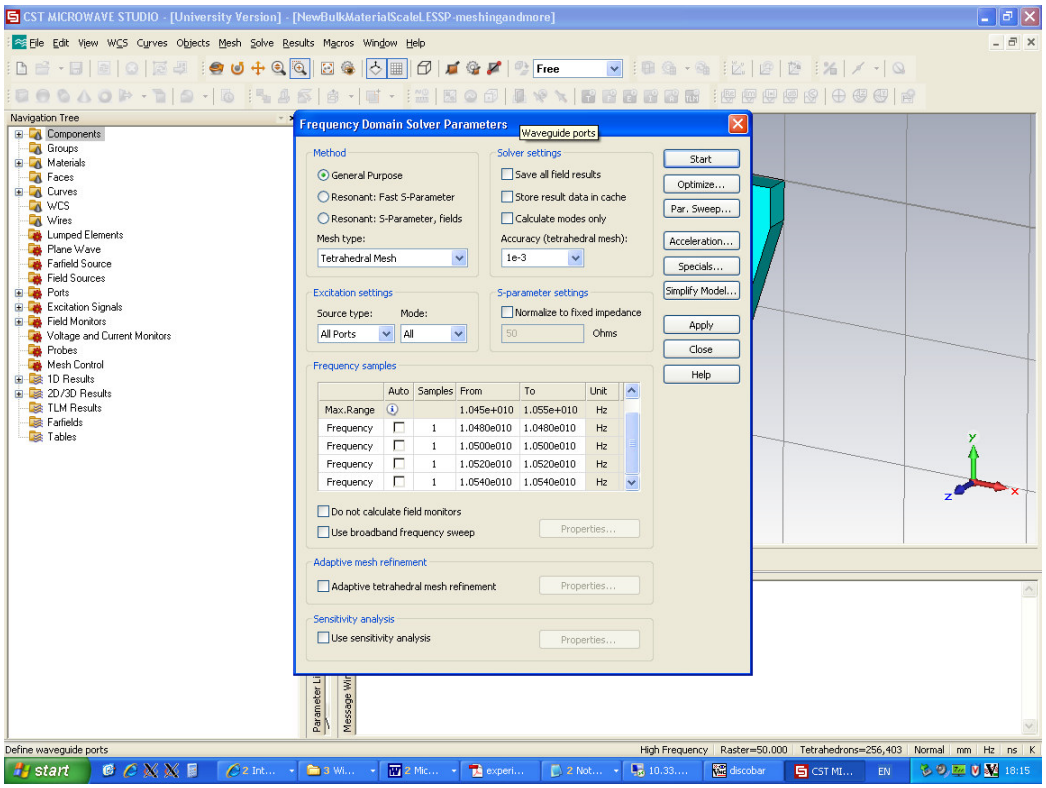

Fig. 1. Configuration set of frequency bands on the solver.

These recommendations were applied, noticing a certain improvement in the speed only for those simulations that did not present problems with the amount of memory. However again a simulation with only three points of the reference dispersion function evaluated in a narrower frequency band –depicted in figure 2- was run, taking these recommendations into account, and it failed to reach any results again.

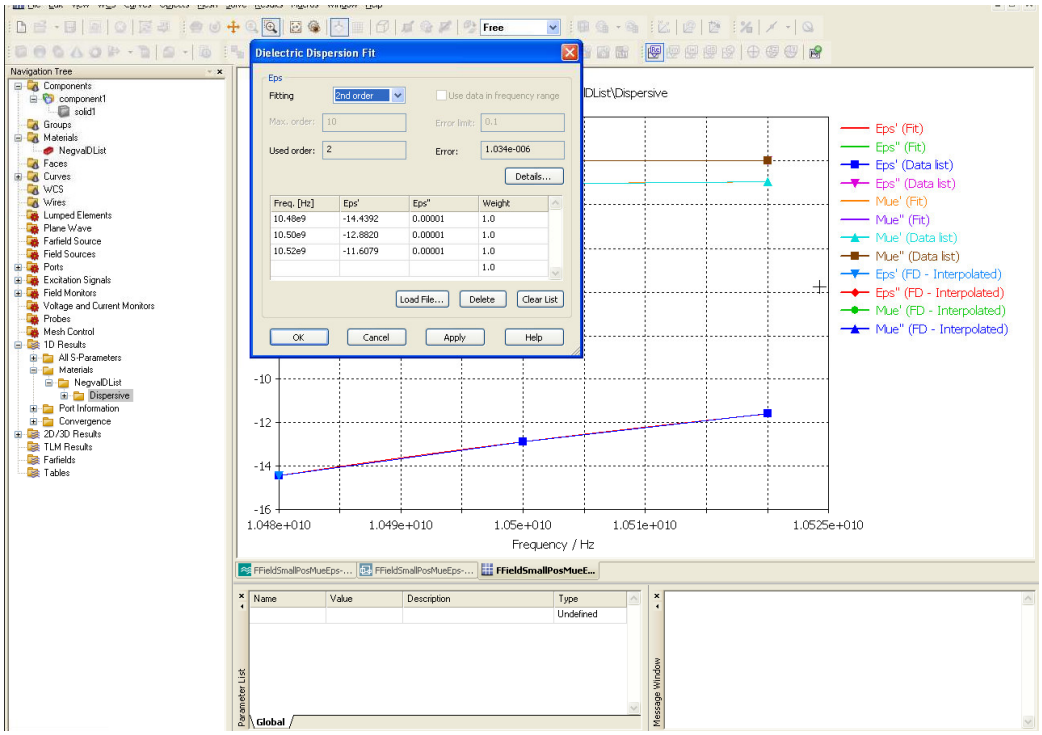

Fig. 2. Negative permittivity values used.

Measurement results of substitute shape design with LS-16

Measurement results compared with simulation results are shown in figure 1 [39].

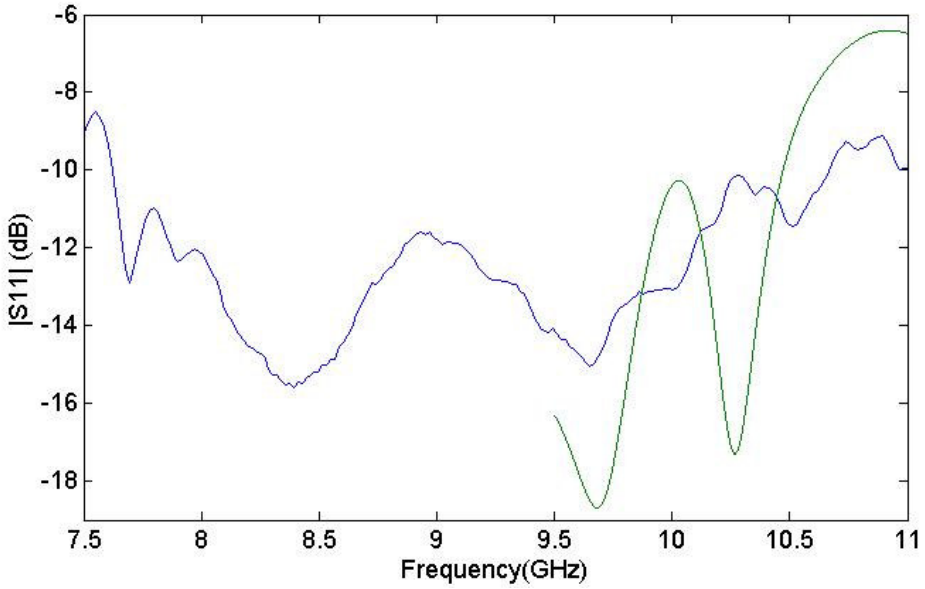

Fig. 1. Processed measurement results (blue line) and simulated results of the polarization insensitive L-shape design to be fabricated with LS-16 material as substrate (green line).

[39] As previously mentioned, it must be said that LS-16 arrived later than foreseen, then further verifications such as material parameter verification could not be performed. Also the Networks Analyzer used to perform the measurements was not the same used with DSF, but an older model. This should in principle not affect the main features of the results.